

FINAL REPORT

Enhanced Reactant-Contaminant Contact through the Use
of Persulfate In Situ Chemical Oxidation (ISCO)

SERDP Project ER-1489

FEBURARY 2011

Richard J. Watts
Washington State University

This document has been cleared for public release



Report Documentation Page		Form Approved OMB No. 0704-0188
Public reporting burden for the collection of information is estimated to average 1 hour per response, including the time for reviewing instructions, searching existing data sources, gathering and maintaining the data needed, and completing and reviewing the collection of information. Send comments regarding this burden estimate or any other aspect of this collection of information, including suggestions for reducing this burden, to Washington Headquarters Services, Directorate for Information Operations and Reports, 1215 Jefferson Davis Highway, Suite 1204, Arlington VA 22202-4302. Respondents should be aware that notwithstanding any other provision of law, no person shall be subject to a penalty for failing to comply with a collection of information if it does not display a currently valid OMB control number.		
1. REPORT DATE FEB 2011	2. REPORT TYPE	3. DATES COVERED 00-00-2011 to 00-00-2011
4. TITLE AND SUBTITLE Enhanced Reactant-Contaminant Contact through the Use of Persulfate In Situ Chemical Oxidation (ISCO)		5a. CONTRACT NUMBER
		5b. GRANT NUMBER
		5c. PROGRAM ELEMENT NUMBER
6. AUTHOR(S)	5d. PROJECT NUMBER	
	5e. TASK NUMBER	
	5f. WORK UNIT NUMBER	
7. PERFORMING ORGANIZATION NAME(S) AND ADDRESS(ES) Washington State University, French Administration Building, Pullman, WA, 99164		8. PERFORMING ORGANIZATION REPORT NUMBER
9. SPONSORING/MONITORING AGENCY NAME(S) AND ADDRESS(ES)		10. SPONSOR/MONITOR'S ACRONYM(S)
		11. SPONSOR/MONITOR'S REPORT NUMBER(S)
12. DISTRIBUTION/AVAILABILITY STATEMENT Approved for public release; distribution unlimited		
13. SUPPLEMENTARY NOTES		
14. ABSTRACT <p>A fundamental study was conducted to investigate the activation and persistence of persulfate in the subsurface with the overlying objective of evaluating the potential for contact between the oxidant source and contaminants. Mechanistic investigation of persulfate activation by naturally occurring iron oxides, manganese oxides, clay minerals, trace minerals, base, iron chelates, and organic compounds was investigated using reaction specific probe compounds hydroxyl radical and sulfate radical scavengers, and electron spin resonance spectroscopy. In addition, the effect of activated persulfate formulations on the permeability and morphology of subsurface minerals and subsurface solids was investigated using falling head permeameters, xray computed tomography, x-ray diffraction, and surface area analysis. Diffusion and transport of different persulfate formulations into low permeability matrices was investigated using specially designed soil columns filled with kaolinite and a low permeability soil. Results of activation studies showed that most minerals do not activate persulfate particularly in the concentrations commonly found in the subsurface. Iron chelate-activated persulfate and base-activated persulfate generate hydroxyl radical, sulfate radical, and reductants and provide the basis for widespread treatment of different classes of contaminants in the subsurface. Many organic compounds activate persulfate including phenoxides and ketones. Because soil organic matter contains phenolic and ketonic moieties, it is a potent activator of persulfate. Depending on the acidity of the soil organic matter, it may activate persulfate with minimal addition of base. Persulfate formulations have varied effects on subsurface morphology. Persulfate has minimal effects on the mineralogy of the subsurface, with the exception of aging ferrihydrite. It can increase the permeability of some subsurface materials. Most importantly, activated persulfate formulations have the potential to diffuse into low permeability strata, such as clays where they have the potential to treat contaminants of concern. In summary, activated persulfate in a highly reactive remediation system that has sufficient longevity and transport characteristics to treat contaminants in low permeability regions of the subsurface.</p>		

15. SUBJECT TERMS					
16. SECURITY CLASSIFICATION OF:			17. LIMITATION OF ABSTRACT	18. NUMBER OF PAGES	19a. NAME OF RESPONSIBLE PERSON
a. REPORT unclassified	b. ABSTRACT unclassified	c. THIS PAGE unclassified	Same as Report (SAR)	290	

This report was prepared under contract to the Department of Defense Strategic Environmental Research and Development Program (SERDP). The publication of this report does not indicate endorsement by the Department of Defense, nor should the contents be construed as reflecting the official policy or position of the Department of Defense. Reference herein to any specific commercial product, process, or service by trade name, trademark, manufacturer, or otherwise, does not necessarily constitute or imply its endorsement, recommendation, or favoring by the Department of Defense.

2. FRONT MATTER

Table of Contents

1. COVER PAGE	i
2. FRONT MATTER	ii
Table of Contents	ii
List of Tables	vi
List of Figures.....	vii
List of Acronyms	xviii
Keywords	xx
Acknowledgements	xx
3. ABSTRACT	0
4. OBJECTIVE	1
5. BACKGROUND	2
6. MATERIALS AND METHODS.....	12
6.1. Factors Controlling the Decomposition of Persulfate in the Subsurface.....	12

6.1.1. Persulfate Activation by Major Subsurface Minerals	12
6.1.2. Persulfate Activation by Subsurface Trace Minerals.....	15
6.1.3. Base-Activated Persulfate Treatment of Contaminated Soils with pH Drift from Alkaline to Circumneutral.....	17
6.2. Persulfate Reactivity Under Different Conditions of Activation.....	19
6.2.1. Oxidative and Reductive Pathways in Iron-Ethylenediaminetetraacetic acid (EDTA) Activated Persulfate Systems.....	19
6.2.2. Effect of Basicity on Persulfate Reactivity	22
6.2.3. Mechanism of Base Activation of Persulfate.....	24
6.2.4. Persulfate Activation By Phenoxide Derivatives.....	27
6.2.5. Persulfate Activation by Alcohols, Aldehydes, Ketones, Organic Acids, and Keto Acids	30
6.2.6. Persulfate Activation by Soil Organic Matter.....	32
6.2.7. Model Contaminants.....	34
6.2.8. Effect of Sorption on Contaminant Oxidation in Activated Persulfate Systems	35
6.3. Effect of Persulfate on Subsurface Characteristics	37
6.3.1. Effect of Persulfate Formulations on Soil Mineralogy	37
6.3.2. Effect of Persulfate Formulations on Soil Permeability	38
6.4. Transport of Persulfate into Low Permeability Matrices	44
6.4.1. Persulfate Transport in Two Low-Permeability Soils.....	44
7. RESULTS AND ACCOMPLISHMENTS.....	47
7.1. Factors Controlling the Decomposition of Persulfate in the Subsurface.....	47

7.1.1. Persulfate Activation by Major Subsurface Minerals	47
7.1.2. Persulfate Activation by Subsurface Trace Minerals.....	67
7.1.3. Base-Activated Persulfate Treatment of Contaminated Soils with pH Drift from Alkaline to Circumneutral.....	79
7.1.4. Summary of Factors Controlling the Decomposition of Persulfate in the Subsurface	99
7.2. Persulfate Reactivity Under Different Conditions of Activation.....	100
7.2.1. Oxidative and Reductive Pathways in Iron-Ethylenediaminetetraacetic acid (EDTA) Activated Persulfate Systems.....	100
7.2.2. Effect of Basicity on Persulfate Reactivity	111
7.2.3. Mechanism of Base Activation of Persulfate.....	122
7.2.4. Persulfate Activation By Phenoxide Derivatives.....	135
7.2.5. Persulfate Activation by Alcohols, Aldehydes, Ketones, Organic Acids, and Keto Acids	146
7.2.6. Persulfate Activation by Soil Organic Matter.....	162
7.2.7. Model Contaminants.....	180
7.2.8. Effect of Sorption on Contaminant Oxidation in Activated Persulfate Systems	186
7.2.9. Summary of Persulfate Activation Conditions	193
7.3. Effect of Persulfate on Subsurface Characteristics	194
7.3.1. Effect of Persulfate Formulations on Soil Mineralogy	194
7.3.2. Effect of Persulfate Formulations on Soil Permeability	235
7.3.3. Summary of the Effect of Persulfate on Subsurface Characteristics	244
7.4. Transport of Persulfate into Low Permeability Matrices.....	245
7.4.1. Persulfate Transport in Two Low-Permeability Soils.....	245
8. CONCLUSIONS AND IMPLICATIONS FOR FUTURE RESEARCH/IMPLEMENTATION	252
9. LITERATURE CITED	255
10. APPENDICES	267

List of Technical Publications.....	267
--	------------

List of Tables

Table 5.1. Second order rate constants for hydroxyl and sulfate radicals.	4
Table 6.1.1.1. Particle size distribution (PSD) of minerals	12
Table 6.1.1.2. Soil characteristics of the total soil and two soil fractions	13
Table 6.1.3.1. Physical properties of soils KB1 and KB2.	18
Table 6.1.3.2. Chemical properties of soils KB1 and KB2.....	18
Table 6.2.6.1. Characteristics of the Carson Valley Soil	32
Table 6.3.2.1. Physical properties of soil KB2 and soil KB1	38
Table 6.3.2.2. Chemical properties of soil KB2 and soil KB1	39
Table 6.4.1.1. Soil characteristics of Palouse loess.	44
Table 7.1.1.1. Persulfate decomposition rate constants in persulfate systems at low and high pH in the presence of iron and manganese oxides.....	49
Table 7.1.1.2. Nitrobenzene decomposition rate constants in persulfate systems at low and high pH in the presence of iron and manganese oxides.....	52
Table 7.1.1.3. HCA decomposition rate constants in persulfate systems at low and high pH in the presence of iron and manganese oxides.....	54
Table 7.1.1.4. Persulfate decomposition rate constants in persulfate systems at low and high pH in the presence of total soil and two soil fractions.....	59
Table 7.1.1.5. Nitrobenzene decomposition rate constants in persulfate systems at low and high pH in the presence of total soil and two soil fractions.....	61
Table 7.1.1.6. HCA decomposition rate constants in persulfate systems at low and high pH in the presence of total soil and two soil fractions.....	63
Table 7.1.4.1. Summary of factors controlling persulfate activation/decomposition.....	99
Table 7.2.5.1. Values of pK_a for ketones and krebs cycle compounds.....	148
Table 7.2.5.2. Isomers of the alcohols used in the study to activate persulfate.....	153
Table 7.2.9.1. Summary of Persulfate Activation.....	193
Table 7.3.1.1. Surface area of minerals after treatment with different persulfate systems.....	234
Table 7.3.3.1. Summary of the Effect of Persulfate on Subsurface Characteristics	244

List of Figures

Figure 6.3.2.1. Falling head permeameter.	41
Figure 6.3.2.2. Flexible wall permeameter	42
Figure 6.3.2.3. XRCT test procedures.	43
Figure 7.1.1.1. Persulfate decomposition in the presence of minerals. a) Low pH; b) high pH..	48
Figure 7.1.1.2. Degradation of the oxidant probe nitrobenzene in persulfate systems containing minerals. a) Low pH; b) high pH.	51
Figure 7.1.1.3. Degradation of the reductant probe HCA in persulfate systems containing minerals. a) Low pH; b) high pH.	53
Figure 7.1.1.4. Degradation of the oxidant probe nitrobenzene in persulfate systems containing clay minerals. a) Low pH; b) high pH.	55
Figure 7.1.1.5. Degradation of the reductant probe HCA in persulfate systems containing clay minerals. a) Low pH; b) high pH.	57
Figure 7.1.1.6. Persulfate decomposition in the presence of a soil and soil fractions. a) Low pH; b) high pH.	58
Figure 7.1.1.7. Degradation of the oxidant probe nitrobenzene in persulfate systems containing a soil and soil fractions. a) Low pH; b) high pH.	60
Figure 7.1.1.8. Degradation of the reductant probe HCA in persulfate systems containing a soil and soil fractions. a) Low pH; b) high pH.	62
Figure 7.1.1.9. Degradation of the oxidant probe nitrobenzene in persulfate systems containing low concentrations of the manganese oxide birnessite. a) Low pH; b) high pH.	64
Figure 7.1.1.10. Degradation of the oxidant probe nitrobenzene in persulfate systems containing low concentrations of the iron oxide goethite. a) Low pH; b) high pH.	65
Figure 7.1.2.1. Degradation of 0.5 M sodium persulfate by 13 various trace minerals with the temperature maintained at $25^{\circ}\text{C} \pm 1^{\circ}\text{C}$	67
Figure 7.1.2.2. Probe compound remaining after treatment in 0.5 M sodium persulfate–trace mineral systems at a temperature of $25^{\circ}\text{C} \pm 1^{\circ}\text{C}$. a) the sulfate + hydroxyl radical probe anisole; b) the hydroxyl radical probe nitrobenzene; c) the hydroperoxide probe 1,3,5-trinitrobenzene; d) the superoxide probe carbon tetrachloride.	69
Figure 7.1.2.3. Degradation of the cumulative sulfate + hydroxyl radical probe anisole by trace mineral–persulfate systems at $25^{\circ}\text{C} \pm 1^{\circ}\text{C}$. a) Calcite; b) Ilmenite; c) Pyrite.	71
Figure 7.1.2.4. Degradation of the hydroxyl radical probe nitrobenzene by trace mineral–persulfate systems at $25^{\circ}\text{C} \pm 1^{\circ}\text{C}$. a) Calcite; b) Ilmenite; c) Pyrite.....	73
Figure 7.1.2.5. Degradation of the hydroperoxide probe 1,3,5-trinitrobenzene by trace mineral–persulfate systems at $25^{\circ}\text{C} \pm 1^{\circ}\text{C}$. a) Calcite; b) Ilmenite; c) Pyrite.....	75
Figure 7.1.2.6. Degradation of reductant probe carbon tetrachloride by trace mineral–persulfate systems at $25^{\circ}\text{C} \pm 1^{\circ}\text{C}$. a) Calcite; b) Ilmenite; c) Pyrite.	76

Figure 7.1.2.7. Degradation of the four probes as relative to corresponding control systems. Duration of reactions was probe-specific: anisole over 24 hr; nitrobenzene over 48 hr; 1, 3, 5-trinitrobenzene over 120 hr; carbon tetrachloride over 4 hr.	78
Figure 7.1.3.1. pH profiles of various molar ratios of sodium hydroxide:sodium persulfate for soils KB1 (a) and KB2 (b).	80
Figure 7.1.3.2. pH profiles for the selected molar ratios of sodium hydroxide: persulfate for soil slurries KB1 (1.25:1) and KB2 (0.375:1). Arrows indicate the approximate times of spiking with probe compounds.	81
Figure 7.1.3.3. pH profiles for the selected molar ratio of 0.375:1 sodium hydroxide: persulfate for soil slurries KB1-No SOM and KB2-No SOM. Arrows indicate the approximate times of spiking with probe compounds. Star indicates that the reaction did not drift down to pH 10 within the time frame of the experiment.	81
Figure 7.1.3.4. Persulfate concentrations in soil slurries KB1 (a) and KB2 (b) in conjunction with hydroxyl radical generation experiments. Time denotes days after the system reached the indicated pH and was spiked with nitrobenzene.	83
Figure 7.1.3.5. Persulfate concentrations in soil slurries KB1-No SOM (a) and KB2-No SOM (b) in conjunction with hydroxyl radical generation experiments. Time denotes days after the system reached the indicated pH and was spiked with nitrobenzene.	84
Figure 7.1.3.6. Persulfate concentrations in soil slurries KB1 (a) and KB2 (b) in conjunction with reductant generation experiments. Time denotes days after the system reached the indicated pH and was spiked with hexachloroethane.	85
Figure 7.1.3.7. Persulfate concentrations in soil slurries KB1-No SOM (a) and KB2-No SOM (b) in conjunction with reductant generation experiments. Time denotes days after the system reached the indicated pH and was spiked with hexachloroethane.	86
Figure 7.1.3.8. pH profiles for soil slurries KB1 (a) and KB2 (b) in conjunction with hydroxyl radical generation experiments. Time denotes days after the system reached the indicated pH and was spiked with nitrobenzene.	88
Figure 7.1.3.9. pH profiles for soil slurries KB1-No SOM (a) and KB2-No SOM (b) in conjunction with hydroxyl radical generation experiments. Time denotes days after the system reached the indicated pH and was spiked with nitrobenzene.	89
Figure 7.1.3.10. pH profiles for soil slurries KB1 (a) and KB2 (b) in conjunction with reductant generation experiments. Time denotes days after the system reached the indicated pH and was spiked with hexachloroethane.	90
Figure 7.1.3.11. pH profiles for soil slurries KB1-No SOM (a) and KB2-No SOM (b) in conjunction with reductant generation experiments. Time denotes days after the system reached the indicated pH and was spiked with hexachloroethane.	91
Figure 7.1.3.12. Hydroxyl radical generation quantified through nitrobenzene degradation in soil slurries KB1 (a) and KB2 (b). Time denotes days after the system reached the indicated pH and was spiked with nitrobenzene.	93

Figure 7.1.3.13. Hydroxyl radical generation quantified through nitrobenzene degradation in soil slurries KB1-No SOM (a) and KB2-No SOM (b). Time denotes days after the system reached the indicated pH and was spiked with nitrobenzene.....	94
Figure 7.1.3.14. Reductant generation quantified through hexachloroethane degradation in soil slurries KB1 (a) and KB2 (b). Time denotes days after the system reached the indicated pH and was spiked with hexachloroethane.	96
Figure 7.1.3.15. Reductant generation quantified through hexachloroethane degradation in soil slurries KB1-No SOM (a) and KB2-No SOM (b). Time denotes days after the system reached the indicated pH and was spiked with hexachloroethane.	97
Figure 7.2.1.1. Persulfate decomposition in the presence of a) 2.5 mM; b) 5.0 mM; c) 10 mM; d) 15 mM of the activators Na ₂ -EDTA, iron (II)-EDTA, and iron (III)-EDTA.....	101
Figure 7.2.1.2. Degradation of the sulfate radical probe anisole in persulfate systems containing 10 mM Na ₂ -EDTA, iron (II)-EDTA, or iron (III)-EDTA.....	103
Figure 7.2.1.3. Degradation of the hydroxyl radical probe nitrobenzene in persulfate systems containing 10 mM Na ₂ -EDTA, iron (II)-EDTA, or iron (III)-EDTA.....	103
Figure 7.2.1.4. Degradation of the reductant probe hexachloroethane in persulfate systems containing 10 mM Na ₂ -EDTA, iron (II)-EDTA, or iron (III)-EDTA.....	104
Figure 7.2.1.5. Scavenging of sulfate radicals and hydroxyl radicals using isopropanol and scavenging of of hydroxyl radicals using <i>tert</i> -butanol in persulfate systems activated by a) iron (II)-EDTA; b) iron (III)-EDTA.	106
Figure 7.2.1.6. ESR spectra for a) iron (II)-EDTA and b) iron (III)-EDTA activated persulfate systems.....	108
Figure 7.2.1.7. Degradation of the model groundwater pollutant TCE with scavenging by isopropanol and <i>tert</i> -butanol in persulfate systems activated by a) iron (II)-EDTA; b) iron (III)-EDTA.....	109
Figure 7.2.2.1. Activity of hydroxyl radical and reductants in persulfate systems at pH 2, 7, and 12. a) Sulfate and hydroxyl radical activity measured by anisole loss; b) Hydroxyl radical activity measured by nitrobenzene loss; c) Reductant activity measured by hexachloroethane loss.	112
Figure 7.2.2.2. Activity of hydroxyl radical in the presence of a hydroxyl radical scavenger (<i>tert</i> -butyl alcohol) and a sulfate/hydroxyl radical scavenger (isopropyl alcohol) measured by a) anisole loss and b) nitrobenzene loss.	114
Figure 7.2.2.3. Activity of hydroxyl radical and reductants in systems with four different persulfate concentrations. a) Hydroxyl radical activity measured by nitrobenzene loss; b) Reductant activity measured by hexachloroethane loss.....	116
Figure 7.2.2.4. Activity of hydroxyl radical in persulfate systems containing varying molar ratios of base:persulfate measured by nitrobenzene loss. a) Base:persulfate ratios from 0.2:1 to 3:1; b) Base:persulfate ratios from 4:1 to 6:1.	118
Figure 7.2.2.5. Activity of reductants in persulfate systems containing varying molar ratios of base:persulfate measured by hexachloroethane loss. a) Base:persulfate ratio of 1:1; b)	

Base:persulfate ratio of 2:1; c) Base:persulfate ratio of 3:1; d) Base:persulfate ratio of 4:1; e) Base:persulfate ratio of 5:1; f) Base:persulfate ratio of 6:1.....	120
Figure 7.2.3.1. a) First order decomposition of base-activated persulfate with varying molar ratios of NaOH:persulfate (reactors: 0.5 M persulfate, 1 M, 1.5 M, 2 M, or 3 M NaOH; 20 mL total volume; $T = 20 \pm 2^\circ\text{C}$). b) First order rate constants for persulfate decomposition in base-activated systems as a function of initial NaOH concentration.....	123
Figure 7.2.3.2. First order decomposition of base-activated persulfate in D_2O vs. H_2O (reactors: 0.5 M persulfate and 3 M NaOH in 20 mL total volume of D_2O or H_2O ; $T = 20 \pm 2^\circ\text{C}$). .	124
Figure 7.2.3.3. Effect of ionic strength on persulfate degradation rate (reactors: 0.5 M persulfate, 3 M NaOH, 0–2 M NaClO_4 ; 20 mL total volume; $T = 20 \pm 2^\circ\text{C}$). Error bars represent the standard error of the mean.	125
Figure 7.2.3.4. Decomposition of persulfate and hydrogen peroxide in a 1:1 persulfate: H_2O_2 system (reactors: 0.5 M persulfate, 0.5 M H_2O_2 , 1.5 M NaOH; 20 mL total volume; $T = 20 \pm 2^\circ\text{C}$). Error bars represent the standard error of the mean.	128
Figure 7.2.3.5. Effect of varying base:persulfate ratio on the degradation rate of added $\text{H}_2\text{O}_2 + \text{HO}_2^-$ (reactors: 0.5 M persulfate, 0.5 M H_2O_2 , and 0.5 M, 1.0 M, or 1.5 M NaOH; 20 mL total volume; $T = 20 \pm 2^\circ\text{C}$). Error bars represent the standard error of the mean.....	128
Figure 7.2.3.6. Stoichiometry for the degradation of added hydroperoxide in base-activated persulfate systems (reactors: 0.5 M persulfate, 1.5 M NaOH, 0.5 M or 1 M H_2O_2 ; 20 mL total volume; $T = 20 \pm 2^\circ\text{C}$). Error bars represent the standard error of the mean.	129
Figure 7.2.3.7. Relative rates of superoxide generation measured by the probe molecule hexachloroethane with varying masses of $\text{H}_2\text{O}_2 + \text{HO}_2^-$ added to base-activated persulfate systems (reactors: 0.5 M persulfate, 1 M NaOH, 0–0.5 M $\text{H}_2\text{O}_2 + \text{HO}_2^-$, $2\mu\text{M}$ HCA; 20 mL total volume; $T = 20 \pm 2^\circ\text{C}$). Error bars represent the standard error of the mean.	130
Figure 7.2.3.8. Effect of copper (II) scavenging of superoxide on HCA degradation in base-activated persulfate systems with added $\text{H}_2\text{O}_2 + \text{HO}_2^-$ (reactors: 0.5 M persulfate, 1 M NaOH, 0.5 M $\text{H}_2\text{O}_2 + \text{HO}_2^-$, $2\mu\text{M}$ HCA, 0 and $2\mu\text{M}$ Cu (II); 20 mL total volume; controls: $\text{H}_2\text{O}_2 + \text{HO}_2^-$ replaced by deionized water; $T = 20 \pm 2^\circ\text{C}$). Error bars represent the standard error of the mean.	131
Figure 7.2.3.9. ESR spectrum for a base-activated persulfate system with added $\text{H}_2\text{O}_2 + \text{HO}_2^-$ (reactors: 0.05 M persulfate, 0.1 M NaOH, 0.05 M $\text{H}_2\text{O}_2 + \text{HO}_2^-$, and 0.09 M DMPO; $T = 20 \pm 2^\circ\text{C}$).	132
Figure 7.2.4.1. Persulfate decomposition in phenoxides activated persulfate systems at basic pH: 0.5 M sodium persulfate, 2M NaOH, 2 mM phenoxide, and $2\mu\text{M}$ hexachloroethane; 20 mL total volume. Error bars represent the standard error of the mean for three replicates.....	135
Figure 7.2.4.2. Degradation of hexachloroethane in phenoxide-activated persulfate systems at basic pH: 0.5 M sodium persulfate, 2M NaOH, 2 mM phenoxide, and $2\mu\text{M}$ hexachloroethane; 20 mL total volume. Error bars represent the standard error of the mean for three replicates.....	136

- Figure 7.2.4.3.** Persulfate decomposition in phenoxid-activated persulfate systems at basic pH: 0.5 M sodium persulfate, 2 M NaOH, 2 mM phenoxide, and 1 mM nitrobenzene; 15 mL total volume. Error bars represent the standard error of the mean for three replicates..... 137
- Figure 7.2.4.4.** Degradation of nitrobenzene in phenoxide-activated persulfate systems at basic pH: 0.5 M sodium persulfate, 2 M NaOH, 2 mM phenoxide, and 1 mM nitrobenzene; 15 mL total volume. Error bars represent the standard error of the mean for three replicates. 138
- Figure 7.2.4.5.** Scavenging of hydroxyl radicals in phenoxide-activated persulfate systems at basic pH: 0.5 M sodium persulfate, 2 M NaOH, 2 mM phenoxide, and 1 mM nitrobenzene; 15 mL total volume, the molar ratio of anisole to *t*-butyl alcohol was 1:1000. Error bars represent the standard error of the mean for three replicates..... 139
- Figure 7.2.4.6.** Degradation of anisole in phenol activated persulfate system at different pH regimes: 0.5 M sodium persulfate, 2 mM phenol, and 1 mM anisole; 15 mL total volume at pH 3–8. Error bars represent the standard error of the mean for three replicates..... 140
- Figure 7.2.4.7.** Degradation of probe compounds in catechol activated persulfate system at different pH regimes: 0.5 M sodium persulfate, 2 mM catechol, at 8, 9, 10, 11, and 13 pH values. Error bars represent the standard error of the mean for three replicates (a) Degradation of nitrobenzene (1 mM nitrobenzene, 15 mL total volume) (b) Degradation of hexachloroethane (2 μ M HCA, 20 mL total volume)..... 141
- Figure 7.2.4.8.** Degradation of nitrobenzene in phenol activated persulfate system at basic pH: 0.5 M sodium persulfate, 2 M NaOH, 1 mM nitrobenzene, and different phenol concentrations ranging from 0.01 to 10 mM; 15 mL total volume. Error bars represent the standard error of the mean for three replicates. 142
- Figure 7.2.4.9.** Degradation of nitrobenzene in pentachlorophenolate activated persulfate system at pH 8.0: 0.5 M sodium persulfate, 2 mM pentachlorophenol and 1 mM nitrobenzene; 15 mL total volume. Error bars represent the standard error of the mean for three replicates. 144
- Figure 7.2.4.10.** Degradation of hexachloroethane in pentachlorophenolate activated persulfate system at pH 8: 0.5 M sodium persulfate, 2 mM pentachlorophenol, and 2 μ M hexachloroethane; 20 mL total volume. Error bars represent the standard error of the mean for three replicates..... 144
- Figure 7.2.5.1.** Degradation of hexachloroethane in ketones activated persulfate systems at basic pH: 0.5 M sodium persulfate, 2 M NaOH, 10 mM ketone, and 2 μ M hexachloroethane; 20 mL total volume. Error bars represent the standard error of the mean for three replicates. 146
- Figure 7.2.5.2.** Degradation of nitrobenzene in ketones activated persulfate systems at basic pH: 0.5 M sodium persulfate, 2 M NaOH, 10 mM ketone, and 1 mM nitrobenzene; 15 mL total volume. Error bars represent the standard error of the mean for three replicates..... 147
- Figure 7.2.5.3.** Degradation of hexachloroethane in Krebs cycle-activated persulfate systems at basic pH: 0.5 M sodium persulfate, 2 M NaOH, 10 mM Krebs cycle compound, and 2 μ M hexachloroethane; 20 mL total volume. Error bars represent the standard error of the mean for three replicates. (a) Keto acids; (b) Alcohol acids; (c) Dicarboxylic acids..... 150
- Figure 7.2.5.4.** Degradation of nitrobenzene in Krebs cycle-activated persulfate systems at basic pH: 0.5 M sodium persulfate, 2 M NaOH, 10 mM Krebs cycle compound, and 1 mM

nitrobenzene; 15 mL total volume. Error bars represent the standard error of the mean for three replicates. (a) Keto acids; (b) Alcohol acids; (c) Dicarboxylic acids.	151
Figure 7.2.5.5. Degradation of hexachloroethane in alcohols activated persulfate systems at basic pH: 0.5 M sodium persulfate, 2 M NaOH, 10 mM alcohol, and 2 μ M hexachloroethane; 20 mL total volume. Error bars represent the standard error of the mean for three replicates. (a) Primary alcohols; (b) Secondary alcohols; (c) Ternary alcohols. .	155
Figure 7.2.5.6. Degradation of nitrobenzene in alcohols activated persulfate systems at basic pH: 0.5 M sodium persulfate, 2 M NaOH, 10 mM alcohol, and 1 mM nitrobenzene; 15 mL total volume. Error bars represent the standard error of the mean for three replicates. (a) Primary alcohols; (b) Secondary alcohols; (c) Ternary alcohols.....	156
Figure 7.2.5.7. Degradation of hexachloroethane in aldehydes activated persulfate systems at basic pH: 0.5 M sodium persulfate, 2 M NaOH, 10 mM aldehyde, and 2 μ M hexachloroethane; 20 mL total volume. Error bars represent the standard error of the mean for three replicates.....	158
Figure 7.2.5.8. Degradation of nitrobenzene in aldehydes activated persulfate systems at basic pH: 0.5 M sodium persulfate, 2 M NaOH, 10 mM aldehyde, and 1 mM nitrobenzene; 15 mL total volume. Error bars represent the standard error of the mean for three replicates. (a) Primary alcohols (b) Secondary alcohols (c) Ternary alcohols.....	159
Figure 7.2.5.9. Scavenging of hydroxyl radicals in persulfate activation by selected organic compounds: 0.5 M sodium persulfate, 2 M NaOH, 10 mM organic compound, and 1 mM nitrobenzene; 15 mL total volume; the molar ratio of nitrobenzene to <i>t</i> -butyl alcohol was 1:1000. Error bars represent the standard error of the mean for three replicates. (a) acetone (C ₃ H ₆ O); (b) pyruvic acid (C ₃ H ₄ O ₃); (c) <i>n</i> -propanol (C ₃ H ₈ O); (d) propionaldehyde (C ₃ H ₆ O).	161
Figure 7.2.6.1. Relative hydroxyl radical generation, as quantified by nitrobenzene degradation, in persulfate systems containing the Carson Valley Soil 1.....	162
Figure 7.2.6.2. Relative hydroxyl radical generation, as quantified by nitrobenzene degradation, in persulfate systems containing the Carson Valley Soil 2.....	163
Figure 7.2.6.3. Relative hydroxyl radical generation, as quantified by nitrobenzene degradation, in persulfate systems containing the Carson Valley Soil 3.....	164
Figure 7.2.6.4. Relative hydroxyl radical generation, as quantified by nitrobenzene degradation, in persulfate systems containing the Carson Valley Soil 4.....	165
Figure 7.2.6.5. Relative hydroxyl radical generation, as quantified by nitrobenzene degradation, in persulfate systems containing the Carson Valley Soil 1 with soil organic matter removed.	166
Figure 7.2.6.6. Relative hydroxyl radical generation, as quantified by nitrobenzene degradation, in persulfate systems containing the Carson Valley Soil 2 with soil organic matter removed.	167
Figure 7.2.6.7. Relative hydroxyl radical generation, as quantified by nitrobenzene degradation, in persulfate systems containing the Carson Valley Soil 3 with soil organic matter removed.	168

Figure 7.2.6.8. Relative hydroxyl radical generation, as quantified by nitrobenzene degradation, in persulfate systems containing the Carson Valley Soil 4 with soil organic matter removed.	169
Figure 7.2.6.9. Relative reductant generation, as quantified by hexachloroethane degradation, in persulfate systems containing the Carson Valley Soil 1.	170
Figure 7.2.6.10. Relative reductant generation, as quantified by hexachloroethane degradation, in persulfate systems containing the Carson Valley Soil 2.	171
Figure 7.2.6.11. Relative reductant generation, as quantified by hexachloroethane degradation, in persulfate systems containing the Carson Valley Soil 3.	172
Figure 7.2.6.12. Relative reductant generation, as quantified by hexachloroethane degradation, in persulfate systems containing the Carson Valley Soil 4.	173
Figure 7.2.6.13. Relative reductant generation, as quantified by hexachloroethane degradation, in persulfate systems containing the Carson Valley Soil 1 with soil organic matter removed.	174
Figure 7.2.6.14. Relative reductant generation, as quantified by hexachloroethane degradation, in persulfate systems containing the Carson Valley Soil 2 with soil organic matter removed.	175
Figure 7.2.6.15. Relative reductant generation, as quantified by hexachloroethane degradation, in persulfate systems containing the Carson Valley Soil 3 with soil organic matter removed.	176
Figure 7.2.6.16. Relative reductant generation, as quantified by hexachloroethane degradation, in persulfate systems containing the Carson Valley Soil 4 with soil organic matter removed.	177
Figure 7.2.6.17. Relative hydroxyl radical generation, as quantified by nitrobenzene degradation, in persulfate systems containing Carson Valley Soil 1 with varying concentrations of soil organic matter.	178
Figure 7.2.7.1. TCE degradation in base-activated persulfate systems containing base to persulfate molar ratios of 1:1, 2:1, and 3:1. Controls: base and persulfate substituted with deionized water.	180
Figure 7.2.7.2. PCE degradation in base-activated persulfate systems containing base to persulfate molar ratios of 1:1, 2:1, and 3:1. Controls: base and persulfate substituted with deionized water.	181
Figure 7.2.7.3. DCA degradation in base-activated persulfate systems containing base to persulfate molar ratios of 1:1, 2:1, and 3:1. Controls: base and persulfate substituted with deionized water.	182
Figure 7.2.7.4. TCA degradation in base-activated persulfate systems containing base to persulfate molar ratios of 1:1, 2:1, and 3:1. Controls: base and persulfate substituted with deionized water.	182

Figure 7.2.7.5. CB degradation in base-activated persulfate systems containing base to persulfate molar ratios of 1:1, 2:1, and 3:1. Controls: base and persulfate substituted with deionized water.....	183
Figure 7.2.7.6. DCB degradation in base-activated persulfate systems containing base to persulfate molar ratios of 1:1, 2:1, and 3:1. Controls: base and persulfate substituted with deionized water.	184
Figure 7.2.7.7. Anisole degradation in base-activated persulfate systems containing base to persulfate molar ratios of 1:1, 2:1, and 3:1. Controls: base and persulfate substituted with deionized water.	184
Figure 7.2.8.1. CHP treatment of PCE sorbed on diatomaceous earth in relation to its rate of gas purge desorption.....	186
Figure 7.2.8.2. Iron (II)–citrate-activated persulfate treatment of PCE sorbed on diatomaceous earth by in relation to its rate of gas purge desorption.....	187
Figure 7.2.8.3. Base-activated persulfate treatment of PCE sorbed on diatomaceous earth in relation to its rate of gas purge desorption.....	188
Figure 7.2.8.4. CHP treatment of HCCP sorbed on diatomaceous earth in relation to its rate of gas purge desorption.	189
Figure 7.2.8.5. Iron (II)–citrate-activated persulfate treatment of HCCP sorbed on diatomaceous earth in relation to its rate of gas purge desorption.....	190
Figure 7.2.8.6. Base-activated persulfate treatment of HCCP sorbed on diatomaceous earth in relation to its rate of gas purge desorption.....	191
Figure 7.3.1.1. XRD spectra for goethite treated with deionized water over 45 days.	196
Figure 7.3.1.2. XRD spectra for goethite treated with persulfate over 45 days.....	197
Figure 7.3.1.3. XRD spectra for goethite treated with iron (III)–EDTA-activated persulfate over 45 days.	198
Figure 7.3.1.4. XRD spectra for goethite treated with base-activated persulfate (2:1 molar ratio of NaOH to persulfate) over 45 days.	199
Figure 7.3.1.5. XRD spectra for hematite treated with deionized water over 45 days.	200
Figure 7.3.1.6. XRD spectra for hematite treated with persulfate over 45 days.....	201
Figure 7.3.1.7. XRD spectra for hematite treated with iron (III)–EDTA-activated persulfate over 45 days.	202
Figure 7.3.1.8. XRD spectra for hematite treated with base-activated persulfate (2:1 molar ratio of NaOH to persulfate) over 45 days.	203
Figure 7.3.1.9. XRD spectra for ferrihydrite treated with deionized water over 45 days.....	204
Figure 7.3.1.10. XRD spectra for ferrihydrite treated with persulfate over 45 days.	205
Figure 7.3.1.11. XRD spectra for ferrihydrite treated with iron (III)–EDTA-activated persulfate over 45 days.	206

Figure 7.3.1.12. XRD spectra for ferrihydrite treated with base-activated persulfate (2:1 molar ratio of NaOH to persulfate) over 45 days.....	207
Figure 7.3.1.13. XRD spectra for birnessite treated with deionized water over 45 days.....	208
Figure 7.3.1.14. XRD spectra for birnessite treated with persulfate over 45 days.	209
Figure 7.3.1.15. XRD spectra for birnessite treated with iron (III)–EDTA-activated persulfate over 45 days.	210
Figure 7.3.1.16. XRD spectra for birnessite treated with base-activated persulfate (2:1 molar ratio of NaOH to persulfate) over 45 days.....	211
Figure 7.3.1.17. XRD spectra for kaolinite treated with deionized water over 45 days.....	212
Figure 7.3.1.18. XRD spectra for kaolinite treated with persulfate over 45 days.....	213
Figure 7.3.1.19. XRD spectra for kaolinite treated with iron (III)–EDTA-activated persulfate over 45 days.	214
Figure 7.3.1.20. XRD spectra for kaolinite treated with base-activated persulfate (2:1 molar ratio of NaOH to persulfate) over 45 days.	215
Figure 7.3.1.21. XRD spectra for montmorillonite treated with deionized water over 45 days.....	216
Figure 7.3.1.22. XRD spectra for montmorillonite treated with persulfate over 45 days.....	217
Figure 7.3.1.23. XRD spectra for montmorillonite treated with iron (III)–EDTA-activated persulfate over 45 days.	218
Figure 7.3.1.24. XRD spectra for montmorillonite treated with base-activated persulfate (2:1 molar ratio of NaOH to persulfate) over 45 days.....	219
Figure 7.3.1.25. Persulfate concentrations over time in control solutions with no minerals containing persulfate alone (unactivated), iron (III)-EDTA-activated persulfate, or base-activated persulfate (with a 2:1 ratio of base to persulfate).	220
Figure 7.3.1.26. Persulfate concentrations over time in goethite systems containing persulfate alone (unactivated), iron (III)-EDTA-activated persulfate, or base-activated persulfate (with a 2:1 ratio of base to persulfate).....	221
Figure 7.3.1.27. Persulfate concentrations over time in hematite systems containing persulfate alone (unactivated), iron (III)-EDTA-activated persulfate, or base-activated persulfate (with a 2:1 ratio of base to persulfate).....	222
Figure 7.3.1.28. Persulfate concentrations over time in ferrihydrite systems containing persulfate alone (unactivated), iron (III)-EDTA-activated persulfate, or base-activated persulfate (with a 2:1 ratio of base to persulfate).....	223
Figure 7.3.1.29. Persulfate concentrations over time in birnessite systems containing persulfate alone (unactivated), iron (III)-EDTA-activated persulfate, or base-activated persulfate (with a 2:1 ratio of base to persulfate).....	224
Figure 7.3.1.30. Persulfate concentrations over time kaolinite systems containing persulfate alone (unactivated), iron (III)-EDTA-activated persulfate, or base-activated persulfate (with a 2:1 ratio of base to persulfate).....	225

Figure 7.3.1.31. Persulfate concentrations over time montmorillonite systems containing persulfate alone (unactivated), iron (III)-EDTA-activated persulfate, or base-activated persulfate (with a 2:1 ratio of base to persulfate).....	226
Figure 7.3.1.32. pH over time in control solutions with no minerals containing persulfate alone (unactivated), iron (III)-EDTA-activated persulfate, or base-activated persulfate (with a 2:1 ratio of base to persulfate).....	227
Figure 7.3.1.33. pH over time in goethite systems containing persulfate alone (unactivated), iron (III)-EDTA-activated persulfate, or base-activated persulfate (with a 2:1 ratio of base to persulfate).	228
Figure 7.3.1.34. pH over time in hematite systems containing persulfate alone (unactivated), iron (III)-EDTA-activated persulfate, or base-activated persulfate (with a 2:1 ratio of base to persulfate).	229
Figure 7.3.1.35. pH over time in ferrihydrite systems containing persulfate alone (unactivated), iron (III)-EDTA-activated persulfate, or base-activated persulfate (with a 2:1 ratio of base to persulfate).	230
Figure 7.3.1.36. pH over time in birnessite systems containing persulfate alone (unactivated), iron (III)-EDTA-activated persulfate, or base-activated persulfate (with a 2:1 ratio of base to persulfate).	231
Figure 7.3.1.37. pH over time in kaolinite systems containing persulfate alone (unactivated), iron (III)-EDTA-activated persulfate, or base-activated persulfate (with a 2:1 ratio of base to persulfate).	232
Figure 7.3.1.38. pH over time in montmorillonite systems containing persulfate alone (unactivated), iron (III)-EDTA-activated persulfate, or base-activated persulfate (with a 2:1 ratio of base to persulfate).....	233
Figure 7.3.2.1. Effect of sodium persulfate and sulfate formulations on sand hydraulic conductivity.....	236
Figure 7.3.2.2. Effect of sodium persulfate and sulfate formulations on kaolinite hydraulic conductivity.....	237
Figure 7.3.2.3. Effect of sodium persulfate and sulfate formulations on soil KB1 hydraulic conductivity.....	238
Figure 7.3.2.4. Effect of sodium persulfate and sulfate formulations on soil KB2 hydraulic conductivity.....	239
Figure 7.3.2.5. Sand porosity distribution with depth and average porosity; a) untreated; b) deionized water; c) persulfate alone; d) persulfate with iron (III)-EDTA.	240
Figure 7.3.2.6. Soil KB1 porosity distribution with depth, average porosity, and mean pore radius; a) dry soil; b) deionized water; c) persulfate alone; d) persulfate with iron (III)-EDTA; e) persulfate with NaOH.	241
Figure 7.3.2.7. Soil KB2 porosity distribution with depth, average porosity and mean pore radius; a) dry soil; b) deionized water; c) persulfate and NaOH	242

Figure 7.4.1.1. Concentration versus depth profile for diffusion of 1 M persulfate in Palouse loess at 149 days.	245
Figure 7.4.1.2. Concentration versus depth profile for diffusion of 1 M persulfate in Palouse loess at 70 days.	246
Figure 7.4.1.3. Concentration versus depth profile for diffusion of 0.1 M persulfate in Palouse loess at 131 days.	247
Figure 7.4.1.4. Concentration versus depth profile for diffusion of 0.1 M persulfate in Palouse loess at 85 days.	248
Figure 7.4.1.5. Concentration versus depth profile for diffusion of 1 M persulfate in kaolin at 81 days.	249
Figure 7.4.1.6. Concentration versus depth profile for diffusion of 0.1 M persulfate in kaolin at 82 days.	250

List of Acronyms

BET	Brunauer, Emmett, and Teller
BTEX	Benzene, toluene, ethylbenzene, and xylenes
CB	Chlorobenzene
CEC	Cation exchange capacity
CHP	Catalyzed H ₂ O ₂ propagations
CT	Carbon tetrachloride
DCB	Dichlorobenzene
DCA	1,1-Dichloroethane
DMPO	5,5-Dimethyl-1-pyrroline-N-oxide
DNAPL	Dense nonaqueous phase liquid
DTPA	Diethylenetriamine-pentaacetic acid
ECD	electron capture detector
EDTA	Ethylenediaminetetraacetic acid
ESR	Electron spin resonance
FID	Flame ionization detector
GC	Gas chromatograph
GC-MS	Gas chromatography/mass spectroscopy
HCA	Hexachloroethane
HCCP	Hexachlorocyclopentadiene
HPLC	High performance liquid chromatography
ICPAES	Inductively coupled plasma-atomic emission spectrometry
ISCO	In situ chemical oxidation
KO ₂	Potassium superoxide
LNAPL	Light nonaqueous phase liquid
NAPL	Nonaqueous phase liquid
NB	Nitrobenzene
NOM	Natural organic matter
NTA	Nitrilotriacetic acid
PCE	Perchloroethylene
PTFE	Polytetrafluoroethylene

SOC	Soil organic carbon
SOM	Soil organic matter
TCA	1,1,1-Trichloroethane
TCE	Trichloroethylene
VOA	Volatile organic analysis
XRCT	X-ray computed tomography
XRD	X-ray diffraction

Keywords

In situ chemical oxidation, activated persulfate, sulfate radical, hydroxyl radical, superoxide radical, contaminant contact, reagent delivery, diffusion in soils

Acknowledgements

The Principal Investigators would like to thank the graduate students and postdoctoral researchers who have worked on the project including Robert Vaughan, Olga Furman, Ana Maria Ocampo, Mike Miraglio, and Mushtaque Ahmad. We would also like to thank the SERDP program manager, Dr. Andrea Leeson, and the SERDP staff for assistance and support throughout the project.

3. ABSTRACT

A fundamental study was conducted to investigate the activation and persistence of persulfate in the subsurface with the overlying objective of evaluating the potential for contact between the oxidant source and contaminants. Mechanistic investigation of persulfate activation by naturally occurring iron oxides, manganese oxides, clay minerals, trace minerals, base, iron chelates, and organic compounds was investigated using reaction specific probe compounds, hydroxyl radical and sulfate radical scavengers, and electron spin resonance spectroscopy. In addition, the effect of activated persulfate formulations on the permeability and morphology of subsurface minerals and subsurface solids was investigated using falling head permeameters, x-ray computed tomography, x-ray diffraction, and surface area analysis. Diffusion and transport of different persulfate formulations into low permeability matrices was investigated using specially designed soil columns filled with kaolinite and a low permeability soil.

Results of activation studies showed that most minerals do not activate persulfate, particularly in the concentrations commonly found in the subsurface. Iron chelate-activated persulfate and base-activated persulfate generate hydroxyl radical, sulfate radical, and reductants, and provide the basis for widespread treatment of different classes of contaminants in the subsurface. Many organic compounds activate persulfate including phenoxides and ketones. Because soil organic matter contains phenolic and ketonic moieties, it is a potent activator of persulfate. Depending on the acidity of the soil organic matter, it may activate persulfate with minimal addition of base.

Persulfate formulations have varied effects on subsurface morphology. Persulfate has minimal effects on the mineralogy of the subsurface, with the exception of aging ferrihydrite. It can increase the permeability of some subsurface materials. Most importantly, activated persulfate formulations have the potential to diffuse into low permeability strata, such as clays, where they have the potential to treat contaminants of concern. In summary, activated persulfate in a highly reactive remediation system that has sufficient longevity and transport characteristics to treat contaminants in low permeability regions of the subsurface.

4. OBJECTIVE

The goal of research conducted under ER-1489 has been to provide definitive information on the physical and chemical processes associated with activated persulfate within aquifer materials, leading to improved application of persulfate ISCO. Specific objectives for the past year were 1) To determine persulfate decomposition rates in the presence of metal oxides and subsurface solids with a wide range of physical and geochemical characteristics, 2) To determine persulfate reactivity with contaminants under varying activation conditions, and 3) To evaluate the effect of persulfate on soil microstructure, porosity, and permeability

5. BACKGROUND

The contamination of soils and groundwater by hazardous organic chemicals has been a significant concern for over thirty years. Even though many contaminated sites have been cleaned up, thousands more remain to be treated (Freeze, 2000) and thousands of hazardous materials spills occur each year (Hackman et al., 2001). Furthermore, despite over two decades of development of innovative technologies, some sites are still not effectively treated. A primary reason for the difficulty in cleaning up many contaminated sites is the difficulty of bringing reactants into contact with contaminants, particularly when the contaminants are found in low permeability matrices (Bedient et al., 1994; Watts, 1998).

Difficulties in reagent transport and contact with contaminants are inherent in most remedial technologies, including the rapidly growing area of in situ chemical oxidation (ISCO). Catalyzed H_2O_2 propagations (CHP—modified Fenton's reagent), permanganate, and ozone have been the most common ISCO processes through the year 2000 (Watts and Teel, 2006). Each of these ISCO reagents has different reactivities with contaminants of concern. CHP has the potential to degrade a wide range of organic contaminants, and can effectively treat sorbed contaminants (Watts and Teel, 2005; Corbin et al., 2007). Furthermore, if CHP process conditions favor the generation of superoxide, the process has the potential to degrade dense nonaqueous phase liquids (DNAPLs) more rapidly than their rate of dissolution (Teel et al., 2002; Smith et al., 2006). Ozone, when decomposed to other reactive oxygen species, is also highly reactive with most contaminants. In contrast, permanganate is stable in the subsurface (Siegrist et al., 2001), but is reactive with a narrow range of contaminants (Tratnyek and Waldemer, 2006).

The use of these reagents is restricted by limitations in the stability, transport, and delivery of the oxidants. Transport of hydrogen peroxide in the subsurface is limited by its low stability, which rarely has a half-life greater than 48 hours (Kakarla and Watts, 1996); depletion of hydrogen peroxide is sometimes found within 1–2 m of the injection well. Ozone is limited by its mass transfer and solubility in groundwater as well as by its often variable reactivity, which is influenced by the subsurface mineralogy (Wong et al., 1997). Permanganate is limited by its reactivity with natural organic material (NOM); in soils with high NOM, permanganate is rapidly consumed, minimizing its transport and delivery to contaminated regions. As a result, both processes may require large oxidant dosages and close spacing of injection wells. The use of permanganate is further limited by its inability to treat several key groundwater contaminants, such as benzene and carbon tetrachloride, and by the formation of manganese oxide precipitates, which may clog subsurface pores (Siegrist et al., 2001). Therefore, the current state of development of ISCO presents a dilemma. The most widely-reactive oxidant, CHP, while able to oxidize nearly all contaminants of concern, is the least stable and therefore most difficult to apply effectively. The most stable oxidant, permanganate, is limited by both the type of contaminant it can oxidize and by the geological matrix.

Sodium persulfate is the newest oxidant source to be used for ISCO. The use of sodium persulfate as an ISCO reagent has the potential to overcome many of the mass transfer limitations characteristic of modified Fenton's reagent and permanganate. Sodium persulfate is a

strong ($E_0 = 2.1$ V), water-soluble (56 g/100 mL @ 20°C) oxidant with unique properties that make it a promising ISCO reagent for treating groundwater contaminants. It is reactive with the same wide range of contaminants as is CHP but is more stable than hydrogen peroxide, with half-lives on the order of 10 to 20 days. Persulfate does not appear to be as reactive with NOM as permanganate, providing the ability to treat organic-rich strata more effectively. Finally, persulfate treatment may actually increase the permeability of certain soils, resulting in improved distribution of the oxidant and contact with contaminants. Thus, persulfate has the potential to be a widely-reactive oxidant that can potentially diffuse into a broad range of geological matrices.

Persulfate has advantages as an ISCO reagent because of its strong oxidation potential and its longevity in the subsurface, which provides the potential for diffusion into lower permeability strata and contact with contaminants. The persulfate anion is the most powerful oxidant of the peroxygen family of compounds and one of the strongest oxidants that can be used in soil and groundwater remediation. The standard oxidation–reduction potential for the reaction:



is 2.1 V, which is higher than the oxidation–reduction potential for hydrogen peroxide (1.8 V) and permanganate anion (1.7 V); however, it is slightly lower than that of ozone (2.2 V).

While persulfate anion can act as a direct oxidant, its reaction rates are limited for more recalcitrant contaminants, such as trichloroethylene (TCE) and perchloroethylene (PCE) (House, 1962; Haikola, 1963). The kinetics of persulfate oxidation can be enhanced significantly by activating persulfate to generate sulfate radical ($SO_4^{\bullet-}$), similar to the generation of hydroxyl radical (OH^{\bullet}) from hydrogen peroxide by Fenton-like reactions. The autodecomposition of persulfate is slow at temperatures $\leq 20^\circ\text{C}$, and initiators, such as heat, light, gamma radiation, and hydroxide anion, are usually used to activate its decomposition. Transition metals also initiate the decomposition of persulfate through a one-electron transfer reaction analogous to the Fenton initiation reaction. Such initiation reactions result in the formation of sulfate radical (Renaud and Sibi, 2001):



Sulfate radical ($SO_4^{\bullet-}$) is a strong oxidant that can potentially oxidize many common groundwater contaminants. Sulfate radical is also an active precursor for the propagation of other free radicals, and has been used as a probe for the reactivity of several compounds:



Another strong, non-specific oxidant, hydroxyl radical (OH^{\bullet}), is also generated during persulfate propagation reactions:



Hydroxyl radical is a relatively non-specific oxidant that reacts with most organic compounds at near diffusion-controlled rates (Table 5.1), and readily attacks even highly chlorinated compounds, such as TCE, PCE, and polychlorinated biphenyls (Haag and Yao, 1992). Hydroxyl radical reacts by addition to the unsaturated bonds of halogenated alkenes and aromatic compounds, displacing halogens and producing organic acids (Walling and Johnson, 1975). In addition, hydroxyl radical can abstract hydrogen atoms from saturated compounds, producing alkyl radicals that are involved in propagation reactions.

Sulfate radical, like hydroxyl radical, is a strong oxidant ($E_0 = 2.6$ V) that degrades organic contaminants through three mechanisms: 1) hydrogen abstraction; 2) addition and substitution reactions with alkenes and aromatic compounds; and 3) electron transfer. Neta et al. (1976) studied the reactivity of sulfate radical by electron spin resonance spectroscopy. Benzene derivatives with ring activating groups, such as anisole, acetanilide, and *p*-hydroxybenzoic acid, showed reactivity with sulfate radical at near diffusion-controlled rates; however, nitrobenzene and *p*-nitrobenzoic acid were essentially nonreactive with sulfate radical (Table 5.1). Oxidation products for benzoic acid derivatives included decarboxylation products and oxidations of the benzene ring. Huie and Clifton (1996) determined the rate constant for reaction of sulfate radical with oxalate. They found rate constants ranging from $1.5 \times 10^7 \text{ M}^{-1} \text{ s}^{-1}$ at 24.3°C to $2.23 \times 10^7 \text{ M}^{-1} \text{ s}^{-1}$ at 60.1°C . Data for sulfate radical reactivity is often sparse, conflicting, or non-existent, especially for long-chain oxygenated organic compounds. George et al. (2001) determined rates for the oxidation of several oxygenated volatile organic compounds (VOCs) with sulfate radical; the reactivity of most were in the $10^7 - 10^8 \text{ M}^{-1} \text{ s}^{-1}$ range. Results to date suggest that sulfate radical has more limited reactivity than hydroxyl radical; however, both sulfate radical and hydroxyl radical are generated in activated persulfate systems.

Table 5.1. Second order rate constants for hydroxyl and sulfate radicals.

Aliphatic compounds	$k_{\text{OH}\cdot} (\text{M}^{-1} \text{ s}^{-1})$	$k_{\text{SO}_4\cdot-} (\text{M}^{-1} \text{ s}^{-1})$
Methanol	8.0×10^8	1.0×10^7
Ethanol	1.8×10^9	4.3×10^7
2-Propanol	2.0×10^9	8.2×10^7
<i>t</i> -Butyl alcohol	5.2×10^8	$\leq 10^6$
1-Hexanol	5.2×10^9	1.6×10^8
1-Octanol	5.6×10^9	3.2×10^8
Aromatic compounds		
Anisole	6.0×10^9	4.9×10^9
Acetanilide	5.0×10^9	3.6×10^9
Benzene	7.8×10^9	3.0×10^9
Benzoic acid	4.0×10^9	1.2×10^9
<i>p</i> -Hydroxybenzoic acid	8.3×10^9	2.5×10^9
Nitrobenzene	3.9×10^9	$< 10^6$
<i>p</i> -Nitrobenzoic acid	2.6×10^9	$< 10^6$

Sources: Neta et al., 1976, Padmaja et al., 1993, Buxton et al., 1988

Persulfate also has the unique property that it hydrolyzes to form two other reactive peroxygen compounds: hydrogen peroxide and peroxymonosulfate, both highly reactive oxidant sources. The peroxymonosulfate anion provides an ionic reaction mechanism as opposed to a free radical mechanism. In addition to the mixture of peroxygen species known to exist within a persulfate solution, activated persulfate may also include a mixture of other free radicals and active oxygen species such as singlet oxygen, superoxide anion, and hydroperoxide anion, similar to the mixture of species that has been documented for CHP (Smith et al., 2004).

Although a modicum of fundamental information is known about activated persulfate in relatively pure aqueous systems, its subsurface chemistry has received little attention. Historical development of ISCO technologies has demonstrated that the subsurface chemistry is a major factor in the effectiveness of these technologies. For example, minerals are known to decompose hydrogen peroxide leading to the formation of reactive oxygen species in CHP systems, resulting in more rapid decomposition of hydrogen peroxide in the subsurface (Watts et al., 1997). Minerals are usually so effective in decomposing H_2O_2 that the addition of soluble iron is usually not required.

Few studies to date have investigated persulfate dynamics in the presence of soils and aquifer solids. Liang et al. (2008b) studied TCE remediation in columns packed with glass beads and a sandy soil. They reported that persulfate preferentially oxidized soil organic matter relative to TCE; however, the authors did not evaluate potential activation of persulfate by the naturally occurring soil minerals. The potential for the iron and manganese oxide minerals commonly found in soils and the subsurface to activate persulfate has not been investigated to date. If naturally occurring minerals in soils or subsurfaces can effectively activate persulfate, then heat or iron chelates would not be required. Such a process modification would be less costly and provide increased ease of persulfate delivery to the subsurface.

The alternative to mineral activation of persulfate is the addition of soluble iron. There are two limitations of using iron (II) to activate persulfate. First, the iron (III) that forms in reaction (1) precipitates as an iron hydroxide at $\text{pH} > 4$ (Stumm and Morgan, 1996). Secondly, unlike CHP systems in which iron (III) is reduced to iron (II) after it is formed, iron (III) is stable in persulfate systems, and the initiation reaction stalls (Liang et al., 2004). However, Liang et al. (2009) reported that iron (III)-EDTA can maintain persulfate activation by promoting the cycling of iron as in CHP systems. The destruction of common groundwater contaminants such as trichloroethylene (TCE) (Liang et al., 2009) and benzene, toluene, ethylbenzene, and xylenes (BTEX) (Killian et al., 2007) has been studied in iron-chelate activated persulfate systems. However, the role of sulfate radical, hydroxyl radical, and reductants in the destruction of groundwater contaminants by iron (II)-EDTA and iron (III)-EDTA activated persulfate has not been investigated.

The first activator used for persulfate ISCO was iron chelates; however, the most common method of persulfate activation in current use for ISCO applications is the addition of base, a pathway that may involve base-catalyzed hydrolysis of persulfate as the initial step in the reaction pathway. Two approaches that can be used for base-activated persulfate are: 1) maintaining the system at $\text{pH} 12$, and 2) adding an equal or excess molar ratio of base:persulfate.

A persulfate ISCO system adjusted to pH 12 has the advantage of initially requiring only small amounts of base to activate the persulfate; however, the sulfuric acid generated through the decomposition of persulfate ultimately lowers the pH into the acidic range (Block et al., 2004), minimizing further activation of persulfate and acidifying the subsurface. The advantage of systems with higher concentrations of base is the potential to maintain a basic pH, and activated persulfate reactivity, as sulfuric acid is generated during persulfate decomposition. In addition, the pH of the groundwater returns to near-neutral when the reaction is complete.

Based on the widespread contaminant transformations observed in field applications, base-activated persulfate formulations may generate multiple reactive species, including sulfate radical, hydroxyl radical, and reductants (Watts and Teel, 2006; Liang and Su, 2009). However, the reactivity of base-activated persulfate systems, with emphasis on the reactive oxygen species responsible for contaminant destruction, has not been investigated to date.

Base activation of persulfate has been used at approximately 60% of sites where persulfate ISCO has been employed (Brown, 2009). Base-activated persulfate technology has successfully destroyed highly chlorinated methanes and ethanes in groundwater and soil systems when base was used in excess (Root et al., 2005; Block et al., 2004). Several mechanisms have been proposed for the base activation of persulfate (Kolthoff and Miller, 1951; House, 1962; Singh and Venkatarao, 1976). Kolthoff and Miller (1951) hypothesized that persulfate decomposes homolytically into two sulfate radicals, which are then transformed to hydroxyl radicals through subsequent reactions. In contrast, Singh and Venkatarao (1976) proposed that persulfate first decomposes to peroxomonosulfate, which then collapses to sulfate and molecular oxygen. However, no proposed mechanisms of persulfate decomposition under alkaline conditions have been thoroughly evaluated and confirmed.

The effectiveness of base-activated persulfate in the subsurface is dependent on pH. Empirical data from field investigations suggest that the reactivity of persulfate formulations decreases dramatically at pH <10. Although Block et al. (2004), suggested that base-activated persulfate is only effective at pH > 10, some results suggest that contaminant oxidation may proceed at pH systems < 10, especially in the presence of subsurface solids.

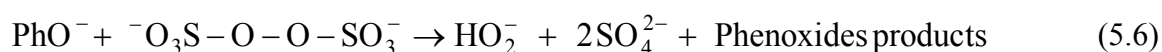
Some organic compounds may also activate persulfate. Elbs (1893) reported the oxidation of *o*-nitrophenol to nitroquinol by reaction with ammonium persulfate in the presence of alkali. In this type of reaction, hydroxyphenyl alkali sulfate was formed as an intermediate product, which was then hydrolyzed in acid solution to quinol. Elbs persulfate oxidation involves nucleophilic displacement where the nucleophile is a phenoxide anion and the main reaction product is an aromatic sulfate with a *para* orientation relative to the phenolic group (Behrman, 2006). Baker and Brown (1948) suggested that during the Elbs persulfate oxidation of phenols, resonance hybrids of the phenoxide ion may be involved.

Merz and Waters (1949) studied the oxidation of aromatic compounds by hydrogen peroxide in the presence of ferrous salts, where the reaction mechanism was a free-radical. The oxidation converted benzene to phenol and biphenyl. It has been suggested that substituted

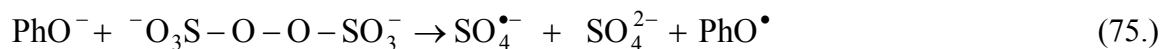
benzenes react with sulfate radicals either by electron transfer from the aromatic ring to sulfate radicals or by addition/elimination (Rosso et al., 1999).

Persulfate activation by organic compounds is an important mechanism given that all soils and sediments contain some amount of organic matter. Phenoxides, which are the salts of phenol and chlorophenols, were the selected organic compounds used to accomplish the study of persulfate activation at alkaline pH. The hypothesized mechanism for persulfate activation by phenoxides included a nucleophilic or reductive pathway.

If phenoxides react with persulfate by nucleophilic attack, sulfate radicals and hydroperoxide can be generated for further chain reactions.



If persulfate activation by phenoxides follows a reductive mechanism, phenoxyl radicals are generated:



The formation of phenoxyl radicals, a product from equation 5.7, should be confirmed by the generation of hydroquinones as degradation byproducts (Sethna, 1951). If the reductive pathway is parallel to the base-activation pathway, the oxidation of phenoxides to hydroquinones would be the dominant pathway.

Organic matter is divided into two basic categories: nonhumic and humic materials. Nonhumic materials include amino acids, carbohydrates, fats, and other biochemicals that occur in the soil as a result of the metabolism of living organisms. Humic substances are present in soil, water and sediments. These substances are derived from plant, algal and microbial material (Scott et al., 1998) and are associated with functional structures such as aromatic carboxyl groups, ketones, esters, ethers, and hydroxyl structures. Some of these compounds found in living organisms are components of the Krebs cycle. Other investigators (David-Gara et al., 2008) have studied the interaction between humic substances and sulfate radicals ($\text{SO}_4^{\bullet-}$) with organic contaminants in water and soil. They emphasized that the presence of humic substances can decrease the effectiveness of oxidants, since these compounds could scavenge sulfate radicals. However, it is also possible that some humic substances could increase the effectiveness of oxidants, such as Krebs cycle compounds that have the potential to activate persulfate in high pH systems.

Some investigators also have evaluated the interaction of sulfate radicals generated by flash photolysis with humic substances and the organic contaminants (David-Gara et al., 2007). These results indicate that the initial step of reaction mechanism involves the reversible binding

of the sulfate radicals by the humic substances. Both the bound and the sulfate radicals then decay to oxidized products. Additionally, Caregnato et al. (2008) performed a mechanistic investigation of the reaction of sulfate radicals with gallic acid, a low molecular weight humic substance. The flash photolysis experiments performed with this system showed the formation of phenoxyl radicals of the organic substrate as reaction intermediates, which supports the H-abstraction by the sulfate radical from gallic acid.

A challenge with some ISCO treatment processes is the slow rate of treatment of sorbed hydrophobic contaminants, which is limited by desorption of the contaminants from soils and subsurface solids (Watts, 1998). Most transformation reactions occur in the aqueous phase, and sorbed contaminants are considered unreactive with water-based reactive species (Sheldon and Kochi, 1981). Surfactants have been used to increase the rate of contaminant desorption; however, high concentrations of surfactants are required and the wash solution must be treated (Suthersan, 1997). One ISCO technology, CHP, has been shown to treat sorbed contaminants more rapidly than the rates at which they desorb (Watts et al., 1994; U.S. DOE, 1999; Watts et al., 2002; Yeh et al., 2003). Watts et al. (1999) found that a nucleophilic or reducing species is responsible for the enhanced desorption of contaminants by CHP, and Corbin et al. (2007) identified the species as superoxide radical anion, generated through propagation reactions with hydrogen peroxide:



The ability of activated persulfate to degrade sorbed contaminants more rapidly than their maximum rates of desorption has not been investigated; however, the process chemistry of activated persulfate systems shares some similarities with CHP systems. Hydroxyl radical is formed in both processes, and hydrogen peroxide may be produced in base-activated persulfate systems. Therefore, superoxide radical may be generated in activated persulfate systems through propagation reactions between hydroxyl radical and hydrogen peroxide, as in CHP systems. As a result, activated persulfate may promote enhanced desorption, similar to CHP.

A significant difficulty in subsurface remediation is promoting contact between the active remediation agents and the contaminant, particularly in low-permeability strata. Often, contaminants have had decades to diffuse into regions of low permeability and the embedded contaminants act as a source of long-term contaminant release, continually diffusing back into the groundwater. Persulfate, because it is long-lived in the subsurface, has the potential to treat contamination in low-permeability regions.

Persulfate formulations are highly complex solutions containing sodium, persulfate, and its decomposition products. Furthermore, the pH drops as the persulfate decomposes to sulfuric acid. The complex chemistry of persulfate may change the permeability of soils and subsurface solids by inducing dispersion and flocculation, or by changes in surface charges. X-ray computed

tomography (XRCT) is a non-destructive technique with wide applications in geological engineering that can be used to evaluate soil morphology related to changes in permeability. XRCT can provide visualization and qualification of the internal structure of subsurface soil. The XRCT process involves measuring the attenuation of X-ray passing through a soil sample and developing three-dimensional CT images (Mees, et al., 2003), which are then further analyzed to determine soil porosity (n).

Diffusion is the dominant mechanism of solute transport in fine-grained soils (Crooks and Quigley, 1984; Rowe et al., 1988). Therefore, a basic understanding of mass transfer theories is necessary for constructing a laboratory experiment and for understanding the analytical solutions used to estimate the diffusion coefficient.

Solutes are transported through the soil by two primary mechanisms: advection and hydrodynamic dispersion (Freeze and Cherry, 1979). Advection describes the transport of the solute due to fluid flow at a rate equal to the seepage (pore-water) velocity. Hydrodynamic dispersion is the combination of two mechanisms, mechanical dispersion and diffusion. Mechanical dispersion is the transport process produced by fluid mixing and diffusion is the movement of molecules due to a concentration gradient.

Assuming saturated conditions in a subsurface porous media and one-dimensional transport, the mass flux of a non-reactive solute in soil can be estimated by (Rowe et al., 1988; Shackelford, 1991):

$$J = n \left(v_s c - D_h \cdot \frac{\partial c}{\partial x} \right) \quad (5.10)$$

where J is the mass flux ($M L^{-2} T^{-1}$; where M is mass, L is length, and T is time); n is the soil porosity (dimensionless); v_s is the seepage velocity of the fluid ($L T^{-1}$); c is the concentration of the solute in pore water ($M L^{-3}$); D_h is the hydrodynamic dispersion coefficient ($L^2 T^{-1}$); and x is the linear distance through which the solute has traveled in the porous media (L). Advection is described mathematically by the first term on the right hand side of the equation, $v_s c$, and the second term, $D_h \cdot \partial c / \partial x$, represents the effects of hydrodynamic dispersion along a decreasing concentration gradient. The hydrodynamic dispersion coefficient is the sum of the mechanical dispersion coefficient ($L^2 T^{-1}$), D_m , and the effective diffusion coefficient ($L^2 T^{-1}$), D^* , which is calculated by:

$$D_h = D_m + D^* \quad (5.11)$$

The effective diffusion coefficient combines the diffusion of a solute in free solution and a factor to account for the tortuous path through the soil matrix given by (Shackelford, 1991):

$$D^* = D_0 \tau \quad (12)$$

where D_0 is the free-solution diffusion coefficient ($L^2 T^{-1}$) and τ is the tortuosity factor (dimensionless). The effective diffusion coefficient is commonly used because it includes the influence of tortuosity, a parameter that is difficult to determine (Shackelford, 1991). However,

Myrand et al. (1992) suggested that porosity, n , is a more accurate parameter for estimating the increased travel distance caused by the pore structure for undisturbed clay materials. In this case, D^* may be represented by equation (5.12) with the substitution of n for τ . Mechanical dispersion is a function of the dispersivity of the soil, $\alpha(L)$, and the seepage velocity (Rowe et al., 1988):

$$D_m = \alpha v_s \quad (5.13)$$

The effects of advection and mechanical dispersion become negligible in fine-grained soils as the seepage velocity approaches zero due to restricted flow caused by minimal void space (Rowe et al., 1988). In this case, the first term of equation (5.10) is neglected and the effective diffusion coefficient is substituted, which results in Fick's first law for diffusion, given by:

$$J_D = -D^* n \cdot \frac{\partial c}{\partial x} \quad (5.14)$$

where J_D is the diffusive flux ($M L^{-2} T^{-1}$).

For a reactive solute in an incompressible fluid moving one-dimensionally at steady state through homogenous, isotropic, and non-deformable soil, the equation for advection-dispersion can be written as (Freeze and Cherry, 1979):

$$\frac{\partial c}{\partial t} = \left(\frac{D_h}{R_d} \right) \cdot \frac{\partial^2 c}{\partial x^2} - \left(\frac{v_s}{R_d} \right) \cdot \frac{\partial c}{\partial x} \quad (5.15)$$

where R_d is the retardation factor (dimensionless). The retardation factor is the ratio of the transport rate of a non-reactive (non-adsorbed) solute relative to a reactive (adsorbing) solute. The retardation factor has been given by (Myrand et al. 1992; Freeze and Cherry, 1979; Shackelford et al., 1989):

$$R_d = 1 + (\rho_d / n) K_d \quad (5.16)$$

and

$$K_d = \frac{dq}{dc} \quad (5.17)$$

where ρ_d is the dry (bulk) density ($M L^{-3}$), K_d is the partition coefficient ($L^3 M^{-1}$), and q is the sorbed concentration of the chemical (mass solute sorbed per mass of soil). The partition coefficient, K_d , can be determined by taking the slope of a q versus c plot, known as a sorption isotherm. In low-permeability soils the seepage velocity becomes negligible and the advection-dispersion equation (eq. 5.10) is reduced to Fick's second law for diffusion of solutes in soil:

$$\frac{\partial c}{\partial t} = \left(\frac{D^*}{R_d} \right) \cdot \frac{\partial^2 c}{\partial x^2} \quad (5.18)$$

The diffusion of a remedial agent through low-permeability strata is characterized by the additional complexity of chemical degradation and loss due to side reactions with organic acids. Hong et al. (2009) investigated the diffusion of Cl^- through a 75% sand and 25% attapulgite clay mixture and calculated diffusion coefficients of $5.86 \times 10^{-6} \text{ cm}^2/\text{s}$ and $7.32 \times 10^{-6} \text{ cm}^2/\text{s}$ for duplicate columns. Diffusion of the chloride ion, a non-reactive species, is essentially the maximum rate of diffusion, which is increased by the addition of sand. Therefore, it is expected that the diffusion of persulfate in clay is expected to be significantly slower.

In recent years, various methods of *in situ* chemical oxidation (ISCO) have been used at Department of Defense (DoD) sites; however, results have been mixed and there is a need for basic research that can be applied to the full-scale use and optimization of ISCO. The distribution and effective transport of remedial amendments is an important element of ISCO effectiveness. The continued growth of ISCO requires an improved understanding of the transport and reactivity of oxidants as well as the development of new ISCO oxidants that can provide superior transport, distribution, and contact.

6. MATERIALS AND METHODS

6.1. Factors Controlling the Decomposition of Persulfate in the Subsurface

6.1.1. Persulfate Activation by Major Subsurface Minerals

Chemicals

Sodium persulfate, sodium citrate, and hexachloroethane (HCA) were purchased from Sigma Aldrich (St. Louis, MO). Sodium hydroxide, sodium bicarbonate, potato starch, and nitrobenzene were obtained from J.T. Baker (Phillipsburg, NJ). Sodium thiosulfate, potassium iodide, and *n*-hexane were purchased from Fisher Scientific (Fair Lawn, NJ). Hydrogen peroxide was provided by Great Western Chemical (Richmond, CA). Sodium dithionate was purchased from EMD Chemicals (Darmstadt, Germany). Hydroxylamine hydrochloride was purchased from VWR (West Chester, PA). Double-deionized water was purified to $> 18 \text{ M}\Omega\cdot\text{cm}$ using a Barnstead NANOpure II Ultrapure system.

Minerals

Six minerals were investigated for their potential to activate persulfate: goethite $[\text{FeOOH}]$, hematite $[\text{Fe}_2\text{O}_3]$, ferrihydrite $[\text{Fe}_5\text{HO}_8\cdot 4\text{H}_2\text{O}]$, birnessite $[\delta\text{-MnO}_2]$, kaolinite $[\text{Al}_2\text{Si}_2\text{O}_5(\text{OH})_4]$, and montmorillonite $[(\text{Na},\text{Ca})(\text{Al},\text{Mg})_6(\text{Si}_4\text{O}_{10})_3(\text{OH})_6\cdot n\text{H}_2\text{O}]$. Goethite and hematite were purchased from Strem Chemicals (Newburyport, MA) and J.T. Baker (Phillipsburg, NJ), respectively. Ferrihydrite was purchased from Mach I (King of Prussia, PA). Birnessite was prepared by the dropwise addition of concentrated hydrochloric acid (2 M) to a boiling solution of 1 M potassium permanganate with vigorous stirring (Mckenzie, 1971). Montmorillonite and kaolinite were provided by the Clay Minerals Society (West Lafayette, IN). Examination of the X-ray diffraction pattern confirmed the minerals were the desired iron and manganese oxides. Mineral surface areas were determined by Brunauer, Emmett, and Teller (BET) analysis under liquid nitrogen on a Coulter SA 3100 (Carter et al. 1986). Particle size distribution of the minerals was determined by the pipette method (Gee and Bauder, 1986) and is listed in Table 6.1.1.1.

Table 6.1.1.1. Particle size distribution (PSD) of minerals

PSD (mm)	Goethite	Hematite	Ferrihydrite	Birnessite	Montmorillonite	Kaolinite
2.00 - 0.05	0.12%	2.40%	0%	2.40%	8.10%	8.10%
0.05 - 0.002	8.24%	89.10%	0%	5.60%	40.10%	56.10%
<0.002	91.64%	8.50%	100%	92.00%	51.80%	35.80%

Soils

A surface soil and two fractions of the soil were used to investigate mineral activation of persulfate. A natural surface soil ("total soil") was collected from the Palouse region of Washington State. The total soil was air dried and ground to pass through a 300 μm sieve. A mineral-only soil fraction ("mineral fraction") was isolated by removing soil organic matter (SOM) from the total soil by heating in the presence of 30% hydrogen peroxide (Robinson, 1927). An iron-only soil fraction ("iron fraction") was produced by removing manganese oxides from the mineral fraction by extracting with hydroxylamine hydrochloride ($\text{NH}_2\text{OH}\cdot\text{HCl}$) (Chao, 1972), leaving the iron oxides. The soil fractions were washed with deionized water (25 ml/g) to remove the residual extractant after each treatment, dried at 55 $^{\circ}\text{C}$, and ground to pass through a 300 μm sieve.

The total soil and soil fractions were analyzed for particle size analysis and amorphous and total iron and manganese oxides. Particle size distribution was measured by the pipette method (Gee and Bauder, 1986). The acid ammonium oxalate in darkness (AOD) method (McKeague and Day, 1966) was used to analyze for amorphous iron and manganese oxides. Total iron and manganese oxides were extracted using the citrate-bicarbonate-dithionite (CBD) method (Jackson et al., 1986), and then analyzed by inductively coupled plasma-atomic emission spectrometry (ICPAES). Characteristics of the soil and soil fractions are listed in Table 6.1.1.2.

Table 6.1.1.2. Soil characteristics of the total soil and two soil fractions

	Total soil	Mineral fraction (after SOM removal)	Iron fraction (After manganese oxides removal)
Organic carbon (%)	1.617	0.083	0.050
Amorphous oxides			
Fe (mg/kg)	4780	4190	3660
Mn (mg/kg)	610	420	170
Crystalline oxides			
Fe (mg/kg)	3900	2700	2700
Mn (mg/kg)	260	210	90
Cation exchange capacity (cmol(+)/kg)	19	12	9
SURFACE AREA (M^2/G)	23.5	24	19
PARTICLE SIZE DISTRIBUTION			
Sand (%)	7.77	9.23	7.83
Clay (%)	69.15	70.67	76.7
Silt (%)	23.08	20.10	15.46
Texture	Silt loam	Silt loam	Silt loam

Probe Compounds

Nitrobenzene (NB) was used as an oxidant probe because of its high reactivity with oxidants such as hydroxyl radical ($k_{\text{OH}\cdot} = 3.9 \times 10^9 \text{ M}^{-1}\text{s}^{-1}$) (Buxton et al., 1988). A suitable probe compound specific to sulfate radical was not identified because all potential sulfate radical probes directly activated persulfate at basic pH. HCA was used as a reductant probe because it is readily degraded by the reductant superoxide in the presence of cosolvents (Smith et al., 2004) and is reduced by alkyl radicals, but is not oxidized by hydroxyl radical ($k_{\text{OH}\cdot} \leq 10^6 \text{ M}^{-1}\text{s}^{-1}$).

Experimental Procedure

All reactions were conducted in 20 ml borosilicate volatile organic analysis (VOA) vials fitted with polytetrafluoroethylene (PTFE) lined caps. Reactions containing minerals were conducted with 5 ml of reactant solution and 2 g of goethite or hematite, 1 g of birnessite, or 0.5 g of ferrihydrite. Smaller masses of the lower-density birnessite and ferrihydrite were used so that the minerals could be completely covered by the reactant solution. Reactions containing soil and soil fractions were conducted using 5 g of the soil and 10 ml of reactant solution. The persulfate reactant solution consisted of 0.5 M persulfate for the low pH systems and 0.5 M persulfate plus 1 M NaOH for the high pH systems. In the low pH systems, the initial pH was 6 and decreased to pH 3 as the reactions proceeded. In the high pH systems, the initial pH was 13 and decreased to pH 12 as the reactions proceeded. For experiments using probe compounds, the solution also contained 1 mM nitrobenzene or 2 μM HCA; triplicate sets of vials were extracted with 5 ml of hexane at selected time points over the course of the reactions. Control experiments were conducted in parallel with deionized water in place of persulfate and without minerals or soils. In addition, positive control experiments were conducted in parallel with persulfate but without minerals or soils, to distinguish between acid/base activation and mineral activation of persulfate. All reactions were conducted in triplicate at $20 \pm 2^\circ\text{C}$.

Extraction and Analysis

Hexane extracts containing probe compounds were analyzed using a Hewlett Packard 5890 series II gas chromatograph (GC) with injection by a Hewlett-Packard 7673A autosampler. For nitrobenzene analysis, the GC was equipped with a flame ionization detector (FID) fitted with a 15 m \times 0.53 mm SPB-5 capillary column. The injector and detector port temperatures were 200 $^\circ\text{C}$ and 250 $^\circ\text{C}$, respectively, the initial oven temperature was 60 $^\circ\text{C}$, the program rate was 30 $^\circ\text{C}/\text{min}$, and the final temperature was 180 $^\circ\text{C}$. For HCA analysis, the GC was equipped with an electron capture detector (ECD) fitted with a 30 m \times 0.53 mm EQUITY-5 capillary column. The injector temperature was 220 $^\circ\text{C}$, the detector temperature was 270 $^\circ\text{C}$, the oven temperature was 100 $^\circ\text{C}$, the program rate was 30 $^\circ\text{C}/\text{min}$, and the final temperature was 240 $^\circ\text{C}$.

Persulfate concentrations were measured in triplicate at different time points by iodometric titration using 0.01 N sodium thiosulfate (Kolthoff and Stenger, 1947). A Fisher Accumet AB15 pH meter was used to measure pH. The Statistical Analysis System package SAS 9.1.3 was used to calculate the differences between the experimental data sets as well as 95% confidence intervals for rate constants.

6.1.2. Persulfate Activation by Subsurface Trace Minerals

Materials

Minerals collected from sites throughout North America were purchased from DJ Minerals (Butte, MT). Thirteen minerals were used: anatase [TiO₂], bauxite [Al(OH)₃], calcite [CaCO₃], cobaltite [CoAsS], cuprite [Cu₂O], hematite [Fe₂O₃], ilmenite [FeTiO₃], magnesite [MgCO₃], malachite [Cu₂(CO₃)(OH)₂], pyrite [FeS₂], pyrolusite [MnO₂], siderite [FeCO₃], willemite [Zn₂SiO₄]. The minerals, which were received as cubes approximately 1 cm x 1 cm x 1 cm, were crushed to a fine powder using a 150 mL capacity Spex shatter box with hardened steel as a grinder. Surface areas were determined by Brunauer, Emmett, Teller (BET) analysis under liquid nitrogen on a Coulter SA 3100 (Carter et al. 1986). The surface areas for the minerals were: anatase [11.7 ± 0.2 m²/g], bauxite [28.8 ± 0.2 m²/g], calcite [38.0 ± 0.2 m²/g], cobaltite [2.21 ± 0.03 m²/g], cuprite [49.5 ± 0.08 m²/g], hematite [28.2 ± 0.2 m²/g], ilmenite [1.7 ± 0.04 m²/g], magnesite [38.0 ± 0.3 m²/g], malachite [3.65 ± 0.03 m²/g], pyrite [2.12 ± 0.01 m²/g], pyrolusite [1.39 ± 0.04 m²/g], siderite [6.8 ± 0.4 m²/g], willemite [1.8 ± 0.02 m²/g]. Sodium persulfate (≥98%) and carbon tetrachloride (99.9%) were purchased from Sigma-Aldrich. Nitrobenzene (99%) and *tert*-butyl alcohol (99.8%) were obtained from J. T. Baker, and anisole (99%) was obtained from Sigma. 1, 3, 5- Trinitrobenzene (TNB) (99%) was purchased from Chem Service and HPLC grade hexanes from Fisher. Double-deionized water (>18 MΩ•cm) was purified using a Barnstead Nanopure II Ultrapure system.

Probe compounds

The probe compounds were selected based on their reactivities with each of the reactive oxygen species. Anisole [$k_{OH\cdot} = 5.4 \times 10^9 \text{ M}^{-1}\text{s}^{-1}$; $k_{SO_4\cdot-} = 4.9 \times 10^9 \text{ M}^{-1}\text{s}^{-1}$] was used because of its high reactivity with both hydroxyl radicals and sulfate radicals (O'Neill et al., 1975; Buxton et al., 1988). Nitrobenzene [$k_{OH\cdot} = 3.9 \times 10^9 \text{ M}^{-1}\text{s}^{-1}$; $k_{SO_4\cdot-} = \leq 10^6$] was used because it is highly reactive with hydroxyl radicals, but is unreactive with sulfate radicals, allowing a comparison between the two radicals (Neta et al., 1977, Buxton et al., 1988). Carbon tetrachloride [$k_{OH\cdot} = < 2 \times 10^6 \text{ M}^{-1}\text{s}^{-1}$] was used to confirm the presence of reductants in the system (Haag and Yao, 1992). 1,3,5- Trinitrobenzene, a highly oxidized nitroaromatic compound resistant to oxidation, was used as a probe for hydroperoxide.

Hydroxyl radical scavenging

tert-Butyl alcohol [$k_{OH\cdot} = 6.0 \times 10^8 \text{ M}^{-1}\text{s}^{-1}$; $k_{SO_4\cdot-} = 8.2 \times 10^7 \text{ M}^{-1}\text{s}^{-1}$] was used to scavenge hydroxyl radicals during reactions (Buxton et al, 1988; Clifton and Huie, 1989). The scavenger:probe molar ratio was 1000:1.

Experimental procedures

All reactions were conducted in 20 ml borosilicate volatile organics analysis (VOA) vials with 2 g of mineral and 5 ml of solution at 25° C. A sodium persulfate concentration of 0.5 M, which is commonly employed in field applications, was used and the pH of the solutions was allowed to drift downward as it would in a natural groundwater system. Probe and persulfate concentrations were analyzed at selected time points. Probe concentrations were measured by extracting each VOA vial with 3 ml of hexane and then analyzing the extract by gas chromatography. Persulfate concentrations were quantified using iodometric titration with 0.01

N sodium thiosulfate (Kolthoff and Belcher, 1957). Solution pH was measured using with a Fisher Accumet 900 pH meter.

Analysis

Extracts containing anisole, nitrobenzene and 1, 3, 5-trinitrobenzene were analyzed on a Hewlett-Packard 5890 gas chromatograph fitted with a 15 m x 0.53 mm (i.d.) SPB-5 capillary column and a flame ionization detector (FID). The injector port and detector port temperatures for anisole and nitrobenzene were 200°C and 250°C, respectively. The initial oven temperature was 70°C. The program rate was 20°C min⁻¹, and the final temperature was 210°C. Gas chromatographic conditions for the analysis of 1,3,5-trinitrobenzene included an initial oven temperature of 160°C and a final temperature of 190°C. The program rate was 10°C min⁻¹, the injector temperature was 200°C, and the detector temperature was 250°C. Extracts containing carbon tetrachloride were analyzed on a Hewlett-Packard 5890A gas chromatograph fitted with a 15 m x 0.53 mm (i.d.) Equity-5 capillary column and an electron capture detector (ECD). The injector port and detector port temperatures were 100°C and 250°C, respectively. A split flow was used with the initial oven temperature at 50°C; the program rate was 30°C min⁻¹, and the final temperature was 170°C.

6.1.3. Base-Activated Persulfate Treatment of Contaminated Soils with pH Drift from Alkaline to Circumneutral

Materials

Sodium persulfate (>98%) and hexachloroethane (99%) were purchased from Sigma-Aldrich. Mixed hexanes, nitrobenzene (99%), sodium hydroxide, sodium bicarbonate, and sodium carbonate were obtained from J.T. Baker. Sodium thiosulfate (99%) and n-hexane were purchased from Fisher Chemical. Potassium iodide (99%) was purchased from Alfa Aesar. Deionized water was purified to $>18.0 \text{ M}\Omega \cdot \text{cm}$ with a Barnstead Nanopure II deionizing system.

Soils

Two horizons of a surface soil, collected from an open slope near Kamiak Butte, WA, were used in base-activated persulfate reactions. The two horizons (KB1 and KB2) were chosen because of their varying soil organic carbon contents but similar mineralogy (Table 6.1.3.1). The soils were crushed using a soil grinder and sieved through a 1.65 mm sieve. Organic carbon content was determined by the Walkley-Black method (Walkley and Black, 1934). Particle size distribution was analyzed using the pipette method (Gee and Bauder, 1986). The citrate-bicarbonate-dithionite extraction method was used to determine amorphous and crystalline iron and manganese oxyhydroxides content (Jackson et al., 1986). Cation exchange capacity was analyzed by saturation with sodium acetate at pH 8.2 (U.S. Soil Conservation Service, 1972). Physical and chemical properties for the KB1 and KB2 soils are listed in Tables 6.1.3.1 and 6.1.3.2.

Soil organic matter (SOM) was removed from the two soils by addition of 20% hydrogen peroxide (H_2O_2) (Robinson, 1927). Soil slurries received periodic additions of H_2O_2 and were heated to 60°C until a visible color change of dark to light in the soil occurred indicating that the SOM was removed. Soils were dried at 55°C , pulverized, and sieved with a 1.65 mm sieve.

Probe Compounds

The probe compounds were selected based on their relative reactivities with each of the reactive oxygen species. Nitrobenzene (NB) was used to detect hydroxyl radicals ($k_{\text{OH}\cdot} = 3.9 \times 10^9 \text{ M}^{-1}\text{s}^{-1}$) but not sulfate radicals ($k_{\text{SO}_4\cdot-} \leq 10^6 \text{ M}^{-1}\text{s}^{-1}$) (Buxton et al., 1988; Neta et al., 1977). Hexachloroethane (HCA) was selected as a probe for superoxide and other reductants ($k_{\text{O}_2\cdot-} = 400 \text{ M}^{-1}\text{s}^{-1}$) because it has negligible reactivity with oxidants; e.g., hydroxyl radicals are nonreactive with perchlorinated aliphatic compounds ($k_{\text{OH}\cdot} \leq 1 \times 10^6 \text{ M}^{-1}\text{s}^{-1}$) (Haag and Yao, 1992; Afanas'ev, 1989).

Experimental Procedures

VOA vials were prepared with 10 g of the KB1, KB2, KB1-No SOM, or KB2-No SOM soils. Each vial received 18 mL of the sodium hydroxide:sodium persulfate solution; the vials were mixed, and then incubated in a water bath at 25°C ($\pm 2^\circ \text{C}$).

Once the pH in the reactors declined to 12, a series of vials received 2 mL of one of the concentrated probe compounds (10 mM NB or 0.005 mM HCA) which yielded final solution concentrations of 1 mM NB or 0.0005 mM HCA, respectively. Probe degradation was then monitored by periodically extracting the entire vial contents with 5 mL of hexane and analyzing

the extract by gas chromatography. All vials were mixed before samples were extracted to ensure homogeneity and minimize volatilization.

The pH in the remaining reactors was monitored until it decreased to 10 and then to 8; these vials then received 2 mL each of the concentrated probe stock solution. Due to lack of drift, the pH in the KB2-No SOM reactors had to be artificially lowered to pH 10 and pH 8 through the addition of dilute sulfuric acid. Control systems were established in parallel using deionized water in place of base-activated persulfate for each soil slurry system.

Analysis

Probe compound concentrations were quantified using Hewlett-Packard 5890A gas chromatographs with an electron capture detector (for HCA) and a flame ionization detector (for NB), each fit with 10 m × 0.53 mm DB-1 capillary columns. Program conditions for HCA analysis included injector temperature of 220°C, detector temperature of 270°C, initial oven temperature of 100°C, program rate of 30°C min⁻¹, and final temperature of 240°C. Program conditions for NB analysis included injector temperature of 200°C, detector temperature of 250°C, initial oven temperature of 60°C, program rate of 30°C min⁻¹, and final temperature of 180°C. Persulfate concentrations were measured by iodometric titration using 0.01 N sodium thiosulfate (Kolthoff and Stenger, 1947). The pH was quantified using a Fisher Accumet Basic AB15 pH meter.

Table 6.1.3.1. Physical properties of soils KB1 and KB2.

Soil	Textural Classification *				Cation Exchange Capacity (Cmol(+)/kg)**
	% Sand	% Clay	% Silt	Texture	
KB1	31.5	10	58.5	Silt Loam	34
KB2	39.5	11.1	49.8	Loam	19

* Method analyzed: Hydrometer

**Method analyzed: EPA 9081

Table 6.1.3.2. Chemical properties of soils KB1 and KB2.

Soil	Amorphous Mn (µg/g)	Total Mn (µg/g)	Amorphous Fe (µg/g)	Crystalline Fe (µg/g)	% Organic Carbon	% Organic Carbon After H ₂ O ₂ Treatment
KB1	194	380	4656	2789	1.01	0.12
KB2	296	510	2196	1697	0.24	0.06

6.2. Persulfate Reactivity Under Different Conditions of Activation

6.2.1. Oxidative and Reductive Pathways in Iron-Ethylenediaminetetraacetic acid (EDTA) Activated Persulfate Systems

Materials

Iron (II) perchlorate (98%), hexachloroethane (99%), TCE (99.5%), ethylenediaminetetraacetic acid iron (III) sodium salt hydrate (iron (III)-EDTA), anisole (99%), and sodium persulfate (> 98%) were purchased from Sigma-Aldrich. Ethylenediaminetetraacetic acid disodium salt (Na₂-EDTA), sodium hydroxide (NaOH), hexane, ethyl acetate, nitrobenzene, *tert*-butanol, and isopropanol were obtained from J.T. Baker. 5,5-Dimethyl-1-pyrroline-N-oxide (DMPO) ($\geq 99\%$) was obtained from Axxora LLC (San Diego, CA). The impurities in DMPO were removed with activated charcoal followed by filtration until no extraneous electron spin resonance spectroscopy (ESR) signals were observed (Das and Misra, 2004). Double-deionized water (> 18 M Ω •cm) was produced using a Barnstead Nanopure II ultrapure system.

Activators

Persulfate activation was investigated using Na₂-EDTA, iron (II)-EDTA, and iron (III)-EDTA. Stock solutions of Na₂-EDTA and iron (III)-EDTA were prepared by dissolving these reagents in deionized water, and adjusting the pH to 7 using dilute NaOH. The iron (II)-EDTA solution was prepared using the procedure described by Sun and Pignatello (1992). Briefly, Na₂-EDTA was dissolved in oxygen-free deionized water, and an equivalent mass of iron (II) perchlorate was added to the solution; the pH of the solution was then adjusted to 7 by adding dilute NaOH.

Probe Compounds

The probe compounds were selected based on their reactivities with each of the reactive oxygen species potentially generated in the iron-EDTA activated persulfate systems. All compounds surveyed that react with sulfate radical also react with hydroxyl radical; therefore, anisole was used to detect both hydroxyl radical and sulfate radical ($k_{\text{OH}\cdot} = 5.4 \times 10^9 \text{ M}^{-1}\text{s}^{-1}$; $k_{\text{SO}_4\cdot-} = 4.9 \times 10^9 \text{ M}^{-1}\text{s}^{-1}$) (Buxton et al., 1988; Padmaja et. al., 1993). Nitrobenzene was used to detect hydroxyl radical but not sulfate radical ($k_{\text{OH}\cdot} = 3.9 \times 10^9 \text{ M}^{-1}\text{s}^{-1}$; $k_{\text{SO}_4\cdot-} \leq 10^6$) (Buxton et al., 1988; Neta et al., 1977). Hexachloroethane (HCA) [$k_{\text{OH}\cdot} = < 1 \times 10^6 \text{ M}^{-1} \text{ s}^{-1}$ (Haag and Yao, 1992); $k_{\text{O}_2\cdot-} = 400 \text{ M}^{-1} \text{ s}^{-1}$ (Afanas'ev, 1989)] was selected as a probe for reductants because it has negligible reactivity with oxidants, but is reactive with reductants (Watts, 1998). TCE was used as a model groundwater contaminant to confirm the reactivity of activated persulfate.

Hydroxyl Radical and Sulfate Radical Scavengers

tert-Butanol was used to scavenge hydroxyl radical but not sulfate radical ($k_{\text{OH}\cdot} = 5.2 \times 10^8 \text{ M}^{-1}\text{s}^{-1}$; $k_{\text{SO}_4\cdot-} = 8.4 \times 10^5 \text{ M}^{-1}\text{s}^{-1}$), and isopropanol was used to scavenge both hydroxyl radical and sulfate radical ($k_{\text{OH}\cdot} = 1.9 \times 10^9 \text{ M}^{-1}\text{s}^{-1}$; $k_{\text{SO}_4\cdot-} = 8.2 \times 10^7 \text{ M}^{-1}\text{s}^{-1}$) (Buxton et al., 1988; Clifton and Huie, 1989). The scavenger concentration was 1 M.

Reaction Procedures

Reactions in which persulfate was monitored were conducted in triplicate in sealed 100 mL borosilicate glass reactors equipped with polytetrafluoroethylene (PTFE)-lined caps. The reactors contained a 0.5 M sodium persulfate solution and concentrations of Na₂-EDTA, iron (II)-EDTA, or iron (III)-EDTA ranging from 2.5 mM to 15 mM in an 80 mL total volume. The system pH was kept constant at pH 5 by the addition of 1 M NaOH. Aliquots were collected daily over a 5 day period and analyzed for persulfate.

Reactions containing the reaction specific probe compounds and the model contaminant TCE were conducted in the dark at 20° C ± 2° C. The initial concentration of anisole and nitrobenzene was 1 mM and the initial concentration of HCA and TCE was 2 µM. The initial persulfate concentration was 0.5 M and the concentration of Na₂-EDTA, iron (II)-EDTA, and iron (III)-EDTA was 10 mM. The reactions were conducted in 20 mL borosilicate glass volatile organic analysis (VOA) vials containing 10 mL of persulfate solution. One set of triplicate vials was established for each time point. At selected time points, the entire vial contents were extracted with 5 mL of hexane and the hexane extract was analyzed by gas chromatography. Reactions containing anisole and TCE were repeated with the addition of *tert*-butanol or isopropanol to investigate the effect of scavenging reactive oxygen species. All reactions were conducted in triplicate, and control reactions were established in parallel without the addition of persulfate.

Detection of Radicals Using Electron Spin Resonance (ESR) Spectroscopy

Radicals were detected by ESR spectroscopy using DMPO as a spin trap agent. The initial reaction mixture for ESR spin trapping consisted of 0.5 M persulfate and 10 mM iron (II)-EDTA or iron (III)-EDTA. Control reactors contained deionized water in place of persulfate. After the reactions had proceeded for 22 hr, 0.25 mL of the reaction mixture was added to a vial containing 2.25 mL of DMPO; the final concentrations during analysis were 0.05 M persulfate, 1 mM iron (II)-EDTA or iron (III)-EDTA, 88 mM DMPO. After mixing for 1 min the reactants were injected into an aqueous sample cell (Bruker, AquaX high sensitivity). All spectra were obtained using a Bruker 6/1 spectrometer with a resonance frequency of 9.86 GHz, microwave power of 2.0 mW, modulation frequency of 100 kHz, modulation amplitude of 1.0 G, sweep width of 100 G, time constant of 164 ms, sweep time of 168 s, and receiver gain of 2.0×10^5 .

Analysis

Extracts containing anisole and nitrobenzene were analyzed using a Hewlett-Packard 5890 gas chromatograph fitted with a 15 m x 0.53 mm (i.d.) SPB-5 capillary column and a flame ionization detector (FID). The injector port and detector port temperatures for nitrobenzene were 200°C and 250°C, respectively. The initial oven temperature was 60°C, the program rate was 30°C min⁻¹, and the final temperature was 220°C. The injector port and detector port temperatures for anisole were 150°C and 180°C, respectively. The initial oven temperature was 40°C, the program rate was 30°C min⁻¹, and the final temperature was 200°C.

Extracts containing HCA and TCE were analyzed on a Hewlett-Packard 5890A gas chromatograph fitted with a 15 m x 0.53 mm (i.d.) Equity-5 capillary column and an electron capture detector (ECD). For HCA and TCE analysis, the injector port and detector port

temperatures were 220°C and 270°C, respectively. The initial oven temperature was 100°C, the program rate was 30°C min⁻¹, and the final temperature was 240°C.

Persulfate concentration was quantified by iodometric titration with 0.01 N sodium thiosulfate (Kolthoff and Stenger, 1947). Solution pH was measured using a Fisher Accumet AB15 pH meter.

6.2.2. Effect of Basicity on Persulfate Reactivity

Materials

Sodium persulfate ($\geq 98\%$), hexachloroethane (99%), sodium phosphate monobasic monohydrate (98%), nitrobenzene (99.9%), and anisole (99%) were purchased from Sigma-Aldrich. Sodium hydroxide (99%), *tert*-butyl alcohol (99.8%), sulfuric acid (97%), hexanes (HPLC grade), isopropyl alcohol ($> 99\%$), and nitrobenzene (99%) were obtained from J. T. Baker. Sodium thiosulfate ($>99\%$) was purchased from Fisher Scientific. Double-deionized water ($>18\text{ M}\Omega\cdot\text{cm}$) was purified using a Barnstead Nanopure II Ultrapure system.

Probe compounds

Three probe compounds were selected based on their reactivities with each of the reactive oxygen species. All compounds surveyed that react with sulfate radical also react with hydroxyl radical; therefore, anisole was used to detect both hydroxyl radical and sulfate radical ($k_{\text{OH}\cdot} = 5.4 \times 10^9\text{ M}^{-1}\text{s}^{-1}$; $k_{\text{SO}_4\cdot-} = 4.9 \times 10^9\text{ M}^{-1}\text{s}^{-1}$) (O'Neill et al., 1975; Buxton et al., 1988). Nitrobenzene was used to detect hydroxyl radical but not sulfate radical ($k_{\text{OH}\cdot} = 3.9 \times 10^9\text{ M}^{-1}\text{s}^{-1}$; $k_{\text{SO}_4\cdot-} \leq 10^6$) (Neta et al., 1977; Buxton et al., 1988). Hexachloroethane was used as a probe compound for reductants ($k_{\text{e}\cdot} = \sim 10^{10}\text{ M}^{-1}\text{s}^{-1}$; $k_{\text{OH}\cdot} < 2 \times 10^6\text{ M}^{-1}\text{s}^{-1}$) (Afanasyev et al., 1979; Haag and Yao, 1992; Furman et al., 2009), such as superoxide and alkyl radicals. Although superoxide is unreactive with compounds such as hexachloroethane in deionized water, its reactivity is significantly increased in systems containing cosolvents and other species that affect the net polarity of the system (Smith et al., 2004; Furman et al., 2009). The initial concentration of the probe compounds was 1 mM for anisole and nitrobenzene and 2 μM for hexachloroethane.

Hydroxyl radical and sulfate radical scavengers

tert-Butyl alcohol was used to scavenge hydroxyl radical but not sulfate radical ($k_{\text{OH}\cdot} = 5.2 \times 10^8\text{ M}^{-1}\text{s}^{-1}$; $k_{\text{SO}_4\cdot-} = 8.4 \times 10^5\text{ M}^{-1}\text{s}^{-1}$), and isopropyl alcohol was used to scavenge both hydroxyl radical and sulfate radical ($k_{\text{OH}\cdot} = 1.9 \times 10^9\text{ M}^{-1}\text{s}^{-1}$; $k_{\text{SO}_4\cdot-} = 8.2 \times 10^7\text{ M}^{-1}\text{s}^{-1}$) (Buxton et al., 1988; Clifton and Huie, 1989). The scavenger:probe molar ratio was 1000:1.

Effect of pH on the generation of reactive oxygen species

Relative rates of sulfate and hydroxyl radical generation and reductant generation in persulfate systems were investigated at pH 2, pH 7, and pH 12. All reactions were conducted at $20 \pm 2\text{ }^\circ\text{C}$ in the dark. Systems containing 0.5 M persulfate, 10 mM sodium phosphate buffer, and one of the probe compounds were adjusted to pH 2, pH 7, or pH 12 using 5 M H_2SO_4 or 5 M NaOH. The base:persulfate molar ratio of the pH 12 system was 0.04:1. Triplicate 20 mL volatile organic analysis (VOA) vials containing 15 mL of reaction solution were prepared for each time point, and were capped to minimize volatilization of the probe compounds. Control reactors were established in parallel using deionized water in place of persulfate. At selected time points over the course of the reaction, a set of vials was shake-extracted with hexane and the extracts were analyzed for residual probe compound concentrations by gas chromatography.

Effect of persulfate concentration on the generation of reactive oxygen species

Solutions of 0.025 M, 0.05 M, 0.25 M, and 0.5 M persulfate were prepared containing one of the probe compounds; each solution was adjusted to pH 12 using 5 M NaOH. All reactions were conducted at $20 \pm 2\text{ }^\circ\text{C}$ in the dark. Triplicate reactors were established for each

time point and were capped to minimize probe compound volatilization. Control reactors were established in parallel using deionized water in place of persulfate. A triplicate set of reactors was then shake-extracted with hexane at each time point, and the extracts were analyzed for residual probe compound concentrations by gas chromatography.

Effect of base:persulfate molar ratios on the generation of reactive oxygen species

Separate solutions containing 0.5 M persulfate with molar ratios of 0.2:1, 0.5:1, 1:1, 2:1, 3:1, 4:1, 5:1, and 6:1 base:persulfate were dispensed in 15 mL aliquots into 20 mL reactors. All reactions were conducted at 20 ± 2 °C in the dark. A set of triplicate vials was analyzed for the probe compounds at each time point after shake extraction with hexane. Control reactors were established in parallel using deionized water in place of persulfate. The hexane extracts were analyzed for nitrobenzene and hexachloroethane by gas chromatography.

Analysis

Solution pH was measured using a Fisher Accumet 900 pH meter. Extracts containing anisole or nitrobenzene were analyzed using a Hewlett-Packard 5890 gas chromatograph fitted with a 15 m x 0.53 mm (i.d.) SPB-5 capillary column and a flame ionization detector (FID). The injector port and detector port temperatures were 200 °C and 250 °C, respectively. The initial oven temperature was 70 °C, the program rate was 20 °C/min, and the final temperature was 210 °C. Extracts containing hexachloroethane were analyzed using a Hewlett-Packard 5890A gas chromatograph fitted with a 15 m x 0.53 mm (i.d.) Equity-5 capillary column and an electron capture detector (ECD). The injector port and detector port temperatures were 200 °C and 250 °C, respectively. A split flow was used with the initial oven temperature at 50 °C. The program rate was 30 °C min⁻¹, and the final temperature was 170 °C.

Results from triplicate data sets were averaged, and the standard error of the mean was displayed on the figures as error bars. Statistical analyses were performed using the SAS software package version 9.1 (SAS 2003).

6.2.3. Mechanism of Base Activation of Persulfate

Materials

Sodium persulfate (98%), hexachloroethane (HCA) (99%), diethylenetriamine pentaacetic acid (DTPA) (97%), and deuterated water (D_2O) were purchased from Sigma-Aldrich (St. Louis, MO). 5,5-Dimethyl-1-pyrroline-N-oxide (DMPO) ($\geq 99\%$) was obtained from Axxora LLC (San Diego, CA). The impurities in DMPO were removed with activated charcoal followed by filtration until no extraneous electron spin resonance spectroscopy (ESR) signals were observed (Das and Misra, 2004). Magnesium chloride (99.6%), hydrogen peroxide (50%), sodium hydroxide (98%), sulfuric acid (96.1%), acetic acid ($> 99\%$), sodium bicarbonate ($> 99\%$), ammonium sulfate ($> 99\%$), and starch were obtained from J.T. Baker (Phillipsburg, NJ). Stock solutions of peroxomonosulfate (SO_5^{2-}) were prepared from oxone ($2KHSO_5 \cdot KHSO_4 \cdot K_2SO_4$), which was obtained from Alfa Aesar (Ward Hill, MA). Potassium iodide (99%) was also purchased from Alfa Aesar (Ward Hill, MA), and titanium sulfate was obtained from GFS Chemicals, Inc. (Columbus, OH). Mixed hexanes and sodium thiosulfate ($> 99\%$) were purchased from Fisher Scientific (Fair Lawn, NJ). Double-deionized water was purified to $> 18 M\Omega \cdot cm$ using a Barnstead E-pure system. Sodium hydroxide solutions were purified to remove transition metals by the addition of magnesium chloride followed by stirring for 8 h and then filtering the solution through $0.45 \mu m$ hydrophilic polypropylene membrane filters (Monig, 1983; Smith et al., 2004).

Persulfate Decomposition Studies

Persulfate decomposition reactions were conducted in 40 mL borosilicate vials containing 20 mL of 0.5 M persulfate activated by 1 M, 1.5 M, 2 M, and 3 M NaOH. Persulfate concentrations were measured by iodometric titration with 0.01 N sodium thiosulfate (Wahba et al., 1959). Persulfate decomposition was also measured in D_2O versus H_2O to examine the kinetic effect of deuterium isotopes on base-catalyzed persulfate hydrolysis; these reactions consisted of 0.5 M persulfate and 3 M NaOH.

Stoichiometry of Hydroperoxide–Persulfate Systems

Persulfate and total hydrogen peroxide species ($H_2O_2 + HO_2^-$) concentrations were monitored simultaneously in reactions containing 0.5 M persulfate, 1.5 M NaOH, and 0.5 M H_2O_2 , which dissociates to hydroperoxide (HO_2^-) in alkaline systems ($pK_a = 11.75$), to examine the stoichiometry of the reaction of hydroperoxide and persulfate. At the 3:1 base:persulfate ratio of the reactions, the initial pH was 12.5; therefore, approximately 85% of the added hydrogen peroxide was in the form of hydroperoxide. To further investigate the reaction of hydroperoxide and persulfate, $H_2O_2 + HO_2^-$ decomposition was monitored in reactions containing different ratios of $H_2O_2 + HO_2^-$ to persulfate. These reactions consisted of 20 mL of 0.5 M persulfate, 1.5 M NaOH, and 0.5 and 1 M $H_2O_2 + HO_2^-$.

Generation of Superoxide in Persulfate–NaOH– $H_2O_2 + HO_2^-$ Systems

HCA was used as a probe to detect superoxide (Furman et al., 2009). Although HCA is unreactive with superoxide in deionized water, its reactivity increases significantly in aqueous systems containing electrolytes such as hydrogen peroxide (Smith et al., 2004). Reactions were conducted with 20 mL of 2 μM HCA, 0.5 M persulfate, 1 M NaOH, and $H_2O_2 + HO_2^-$ concentrations ranging from 0.1 M–0.5 M. At the 2:1 base:persulfate ratio of the reactions, the initial pH was 12.1; therefore, approximately 70% of the added hydrogen peroxide was in the

form of hydroperoxide. Control reactions were performed in parallel with double deionized water in place of $\text{H}_2\text{O}_2 + \text{HO}_2^-$. The reactions were conducted in borosilicate vials capped with PTFE-lined septa in the dark at $20 \pm 2^\circ\text{C}$. A triplicate set of reactors was established for each time point in the experiment; as the reactions preceded, the total reactor contents were extracted with hexane, and the extracts were analyzed for HCA by gas chromatography.

Dismutation of Superoxide

Copper (II) was used to dismutate superoxide ($k = 8 \times 10^9 \text{ M}^{-1}\text{s}^{-1}$) as a means of confirming superoxide generation in base-activated persulfate systems (Piechowski et al., 1993; Zafiriou et al., 1998). The base-activated persulfate decomposition of HCA was repeated using 0.5 M persulfate, 1 M NaOH, 0.5 M $\text{H}_2\text{O}_2 + \text{HO}_2^-$, and 2 μM HCA with the addition of 2 μM CuCl_2 to dismutate superoxide. This low concentration of Cu (II) did not promote persulfate decomposition and activation, as documented in parallel control reactions conducted without the addition of Cu (II).

Detection of Radicals Using ESR Spectroscopy

Radicals generated in base-activated persulfate systems were detected by ESR spectroscopy using DMPO as a spin trap agent. The reaction mixture for ESR spin trapping consisted of 3 mL of 0.05 M persulfate, 0.1 M NaOH, 0.05 M $\text{H}_2\text{O}_2 + \text{HO}_2^-$, and 0.09 M DMPO. The reactants were injected into an aqueous sample cell (Bruker, AquaX high sensitivity) 1 min after the reaction was initiated. All spectra were obtained using a Bruker 6/1 spectrometer with a resonance frequency of 9.86 GHz, microwave power of 2.0 mW, modulation frequency of 100 kHz, modulation amplitude of 1.0 G, sweep width of 100 G, time constant of 164 ms, sweep time of 168 s, and receiver gain of 2.0×10^5 .

Measurement of Oxygen Evolution

A U-tube manometer filled with water was used to measure the differential pressure in reactions containing 0.5 M persulfate and 3 M NaOH. A reactor was attached to one end of the U-tube manometer, and the other end of the U-tube was open to the atmosphere. The ideal gas law was applied to calculate the moles of gas evolved during the reaction. Persulfate concentrations were quantified in parallel by iodometric titration as the reactions proceeded. The presence of oxygen in the manometer tubes was confirmed by conducting reactions in parallel in Exetainer vials equipped with a pierceable rubber septum. The headspaces of the vials were sampled with a gas-tight syringe and introduced into a vacuum line where water and CO_2 were cryogenically removed (Barkan and Luz, 2003). The collected gas samples were analyzed using an isotope-ratio mass spectrometer (Delta Plus XP, ThermoFinnigan, Bremen, Germany); the evolved gas was found to be $> 99\% \text{ O}_2$.

Analysis

Persulfate concentrations in systems with no hydrogen peroxide addition were measured using iodometric titration with 0.01 N sodium thiosulfate (Wahba et al., 1959). In reactions containing both persulfate and hydrogen peroxide, iodometric titration was used to measure the total peroxygen concentrations, and $\text{H}_2\text{O}_2 + \text{HO}_2^-$ concentrations were quantified by complexation with titanium sulfate followed by visible spectrophotometry at 407 nm using a Spectronic 20 Genesys spectrophotometer (Eisenberg, 1943; Cohen and Purcell, 1967); the $\text{H}_2\text{O}_2 + \text{HO}_2^-$

concentration was then subtracted from the total peroxygen concentration to obtain the concentration of persulfate.

Peroxomonosulfate concentrations were measured in activated persulfate reactions using a Metrohm 690 ion chromatograph equipped with a Super-Sep anion-exchange column. The mobile phase consisted of a degassed solution of 2.0 mmol/L phthalic acid containing 5% (v/v) acetonitrile (pH 3); the flow rate of the mobile phase was 1.5 ml/min (Ossadnik and Schwedt, 2001).

Hexane extracts were analyzed for HCA using a Hewlett-Packard 5890A gas chromatograph fitted with a 0.53 mm (i.d.) \times 60 m Equity 1 capillary column and electron capture detector (ECD). Chromatographic parameters included an injector temperature of 220 °C, detector temperature of 270 °C, initial oven temperature of 100 °C, program rate of 30 °C/min, and final temperature of 240 °C.

Statistical analyses were performed using the SAS software package version 9.1 (SAS, 2003). Linear regressions were performed to calculate first-order rate constants for persulfate decomposition. Contrast tests were conducted using a general linear model to compare regression coefficients (first-order rate constants for persulfate decomposition) across different treatments. Pearson's correlation test was used to determine correlations between measured and predicted oxygen evolved in base-activated persulfate systems.

6.2.4. Persulfate Activation By Phenoxide Derivatives

Materials

Sodium hydroxide (reagent grade, 98%), sulfuric acid, sodium bicarbonate, nitrobenzene, isopropanol (>99%), *tert*-butyl alcohol, potato starch, sodium phosphate dibasic, and hexane (>98%) were obtained from J.T. Baker (Phillipsburg, NJ). Sodium persulfate ($\text{Na}_2\text{S}_2\text{O}_8$) (reagent grade, >98%), magnesium chloride (MgCl_2) (99.6%), methyl formate (97%), sodium phosphate monobasic monohydrate (98.0–102.0%), xylenes, toluene, aniline (99.5%), and hexachloroethane (HCA) (99%) were purchased from Sigma Aldrich (St. Louis, MO). Carbon adsorbent tubes (ORBO-32) were obtained from Supelco (St. Louis, MO). A purified solution of sodium hydroxide was prepared by adding 10 mM of MgCl_2 to 1 L of the 8 M NaOH solution, which was then stirred for a minimum 8 hr and passed through a 0.45 μm membrane filter. Sodium thiosulfate (99%), potassium iodide, and methylene chloride were purchased from Fisher Scientific (Fair Lawn, NJ). Deionized water was purified to > 18 $\text{M}\Omega\cdot\text{cm}$ with a Barnstead Nanopure II ultrapure system (Dubuque, Iowa).

Potential Persulfate Activators

Phenol ($\text{C}_6\text{H}_5\text{OH}$) (89.6%) was obtained from J.T. Baker. (Phillipsburg, NJ). Catechol (http://en.wikipedia.org/wiki/Chemical_formula $\text{C}_6\text{H}_6\text{O}_2$) (98%), 2-chlorophenol ($\text{C}_6\text{H}_5\text{ClO}$) (>99%), 2,3-dichlorophenol ($\text{C}_6\text{H}_4\text{Cl}_2\text{O}$) (98%), 2,4,6-trichlorophenol ($\text{C}_6\text{H}_3\text{Cl}_3\text{O}$) (98%), 2,3,4,6-tetrachlorophenol ($\text{C}_6\text{H}_2\text{Cl}_4\text{O}$) (>99%), and pentachlorophenol ($\text{C}_6\text{HCl}_5\text{O}$) (98%) were purchased from Sigma-Aldrich (St. Louis, MO).

Probe Compounds and Scavengers

Nitrobenzene was used as a hydroxyl radical probe due to its high reactivity with hydroxyl radical ($k_{\text{OH}\cdot} = 3.9 \times 10^9 \text{ M}^{-1}\text{s}^{-1}$) and negligible reactivity with sulfate radical ($k_{\text{SO}_4\cdot-} \leq 10^6 \text{ M}^{-1}\text{s}^{-1}$) (Neta et al., 1977; Buxton et al., 1987; Clifton and Huie, 1989). HCA was used as a reductant probe because it is unreactive with hydroxyl and sulfate radicals ($k_{\text{OH}\cdot} = < 1 \times 10^6 \text{ M}^{-1}\text{s}^{-1}$) (Haag and Yao, 1992), but is readily reduced. Hydroxyl radicals were scavenged from the system using *tert*-butyl alcohol ($k_{\text{OH}\cdot} = 5.2 \times 10^8 \text{ M}^{-1} \text{ s}^{-1}$), which is unreactive with sulfate radicals ($k_{\text{SO}_4\cdot-} \leq 1 \times 10^6 \text{ M}^{-1} \text{ s}^{-1}$) (Neta et al, 1977; Buxton et al, 1987). The scavenger:probe molar ratio was 1000:1. Sulfate radical and hydroxyl radical were scavenged from the system using isopropanol ($k_{\text{OH}\cdot} = 8.2 \times 10^7 \text{ M}^{-1} \text{ s}^{-1}$) (Clifton and Huie, 1989; Buxton et al, 1987). The scavenger: probe molar ratio was 1000:1.

General Reaction Procedures

All reactions were conducted in 20 mL borosilicate vials capped with polytetrafluoroethylene (PTFE) lined septa. Each reaction vial contained 0.5 M sodium persulfate and 2 M NaOH (for a base to persulfate molar ratio of 4:1), 2 mM phenoxide, and 1 mM of nitrobenzene or 2 μM of HCA. At several times during the course of the reactions, sodium persulfate was measured by iodometric titration and probe concentrations were analyzed by gas chromatography (GC) after extracting the contents of the reactors with hexane. All reactions were performed in triplicate, and the data were reported as the mean of the three replicates. The standard error of the mean was calculated and included as error bars for each data point. All reactions were conducted at a temperature of $\pm 20^\circ\text{C}$. Triplicate control systems for each phenoxide system were evaluated in parallel at a pH above 12 using deionized water instead

of the phenoxide solution. Solution pH was monitored using a Fisher Accumet pH meter 900 (Fisher Scientific, Hampton, NH).

Detection of the Dominant Radical Oxidant

tert-Butyl alcohol was used as a hydroxyl scavenger to distinguish between hydroxyl radical and sulfate radical. Reactions consisted of a 15 mL solution of 2 mM phenoxide, 0.5 M sodium persulfate, 1 mM nitrobenzene, a molar ratio of sodium persulfate to NaOH of 1:4, and a molar ratio of nitrobenzene to *t*-butyl alcohol of 1:1000. Control reactions were conducted in parallel using double-deionized water in place of phenoxide.

Effect of pH on Persulfate Activation by Phenoxides

Persulfate activation was studied at various pH regimes. The characteristics of the organic compounds used in this study are highly pH dependent; therefore experiments were run from a pH starting at 12 down to a pH below the pK_a of the corresponding phenoxide. Vials were filled with 15 mL of a solution containing 2 mM phenol, 0.5 M sodium persulfate, and 1 mM nitrobenzene. The initial pH was adjusted with a 0.1 M phosphate buffer (a mixture of monosodium and disodium phosphate). As the reaction proceeded, the pH was monitored and sulfuric acid (0.1 N) and sodium hydroxide (0.1 N, 1 N and 4 N) were used to maintain the pH close to the initial value. Control reactions were conducted in parallel using double-deionized water in place of phenol. Also, a catechol-activated system was studied at 2 pH units above and below the pK_a of catechol to observe the degradation rates of nitrobenzene and hexachloroethane.

Mechanisms for Phenoxide-Persulfate Activation

Reductive and nucleophilic mechanisms were studied as possible mechanisms in phenoxide-persulfate activation. Pentachlorophenol was used in this study as the selected phenoxide. Experiments were conducted at a pH 8.0, which is mid-way between the pK_a of pentachlorophenol (4.8) and hydroperoxide (11.8). Vials were filled with 15 mL of the following solution: 2 mM pentachlorophenol, 0.5 M sodium persulfate, and either 1 mM of nitrobenzene or 2 μ M HCA. The initial pH was adjusted with a 0.1 M phosphate buffer. As the reaction proceeded, the pH was monitored and sulfuric acid (0.1 N) and sodium hydroxide (0.1 N, 1 N and 4 N) were used to maintain the pH close to 8. Control reactions were conducted in parallel using double-deionized water in place of pentachlorophenol. At several times during the course of the reactions, hydrogen peroxide was measured by spectrometry, and nitrobenzene or HCA concentrations were analyzed by GC after extracting the contents of the reactors with hexane. Pentachlorophenol and their derivatives were analyzed by GC/MS after extracting the contents of the reactors with methylene chloride.

Analytical Procedures

Hexane extracts were analyzed for nitrobenzene using a Hewlett Packard Series 5890 GC with a 0.53 mm (i.d.) x 15 m SPB-5 capillary column and flame ionization detector (FID). Chromatographic parameters included an injector temperature of 200 °C, detector temperature of 250 °C, initial oven temperature of 60 °C, program rate of 30 °C/min, and a final temperature of 180 °C. Hexane extracts were analyzed for HCA using a Hewlett Packard Series 5890 GC with electron capture detector (ECD) by performing splitless injections onto a 0.53 mm (i.d.) x 30 m Equity-5 capillary column. Chromatographic parameters included an injector temperature of 220

°C, detector temperature of 270 °C, initial oven temperature of 100 °C, program rate of 30 °C/min, and a final temperature of 240 °C. Six-point calibration curves were developed using solutions of known concentrations of nitrobenzene and HCA.

Phenolic compounds and their derivatives were analyzed on a Hewlett-Packard model 7890A GC/5975C mass spectrometer. Samples were acidified to a pH of 1–2 with sulfuric acid, followed by extraction with methylene chloride. Methylene chloride extracts were analyzed by GC/MS. Chromatographic parameters included an injector in splitless mode and maintained at 250 °C; an initial oven temperature of 40 °C for 2 min, then programmed at a rate of 40 °C/min to 100 °C and held for 0.5 min, and finally raised to 300 °C at a rate of 10 °C/min and held for 3 min. The column used was a 30 m MDB-5ms Agilent column (Santa Clara, CA) with a 0.5 µm i.d. and 250 µm film thickness. Helium was used as the carrier gas at a constant flow rate of 1.5 ml/min.

Sodium persulfate concentrations were determined by iodometric titration with 0.01 N sodium thiosulfate (Kolthoff and Stenger, 1947). Hydrogen peroxide was measured by the reaction between titanium sulfate and H₂O₂ (Cohen and Purcell, 1967). The absorbance at 407 nm was read on a Spectronic 20 Genesys spectrophotometer. The Statistical Analysis System package S.A.S version 9.1 was used to calculate the variances between the experimental data sets and 95% confidence intervals for rate constants.

6.2.5. Persulfate Activation by Alcohols, Aldehydes, Ketones, Organic Acids, and Keto Acids

Chemicals

Sodium hydroxide (reagent grade, 98%), sodium bicarbonate, nitrobenzene, potato starch, and hexane (>98%) were obtained from J.T. Baker (Phillipsburg, NJ). Sodium persulfate ($\text{Na}_2\text{S}_2\text{O}_8$) (reagent grade, >98%), magnesium chloride (MgCl_2) (99.6%), and hexachloroethane (HCA) (99%) were purchased from Sigma Aldrich (St. Louis, MO). A purified solution of sodium hydroxide was prepared by adding 5–10 mM of MgCl_2 to 1 L of 8 M NaOH, which was then stirred for a minimum 8 hours and passed through a 0.45 μM membrane filter. Sodium thiosulfate (99%), potassium iodide, methylene chloride, and mixed hexanes were purchased from Fisher Scientific (Fair Lawn, NJ). Deionized water was purified to >18 $\text{M}\Omega\cdot\text{cm}$ with a Barnstead Nanopure II ultrapure system (Dubuque, Iowa).

Potential Persulfate Activators

Different classes of organic compounds were evaluated for their potential to activate persulfate under basic conditions. Acetone, sodium pyruvate, pyruvic acid, citrate, 1-propanol (>99%), 2-propanol (>99%), *t*-butyl alcohol (>99%), and formaldehyde were obtained from J.T. Baker (Phillipsburg, NJ). 2-Butanone (>99%), 2-pentanone (>99%), 2-heptanone (99%), oxalic acid, acetoacetic acid (98%), L(-) malic acid disodium, succinic acid, 1-pentanol (>99%), 2-pentanol (98%), 3-pentanol (98%), acetaldehyde (99%), propionaldehyde (97%), and butyraldehyde (>99%) were purchased from Sigma Aldrich (St. Louis, MO). Levulinic acid (98%) and isobutanol (>99%) were obtained from Alfa Aesar (Ward Hill, MA). *sec*-Butanol (>99%) was obtained from Acros Organics (Morris Plains, NJ).

Probe Compounds and Scavengers

Nitrobenzene, which has a high reactivity with hydroxyl radicals ($k_{\text{OH}\cdot} = 3.9 \times 10^9 \text{ M}^{-1}\text{s}^{-1}$) and negligible reactivity with sulfate radicals ($k_{\text{SO}_4\cdot-} = \leq 10^6 \text{ M}^{-1}\text{s}^{-1}$), was used to detect hydroxyl radicals (Neta et al., 1977; Buxton et al., 1987; Clifton and Huie, 1989). HCA was used as a reductant probe because it is not oxidized by hydroxyl radicals ($k_{\text{OH}\cdot} = < 1 \times 10^6 \text{ M}^{-1}\text{s}^{-1}$) (Haag and Yao, 1992). *t*-Butyl alcohol was used to scavenge hydroxyl radicals ($k_{\text{OH}\cdot} = 5.2 \times 10^8 \text{ M}^{-1}\text{s}^{-1}$) without scavenging sulfate radicals ($k_{\text{SO}_4\cdot-} = < 1 \times 10^6 \text{ M}^{-1}\text{s}^{-1}$) (Buxton et al., 1987). The scavenger: probe molar ratio used was 1000:1.

General Reaction Procedures

All reactions were conducted in 20 mL borosilicate vials capped with polytetrafluoroethylene (PTFE) lined septa. Each reaction vial contained 0.5 M sodium persulfate, 2M NaOH, 10 mM of the organic compound used as an activator, and the selected probe (1 mM of nitrobenzene or 2 μM of hexachloroethane). At selected time points, sodium persulfate was measured using iodometric titrations, and the residual probe concentration was analyzed with gas chromatography (GC) after extracting the contents of the reactor with hexane. All reactions were performed in triplicate, and the data were reported as the mean of the three replicates. The standard error of the mean was calculated and included as error bars for each data point. All reactions were conducted at a temperature of $\pm 20^\circ\text{C}$. Triplicate control systems for each organic system were evaluated in parallel at a pH above 12 using deionized water in place of the organic activator solution. Solution pH was monitored by using a Fisher Accumet pH meter 900 (Fisher Scientific, Hampton, NH).

Analytical Procedures

Hexane extracts were analyzed for nitrobenzene using a Hewlett Packard Series 5890 GC with a 0.53 mm (i.d.) x 15 mSPB-5 capillary column and flame ionization detector (FID). Chromatographic parameters included an injector temperature of 200 °C, detector temperature of 250 °C, initial oven temperature of 60 °C, program rate of 30 °C/min, and a final temperature of 180 °C. Hexane extracts were analyzed for HCA using a Hewlett Packard Series 5890 GC with electron capture detector (ECD) by performing splitless injections onto a 0.53 mm (i.d.) x 30 m Equity-5 capillary column. Chromatographic parameters included an injector temperature of 220 °C, detector temperature of 270 °C, initial oven temperature of 100 °C, program rate of 30 °C/min, and a final temperature of 240 °C. A 6-point calibration curve was developed using known concentrations of nitrobenzene or hexachloroethane solutions respectively.

Sodium persulfate concentrations were determined by iodometric titration with 0.01 N sodium thiosulfate (Kolthoff and Stenger, 1947). The Statistical Analysis System package SAS 9.1.3 was used to calculate the variances between the experimental data sets and 95% confidence intervals for rate constants.

6.2.6. Persulfate Activation by Soil Organic Matter

Materials

Sodium hydroxide (reagent grade, 98%), sulfuric acid, sodium bicarbonate, nitrobenzene, isopropanol (>99%), *tert*-butyl alcohol, potato starch, sodium phosphate dibasic, and hexane (>98%) were obtained from J.T. Baker (Phillipsburg, NJ). Sodium persulfate ($\text{Na}_2\text{S}_2\text{O}_8$) (reagent grade, >98%), magnesium chloride (MgCl_2) (99.6%), methyl formate (97%), sodium phosphate monobasic monohydrate (98.0–102.0%), and hexachloroethane (HCA) (99%) were purchased from Sigma Aldrich (St. Louis, MO). A purified solution of sodium hydroxide was prepared by adding 10 mM of MgCl_2 to 1 L of the 8 M NaOH solution, which was then stirred for a minimum 8 hours and passed through a 0.45 μm membrane filter. Sodium thiosulfate (99%), potassium iodide, and methylene chloride were purchased from Fisher Scientific (Fair Lawn, NJ). Deionized water was purified to > 18 $\text{M}\Omega\cdot\text{cm}$ with a Barnstead Nanopure II ultrapure system (Dubuque, Iowa).

Soils

Four horizons of a surface soil, collected from an alluvial fan in the Carson Valley, NV, were used in base-activated persulfate reactions. The four horizons were chosen because of their varying soil organic carbon contents but similar mineralogy (Table 7.2.6.1). The soils were crushed using a soil grinder and sieved through a 1.65 mm sieve. Organic carbon content was determined by the Walkley-Black method (Walkley and Black, 1934). Particle size distribution was analyzed using the pipette method (Gee and Bauder, 1986). The citrate-bicarbonate-dithionite extraction method was used to determine amorphous and crystalline iron and manganese oxyhydroxides content (Jackson et al., 1986). Cation exchange capacity was analyzed by saturation with sodium acetate at pH 8.2 (U.S. Soil Conservation Service, 1972). Physical and chemical properties for the Carson Valley soils are listed in Table 6.2.6.1.

Table 6.2.6.1. Characteristics of the Carson Valley Soil

Characteristic	Soil I	Soil 2	Soil 3	Soil 4
Organic carbon content (mg kg^{-1})	2000	5000	10000	16000
Sand (%)	85.3	86.5	86.3	86.1
Silt (%)	12.3	11.0	10.9	10.8
Clay (%)	2.4	2.5	2.8	3.1
Crystalline Fe oxides (mg kg^{-1})	4400	4400	4300	4300
Crystalline Mn oxides (mg kg^{-1})	100	100	100	100
Amorphous Fe oxides (mg kg^{-1})	3400	4400	4200	4000
Amorphous Mn oxides (mg kg^{-1})	100	100	100	100
Cation exchange capacity (cmol kg^{-1})	4.04	4.28	4.59	4.90
pH	6.6	6.4	6.5	6.6

Soil organic matter (SOM) was removed from the two soils by addition of 20% hydrogen peroxide (H_2O_2) (Robinson, 1927). Soil slurries received periodic additions of H_2O_2 and were heated to 60° C until a visible color change of dark to light in the soil occurred indicating that the SOM was removed. Soils with the SOM removed were dried at 55° C, pulverized, and sieved with a 1.65 mm sieve.

Probe Compounds and Scavengers

Nitrobenzene was used as a hydroxyl radical probe due to its high reactivity with hydroxyl radicals ($k_{\text{OH}\cdot} = 3.9 \times 10^9 \text{ M}^{-1}\text{s}^{-1}$) and negligible reactivity with sulfate radicals ($k_{\text{SO}_4\cdot-} = \leq 10^6 \text{ M}^{-1}\text{s}^{-1}$) (Neta et al., 1977; Buxton et al., 1987; Clifton and Huie, 1989). HCA was used as a reductant probe because it is unreactive with hydroxyl and sulfate radicals ($k_{\text{OH}\cdot} = < 1 \times 10^6 \text{ M}^{-1}\text{s}^{-1}$) (Haag and Yao, 1992), but is readily reduced.

General Reaction Procedures

All reactions were conducted in 20 mL borosilicate vials capped with polytetrafluoroethylene (PTFE) lined septa. Each reaction vial contained 0.5 M sodium persulfate and 1.5 M NaOH in a base to persulfate molar ratio of 3:1, and 1 mM of nitrobenzene or 2 μM of HCA, which was added to 10 g of one of the Carson Valley soils. At several times during the course of the reactions, sodium persulfate was measured by iodometric titration and probe concentrations were analyzed by gas chromatography (GC) after extracting the contents of the reactors with hexane. All reactions were performed in triplicate, and the data were reported as the mean of the three replicates. The standard error of the mean was calculated and included as error bars for each data point. All reactions were conducted at a temperature of $\pm 20^\circ \text{C}$. Triplicate control systems for each soil system were evaluated in parallel at a pH above 12 using deionized water without the presence of soil. Solution pH was monitored using a Fisher Accumet pH meter 900 (Fisher Scientific, Hampton, NH).

Analysis

Probe compound concentrations were quantified using Hewlett-Packard 5890A gas chromatographs with an electron capture detector (for HCA) and a flame ionization detector (for NB), each fit with 10 m x 0.53 mm DB-1 capillary columns. Program conditions for HCA analysis included injector temperature of 220°C, detector temperature of 270°C, initial oven temperature of 100°C, program rate of 30°C min⁻¹, and final temperature of 240°C. Program conditions for nitrobenzene analysis included injector temperature of 200°C, detector temperature of 250°C, initial oven temperature of 60°C, program rate of 30°C min⁻¹, and final temperature of 180°C. Persulfate concentrations were measured by iodometric titration using 0.01 N sodium thiosulfate (Kolthoff and Stenger, 1947). The pH was quantified using a Fisher Accumet Basic AB15 pH meter.

6.2.7. Model Contaminants

Materials

Seven model substrates were evaluated for their potential to be treated by base activated persulfate: anisole, 1,1-dichloroethane (DCA), 1,1,1-trichloroethane (TCA), chlorobenzene (CB), 1,2-dichlorobenzene (DCB), trichloroethylene (TCE), and perchloroethylene (PCE). Each was purchased from Sigma-Aldrich. Sodium persulfate was also obtained from Sigma-Aldrich, and sodium hydroxide was purchased from J. T. Baker.

Reaction Procedures

Each of the seven probe compounds was dissolved in deionized water at a concentration of 2 mM. Persulfate formulations were prepared with concentrations of 1 M sodium persulfate in sodium hydroxide to persulfate molar ratios of 1:1, 2:1, and 3:1. To initiate the reactions, 40 mL volatile organic analysis (VOA) vials received 15 mL of one of the probe solutions and 15 mL of one persulfate formulation, for a total volume of 30 mL. A set of triplicate vials was prepared for each time point of analysis. After mixing the model contaminant solution and persulfate solution, the initial contaminant concentration was 1 mM, and the initial persulfate concentration was 0.5 M.

The reactions were allowed to proceed between 4 and 12 hr (depending on the rate of contaminant degradation). At selected time points the entire contents of the triplicate vials were extracted with 3 mL of hexane, and the hexane extracts were analyzed for the specific contaminant by gas chromatography.

6.2.8. Effect of Sorption on Contaminant Oxidation in Activated Persulfate Systems

Materials

Hexane and sodium hydroxide (99.3%) were obtained from J.T. Baker (Phillipsburg, NJ). Perchloroethylene (99.5%), hexachlorocyclopentadiene (98%), diatomaceous earth (95%), and sodium persulfate ($\geq 98\%$) were purchased from Sigma-Aldrich (Milwaukee, WI). ORBO tubes were purchased from Supelco (Bellefonte, PA). Double deionized water ($>18\text{ M}\Omega\text{-cm}$) was purified using a Barnstead Nanopure II deionizing system.

Vapor Deposition of Probe Compounds

Diatomaceous earth was used as a model sorbent because it was employed previously to investigate desorption–oxidation relationships (Sedlak and Andren, 1994). Perchloroethylene (tetrachloroethene, PCE) and hexachlorocyclopentadiene (HCCP) were sorbed to diatomaceous earth in separate batches using vapor deposition (Corbin et al., 2007) for an initial concentration of 0.05 mmol/kg. PCE was added directly to 35 g of diatomaceous earth in a 500 mL Pyrex bottle, which was then heated at 135°C for five hours and shaken hourly to promote sorption of the PCE. HCCP was diluted in methylene chloride prior to addition to the diatomaceous earth. The bottle containing the sorbent and methylene chloride–HCCP was then heated at 70°C in a fume hood for two hours and shaken every half hour to promote even distribution of HCCP until the methylene chloride volatilized.

Gas-Purge Desorption

Gas-purge methodology was used to determine the maximum natural rate of desorption of PCE and HCCP (Brusseau et al., 1990). Desorption was measured in triplicate using 3 g aliquots of diatomaceous earth containing one of the sorbed probe compounds mixed with 20 mL of deionized water in 40 mL volatile organic analysis (VOA) vials. The slurry was purged with nitrogen gas at a rate of 100 mL/min, and volatilized probe compounds were trapped in ORBO tubes fitted to the vial caps. At each time point the ORBO tubes were replaced with new tubes, the spent ORBO tubes were extracted with mixed hexanes, and the extracts were analyzed by gas chromatography.

Reaction Conditions

Batch reactions were conducted in triplicate 40 mL VOA vials with 3 g diatomaceous earth sorbed with PCE or HCCP and 20 mL of persulfate or CHP reaction solution. Reactions were conducted over 60 minutes for PCE and 120 minutes for HCCP. At each time point, the contents of a triplicate set of reactors were extracted with hexane and analyzed by gas chromatography. CHP reactions were catalyzed by 5 mM iron (III) sulfate and conducted at pH 3; hydrogen peroxide concentrations of 0.6, 1.8, 3.6, and 5.4 M were used for PCE, while concentrations of 2, 5, and 10 M hydrogen peroxide were used for HCCP. Iron (II)–citrate-activated persulfate reactions were conducted at an initial pH of 7.0 and contained 5, 10, and 20 mM iron (II)–citrate and 1 M persulfate. Base-activated persulfate reactions contained a 2:1 molar ratio of NaOH to persulfate with persulfate concentrations of 0.1, 0.25, 0.5, and 1.0 M, and corresponding NaOH concentrations of 0.2, 0.5, 1.0, and 2.0 M, respectively. The concentrations of persulfate used were lower than hydrogen peroxide concentrations due to the lower water solubility of sodium persulfate.

Analysis

Extracts were analyzed using a Hewlett-Packard 5890A gas chromatograph fitted with a 30 m x 0.53 mm (i.d.) DB-5 capillary column and electron capture detector. For PCE analysis, the injector port and detector port temperatures were 240°C and 260°C, the program rate was 20°C min⁻¹, initial temperature was 100° C, and the final temperature was 200°C. For HCCP analysis the injector port was 240°C, the detector port was 260°C, the program rate was 20°C min⁻¹ and the initial and final temperatures were 140°C and 280°C. Hydrogen peroxide concentrations were determined by iodometric titration using 0.1 N sodium thiosulfate (Schumb et al., 1955).

6.3. Effect of Persulfate on Subsurface Characteristics

6.3.1. Effect of Persulfate Formulations on Soil Mineralogy

Materials

Six minerals were investigated for the potential of activated persulfate to change mineral structure: goethite [FeOOH], hematite [Fe₂O₃], ferrihydrite [Fe₅HO₈•4H₂O], birnessite [δ-MnO₂], kaolinite [Al₂Si₂O₅(OH)₄], and montmorillonite [(Na,Ca)(Al,Mg)₆(Si₄O₁₀)₃(OH)₆•nH₂O]. Goethite and hematite were purchased from Strem Chemicals (Newburyport, MA) and J.T. Baker (Phillipsburg, NJ), respectively. Ferrihydrite was purchased from Mach I (King of Prussia, PA). Birnessite was prepared by the drop-wise addition of concentrated hydrochloric acid (2 M) to a boiling solution of 1 M potassium permanganate with vigorous stirring (Mckenzie, 1971). Montmorillonite and kaolinite were provided by the Clay Minerals Society (West Lafayette, IN). Examination of the X-ray diffraction pattern confirmed the minerals were the desired iron and manganese oxides. Mineral surface areas were determined by Brunauer, Emmett, and Teller (BET) analysis under liquid nitrogen on a Coulter SA 3100 (Carter et al. 1989).

Persulfate process conditions

Reactions were conducted with 1) persulfate alone (0.5 M persulfate), 2) iron-EDTA activated persulfate (0.5 M persulfate activated by 10 mM iron (III)-EDTA), and 3) base-activated persulfate (0.5 M persulfate activated by 1.5 M NaOH). In addition, control systems receiving only deionized water were conducted in parallel.

Treatment procedures

Reactions in which persulfate effects on dominant soil minerals were monitored were conducted in triplicate in 250 mL I-Chem borosilicate glass media bottles equipped with polytetrafluoroethylene (PTFE)-lined caps. The reactors contained 70 mL of one of the persulfate formulations. The reactions were conducted in the dark at 20° C ± 2° C. After 15, 30, and 45 days, one bottle containing each mineral was selected for analysis. The persulfate solution (or deionized water for control reactors) was decanted, and the mineral was rinsed out of the bottle using deionized water. The mineral was then spread on a Whatman No. 2 filter and rinsed with at least 500 mL of deionized water. The mineral was then allowed to air dry, and aliquots were separated for different analyses.

6.3.2. Effect of Persulfate Formulations on Soil Permeability

Materials

Sodium persulfate ($\geq 98\%$) and sodium sulfate were purchased from Sigma Aldrich (St. Louis, MO). Sodium hydroxide (98.6%) and iron (III)-EDTA were obtained from J.T. Baker Inc. (Phillipsburg, NJ). Deionized water was purified to $>18 \text{ M}\Omega\cdot\text{cm}$ with a Barnstead Nanopure II deionizing system. Four materials were used to investigate the effect of persulfate formulations on hydraulic conductivity: commercial sand (silica sand 20/30), kaolinite and two horizons of a natural soil. Commercial sand was purchased from Lane Mountain Company (Valley, WA). Kaolinite ($\text{Al}_2\text{Si}_2\text{O}_5(\text{OH})_4$) was purchased from Dry Branch Kaolin Company (Dry Branch, GA).

Two natural soils, which were termed soil KB1 and soil KB2, were collected from two separate horizons near Kamiak Butte in the Palouse region of Washington State. Although surface soils and subsurface soils are classified as separate soil types, they exhibit many of the same characteristics. The organic carbon content is one of the primary distinguishing characteristics between these two soil classifications (McBride, 1994). Subsurface soils are classified as those soils below the root zone. These soils typically have organic carbon contents $< 0.1\%$, although organic carbon contents can be higher, especially in clay layers. The KB2 soil was collected below the root zone and may be considered to represent subsurface soils.

The natural soils were air dried and passed through a $300 \mu\text{m}$ sieve. The total soil and soil fractions were analyzed for particle size analysis and amorphous and total iron and manganese oxides. Particle size distribution was measured by the pipette method (Gee and Bauder, 1986). The acid ammonium oxalate in darkness (AOD) method (McKeague and Day, 1966) was used to analyze for amorphous iron and manganese oxides. Total iron and manganese oxides were extracted using the citrate-bicarbonate-dithionite (CBD) method (Jackson et al., 1986), and then analyzed by inductively coupled plasma-atomic emission spectrometry (ICPAES). The physical and chemical properties of the soils are shown in Table 6.3.2.1 and Table 6.3.2.2.

Table 6.3.2.1. Physical properties of soil KB2 and soil KB1

Soil	% Sand	% Clay	% Silt	Texture	CEC ($\text{Cmol}(+)/\text{kg}$)
KB1	7.77	69.15	23.08	Silt Loam	34
KB2	39.5	11.1	49.8	Loam	19

*CEC: Cation Exchange Capacity

Table 6.3.2.2. Chemical properties of soil KB2 and soil KB1

Soil	Amorphous Mn ($\mu\text{g/g}$)	Total Mn ($\mu\text{g/g}$)	Amorphous Fe ($\mu\text{g/g}$)	Crystalline Fe ($\mu\text{g/g}$)	% Organic Carbon
KB1	194	380	4656	2789	1.61
KB2	296	510	2196	1697	0.24

Persulfate Reactions

Unactivated persulfate was used at a concentration of 0.5 M. The same concentration of persulfate was used in activated persulfate formulations with the addition of 1) iron (III)-EDTA (10 mM) and 2) sodium hydroxide (1 M, for a 2:1 ratio of base to persulfate) as activators. Sodium sulfate solutions (0.5 M) were used in place of persulfate as positive control reactions for hydraulic conductivity tests. Sulfate served as a positive control because it is a sulfur-oxygen based compound with the same charge as persulfate, but without the potential to proceed through oxidation-reduction pathways. Deionized water was used in place of persulfate for control reactions for XRCT.

Hydraulic Conductivity

Hydraulic conductivity was measured to evaluate potential changes in soil permeability after the application of persulfate formulations. The permeameters and test methods used varied according to the physical characteristics of different soils. Permeability tests of commercial sand were conducted using a falling head permeameter as shown in Figure 6.3.2.1. Sand in 300 g quantities was added to the column of the permeameter, which was then filled with persulfate or control solutions and compacted in the column to a height of 13 cm. The initial head h_1 at time $t=0$ was recorded and the solution was passed through the sample in order to obtain the final head h_2 at time t . The hydraulic conductivity K governed by Darcy's Law was calculated using equation 7:

$$K = \frac{l}{t} \ln \left(\frac{h_1}{h_2} \right) \quad (6.3.2.1)$$

where l is the height of sample (13 cm), t is the time interval between readings of h_1 and h_2 , h_1 is the initial height of the solution in the column, and h_2 is the final height of the solution.

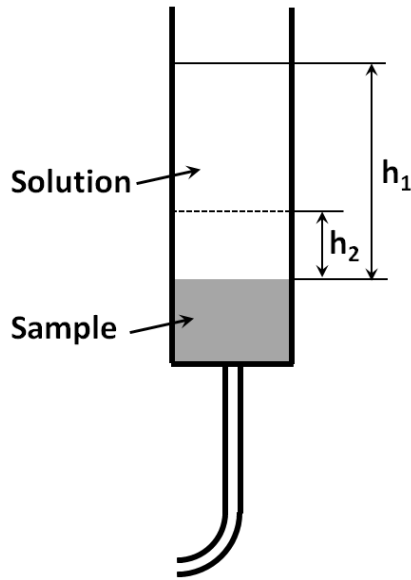


Figure 6.3.2.1. Falling head permeameter.

Hydraulic conductivity tests for kaolinite, soil KB1, and soil KB2 were conducted with a flexible wall permeameter (ASTM D5856-95) (Hamdi et al., 2005) as shown in Figure 6.3.2.2. The permeameter column and sample holder ring were made of polyvinyl chloride (PVC). The sample holder ring was fitted tightly with an O-ring fitting which was set between the sample ring and the column to prevent leakage from the inner edge of column. Kaolinite and the natural soils were mixed with 10% of their mass in deionized water before compaction and saturation. Kaolinite in a mass of 90 g was compacted in the mold to a 2 cm layer. Similarly, 123 g of soil KB2 and 114 g of soil KB1 were compacted in the same way; the different masses were used to provide the same volume of soil. Compacted samples were saturated with deionized water, persulfate, or sulfate solutions for 24 hr before the permeability tests were initiated. The soil samples were placed on a porous stone to hold the sample and allow transport of solutions. The solutions passed through the soil sample with head changing from h_1 to h_2 . Hydraulic conductivity K was then calculated using equation 8:

$$K = \frac{la}{tA} \ln \left(\frac{h_1}{h_2} \right) \quad (6.3.2.2)$$

where l is the thickness of sample (2 cm), t is the time interval between readings of h_1 and h_2 , h_1 is the initial level of solution, h_2 is the final level of solution, A is the cross-sectional area of the soil sample (45.58 cm^2), and a is the cross-sectional area of the solution column (0.064 cm^2). Because kaolinite and the natural soils were not very permeable, the ratio between A and a was designed to be large enough in order to conduct the tests within a reasonable time.

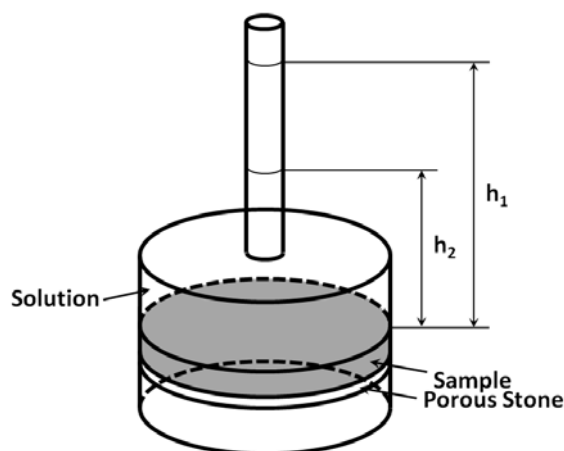


Figure 6.3.2.2. Flexible wall permeameter

XRCT

For each XRCT analysis, equal volumes (74 g of sand or 68 g of the natural soil) were packed in 3.4 cm-diameter PVC columns. Deionized water, unactivated persulfate, or iron (III)-EDTA activated persulfate solutions were passed through the sand samples before X-ray scanning. Each of the soil samples were saturated with one of the persulfate formulations or deionized water for 24 hr prior to conducting the X-ray scans. Dry soil samples and deionized water treated soil samples served as controls. The XRCT scan apparatus has two X-ray sources that are able to generate 420 keV and 225 keV voltages, respectively. The voltage for the X-ray source used in this study was 350 keV and the source current was 1.6 amp. The X-ray sources are connected to a central work station, which is comprised of four parallel computing processors and software.

Three FlashCT programs were used to generate images of the materials. The first program, FlashCT DAQ, initiates the scanning of samples and outputs raw data. The data are processed by the second program, FlashCT DPS, which provides reconstructed cross-sectional images of the scanned slices. The third program, FlashCT VIZ, converts the cross-sectional images into three-dimensional images. Finally, these three-dimensional images are re-processed to two-dimensional (XY, YZ, XZ) format images for further analysis. Analysis of these 2-D images was carried out by Image Pro Plus software to determine soil structure data, including soil porosity (n) and mean pore radius (r). The algorithm for obtaining final X-ray results is shown in Figure 6.3.2.3.

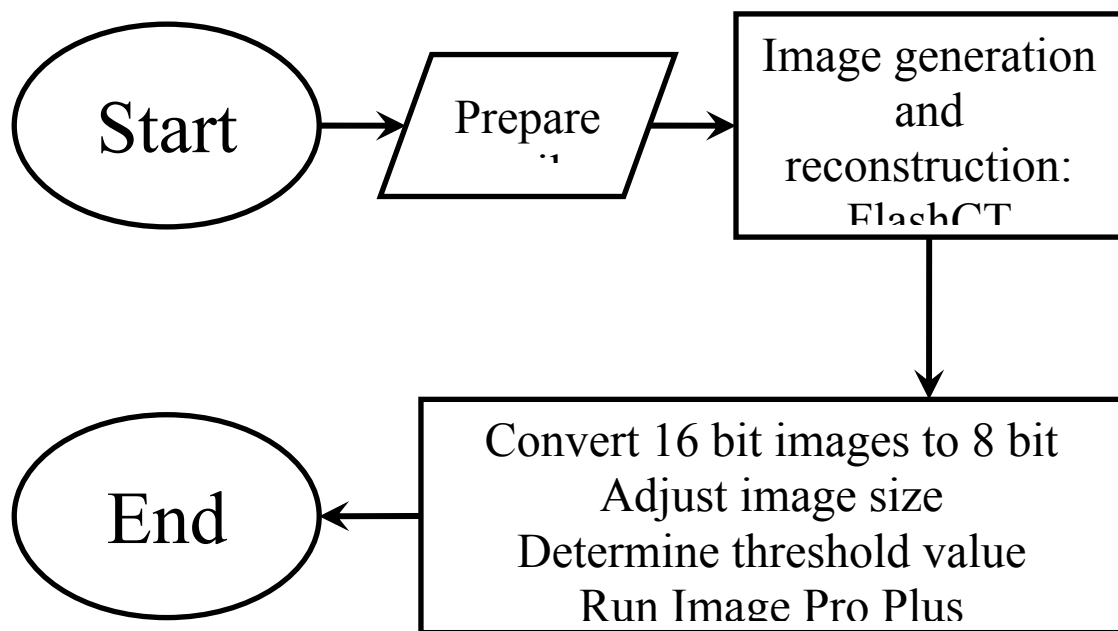


Figure 6.3.2.3. XRCT test procedures.

6.4. Transport of Persulfate into Low Permeability Matrices

6.4.1. Persulfate Transport in Two Low-Permeability Soils

Chemicals

Sodium persulfate ($\geq 98\%$) and iron (III) ethylenediaminetetraacetic acid (Fe(III)EDTA) were purchased from Sigma Aldrich (St. Louis, MO). Sodium hydroxide (98.6%), sodium bicarbonate and potato starch were obtained from J.T. Baker Inc. (Phillipsburg, NJ). Sodium thiosulfate (99%) and potassium iodide were purchased from Fisher Scientific (Fair Lawn, NJ). Double-deionized water ($>18 \text{ M}\Omega\cdot\text{cm}$) was generated with a Barnstead NANOpure II Ultrapure system.

Soils

Two soil types were used in this study. Kaolin was purchased from Dry Branch Kaolin Company (Dry Branch, GA) and Palouse loess was collected from a site near Pullman, WA. The soil characteristics of the Palouse loess are summarized in Table 6.4.1.1.

Table 6.4.1.1. Soil characteristics of Palouse loess.

Characteristic	Palouse loess	Standard
Classification	Lean clay	ASTM D 2487
Passing #200 sieve, %	98.2	
Liquid limit, %	33.0	ASTM D 4318
Plastic limit, %	20.7	ASTM D 4318
Plasticity index, %	12.3	ASTM D 4318
Maximum dry unit weight, (KN/m^3)	17.0	ASTM D 698
Optimum water content, %	18.7	ASTM D 698

Column Materials

Polyvinyl chloride (PVC) pipe (ASTM D 3034) with a 10.2-cm inner diameter was purchased from Cresline[®] (Evansville, IN). Styrene caps were obtained from Genova Products (Davison, MI). PVC couplers were purchased from Savko Plastic Pipe & Fittings (Columbus, OH). Polyethylene caps and 5.1 cm tenite butyrate tubing were purchased from U.S. Plastic Corp. (Lima, OH).

Column Preparation

Palouse loess columns. The soil and column preparation was adapted from Cotton et al. (1998). Double deionized water was added to the Palouse loess until a water content of 17% was reached (1.7% below optimum). The soil was stored in double Glad[®] 4-L bags and allowed to

cure for 24 hr. The Palouse loess was then compacted in accordance with ASTM D 698 in 11.6-cm high by 10.2-cm diameter PVC molds. A styrene cap with 5 symmetrically drilled 0.4-cm holes was attached to the column. The holes relieved the pressure created within the column as the cap was attached and allowed for water infiltration during the saturation period. Finally, the columns were submerged in a water bath to saturate the soil and the soil was routinely trimmed to the height of the column. Once the soil swelling was negligible, the columns were removed from the water bath and the cap was sealed with DAP[®] silicone sealant.

Kaolin columns. Kaolin was mixed with 150% double deionized water (mass/mass) to make a slurry and was poured into two consolidation cylinders with drains (Hammar, 2004; Sheeran and Krizek, 1971). The slurry was allowed to settle for 5 d and then 2 kg, 1 kg, and 4 kg weights were loaded every 48 hr to the pressure plates of each cylinder for a total pressure of 4.5 kPa. The weight was removed following the final 48 hr of loading and 69 kPa of air pressure was applied for 5 d. A final pressure of 276 kPa was achieved by incrementally increasing the pressure by 34 kPa every 72 hr. The soil was slowly removed from the cylinders with a modified hydraulic jack. Eight-cm high tenite butyrate tubing was pressed into the kaolin and the kaolin was trimmed to a height of 4 cm, which left room for a solution reservoir. Polyethylene caps were attached to the bottoms of the columns.

Diffusion Testing Procedure

The single reservoir with a decreasing source concentration method was used (Shackelford, 1991). For testing the persulfate diffusion in Palouse loess, a solution reservoir was created by attaching 11.6-cm high PVC cylinders to the columns with a PVC coupler. The reservoir was filled with solution to a height of 10.3 cm. The solution reservoir was filled to a height of 3 cm for testing diffusion in the kaolin columns.

The diffusion test consisted of 2 solution sets: a 1M persulfate set and a 0.1M persulfate set. Within each set there were 4 treatments: persulfate, persulfate activated by 5mM Fe(III)EDTA, 2:1 molar ratio of NaOH:persulfate, and persulfate with no soil (control). Each treatment was replicated three times. Two 1M persulfate and two 0.1M persulfate sets were made (long and short duration) and the persulfate was allowed to diffuse into the soil for a period of 70-149 days. The persulfate diffusion test for the kaolin columns was conducted over 82 d.

Biweekly diffusion test monitoring. Solution sampling was conducted every two weeks; 0.05 ml and 0.1 ml of solution was removed from the kaolin and Palouse loess reservoirs, respectively, and the persulfate concentration was determined by iodometric titration. The solution from the Palouse loess columns was filtered with Millipore 0.22 Millex[®] GP filters prior to titration in order to prevent the reaction of soil particles with iodide. The pH was also recorded biweekly with a Fisher Accumet AB15 pH meter.

Persulfate Analysis in Column Segments

For the Palouse loess systems, the soil was removed from the PVC columns in 1-cm increments with a hydraulic jack and a 10-g sample was taken from each 1-cm section and placed in 20-ml borosilicate volatile organic analysis (VOA) vials capped with PTFE (polytetrafluoroethylene) lined septa. The same procedure was followed for the kaolin columns with the exception that 0.5 cm sections were collected and 5 g of kaolin was used for persulfate analysis. The remaining soil from each section was dried at 105° C for 24 hr to determine the

water content. For the Palouse loess system, 10 ml of double deionized water was added to the 10 g soil sample, mixed with a Scientific Industries vortex for 15 sec, and centrifuged for 4 min. For the kaolin system, the sample was centrifuged for 6 min and was not filtered. A 0.1 ml sample of the supernatant was removed and filtered with Millipore 0.22 Millex[®] GP filters. The persulfate concentration was determined by iodometric titration, and concentration versus depth profiles were plotted in order to determine the depth of persulfate diffusion. The pH was also determined for each soil section.

Statistical Analysis

Statistical analyses were performed using Minitab version 15. Tukey's procedure with a 95% confidence level was used to compare treatments.

7. RESULTS AND ACCOMPLISHMENTS

7.1. Factors Controlling the Decomposition of Persulfate in the Subsurface

7.1.1. Persulfate Activation by Major Subsurface Minerals

Persulfate Decomposition in the Presence of Minerals

Persulfate activation was investigated in the presence of three iron oxides, one manganese oxide, and two clay minerals. Persulfate decomposition over 30 d in mineral systems at low pH (< 7) and at high pH (> 12) is shown in Figure 7.1.1.1a-b. In the low pH systems (Figure 7.1.1.1a), $\leq 15\%$ persulfate decomposition was observed in the presence of all of the minerals. The greatest persulfate decomposition occurred in the presence of birnessite (15%) followed by goethite (13%), while the other minerals (hematite, ferrihydrite, montmorillonite, and kaolinite) promoted persulfate decomposition of $\leq 8\%$. In the high pH systems, persulfate decomposed most rapidly in the presence of ferrihydrite with 24% loss over 30 d (Figure 7.1.1.1b). Persulfate decomposition did not vary significantly between hematite, birnessite, and goethite ($\alpha = 0.05$) and was 15–18% relative to the control. Persulfate decomposition in the presence of the clays montmorillonite and kaolinite (< 6%) was similar to that of the control ($\alpha = 0.05$).

In both the low pH and the high pH systems, the highest rates of persulfate decomposition occurred in the presence of iron and manganese oxides, and the lowest rates in the presence of the clay minerals. Rates of mineral-mediated catalysis are often proportional to the surface area of the mineral (Khan and Watts, 1996; Valentine and Wang, 1998; Kwan and Voelker 2003). Therefore, the data of Figure 7.1.1.1a-b were fit to first order kinetics, and the observed persulfate decomposition rate constants (k_{obs}) were normalized to the surface areas of the iron and manganese oxide minerals (Table 7.1.1.1). In the low pH systems, the normalized rate constant for persulfate decomposition (k_{norm}) for goethite was greater than for hematite. However, in the high pH systems, the k_{norm} for goethite was lower than for hematite. Liang et al. (2008b) postulated that soil organic matter, iron, manganese, and copper in soils could accelerate the decomposition of persulfate, although they did not investigate this hypothesis. Although mineral-mediated persulfate decomposition has not been studied to date, similar results were found during the mineral-mediated decomposition of hydrogen peroxide (Watts and Teel, 2005) Watts et al. (2007) similarly found that hydrogen peroxide decomposition rates were greater with goethite than with hematite at low pH, but lower with goethite than with hematite at high pH. Although the surface area of ferrihydrite was the highest among the minerals studied, relative persulfate decomposition was lower, which may be due to surface scavenging of reactive intermediates resulting in the generation of oxygen on the surface of ferrihydrite. Huang et al. (2001) and Miller and Valentine (1999) reported that in ferrihydrite-catalyzed hydrogen peroxide decomposition, the surface scavenging rate was larger than the hydrogen peroxide decomposition rate, which resulted in lower oxidant decomposition. A similar mechanism may be occurring in the ferrihydrite-mediated decomposition of persulfate.

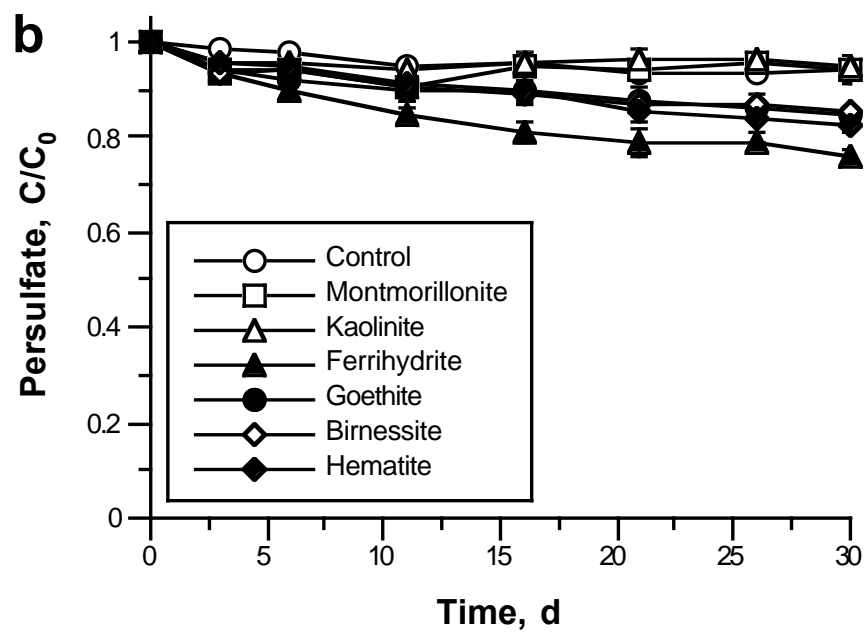
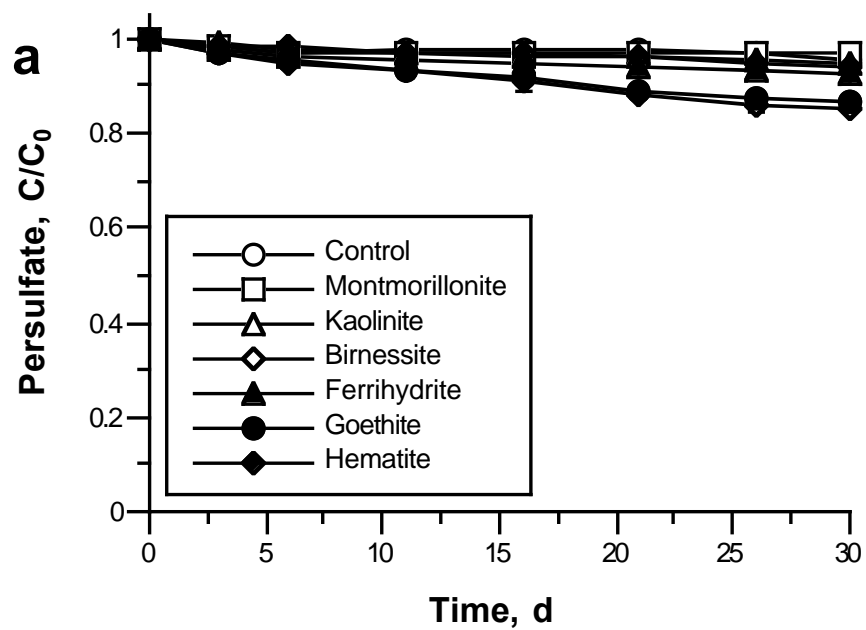


Figure 7.1.1.1. Persulfate decomposition in the presence of minerals. a) Low pH; b) high pH.

Table 7.1.1.1. Persulfate decomposition rate constants in persulfate systems at low and high pH in the presence of iron and manganese oxides

		Iron oxides			Manganese oxide
		Ferrihydrite	Goethite	Hematite	Birnessite
	Mass used (g)	0.5	2	2	1
	Surface area (m ² /g)	233	37	28	44
Low pH (< 7)	k _{obs}	$2.1 \pm 0.6 \times 10^{-3}$	$4.5 \pm 0.8 \times 10^{-3}$	$1.6 \pm 0.5 \times 10^{-3}$	$5.4 \pm 0.7 \times 10^{-3}$
	k _{norm}	$1.8 \pm 0.5 \times 10^{-5}$	$6.0 \pm 1.1 \times 10^{-5}$	$2.9 \pm 1.0 \times 10^{-5}$	$1.2 \pm 0.2 \times 10^{-4}$
High pH (> 12)	k _{obs}	$8.0 \pm 1.5 \times 10^{-3}$	$5.0 \pm 0.6 \times 10^{-3}$	$6.3 \pm 0.3 \times 10^{-3}$	$4.8 \pm 0.2 \times 10^{-3}$
	k _{norm}	$6.9 \pm 1.3 \times 10^{-5}$	$6.7 \pm 0.8 \times 10^{-5}$	$1.1 \pm 0.05 \times 10^{-4}$	$1.1 \pm 0.04 \times 10^{-4}$

95% confidence intervals shown

k_{obs} = observed 1st order rate constant (d⁻¹) calculated from the data of Figure 1a-b; k_{norm} = k_{obs}/((surface area)(mass)), (d⁻¹/m²)

Oxidant Generation in Mineral-Activated Persulfate Systems

Nitrobenzene was used as a probe to investigate the generation of oxidants in low and high pH mineral-catalyzed persulfate systems. Relative rates of oxidant generation in the low pH mineral-catalyzed systems, as measured by the oxidation of nitrobenzene, are shown in Figure 7.1.1.2a. In control systems containing no persulfate, no measurable loss of nitrobenzene was observed over the 7 d reaction time. In contrast, > 99% nitrobenzene degradation was achieved over 6 d in the presence of birnessite. However, nitrobenzene degradation in the presence of the other minerals was < 50% over 7 d, and did not vary significantly from the degradation achieved in the positive control system containing persulfate without minerals ($\alpha = 0.05$). These results demonstrate that the manganese oxide mineral birnessite promotes significant generation of oxidants in low pH persulfate systems, while the iron oxide minerals evaluated do not.

Relative oxidant generation rates in high pH persulfate systems in the presence of minerals, as quantified by loss of nitrobenzene, are shown in Figure 7.1.1.2b. The greatest oxidant generation over the 3 d reaction time occurred in the birnessite system with 92% nitrobenzene degradation. Liang et al. (2008a) found that degradation of BTEX in soil slurries was more rapid than in parallel aqueous systems. They postulated that naturally occurring soil minerals may activate persulfate. The results shown in Figure 7.1.1.2a-b demonstrate that the crystalline manganese oxide birnessite is responsible for oxidant generation from persulfate in soils. In the goethite system, 57% of the nitrobenzene degraded, which was not significantly different from the positive control ($\alpha = 0.05$). However, relative rates of oxidant generation in the hematite and ferrihydrite systems were lower than in the positive control. Some iron oxides may inhibit oxidant generation or scavenge oxidants; for example, quenching of hydroxyl radical

by iron oxides was reported by Miller and Valentine (1995). To account for differences in mineral surface area, the data of Figure 7.1.1.2a-b were fit to first order kinetics and the k_{obs} were normalized to the surface areas of the oxide minerals (Table 7.1.1.2). Normalizing the rate constants for surface area did not change the overall findings from Figure 7.1.1.2a-b; birnessite still promoted more rapid generation of oxidants than did the iron oxide minerals by a factor of almost two orders of magnitude in the low pH system, and almost one order of magnitude in the high pH system. The higher rate of manganese oxide-mediated oxidant generation may be due to the higher redox potential of manganese compared to iron (McBride, 1994), which has the potential to more rapidly decompose peroxygens.

Reductant Generation in Mineral-Activated Persulfate Systems

HCA was used as a probe compound to investigate the generation of reductants, such as superoxide radical and alkyl radicals, in low and high pH mineral-catalyzed persulfate systems. The degradation of HCA in low pH systems containing iron and manganese oxide minerals over 3 d is shown in Figure 7.1.1.3a. The highest relative rate of reductant generation was in the goethite system, with 75% loss of HCA over 3 d. Degradation of HCA in ferrihydrite and hematite systems was 24% and 19%, respectively. HCA degradation in the birnessite system was similar to that of the positive control at approximately 12% ($\alpha = 0.05$). In the control system, 6% of the HCA was lost, likely due to volatilization. The degradation of HCA in high pH mineral-catalyzed systems is shown in Figure 7.1.1.3b. In the presence of goethite, 89% of the HCA degraded in 24 hr, with > 99% degradation after 2 d. Degradation of HCA after 2 d in the hematite and ferrihydrite systems was 26% and 22%, respectively. HCA degradation in the birnessite system was 17%, similar to that of the positive control ($\alpha = 0.05$).

To account for differences in mineral surface area, the data of Figure 7.1.1.3a-b were fit to first order kinetics and the k_{obs} were normalized to the surface areas of the metal oxide minerals (Table 7.1.1.3). The normalized rate constants confirm that the order of mineral reactivity for relative reductant generation rates was similar between low pH and high pH systems, with goethite generating the greatest flux of reductants, hematite less, and birnessite and ferrihydrite the least. The data of Table 7.1.1.3 indicate that the iron mineral goethite catalyzes the generation of a reductant in both low and high pH systems, while hematite and ferrihydrite have only a small effect at both pH regimes. HCA degradation in the presence of the manganese oxide mineral birnessite was the lowest among all the minerals evaluated, and was similar to the positive control containing no minerals. The minimal reductant generation in the manganese oxide-activated persulfate systems is different from the rapid generation of reductants in manganese oxide-catalyzed hydrogen peroxide systems documented by Hasan et al. (1999), Watts et al. (2005), and Furman et al. (2009a). Reductant activity has also been documented in base-activated persulfate systems (Watts et al., 2008; Furman et al., 2009b), and is likely an important pathway that contributes to the widespread reactivity of persulfate formulations.

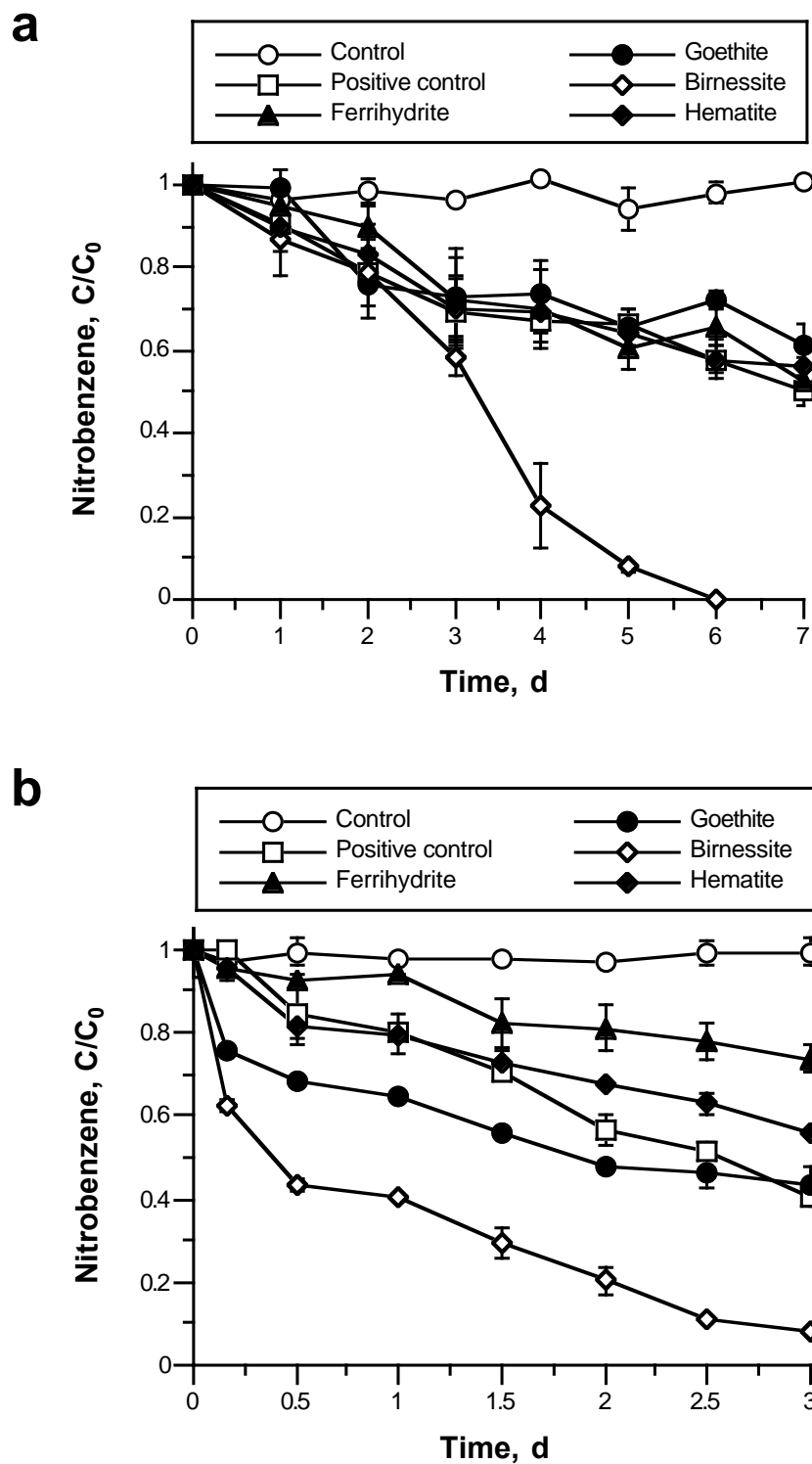


Figure 7.1.1.2. Degradation of the oxidant probe nitrobenzene in persulfate systems containing minerals. a) Low pH; b) high pH.

Table 7.1.1.2. Nitrobenzene decomposition rate constants in persulfate systems at low and high pH in the presence of iron and manganese oxides

		Iron oxides			Manganese oxide
		Ferrihydrite	Goethite	Hematite	Birnessite
	Mass used (g)	0.5	2	2	1
	Surface area (m ² /g)	233	37	28	44
Low pH (< 7)	k _{obs}	$6.4 \pm 1.7 \times 10^{-2}$	$5.1 \pm 1.2 \times 10^{-2}$	$5.6 \pm 1.3 \times 10^{-2}$	$2.2 \pm 0.5 \times 10^0$
	k _{norm}	$5.5 \pm 1.5 \times 10^{-4}$	$6.9 \pm 1.6 \times 10^{-4}$	$1.0 \pm 0.2 \times 10^{-3}$	$5.0 \pm 1.1 \times 10^{-2}$
High pH (> 12)	k _{obs}	$8.3 \pm 1.4 \times 10^{-2}$	$3.2 \pm 0.4 \times 10^{-1}$	$1.7 \pm 0.1 \times 10^{-1}$	$7.7 \pm 0.4 \times 10^{-1}$
	k _{norm}	$7.1 \pm 0.3 \times 10^{-4}$	$6.7 \pm 0.8 \times 10^{-3}$	$3.0 \pm 0.2 \times 10^{-3}$	$1.8 \pm 0.1 \times 10^{-2}$

95% confidence intervals shown

k_{obs} = observed 1st order rate constant (d⁻¹) calculated from the data of Figure 2a-b; k_{norm} = k_{obs}/((surface area)(mass)), (d⁻¹/m²)

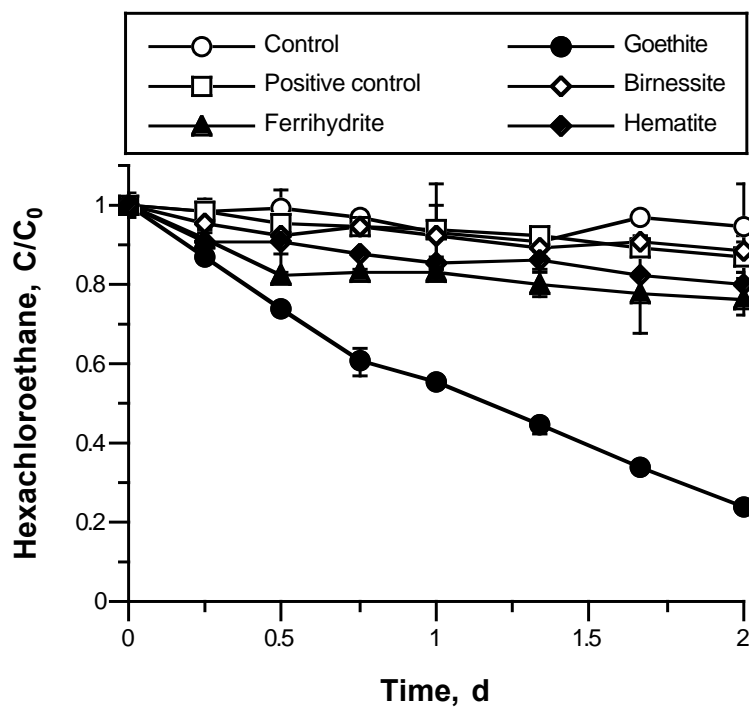
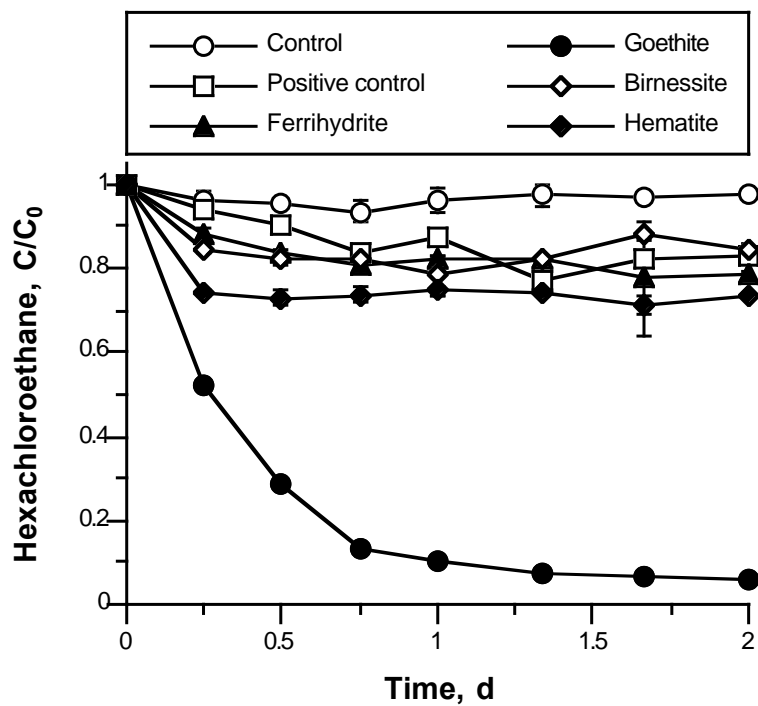
a**b**

Figure 7.1.1.3. Degradation of the reductant probe HCA in persulfate systems containing minerals. a) Low pH; b) high pH.

Table 7.1.1.3. HCA decomposition rate constants in persulfate systems at low and high pH in the presence of iron and manganese oxides

		Iron oxides			Manganese oxide
		Ferrihydrite	Goethite	Hematite	Birnessite
	Mass used (g)	0.5	2	2	1
	Surface area (m ² /g)	233	37	28	44
Low pH (< 7)	k _{obs}	$9.2 \pm 2.1 \times 10^{-2}$	$6.9 \pm 0.2 \times 10^{-1}$	$8.6 \pm 1.5 \times 10^{-2}$	$5.9 \pm 1.5 \times 10^{-2}$
	k _{norm}	$7.9 \pm 1.8 \times 10^{-4}$	$9.3 \pm 0.3 \times 10^{-3}$	$1.5 \pm 0.3 \times 10^{-3}$	$1.3 \pm 0.3 \times 10^{-3}$
High pH (> 12)	k _{obs}	$9.3 \pm 3.1 \times 10^{-2}$	$1.4 \pm 0.1 \times 10^0$	$8.1 \pm 2.9 \times 10^{-2}$	$3.3 \pm 2.5 \times 10^{-2}$
	k _{norm}	$8.0 \pm 2.7 \times 10^{-4}$	$1.9 \pm 0.1 \times 10^{-2}$	$1.4 \pm 0.5 \times 10^{-3}$	$7.5 \pm 5.7 \times 10^{-4}$

95% confidence intervals shown

k_{obs} = observed 1st order rate constant (d⁻¹) calculated from the data of Figure 3a-b; k_{norm} = k_{obs}/((surface area)(mass)), (d⁻¹/m²)

Oxidant Generation in Clay Mineral-Activated Persulfate Systems

The effect of the clay minerals montmorillonite and kaolinite on oxidant generation was investigated in the low and high pH persulfate systems. Relative rates of oxidant generation, quantified by nitrobenzene degradation, in the low pH system over 4.5 d is shown in Figure 7.1.1.4a. In the low pH kaolinite system nitrobenzene degradation was 45%, which was the same as the positive control ($\alpha = 0.05$). Nitrobenzene degradation in the montmorillonite system was lower, at 29%. In the high pH system (Figure 7.1.1.4b), nitrobenzene degradation was approximately 92% in the presence of kaolinite as well as in the positive control, while degradation was approximately 82% in the montmorillonite system. These data show that clay minerals do not promote the generation of oxidants in either the low pH or high pH systems. Furthermore, montmorillonite may scavenge oxidants or inhibit their generation, similar to scavenging of hydroxyl radical by iron oxides (Miller and Valentine, 1995).

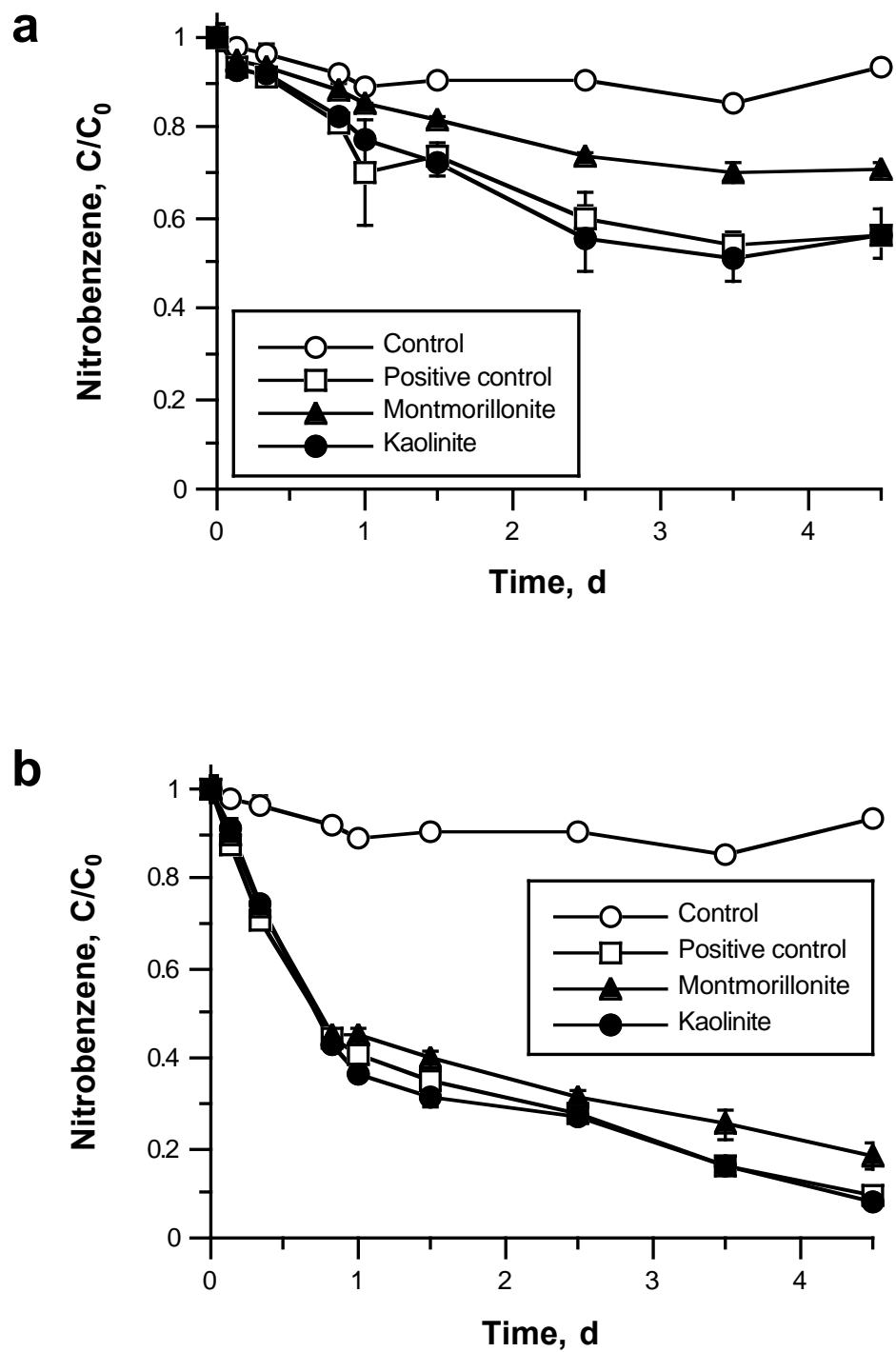


Figure 7.1.1.4. Degradation of the oxidant probe nitrobenzene in persulfate systems containing clay minerals. a) Low pH; b) high pH.

Reductant Generation in Clay Mineral-Activated Persulfate Systems

The relative generation rates of reductants were quantified in low pH and high pH persulfate systems containing the clay minerals montmorillonite and kaolinite. The degradation of the reductant probe HCA over 2 d is shown in Figure 7.1.1.5a-b. In the low pH systems < 15% loss of HCA was observed in the presence of both montmorillonite and kaolinite, which was not significantly different from the control or the positive control ($\alpha = 0.05$). In the high pH systems, HCA loss was approximately 19% with both kaolinite and montmorillonite, which was again similar to the control and positive control. These results demonstrate that at both low and high pH regimes, clay minerals do not promote significant reductant generation in persulfate systems.

In summary, the results of the mineral-activated persulfate studies using stocks of pure minerals as catalysts show that 1) most of the minerals studied did not activate persulfate, 2) birnessite activated persulfate to generate hydroxyl radical at low and high pH regimes, and 3) goethite activated persulfate to generate reductants at both low and high pH regimes. The results of Figure 7.1.1.2a-b and Figure 7.1.1.4a-b demonstrate that hydroxyl radical is generated in acid-activated and base-activated persulfate systems, and that some minerals quench hydroxyl radical while others have no influence relative to the positive control. The mineralogy of a contaminated site affects the activation and reactivity of persulfate that is injected into the subsurface; therefore, understanding characteristics of the subsurface, such as the crystalline and amorphous iron and manganese oxide content, will aid in predicting persulfate reactivity in the subsurface. For example, goethite is a primary form of crystalline iron oxide and birnessite is a primary form of crystalline manganese oxide. Subsurface solids containing high concentrations of crystalline iron or manganese oxides may exhibit enhanced persulfate activation. In contrast, subsurface solids with high amorphous iron oxide contents would contain ferrihydrite, which scavenges hydroxyl radical.

Persulfate Decomposition in the Presence of Soil and Soil Fractions

To further investigate mineral activation of persulfate during ISCO, a natural soil from Palouse, WA, (“total soil”) was treated with specific reagents to generate a fraction containing minerals but no soil organic matter (“mineral fraction”), and a fraction containing iron oxides but no manganese oxides (“iron fraction”). The total soil and the soil fractions were investigated for their potential to promote persulfate decomposition in low and high pH regimes over 7 d (Figure 7.1.1.6a-b). In the low pH persulfate system, minimal persulfate decomposition of < 12% was observed in the total soil as well as the two soil fractions and the positive control. In the high pH system, persulfate decomposition was similarly low in slurries of the modified soil fractions; however, 85% persulfate decomposition over 7 d was observed in the presence of the total soil. To account for differences in surface areas, the persulfate decomposition data of Figure 7.1.1.6a-b were fit to first order kinetics and the k_{obs} were normalized to the surface areas of the soil and soil fractions (Table 7.1.1.4). The small differences in surface areas did not affect trends in persulfate decomposition. These results indicate that, at high pH, the soil organic matter that was present in the total soil promoted persulfate decomposition. The presence of phenols at basic pH has been shown to activate persulfate via Elbs oxidation (Sethna, 1951); soil organic matter contains a large proportion of phenolic compounds and a similar mechanism is likely occurring in the presence of soil organic matter at high pH.

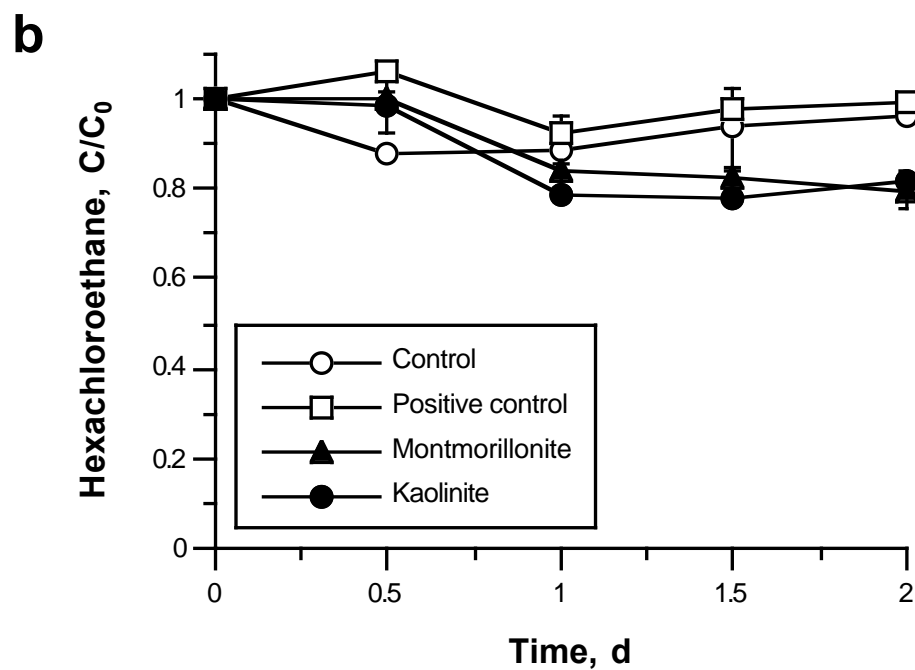
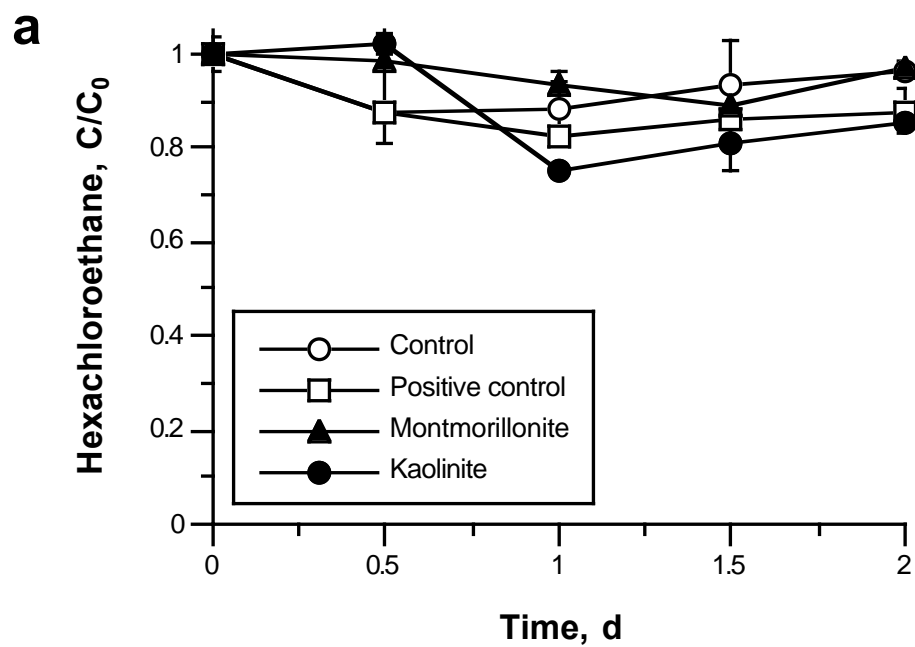


Figure 7.1.1.5. Degradation of the reductant probe HCA in persulfate systems containing clay minerals. a) Low pH; b) high pH.

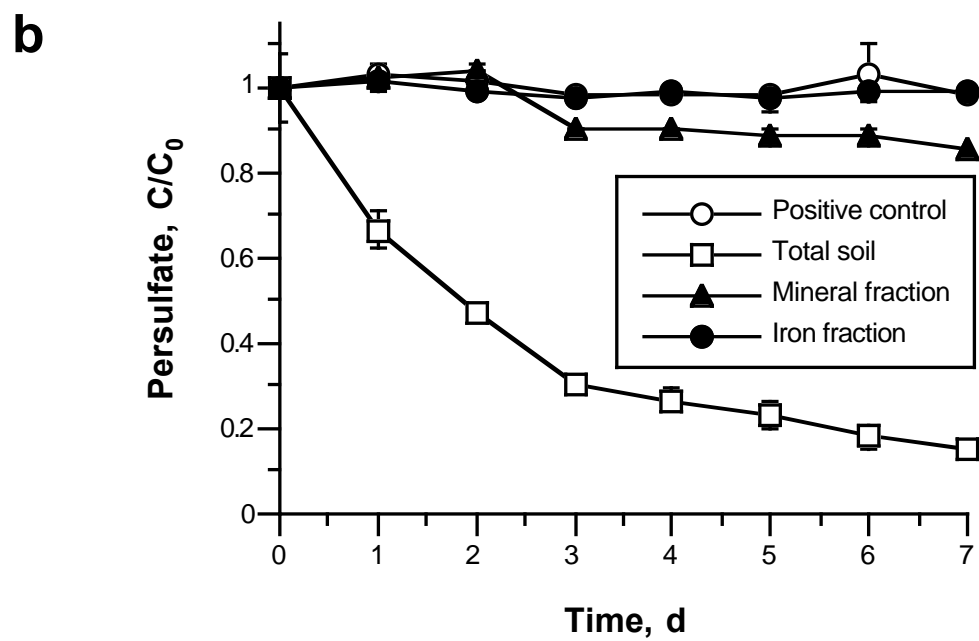
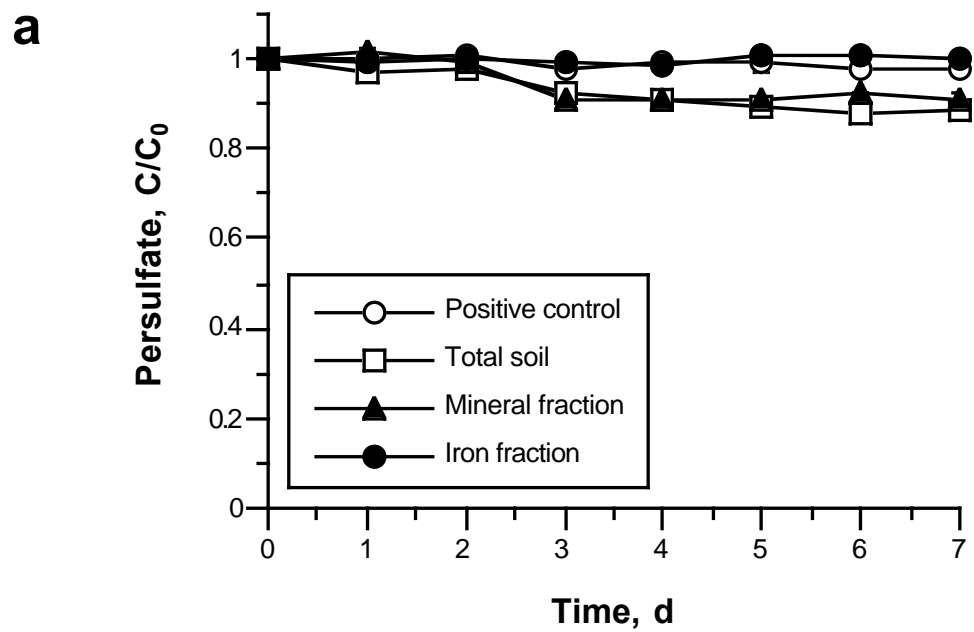


Figure 7.1.1.6. Persulfate decomposition in the presence of a soil and soil fractions. a) Low pH; b) high pH.

Table 7.1.1.4. Persulfate decomposition rate constants in persulfate systems at low and high pH in the presence of total soil and two soil fractions

		Total soil	Mineral fraction (After SOM removal)	Iron fraction (After manganese oxides removal)
	Mass used (g)	5	5	5
	Surface area (m ² /g)	23.5	24	19
Low pH (< 7)	k _{obs}	$2.0 \pm 0.2 \times 10^{-2}$	$1.5 \pm 0.3 \times 10^{-2}$	$8.5 \pm 11 \times 10^{-4}$
	k _{norm}	$1.7 \pm 0.2 \times 10^{-4}$	$1.3 \pm 0.9 \times 10^{-4}$	$8.9 \pm 12 \times 10^{-6}$
High pH (> 12)	k _{obs}	$2.6 \pm 1.3 \times 10^{-1}$	$2.9 \pm 0.4 \times 10^{-2}$	$2.9 \pm 2.0 \times 10^{-3}$
	k _{norm}	$2.2 \pm 1.1 \times 10^{-3}$	$2.4 \pm 0.3 \times 10^{-4}$	$3.1 \pm 2.1 \times 10^{-5}$

95% confidence intervals shown

k_{obs} = observed 1st order rate constant (d⁻¹) calculated from the data of Figure 6a-b; k_{norm} = k_{obs}/((surface area)(mass)), (d⁻¹/m²)

Oxidant Generation in the Presence of Soil and Soil Fractions

Relative rates of oxidant generation were investigated in low and high pH persulfate systems containing the total soil and soil mineral fractions. The degradation of the oxidant probe nitrobenzene in the low pH system over 7 d is shown in Figure 7.1.1.7a. Nitrobenzene degradation was not significantly different between any of the soil fractions ($\alpha = 0.05$). Although the total soil and the mineral fraction contained manganese oxides, they did not promote the generation of oxidants, unlike the synthetic manganese oxide birnessite in the low pH mineral system (Figure 7.1.1.2a). The results of Figure 7.1.1.7a show that none of the soil fractions activated persulfate to generate oxidants at low pH regimes, which may be due to the low concentrations of birnessite in the soil (Table 6.1.1.2).

Relative oxidant generation rates over 7 d in the total soil and the two soil mineral fractions at high pH, quantified by the degradation of nitrobenzene, are shown in Figure 7.1.1.7b. The greatest nitrobenzene degradation occurred in the positive control at 87%. Nitrobenzene degradation was not significantly different ($\alpha = 0.05$) between the total soil and the iron fraction (68%-79%), while nitrobenzene degraded 52% in the mineral fraction. The results of Figure 7.1.1.7b show that oxidant reactivity was lower in all soil fractions relative to the positive control (i.e., persulfate without soil). The lower reactivity is likely due to scavenging of oxidant as has been reported for hydroxyl radical by soil organic matter (Bissey et al., 2006; Liang et al., 2008a) or the inorganic fraction of the soil (Miller and Valentine, 1995). When the rate constants were normalized for the small differences in surface area, there was no effect on these trends (Table 7.1.1.5).

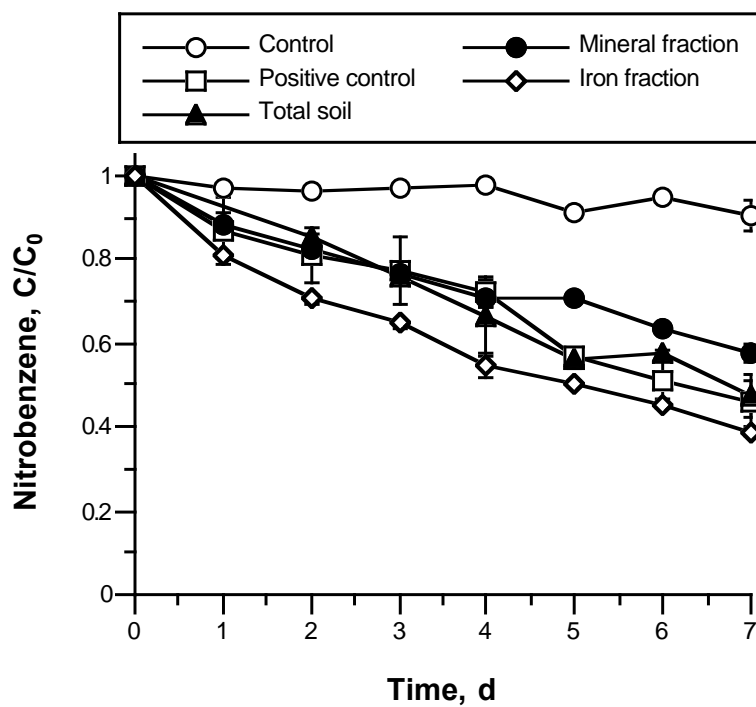
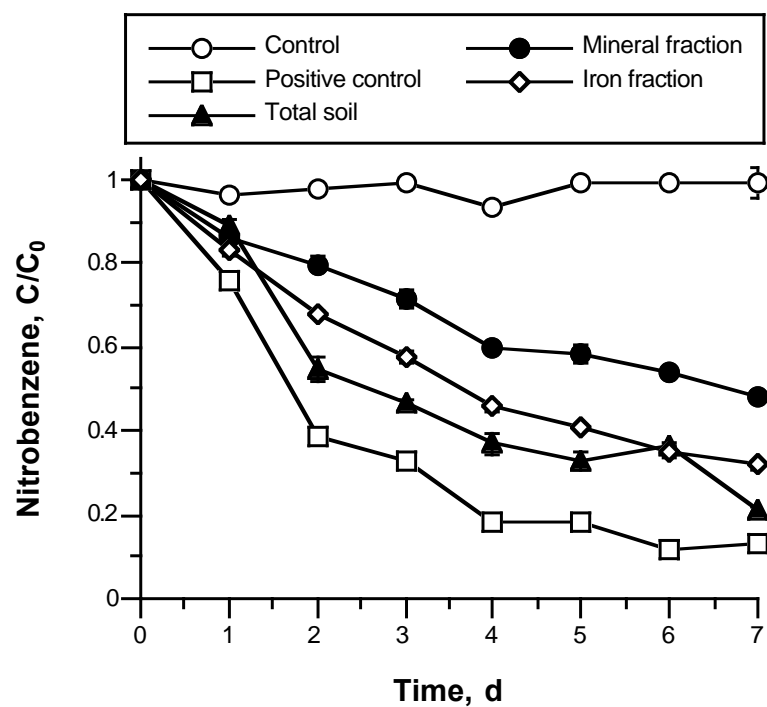
a**b**

Figure 7.1.1.7. Degradation of the oxidant probe nitrobenzene in persulfate systems containing a soil and soil fractions. a) Low pH; b) high pH.

Table 7.1.1.5. Nitrobenzene decomposition rate constants in persulfate systems at low and high pH in the presence of total soil and two soil fractions

		Total soil	Mineral fraction (After SOM removal)	Iron fraction (After manganese oxides removal)
	Mass used (g)	5	5	5
	Surface area (m ² /g)	23.5	24	19
Low pH	k _{obs}	$9.5 \pm 1.1 \times 10^{-2}$	$7.2 \pm 0.3 \times 10^{-2}$	$1.3 \pm 0.05 \times 10^{-1}$
(< 7)	k _{norm}	$8.1 \pm 0.9 \times 10^{-4}$	$6.0 \pm 0.3 \times 10^{-4}$	$1.4 \pm 0.05 \times 10^{-3}$
High pH	k _{obs}	$2.0 \pm 0.2 \times 10^{-1}$	$1.0 \pm 0.04 \times 10^{-1}$	$1.7 \pm 0.05 \times 10^{-1}$
(> 12)	k _{norm}	$1.7 \pm 1.7 \times 10^{-3}$	$8.3 \pm 0.03 \times 10^{-4}$	$1.8 \pm 0.05 \times 10^{-3}$

95% confidence intervals shown

k_{obs} = observed 1st order rate constant (d⁻¹) calculated from the data of Figure 7a-b; k_{norm} = k_{obs}/((surface area)(mass)), (d⁻¹/m²)

Reductant Generation in the Presence of Soil and Soil Fractions

Degradation of the reductant probe HCA in the total soil and soil fractions at low pH is shown in Figure 7.1.1.8a. After 2 d, the degradation of HCA in the mineral fraction was 66% and in the total soil was 45%. HCA degradation was < 20% in the control, positive control, and iron fraction systems, which indicates that iron minerals did not activate persulfate to form reductants. HCA degradation in the high pH persulfate systems over 2 d is shown in Figure 7.1.1.8b. In the presence of the total soil at high pH, HCA degraded rapidly to an undetectable concentration in 4 h; in contrast, HCA loss in the soil fractions without SOM was 22%–33% after 2 d, and was not significantly different from the control or the positive control ($\alpha = 0.05$). In the high pH persulfate system, the rapid degradation of HCA in the presence of the total soil was likely the result of reductant generation through reactions of persulfate with the phenolic compounds in SOM through the Elbs persulfate oxidation mechanism (Sethna, 1951). Similar to the results of relative rates of hydroxyl radical generation (Table 7.1.1.5), normalizing the rate constants for surface area provided no difference in reductant generation trends (Table 7.1.1.6).

The results of persulfate activation by different fractions of a natural soil at low pH show that 1) persulfate decomposition was slow in all soil fractions, 2) rates of hydroxyl radical generation were not significantly different from the controls, and 3), rates of reductant generation were highest in the mineral fraction, followed by the total soil. In the systems at high pH, 1) persulfate decomposition was high only in the total soil, 2) hydroxyl radical generation in all soil fractions was lower than in the positive control, and 3) reductant generation was rapid in the total soil and negligible in all of the other soil fractions.

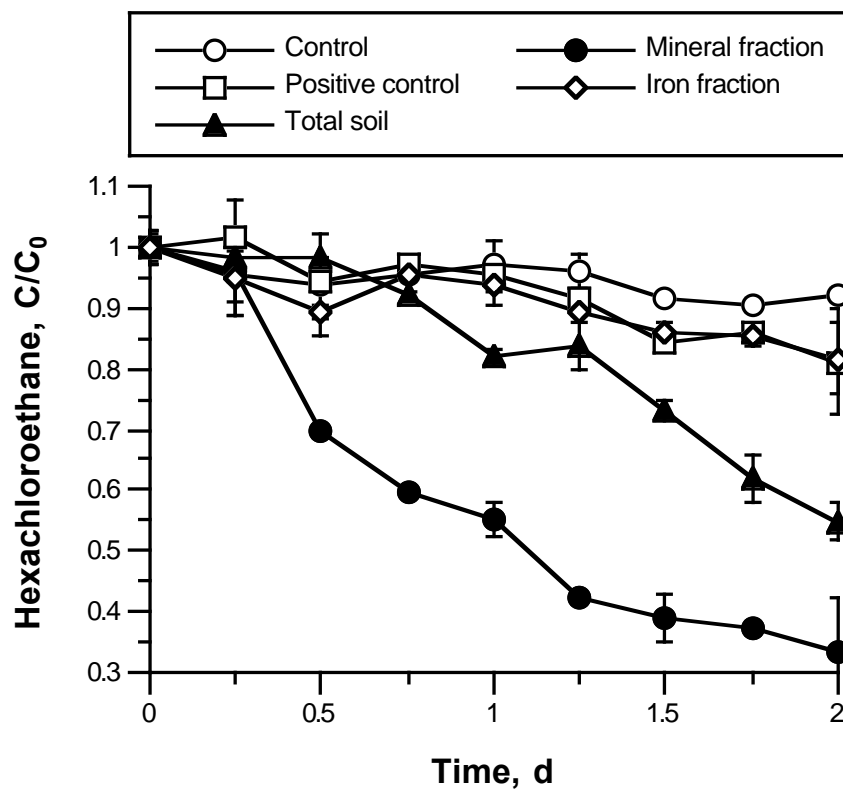
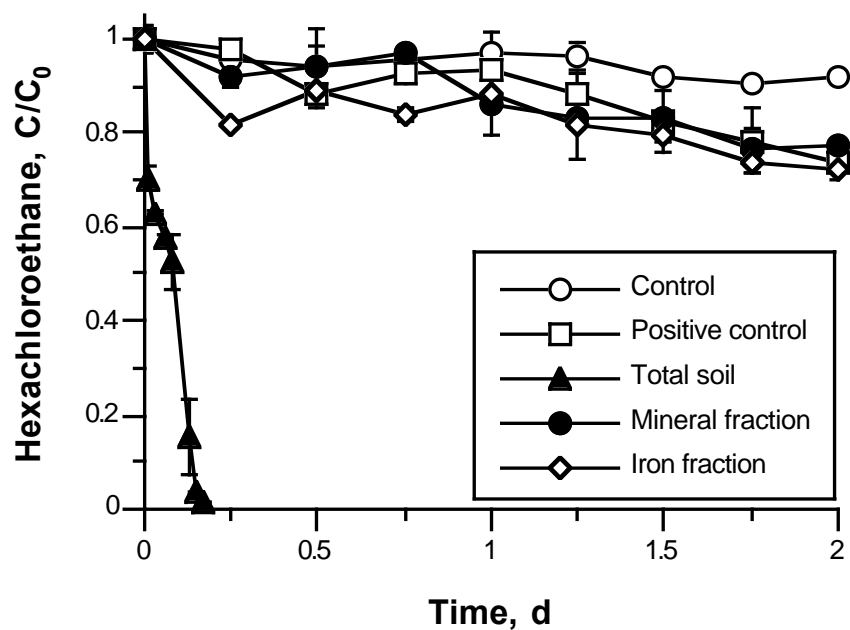
a**b**

Figure 7.1.1.8. Degradation of the reductant probe HCA in persulfate systems containing a soil and soil fractions. a) Low pH; b) high pH.

Table 7.1.1.6. HCA decomposition rate constants in persulfate systems at low and high pH in the presence of total soil and two soil fractions

		Total soil	Mineral fraction (After SOM removal)	Iron fraction (After manganese oxides removal)
	Mass used (g)	5	5	5
	Surface area (m ² /g)	23.5	24	19
Low pH	k _{obs}	$3.0 \pm 0.3 \times 10^{-1}$	$5.8 \pm 0.5 \times 10^{-1}$	$7.8 \pm 2.7 \times 10^{-2}$
(< 7)	k _{norm}	$2.6 \pm 0.3 \times 10^{-3}$	$4.8 \pm 0.5 \times 10^{-3}$	$8.2 \pm 2.8 \times 10^{-4}$
High pH	k _{obs}	$2.5 \pm 0.3 \times 10^1$	$1.3 \pm 0.3 \times 10^{-1}$	$9.7 \pm 3.1 \times 10^{-2}$
(> 12)	k _{norm}	$2.1 \pm 0.3 \times 10^{-1}$	$1.1 \pm 0.3 \times 10^{-3}$	$1.0 \pm 0.3 \times 10^{-3}$

95% confidence intervals shown

k_{obs} = observed 1st order rate constant (d⁻¹) calculated from the data of Figure 8a-b; k_{norm} = k_{obs}/((surface area)(mass)), (d⁻¹/m²)

The results of Figure 7.1.1.7-8 are not in agreement with the data of Figure 7.1.1.2-3; i.e., birnessite did not appear to promote the generation and reactivity of oxidants and goethite did not appear to promote the generation of reductants in the total soil. A possible reason for the negligible amount of birnessite- and goethite-mediated reactivity in the total soil and soil fractions may be the lower masses of these minerals in the soil. To evaluate this possibility, persulfate decomposition was catalyzed by birnessite and goethite with lower masses than those used in Figure 7.1.1.2-3 (0.004 g – 1.75 g birnessite and 0.03 g – 1.00 g goethite). The results of birnessite-catalyzed generation of oxidants and reductants at low and high pH are shown in Figure 7.1.1.9a-b. Birnessite masses ≤ 0.05 g promoted oxidant generation in the low pH system at rates slower than the positive control (Figure 7.1.1.9a). Similarly, birnessite masses ≤ 0.02 g promoted oxidant generation in high pH systems at rates that were not significantly different from the positive control ($\alpha = 0.05$) (Figure 7.1.1.9b). Similar trends were evident in the generation of reductants (Figure 7.1.1.10a-b). Goethite-mediated reductant generation rates at low pH were not significantly greater than in the positive control when the mass of goethite was ≤ 0.10 g ($\alpha = 0.05$) (Figure 7.1.1.10a). At high pH, reductant generation with goethite masses ≤ 0.03 g did not generate reductants at rates different from the positive control ($\alpha = 0.05$) (Figure 7.1.1.10b). The mass of crystalline manganese oxides in the total soil was 0.00026 g, and the total mass of crystalline iron oxides was 0.0039 g. Each of these masses is well below the mineral mass that would activate persulfate; therefore, the masses of birnessite and goethite in the soil used in this study were too low to activate persulfate.

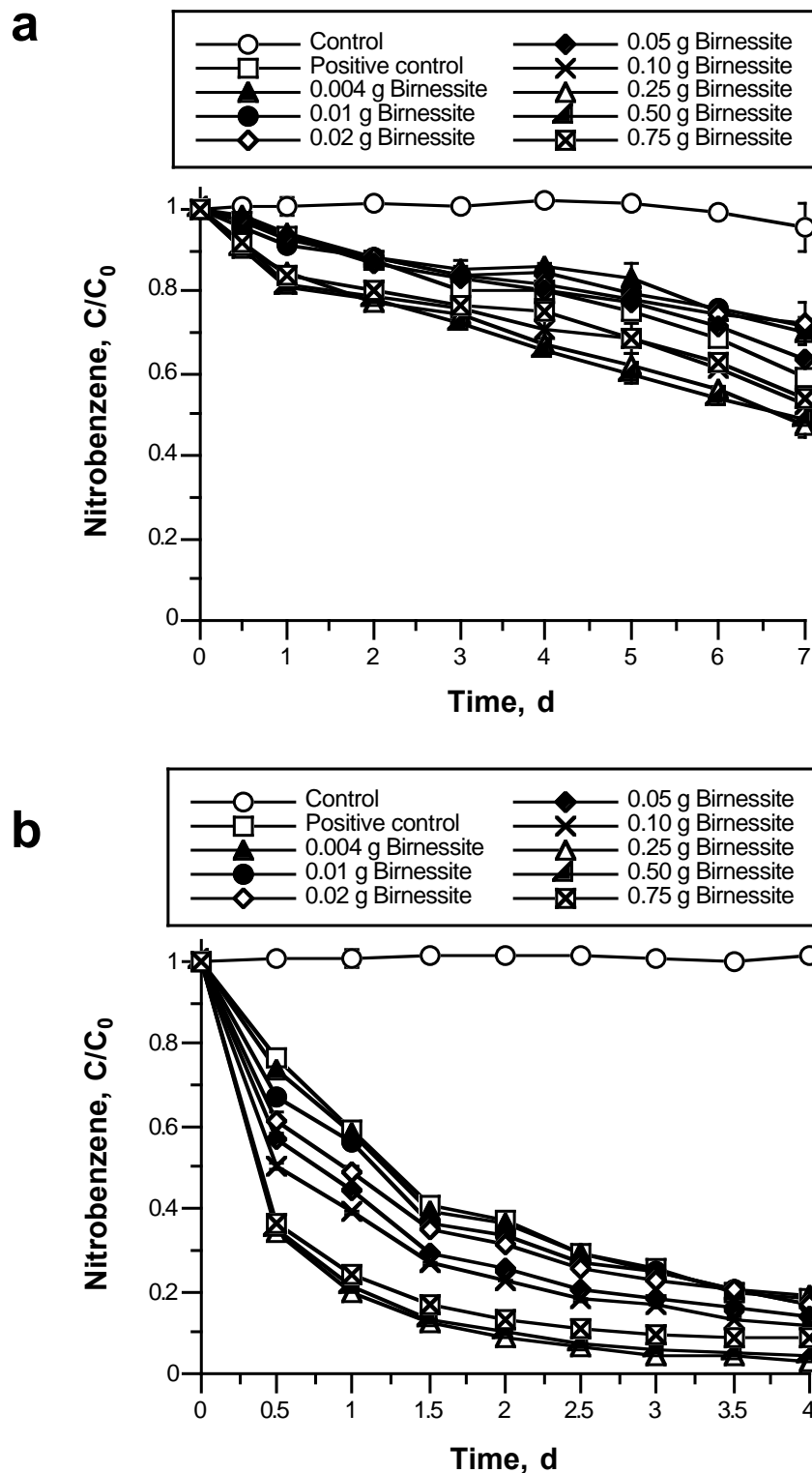


Figure 7.1.1.9. Degradation of the oxidant probe nitrobenzene in persulfate systems containing low concentrations of the manganese oxide birnessite. a) Low pH; b) high pH.

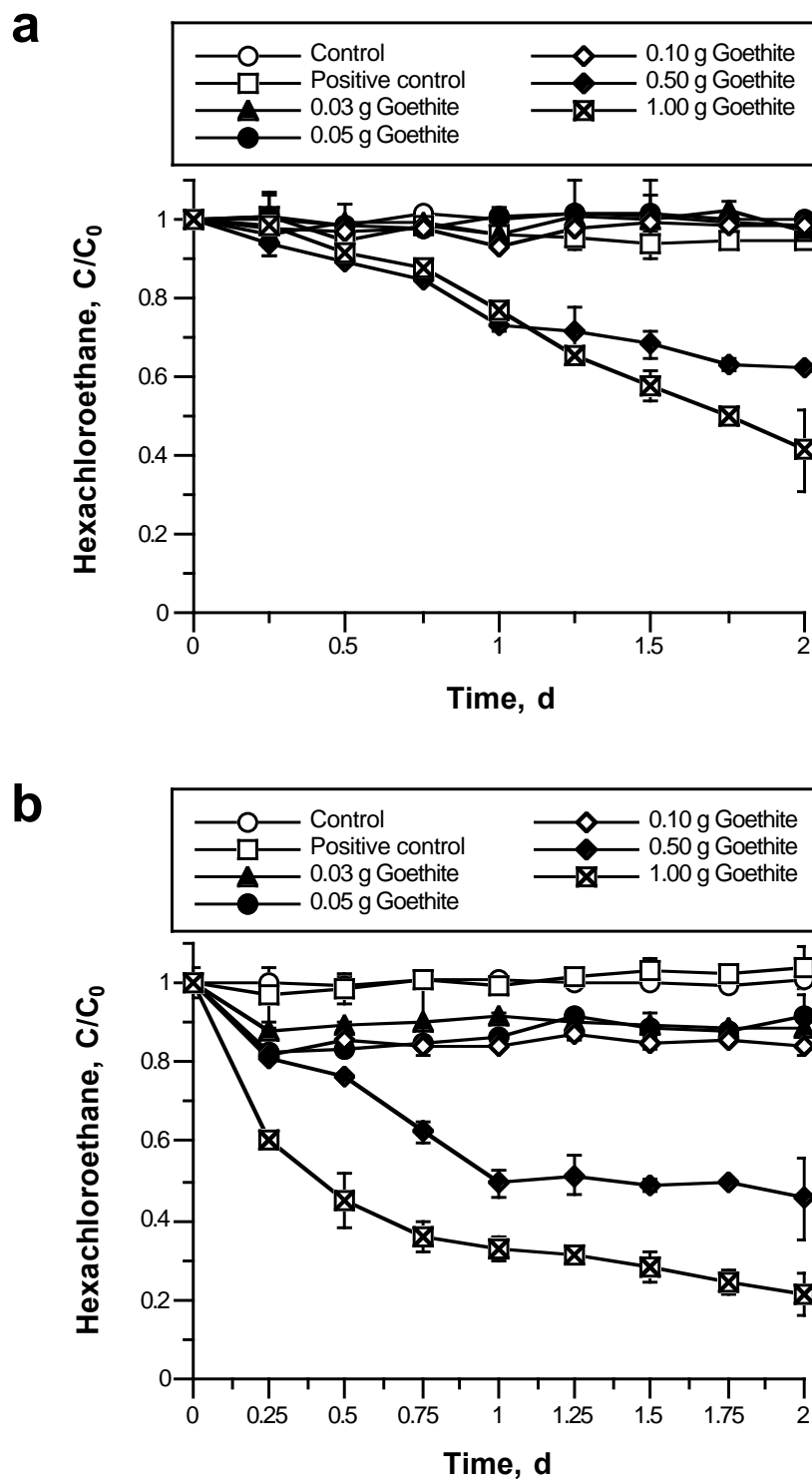


Figure 7.1.1.10. Degradation of the oxidant probe nitrobenzene in persulfate systems containing low concentrations of the iron oxide goethite. a) Low pH; b) high pH.

Conclusions

The potential for persulfate activation by three iron oxides, a manganese oxide, and two clay minerals was investigated in high pH (> 12) and low pH (< 7) systems. Positive control systems consisting of acid-activated and base-activated persulfate without minerals provided relatively high rates of oxidant generation. In both the high and low pH systems, the manganese oxide mineral birnessite was the most active initiator for generating additional fluxes of oxidants, and the iron oxide mineral goethite was the most active initiator for generating reductants relative to the positive controls. The clay minerals kaolinite and montmorillonite did not show detectable persulfate activation in the generation either oxidants or reductants relative to positive controls.

A natural soil and two fractions of the soil were also studied. The natural soil minerals in the total soil and soil fractions were not effective in catalyzing persulfate to generate reactive oxygen species. However, SOM was highly active in promoting the generation of reductants in the high pH persulfate system.

Minimal persulfate decomposition was seen in both mineral systems and soil fractions at low pH. However, persulfate decomposition at high pH was approximately 85% in the presence of the total soil after 7 d. In the presence of each of the minerals, persulfate decomposition was $< 25\%$ after 30 d. At high pH, the surface area-normalized rate of persulfate decomposition in the presence of all of the iron and manganese oxides did not vary significantly. Persulfate was not activated by crystalline iron oxides and manganese oxides in the natural soil because the masses of crystalline iron and manganese oxides were too low to provide significant activation.

The results of this research demonstrate that, although relatively high masses of birnessite and goethite can activate persulfate to generate reactive oxygen species, the mineral components of the soil evaluated did not promote measurable activation of persulfate. These findings suggest that the crystalline iron and manganese oxide contents typically found in soils are not sufficient to promote persulfate activation during ISCO applications. In contrast, the presence of SOM in high pH persulfate systems promoted significant reductant activity. SOM has traditionally been considered a negative in ISCO applications because it creates a demand on the oxidant; however, the results of this research demonstrate that SOM can promote the generation of reductants during persulfate ISCO applications.

7.1.2. Persulfate Activation by Subsurface Trace Minerals

Trace Mineral-Mediated Decomposition of Persulfate

The decomposition of persulfate mediated by 13 trace minerals is shown in Figure 7.1.2.1. The rates of mineral-mediated persulfate decomposition ranged substantially; therefore, the minerals were classified into four distinct groups based on the rates at which they promoted the decomposition of persulfate. The group of minerals that promoted rapid persulfate decomposition (cobaltite and pyrite) was characterized by >90% decomposition of persulfate within 12-36 hr. The minerals classified as slowly decomposing persulfate (ilmenite and siderite) promoted the decomposition of persulfate over approximately 20 d. The control group (pyrolusite and hematite) was characterized by an undetectable change in persulfate decomposition compared to aqueous controls. The fourth group of minerals (calcite, anatase, bauxite, cuprite, malachite, willemite, magnesite) demonstrated persulfate decomposition rates that were slower than that of persulfate decomposition in deionized water controls.

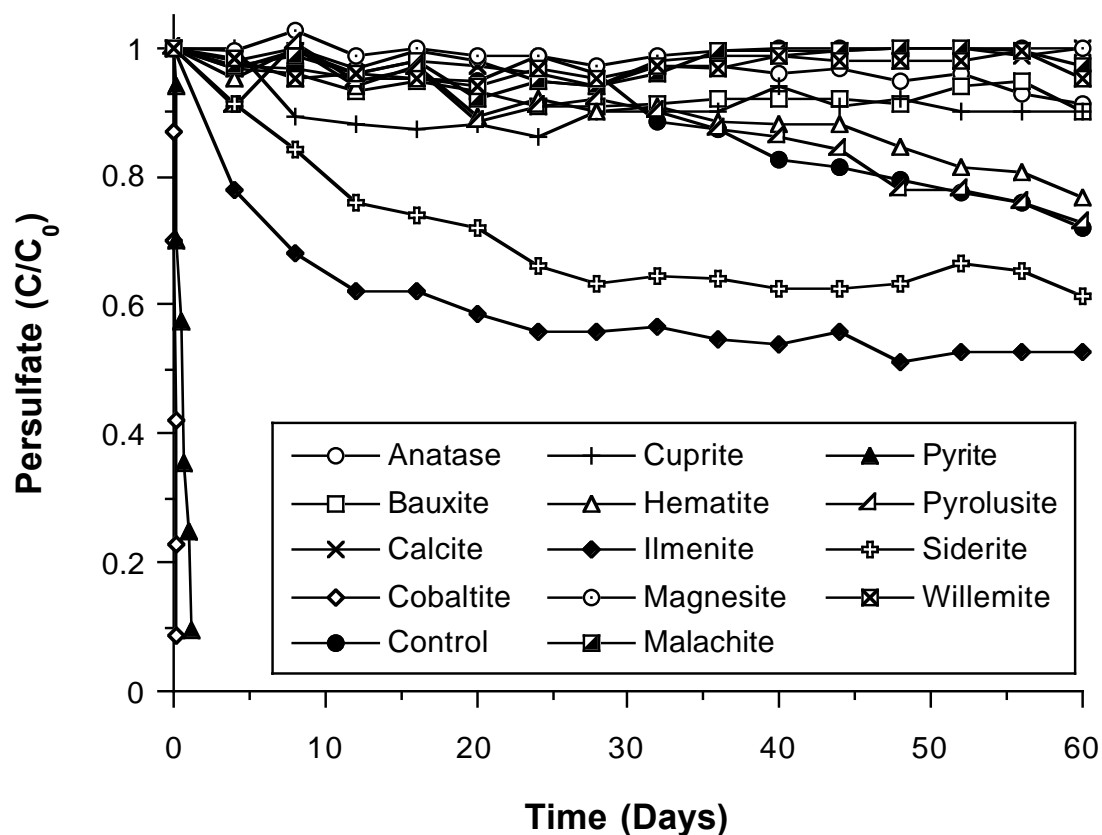


Figure 7.1.2.1. Degradation of 0.5 M sodium persulfate by 13 various trace minerals with the temperature maintained at 25°C ± 1°C.

Most of the minerals retarded or had minimal effect on the rate of persulfate decomposition, while four minerals (pyrite, cobaltite, ilmenite, and siderite) increased the rate of persulfate decomposition. There was no correlation found between mineral surface areas and rates of persulfate decomposition. In addition, the metal composition of the minerals appeared to be a weak predictor of the potential for a mineral to decompose persulfate. For example, ilmenite, pyrite, and siderite are Fe (II) minerals. Ilmenite and siderite were slow in decomposing persulfate, whereas pyrite was the rapid. Persulfate decomposition mediated by Fe (II)-based minerals was no greater than hematite-mediated persulfate decomposition (hematite was the only Fe (III) mineral evaluated). Unlike the iron minerals, the copper-based minerals showed no difference in persulfate decomposition rates between the Cu (I) of cuprite and the Cu (II) of malachite.

Survey of Generation of Reactive Oxygen Species

Anisole-persulfate decomposition studies were conducted over 24 hr; 60% degradation of the cumulative sulfate + hydroxyl radical probe compound anisole was observed in persulfate systems containing no minerals. Mineral-mediated persulfate decomposition rates correlated with corresponding rates of sulfate + hydroxyl radical generation, which was quantified by the oxidation of anisole. However, a few exceptions were found. Cobaltite promoted the most rapid decomposition of persulfate, but slowed the relative rate of sulfate + hydroxyl radical generation (measured by anisole loss) by 20%. Conversely, malachite mediated minimal decomposition of persulfate, but promoted rapid generation of sulfate + hydroxyl radicals.

Relative rates of hydroxyl radical generation (quantified by nitrobenzene oxidation) are shown in Figure 7.1.2.2b. Minimal loss of nitrobenzene occurred in nitrobenzene-deionized water systems, and nitrobenzene loss was 40% in persulfate-deionized water systems. Similar to the data shown in Figure 7.1.2.2a, relative hydroxyl radical generation rates usually correlated with persulfate decomposition rates. Cobaltite and pyrolusite-mediated persulfate systems promoted less hydroxyl radical generation relative to persulfate decomposition compared to the other 11 minerals.

Relative rates of hydroperoxide generation, quantified by the loss of TNB, in mineral-persulfate systems are shown in Figure 7.1.2.2c. Cobaltite-, cuprite-, ilmenite-, and magnesite-persulfate systems promoted the generation of hydroperoxide more rapidly than persulfate-deionized water systems. Conversely, pyrite-, and siderite-persulfate systems promoted lower rates of hydroperoxide generation relative to persulfate-deionized water systems. Relative hydroperoxide generation rates for anatase, bauxite, calcite, pyrolusite, malachite and willemite were not significantly different from hydroperoxide generation rates in persulfate-deionized water systems. These results demonstrate that pyrite-mediated decomposition of persulfate is proceeding through oxidative pathways, and not generating a significant flux of nucleophiles. Although cobaltite rapidly promotes the decomposition of persulfate, it slowly generates hydroperoxide.

The relative generation of reductants, such as superoxide, using carbon tetrachloride as a reductant probe, is shown in Figure 7.1.2.2d. Calcite-, ilmenite-, magnesite-, and pyrolusite-persulfate systems promoted the generation of reductants at rates exceeding that of persulfate-deionized water systems. The nine other minerals promoted the generation of reductants at rates lower than or equal to that of the persulfate-deionized water system.

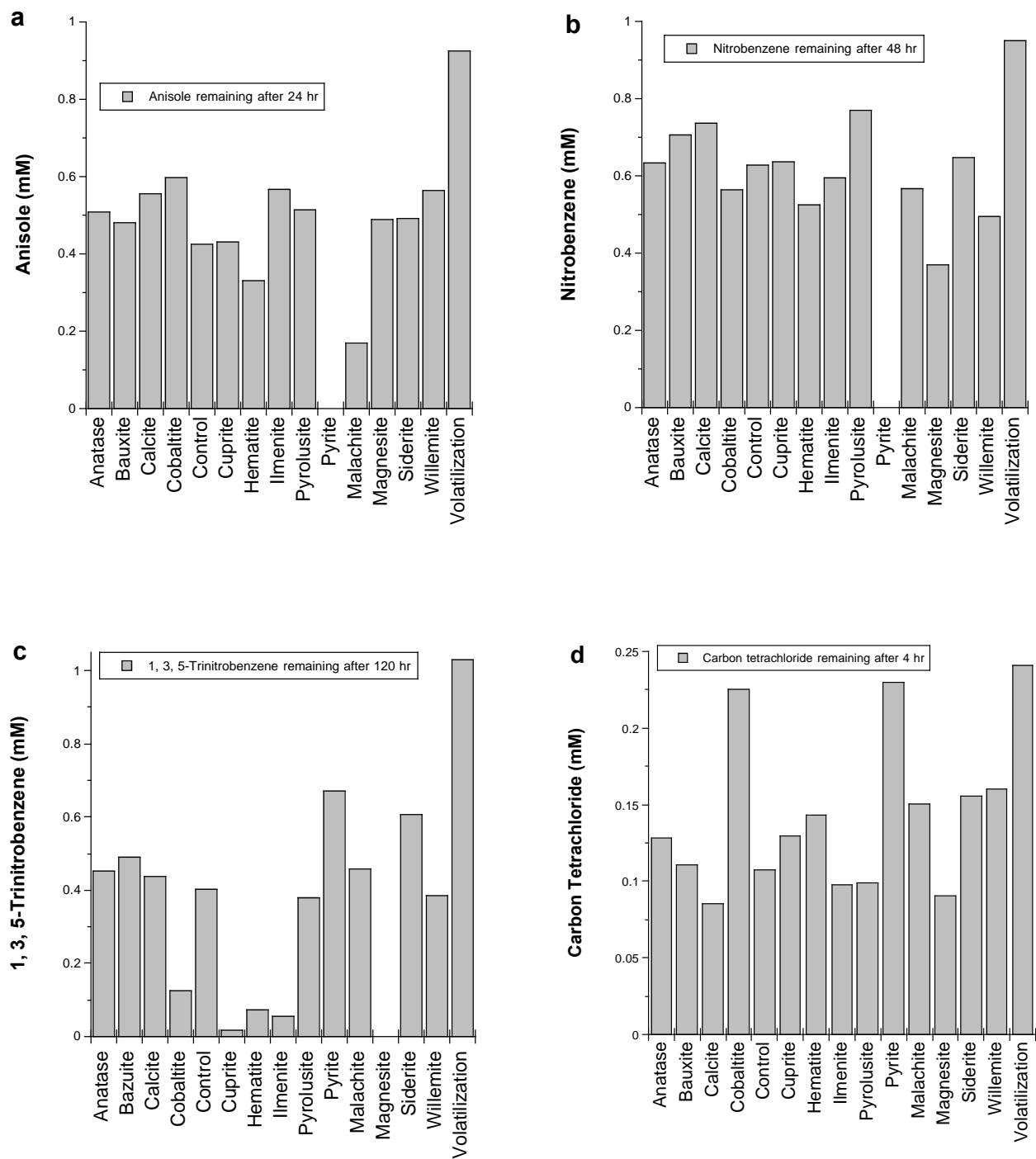


Figure 7.1.2.2. Probe compound remaining after treatment in 0.5 M sodium persulfate–trace mineral systems at a temperature of $25^{\circ}\text{C} \pm 1^{\circ}\text{C}$. a) the sulfate + hydroxyl radical probe anisole; b) the hydroxyl radical probe nitrobenzene; c) the hydroperoxide probe 1,3,5-trinitrobenzene; d) the superoxide probe carbon tetrachloride.

The results of Figure 7.1.2.2a-d suggest that numerous mechanisms may be occurring in mineral-persulfate systems. Ilmenite- and magnesite-persulfate systems do not promote the generation of sulfate and hydroxyl radicals, but promote the generation of nucleophiles and reductants. In contrast, pyrite-persulfate systems promote the rapid generation of sulfate and hydroxyl radical, but do not promote the generation of nucleophiles and reductants.

Detection of Sulfate and Hydroxyl Radical

Pyrite, ilmenite, and calcite were used as representative minerals of those that decompose persulfate rapidly, slowly, and less than persulfate-deionized water systems. The capacity of these three minerals to promote the degradation of anisole was studied as a basis for quantifying relative cumulative generation rates of sulfate + hydroxyl radicals.

The calcite-mediated degradation of anisole is shown in Figure 7.1.2.3a. Loss of anisole in the calcite-persulfate system was not significantly different than its loss in the persulfate-deionized system. The minimal degradation of anisole in the persulfate-deionized water system is likely due to the direct oxidation of anisole by persulfate ($E^0 = 2.01 \text{ V}$) (Latimer, 1952). These results demonstrate that calcite does not activate persulfate and, thus, sulfate and hydroxyl radicals are not generated in the calcite-persulfate system. Although carbonates are known scavengers of the sulfate ($k_{\text{SO}_4^{\bullet-}} = 9.1 \times 10^6 \text{ M}^{-1}\text{s}^{-1}$) and hydroxyl radicals ($k_{\text{OH}^{\bullet}} = 1.5 \times 10^7 \text{ M}^{-1}\text{s}^{-1}$), no scavenging effects were observed (Dogliotti and Hayon, 1967; Watts, 1997). These results suggest that carbonate concentrations were not high enough to scavenge sulfate or hydroxyl radicals. The pH of these systems was <4 ; the pK_a of bicarbonate-carbonic acid is 4.5. Therefore, any dissolved calcite likely escaped from the system as carbon dioxide.

Relative rates of sulfate and hydroxyl radical generation in ilmenite-persulfate systems is shown in Figure 7.1.2.3b. Over 99% anisole degradation in the ilmenite-persulfate system within 40 min demonstrates a significant generation rate of sulfate and hydroxyl radicals.

The pyrite-mediated degradation of anisole in persulfate systems is shown in Figure 7.1.2.3c. Anisole degradation was significantly higher in the presence of pyrite ($>90\%$ degraded) compared to systems containing only persulfate ($<10\%$ anisole degraded). These results demonstrate rapid generation of sulfate + hydroxyl radicals in pyrite-persulfate systems.

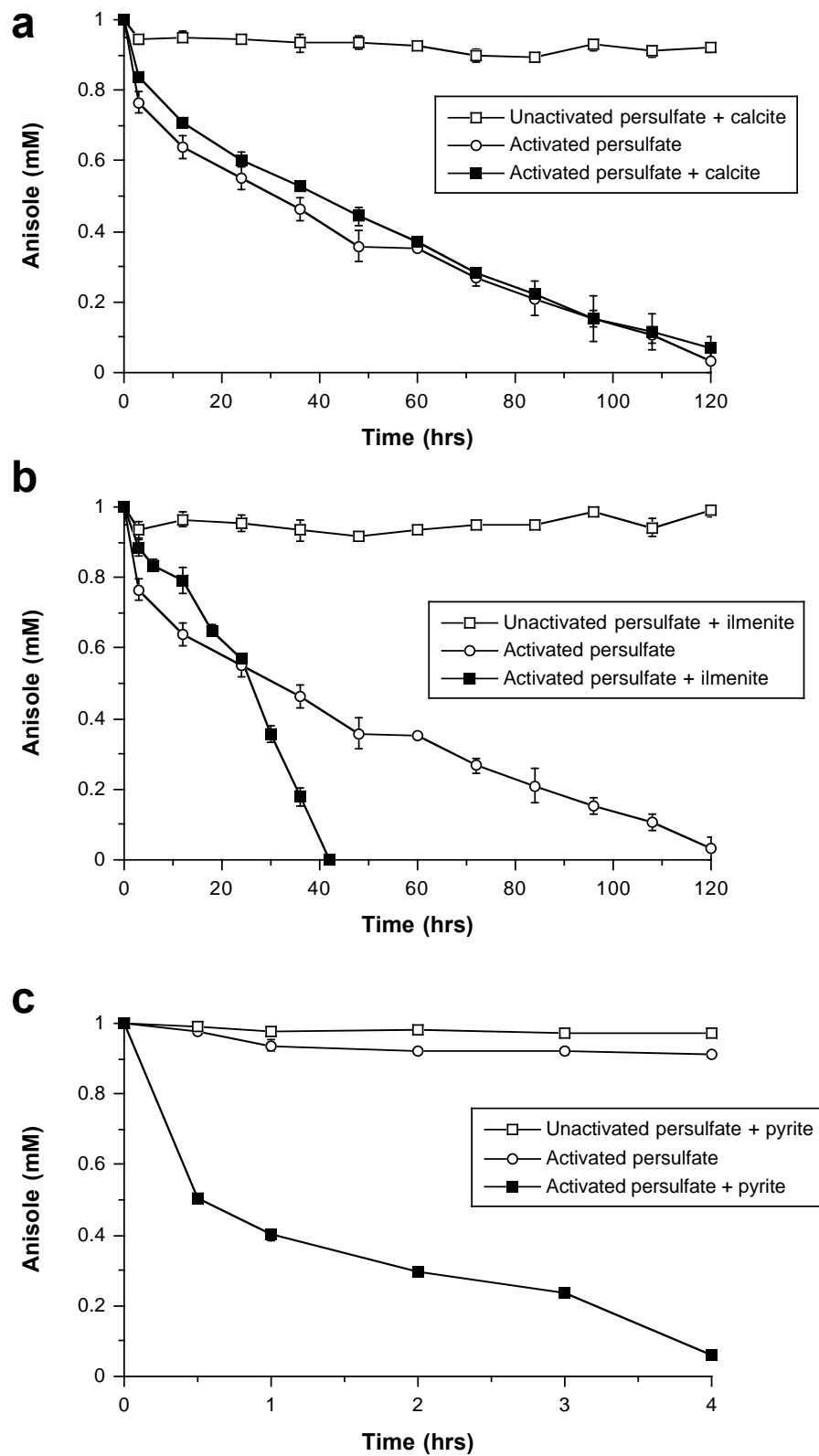


Figure 7.1.2.3. Degradation of the cumulative sulfate + hydroxyl radical probe anisole by trace mineral–persulfate systems at 25°C ± 1°C. a) Calcite; b) Ilmenite; c) Pyrite.

Detection of Hydroxyl Radicals

The detection of hydroxyl radical was evaluated through the oxidation of the hydroxyl radical probe nitrobenzene in persulfate systems containing pyrite, ilmenite and calcite.

Nitrobenzene was oxidized more slowly in calcite-persulfate systems than in persulfate-deionized water systems (Figure 7.1.2.4a). In the persulfate-deionized water systems >99% of the nitrobenzene was oxidized within 144 hr while only 60% of the nitrobenzene was oxidized in calcite-persulfate systems. Unlike the data of Figure 7.1.2.3a, these results suggest that calcite is scavenging hydroxyl radicals. Scavenging may be occurring in the nitrobenzene system, while not the anisole system, because the nitrobenzene systems react longer allowing for more dissolution of carbonates. Hydroxyl radical generation was promoted in the ilmenite-persulfate system compared to systems containing only persulfate and deionized water (Figure 7.1.2.4b). Over 72 hr, >99% of the hydroxyl radical probe nitrobenzene was oxidized in ilmenite-persulfate systems, while approximately 50% of the nitrobenzene was oxidized in persulfate-deionized water systems.

Relative rates of hydroxyl radical generation measured by the oxidation of nitrobenzene in pyrite-persulfate systems are shown in Figure 7.1.2.4c. Approximately 90% of the nitrobenzene was degraded in pyrite-persulfate systems over 11 hr compared to <10% in persulfate-deionized water systems. These results demonstrate that pyrite can promote the rapid generation of hydroxyl radical in persulfate systems.

The results of Figure 7.1.2.4a-d demonstrate that the three trace minerals pyrite, ilmenite, and calcite promote the generation of hydroxyl radical in persulfate slurries. Generation of hydroxyl radical in pyrite slurries is rapid, which is likely due to dissolution of the pyrite, providing soluble iron (II) to activate persulfate:



Hydroxyl radical generation was slower in ilmenite systems and calcite systems. The mechanism of activation of persulfate in the presence of these minerals is unknown, but may involve the dissolution of the metal oxides or heterogeneous catalysis on the mineral surfaces.

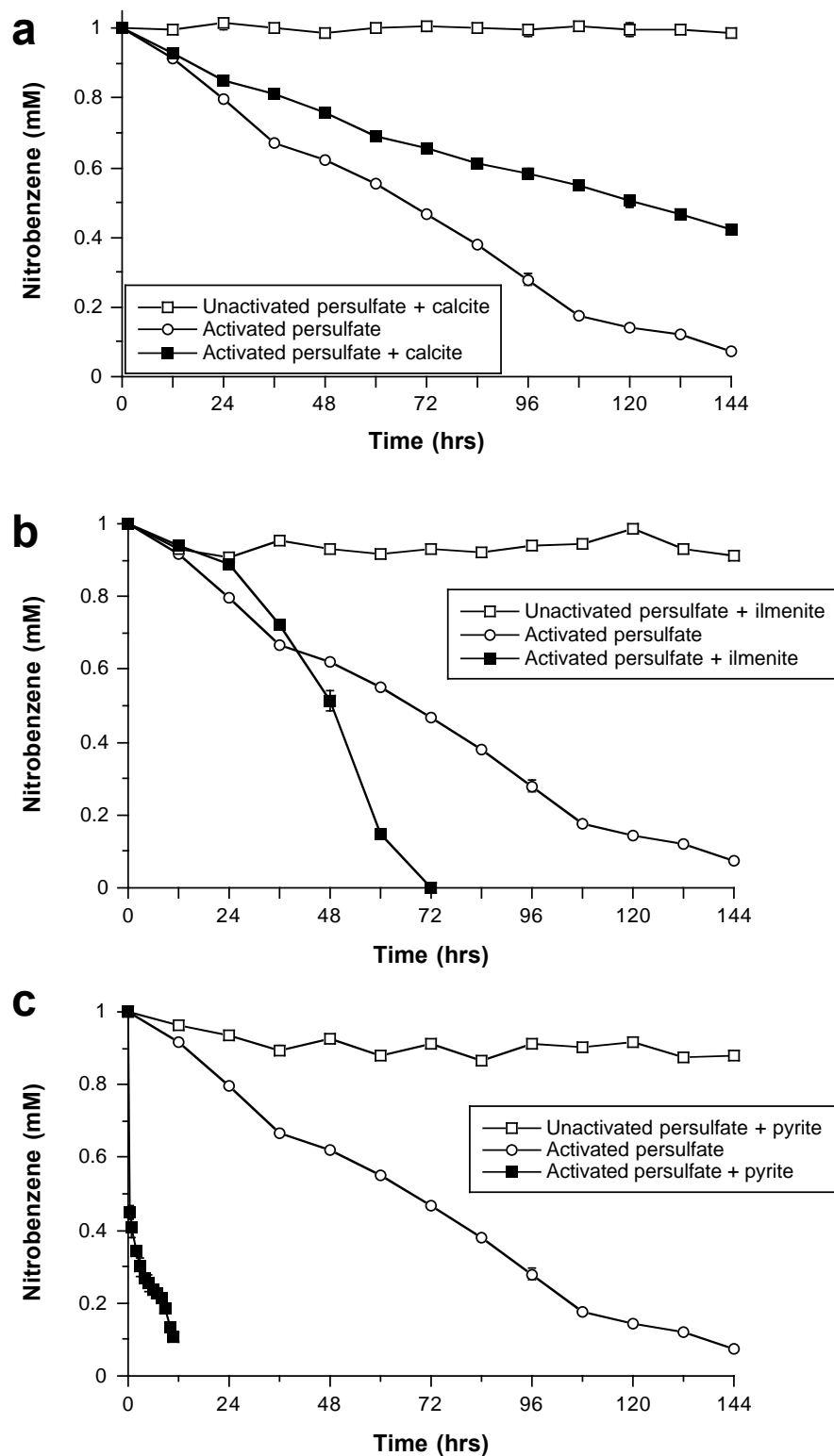


Figure 7.1.2.4. Degradation of the hydroxyl radical probe nitrobenzene by trace mineral–persulfate systems at $25^{\circ}\text{C} \pm 1^{\circ}\text{C}$. a) Calcite; b) Ilmenite; c) Pyrite.

Detection of Hydroperoxide

Degradation of the nucleophile probe TNB in calcite-persulfate systems is shown in Figure 7.1.2.5a. The addition of calcite to the persulfate system had no observable impact on the degradation of TNB. Approximately 90% of the TNB was degraded over 216 hr in both the persulfate-deionized water systems and the calcite-persulfate systems. Approximately 40% of the TNB loss occurred in the first hr.

A large portion (40%) of the TNB degradation occurred within the first hr; thereafter, TNB degraded slowly, and after 120 hr there was a >90% loss of TNB in ilmenite-persulfate systems (Figure 7.1.2.5b). TNB loss in persulfate-deionized water systems also declined rapidly over the first hr, followed by a slow reaction; 90% loss of the TNB then occurred over 220 hr.

The degradation of TNB by pyrite is shown in Figure 7.1.2.5c. Dissolution of pyrite may be increasing the extraction efficiency during the analysis of the TNB, resulting in an apparent increasing concentration of TNB. Nonetheless, the persulfate-pyrite system showed significant loss relative to the control systems, demonstrating the generation of nucleophiles in pyrite-persulfate systems.

Detection of Reductants

Carbon tetrachloride was used as probe for superoxide, a reductant generated in CHP systems and likely generated in activated persulfate systems as well. In CHP systems superoxide is responsible for degrading highly oxidized compounds, and it is also important in the enhanced desorption of hydrophobic organic contaminants (Corbin et al., 2007).

Degradation of carbon tetrachloride in calcite-persulfate systems is shown in Figure 7.1.2.6a; >80% carbon tetrachloride degradation was observed in both calcite-deionized water and calcite-persulfate systems after 8 hr. Approximately 70% of the carbon tetrachloride degradation occurred within the first hour, after which the rate slowed significantly. Most of the carbon tetrachloride loss was likely due to volatilization; therefore, calcite-persulfate systems do not promote the generation of reductants. Loss of carbon tetrachloride in ilmenite-persulfate systems is shown in Figure 7.1.2.6b. Reductant activity was lower in ilmenite-persulfate systems than in persulfate-deionized water systems and, therefore, reductant generation is negligible in ilmenite-persulfate systems.

Degradation of carbon tetrachloride in pyrite-persulfate slurries is shown in Figure 7.1.2.6c. Carbon tetrachloride degradation in pyrite-persulfate systems was less than that of the persulfate-deionized water systems; these data demonstrate that no reductants are generated in pyrite-persulfate slurries. Furthermore, minimal generation of reductants was observed in any of the mineral-persulfate systems evaluated.

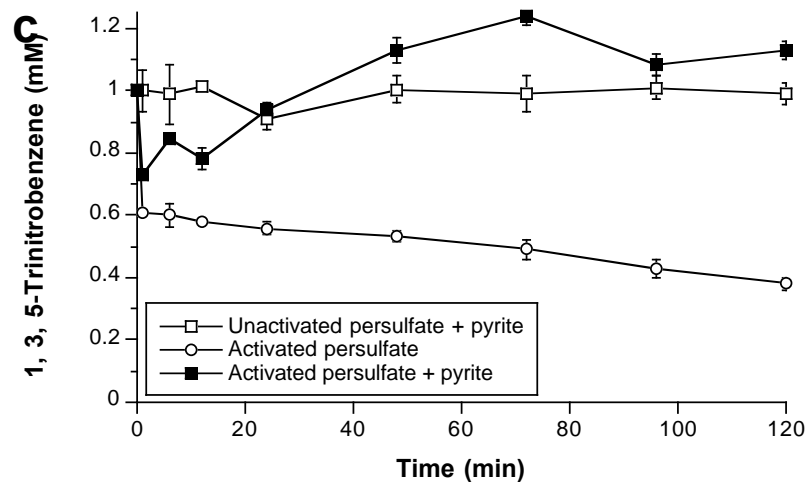
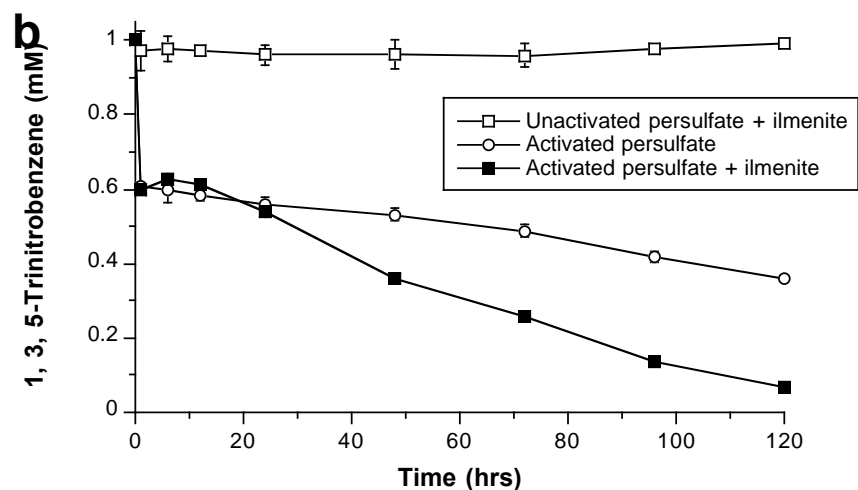
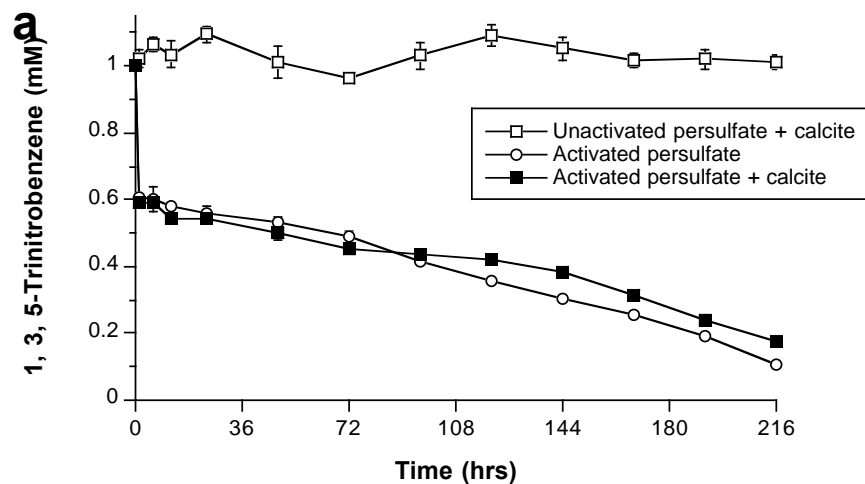


Figure 7.1.2.5. Degradation of the hydroperoxide probe 1,3,5-trinitrobenzene by trace mineral–persulfate systems at $25^{\circ}\text{C} \pm 1^{\circ}\text{C}$. a) Calcite; b) Ilmenite; c) Pyrite.

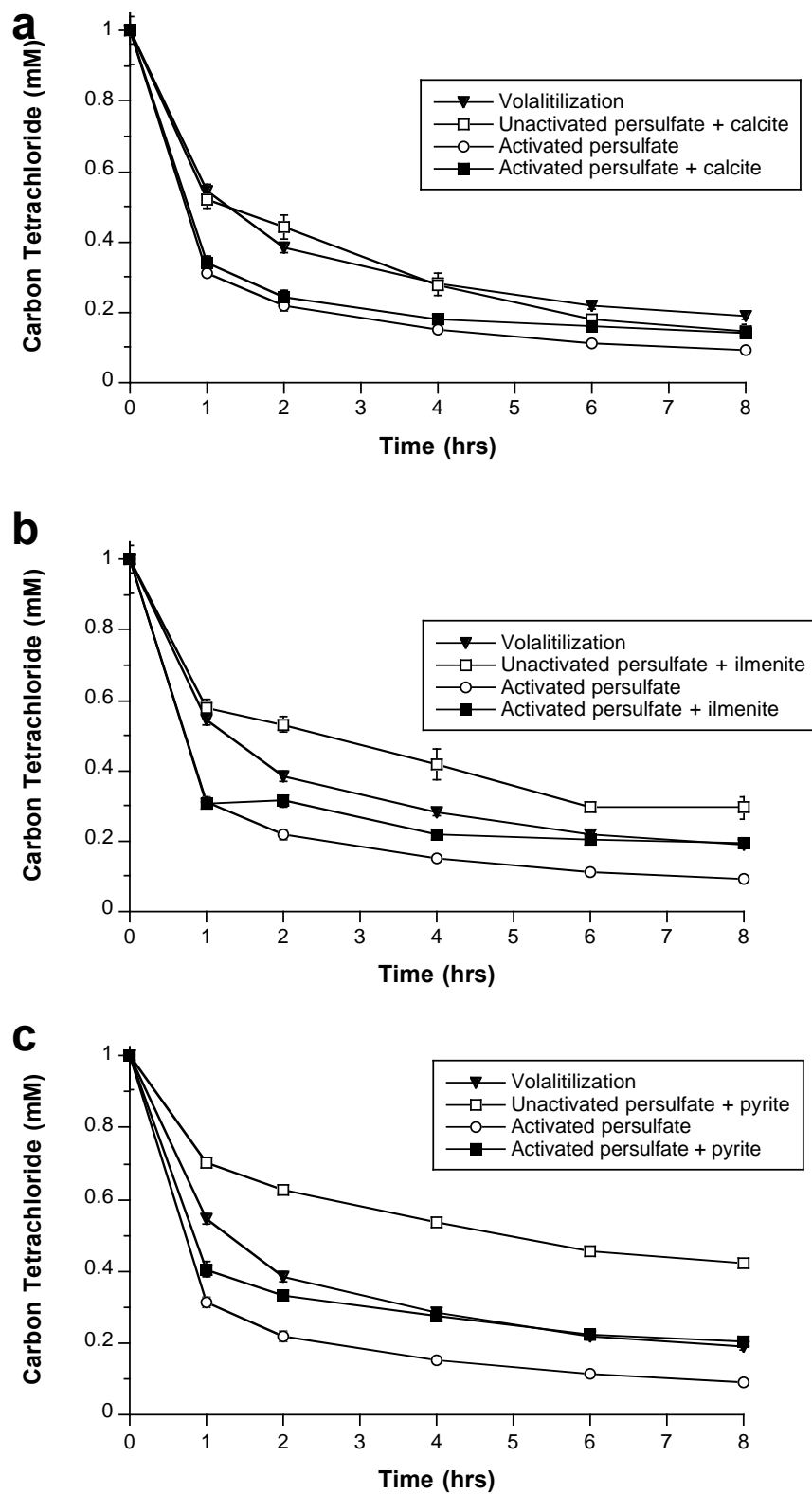


Figure 7.1.2.6. Degradation of reductant probe carbon tetrachloride by trace mineral–persulfate systems at 25°C ± 1°C. a) Calcite; b) Ilmenite; c) Pyrite.

All of the mineral persulfate systems exhibited lower reactivity with carbon tetrachloride than the persulfate-deionized water control systems, denoting lower generation rates for reductants. A significant trend can be found between the total oxidant (sulfate and hydroxyl radical) generation and reductant generation in mineral-persulfate systems. The relative rate of total oxidant generation was inversely proportional to the relative rate of reductant generation.

The degradation of anisole, nitrobenzene, TNB and carbon tetrachloride in 13 mineral-persulfate systems compared to corresponding persulfate-deionized water systems over 4 hr, 24 hr, 48 hr, and 120 hr, is shown in Figure 7.1.2.7. The probe compounds were degraded at rates slower than persulfate-deionized water controls in most of the mineral-persulfate systems. These results suggest that, in most cases, the minerals scavenge the reactive oxygen species or inhibit activation of persulfate.

Conclusion

The results of this research demonstrate that most trace minerals promote the decomposition of persulfate; however, the decomposition of persulfate appears to have varied consequences in the generation of reactive oxygen species with some minerals increasing reactivity and others lowering the reactivity of the persulfate.

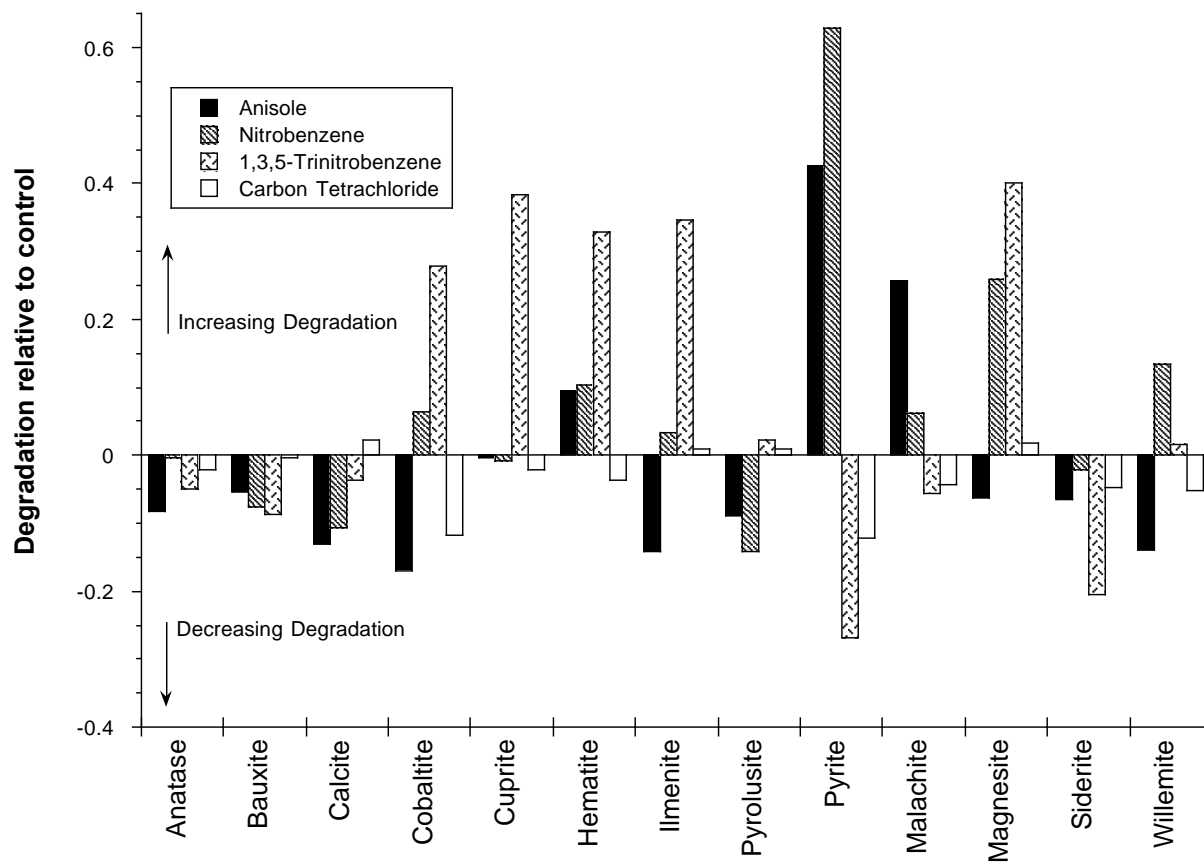


Figure 7.1.2.7. Degradation of the four probes as relative to corresponding control systems. Duration of reactions was probe-specific: anisole over 24 hr; nitrobenzene over 48 hr; 1, 3, 5-trinitrobenzene over 120 hr; carbon tetrachloride over 4 hr.

7.1.3. Base-Activated Persulfate Treatment of Contaminated Soils with pH Drift from Alkaline to Circumneutral

Four different soil systems were investigated for hydroxyl radical and reductant activity as basic persulfate formulations were allowed to drift toward circumneutral pH: soils KB1 and KB2 with 1.01% and 0.24% organic carbon, respectively, and soils KB1-No SOM and KB2-No SOM on which the SOM was removed. Persulfate concentration, pH, and either hydroxyl radical or reductant generation were quantified concurrently as the reactions proceeded.

Screening of Base Dosages

Several persulfate formulations of varied sodium hydroxide to persulfate molar ratios were added to the KB1 and KB2 soils to obtain a base dosage that would drift from basic to circumneutral (Figure 7.1.3.1a-b). Using a sodium persulfate concentration of 0.5 M, molar ratios of 0.375:1 to 2.5:1 hydroxide:persulfate were prepared; 20 mL of each were added to 10 g of soil in 40 mL volatile organic analysis (VOA) vials. The pH was monitored over time to obtain pH profiles for each molar ratio; each vial was mixed prior to pH measurements. The vials were incubated in a water bath at 25°C ($\pm 2^\circ\text{C}$) between measurements.

From the results in Figure 7.1.3.1a-b, molar ratios of 1.25:1 were used in the KB1 soil slurries and 0.375:1 were used in the KB2 soil slurries to evaluate persulfate reactivity as the pH drifted from basic to circumneutral. Approximate spike times for the probe compounds were determined from these profiles at pH levels of 12, 10, and 8 (Figure 7.1.3.2). Furthermore, molar ratios of 0.375:1 were used once the SOM was removed for soils KB1-No SOM and KB2-No SOM because a smaller ratio would not bring the starting pH above 12 in these soil slurries. Changes in pH in these soil slurries with approximate spike times are shown in Figure 7.1.3.3.

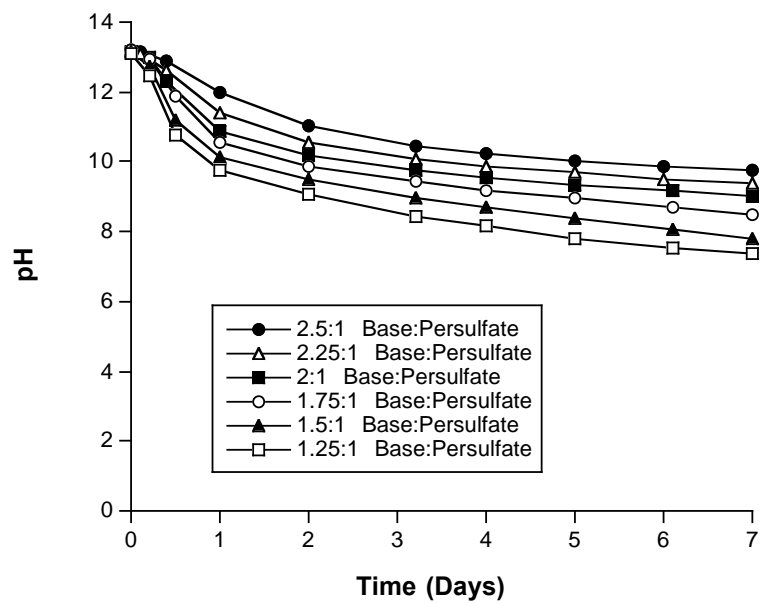
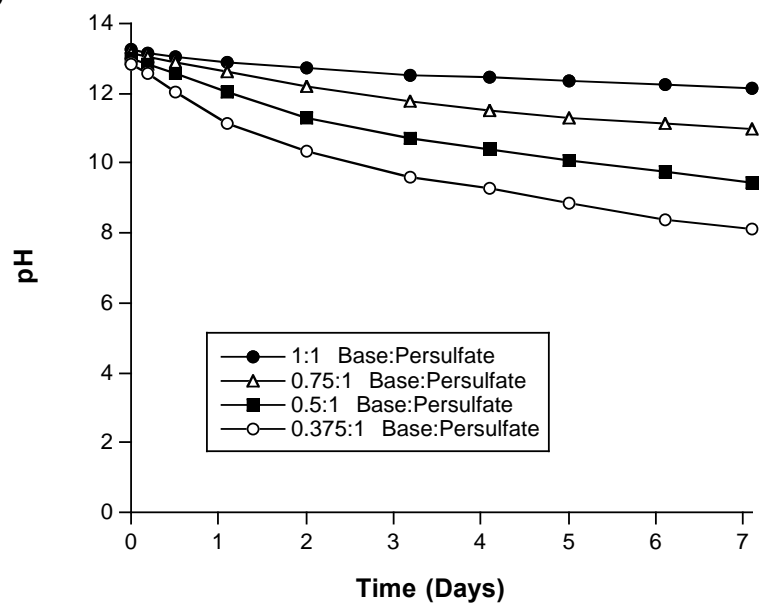
a**b**

Figure 7.1.3.1. pH profiles of various molar ratios of sodium hydroxide:sodium persulfate for soils KB1 (a) and KB2 (b).

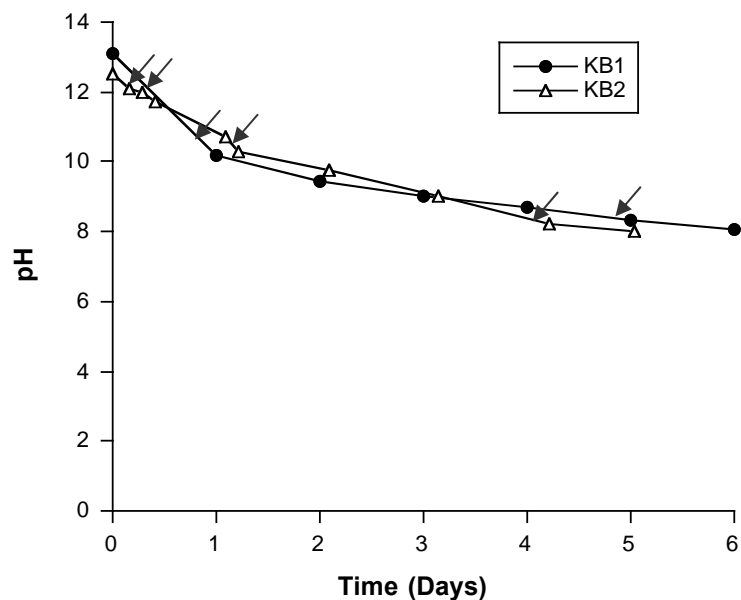


Figure 7.1.3.2. pH profiles for the selected molar ratios of sodium hydroxide: persulfate for soil slurries KB1 (1.25:1) and KB2 (0.375:1). Arrows indicate the approximate times of spiking with probe compounds.

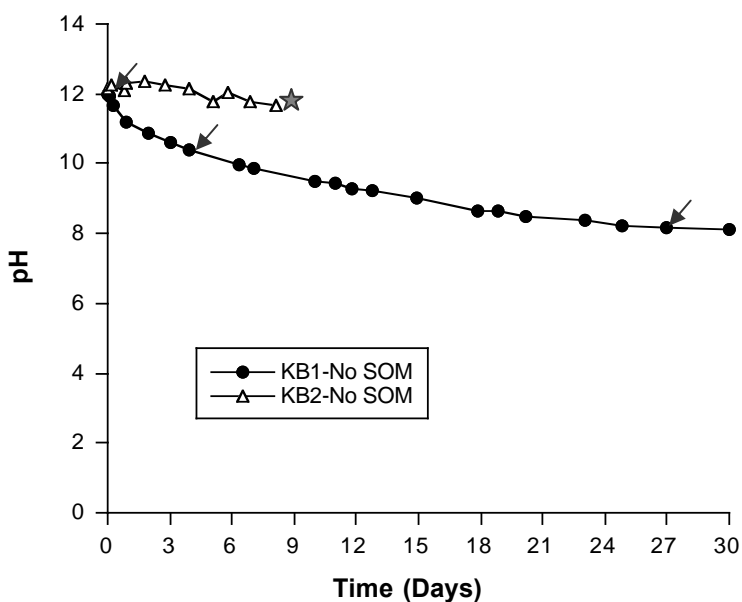


Figure 7.1.3.3. pH profiles for the selected molar ratio of 0.375:1 sodium hydroxide: persulfate for soil slurries KB1-No SOM and KB2-No SOM. Arrows indicate the approximate times of spiking with probe compounds. Star indicates that the reaction did not drift down to pH 10 within the time frame of the experiment.

Persulfate Decomposition and pH Changes in Soil Slurries

Persulfate decomposition was monitored as the pH drifted toward neutral during the experiments that tracked hydroxyl radical and reductant generation. Persulfate decomposition in the KB1 and KB2 soil slurries in which hydroxyl radical generation was tracked is shown in Figure 7.1.3.4a-b. The persulfate concentration decreased from 0.5 M to 0.27 M as the pH in the KB1 reactors reached pH 12, likely due to persulfate consumption by SOM. Initial persulfate concentrations for the three starting pH regimes of pH 12, pH 10, and pH 8, were 0.27 M, 0.25 M, and 0.22 M, respectively. Persulfate decomposed an additional 33%, 28%, and 23% in these systems over the 30 d reactions. The bulk of the persulfate loss occurred in the first few days with less consumption over the remaining 30 d. The persulfate concentration decreased from 0.5 M to 0.48 M as the pH in the KB2 reactors reached pH 12. Initial persulfate concentrations were 0.48 M, 0.47 M, and 0.46 M for the starting pH regimes of pH 12, pH 10, and pH 8. Persulfate decomposed an additional 17%, 15%, and 13% in the three pH regimes over 30 d.

Persulfate concentrations in the KB1-No SOM and KB2-No SOM soil slurries in which hydroxyl radical generation was tracked are shown in Figure 7.1.3.5a-b. Rates of persulfate decomposition in persulfate slurries containing KB1-No SOM and KB2-No SOM were less than in the slurries containing SOM; persulfate consumption was <2% in these slurries once the pH reached 12. Initial persulfate concentrations in the KB1-No SOM were 0.50 M, 0.48 M, and 0.45 M for the three pH regimes. Persulfate decomposed an additional 10%, 8%, and 7% over 30 d. The rates of persulfate consumption in the three pH regimes were relatively constant over the 30 d reactions compared to the KB1 and KB2 soil slurries. Initial persulfate concentrations in the KB2-No SOM slurries were 0.48 M, 0.47 M, and 0.47 M; the initial persulfate concentrations in these systems were nearly identical at pH 10 and pH 8 because the pH in these reactors had to be artificially lowered through the addition of dilute sulfuric acid. Only 4% persulfate decomposition was observed in the KB2-No SOM soil slurries over each reaction period for all three pH systems; 6 d for pH 12 system, and 14 d for the pH 10 and pH 8 systems.

Persulfate concentrations monitored in conjunction with reductant generation experiments are illustrated in Figure 7.1.3.6a-b for soil slurries KB1 and KB2, and Figure 7.1.3.7a-b for soil slurries KB1-No SOM and KB2-No SOM. The persulfate decomposition trends are nearly the same as the persulfate decomposition in the hydroxyl radical generation experiments (Figure 7.1.3.4a-b and Figure 7.1.3.5a-b).

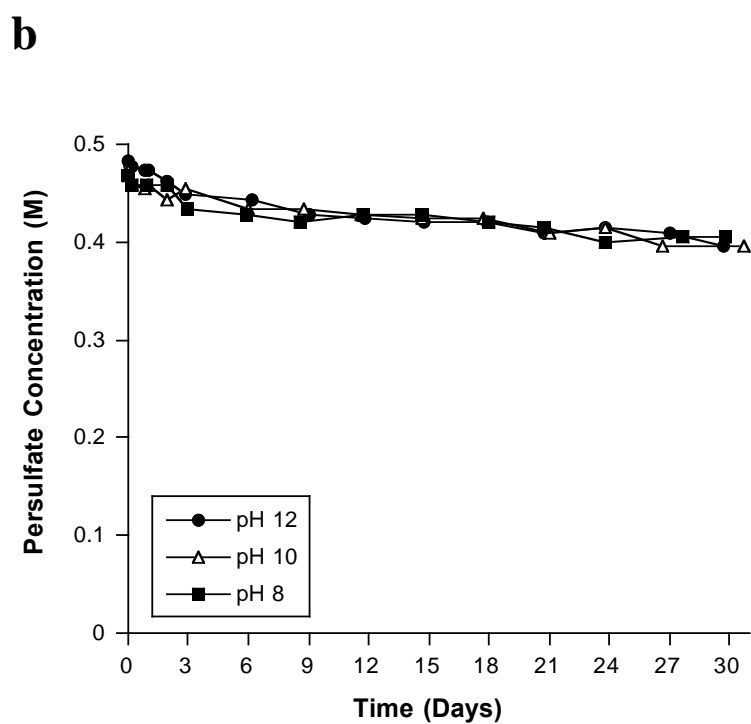
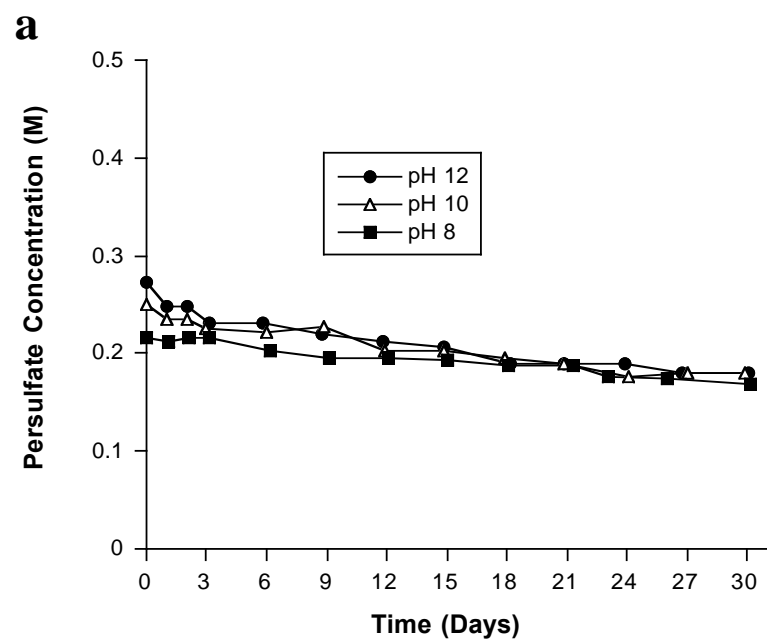


Figure 7.1.3.4. Persulfate concentrations in soil slurries KB1 (a) and KB2 (b) in conjunction with hydroxyl radical generation experiments. Time denotes days after the system reached the indicated pH and was spiked with nitrobenzene.

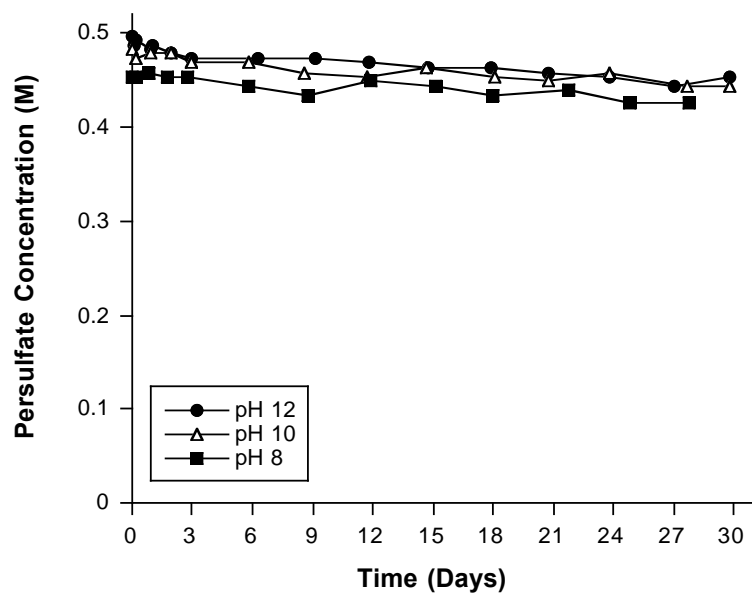
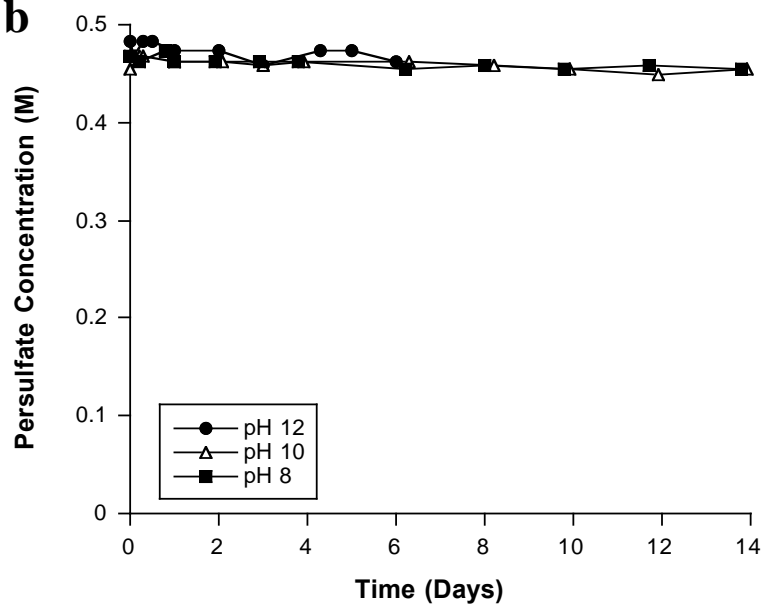
a**b**

Figure 7.1.3.5. Persulfate concentrations in soil slurries KB1-No SOM (a) and KB2-No SOM (b) in conjunction with hydroxyl radical generation experiments. Time denotes days after the system reached the indicated pH and was spiked with nitrobenzene.

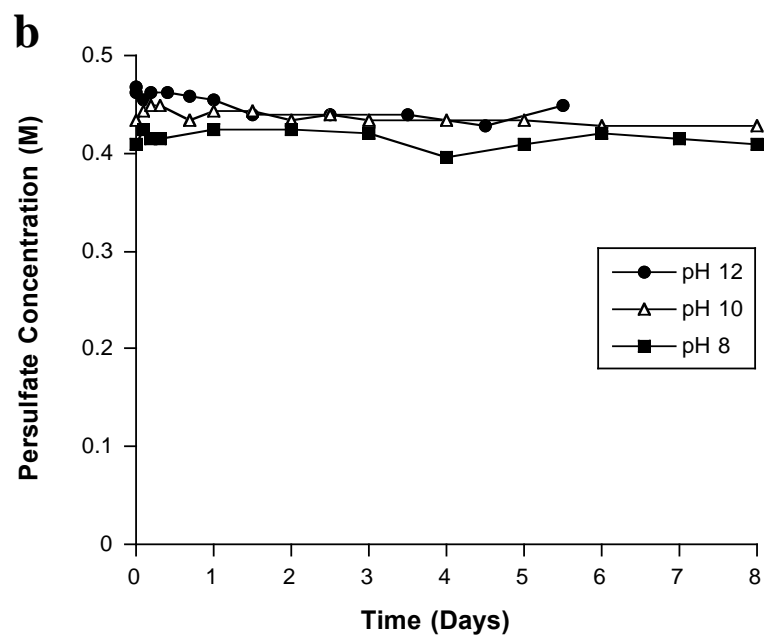
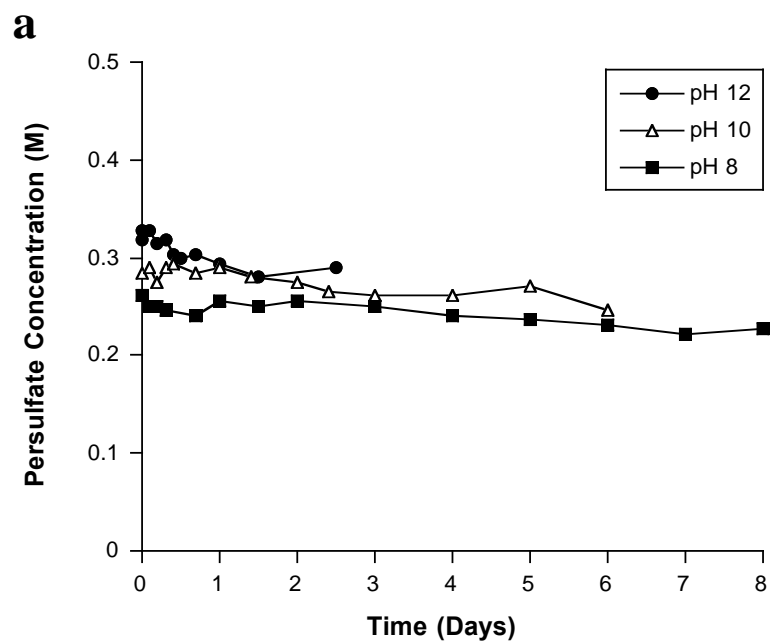


Figure 7.1.3.6. Persulfate concentrations in soil slurries KB1 (a) and KB2 (b) in conjunction with reductant generation experiments. Time denotes days after the system reached the indicated pH and was spiked with hexachloroethane.

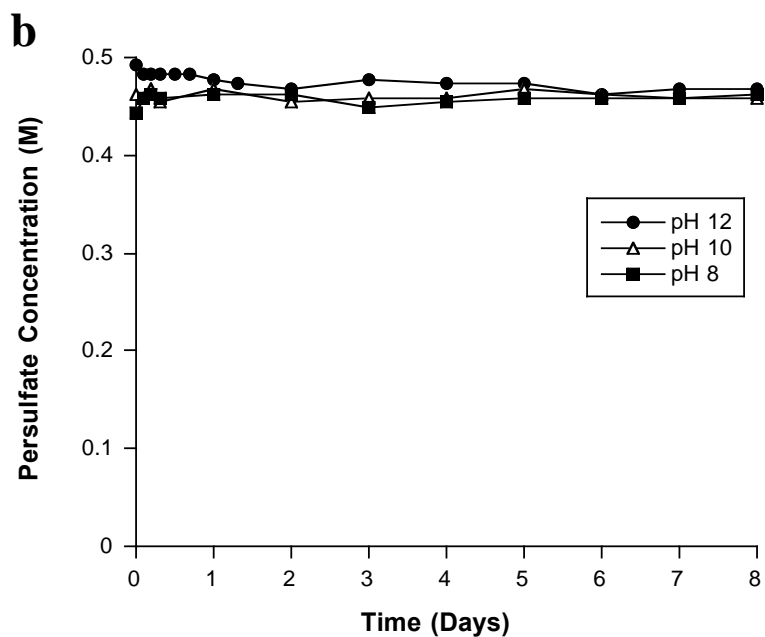
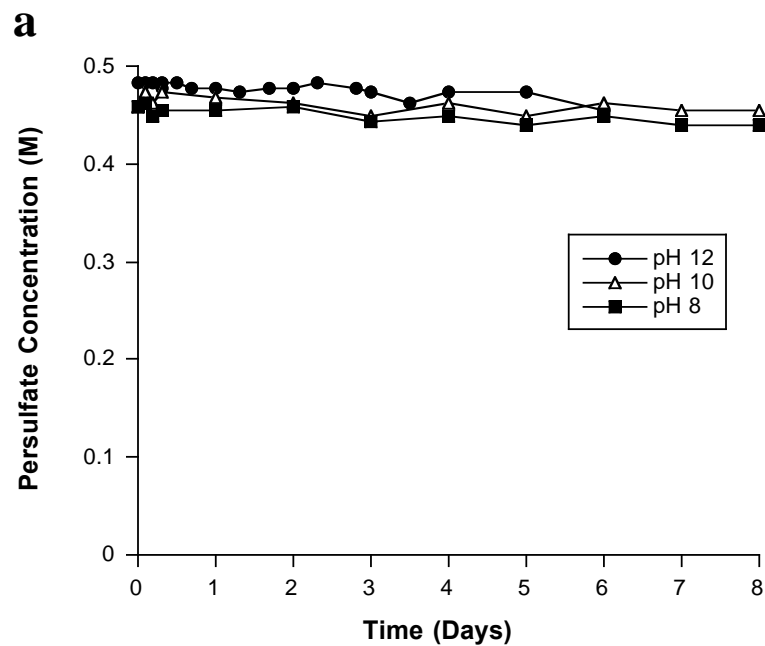


Figure 7.1.3.7. Persulfate concentrations in soil slurries KB1-No SOM (a) and KB2-No SOM (b) in conjunction with reductant generation experiments. Time denotes days after the system reached the indicated pH and was spiked with hexachloroethane.

pH Drift in Soil Slurries

pH was monitored in the four different soil systems in conjunction with hydroxyl radical and reductant activity as basic persulfate formulations drifted from alkaline circumneutral pH. The rate of pH change followed a pattern similar to persulfate decomposition and decreased most rapidly in the early stages of the reactions. pH drift in soil slurries is due to the generation of sulfuric acid as the persulfate decomposed; based on reaction stoichiometry, two moles of sulfuric acid are produced from one mole of persulfate:



Changes in pH over time for the KB1 and KB2 soil slurries during the hydroxyl radical generation experiments is shown in Figure 7.1.3.8a-b. In parallel to rapid persulfate consumption, the pH dropped most rapidly in the early stages of persulfate decomposition in the KB1 soil systems because of the greater SOD; e.g., the pH in the KB1 soil slurries declined from pH 12 to pH 10 over 24 hours after addition of nitrobenzene probe. After 24 hours, the rate of pH change in the KB1 soil slurries continued to change somewhat rapidly but with a lower rate of change until day 15. At that time, the rate of pH change in the three soil systems slowed and was nearly identical for the remaining 30 d.

The rate of pH change in the KB2 soil slurries was less than the rate in the KB1 soil slurries. The pH declined most rapidly in the first 6 d in all three pH systems; e.g., the pH in the KB2 soil slurries declined from pH 12 to pH 10 over 48 hours after addition of nitrobenzene probe. After 6 d, the rate of pH change in the three soil systems slowed significantly and was nearly identical for the next 18 d. After 24 d, the rate of pH change increased slightly as the pH in all three systems decreased below pH 6.

Changes in pH over time for the KB1-No SOM and KB2-No SOM soil slurries in which relative hydroxyl radical generation was quantified is shown in Figure 7.1.3.9a-b. The rate of pH change in both of these systems was less than in the soil systems with SOM; in addition, less persulfate decomposed which decreased the rate of pH drift. The rates of pH drift in the KB1-No SOM soil systems were slightly greater than the KB2-No SOM soil systems, which may be due to the degree to which the SOM was removed; slightly more SOM remained in the KB1-No SOM soil (0.12%) than in the KB2-No SOM soil (0.06%) after SOM removal. The pH then declined linearly for both KB1-No SOM and KB2-No SOM soil slurries throughout the reactions. A small pH increase was observed in the early stages of the pH 8 and pH 10 systems of the KB2-No SOM after the injection of the probe compounds (The probe solutions were added at acidic pH to obtain the desired pH in the system).

pH drift monitored in conjunction with the reductant generation experiments is shown in Figure 7.1.3.10a-b for soil slurries KB1 and KB2, and Figure 7.1.3.11a-b for soil slurries KB1-No SOM and KB2-No SOM. These results are nearly the same as the pH profiles in the hydroxyl radical generation experiments (Figure 7.1.3.8a-b and Figure 7.1.3.9a-b).

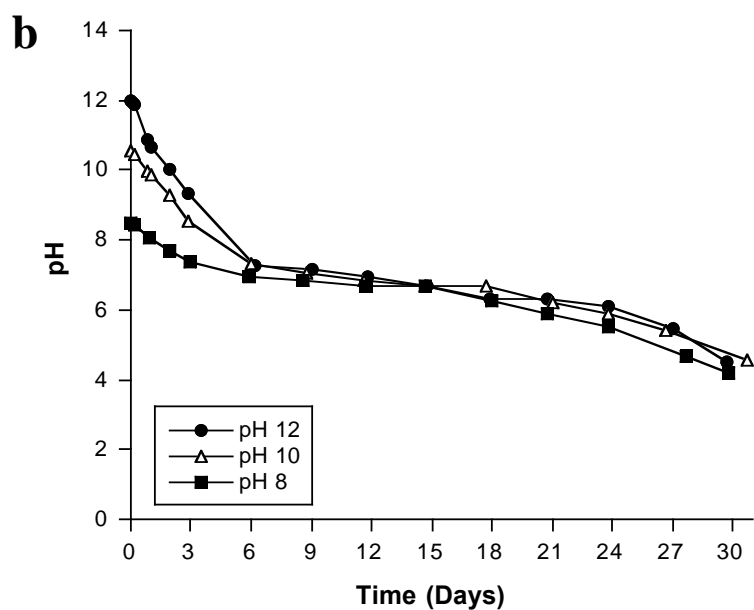
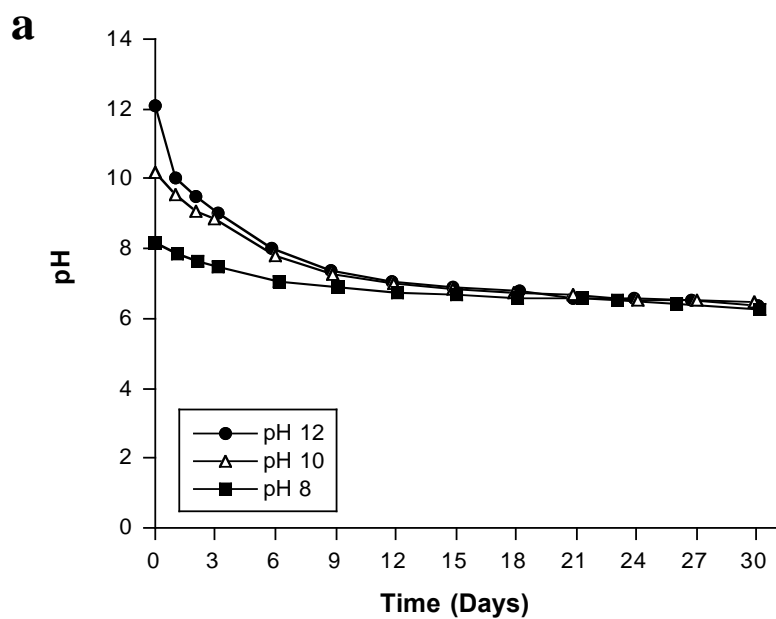
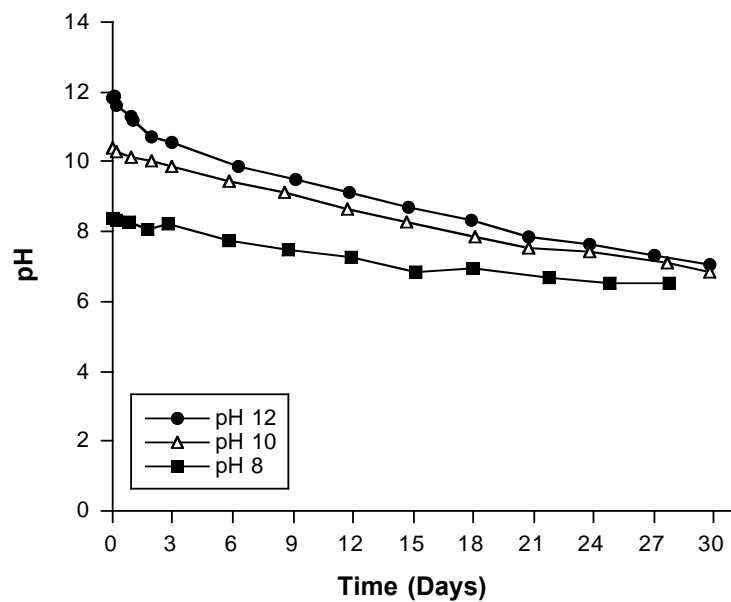


Figure 7.1.3.8. pH profiles for soil slurries KB1 (a) and KB2 (b) in conjunction with hydroxyl radical generation experiments. Time denotes days after the system reached the indicated pH and was spiked with nitrobenzene.

a



b

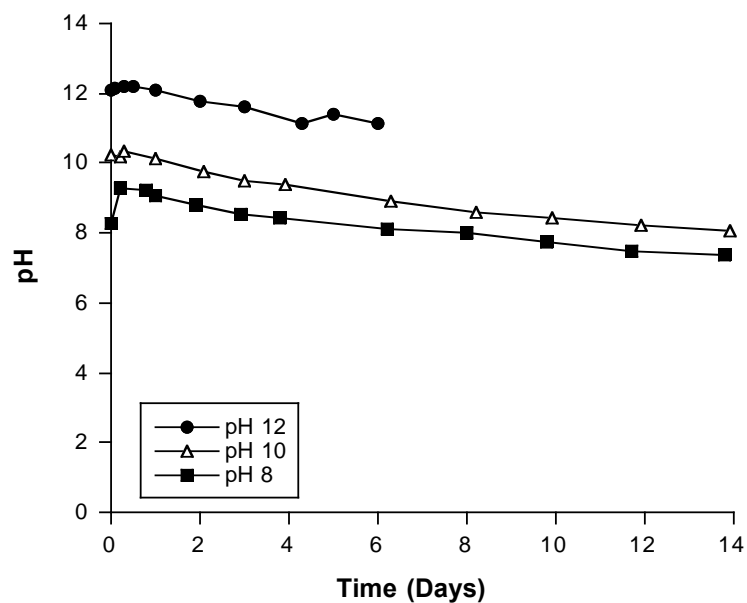


Figure 7.1.3.9. pH profiles for soil slurries KB1-No SOM (a) and KB2-No SOM (b) in conjunction with hydroxyl radical generation experiments. Time denotes days after the system reached the indicated pH and was spiked with nitrobenzene.

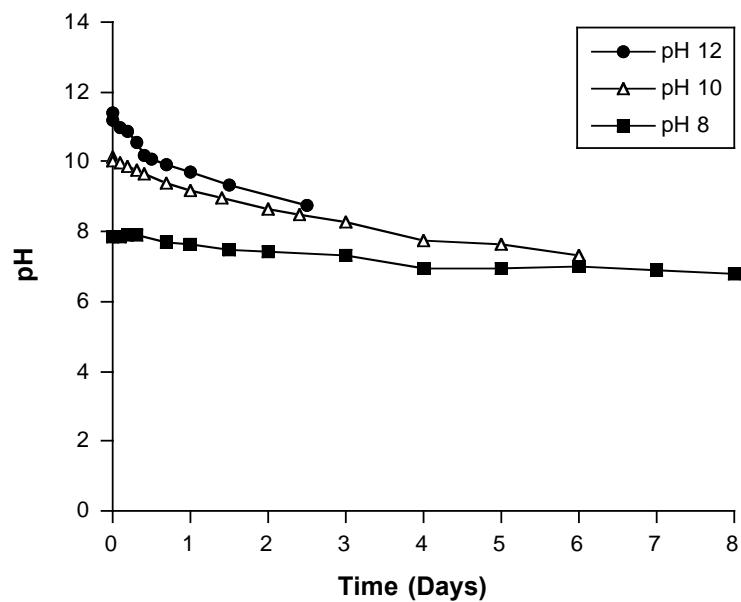
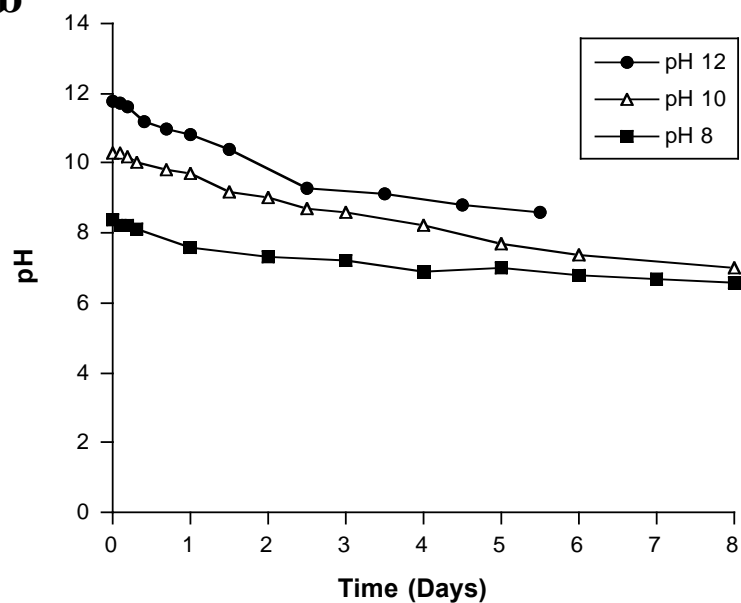
a**b**

Figure 7.1.3.10. pH profiles for soil slurries KB1 (a) and KB2 (b) in conjunction with reductant generation experiments. Time denotes days after the system reached the indicated pH and was spiked with hexachloroethane.

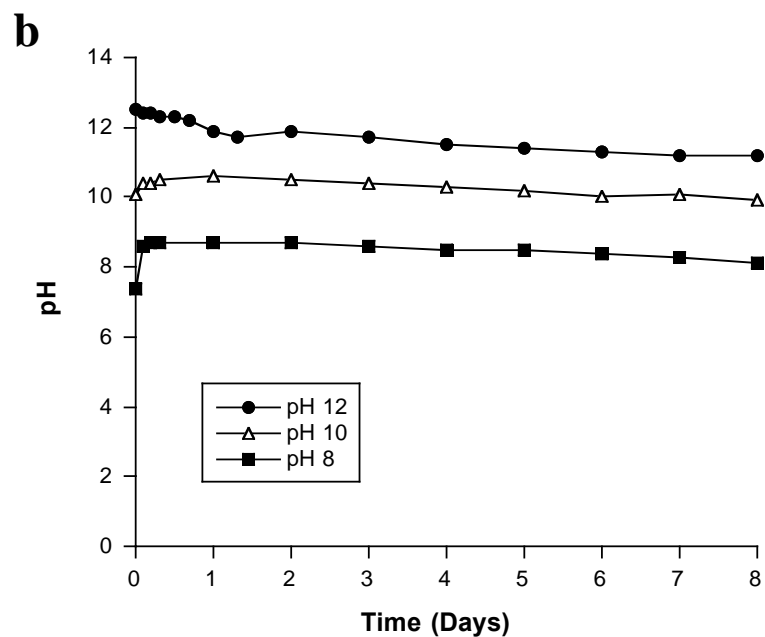
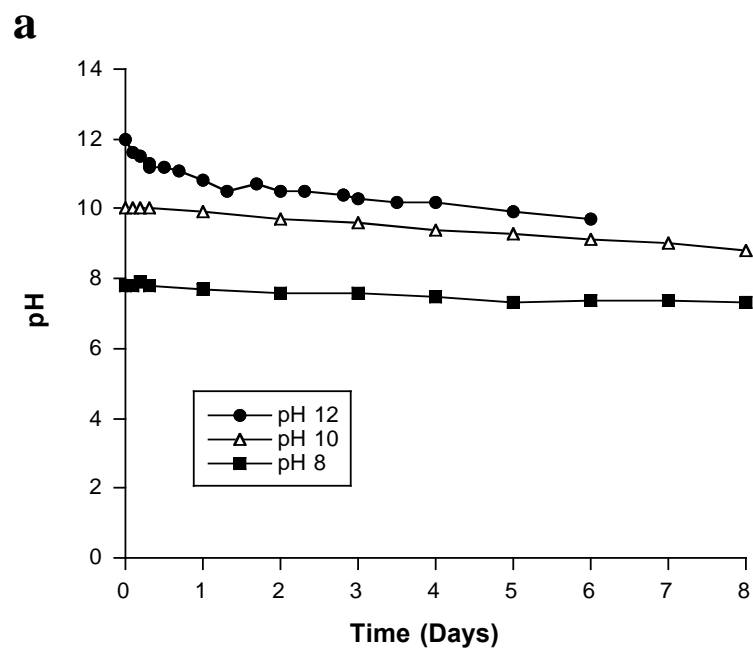


Figure 7.1.3.11. pH profiles for soil slurries KB1-No SOM (a) and KB2-No SOM (b) in conjunction with reductant generation experiments. Time denotes days after the system reached the indicated pH and was spiked with hexachloroethane.

Hydroxyl Radical Generation as pH Drifts to Circumneutral

Relative rates of hydroxyl radical generation were quantified by the oxidation of nitrobenzene as the pH drifted toward neutrality. Nitrobenzene concentrations in the KB1 and KB2 soil slurries are shown in Figure 7.1.3.12a-b. Nitrobenzene degradation in the KB1 soil slurries was 67% in the pH 12 system, 60% in the pH 10 system, and 34% in the pH 8 system over 30 d. Minimal nitrobenzene loss occurred in parallel control systems. Initial rates of hydroxyl radical generation were greater in early stages of the reactions, with a more constant degradation rate occurring after 3 d. Since less persulfate remained in the KB1 soil slurries due to the large SOD, less persulfate was available to react with nitrobenzene. Furthermore, due to the high amount of SOM, the hydroxyl radicals, catalyzed from the remaining persulfate, were likely scavenged by the SOM.

Nitrobenzene degradation in the KB2 soil slurries was 97% in the pH 12 system, 96% in the pH 10 system, and 94% in the pH 8 system over the 30 d. Initial rates of hydroxyl radical generation were greater in the higher pH systems, with near constant degradation rates occurring after 6 d in the three different pH regimes. Minimal nitrobenzene loss occurred in parallel control systems. In general, hydroxyl radical generation was greater in the KB2 systems compared to the KB1 systems likely due to a combination of more persulfate available for catalysis and less scavenging of hydroxyl radicals by SOM. These results demonstrate that relative rates of hydroxyl radical generation decreased as the pH drifted from alkaline toward circumneutral conditions, but hydroxyl radicals were still generated.

Relative rates of hydroxyl radical generation quantified through the oxidation of nitrobenzene in the KB1-No SOM and KB2-No SOM slurries are shown in Figure 7.1.3.13a-b. Nitrobenzene was oxidized to nondetectable concentrations in all KB1-No SOM pH slurries after 30 d and after 14 d for the KB2-No SOM slurries with minimal nitrobenzene loss in parallel soil control systems. The differing rates of hydroxyl radical generation in these two systems may be partly from oxidant scavenging by lingering SOM; slightly more SOM remained in the KB1-No SOM soil (0.12%) than the KB2-No SOM soil (0.06%) after SOM removal. Another possible explanation may be varying mechanisms that are activating persulfate in these two systems, which include catalysis by the soil minerals or a radical chain reaction that is initiated at high pH.

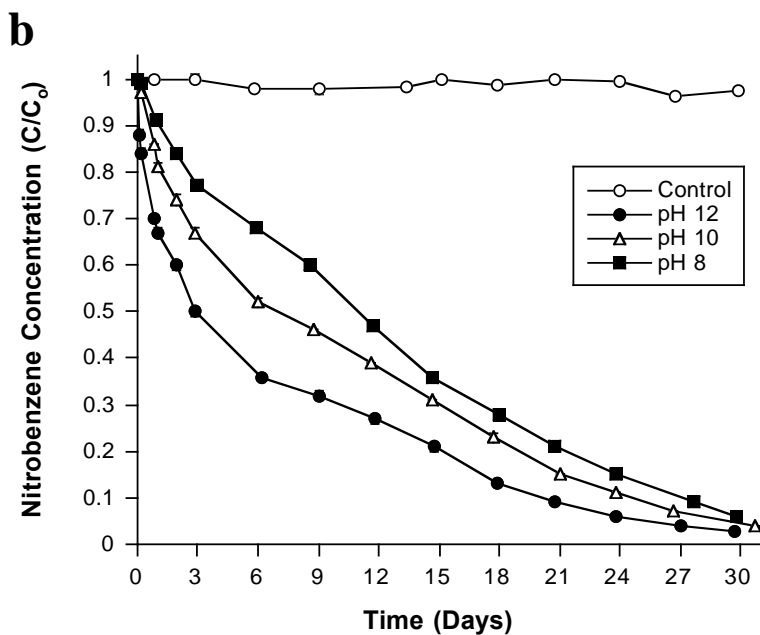
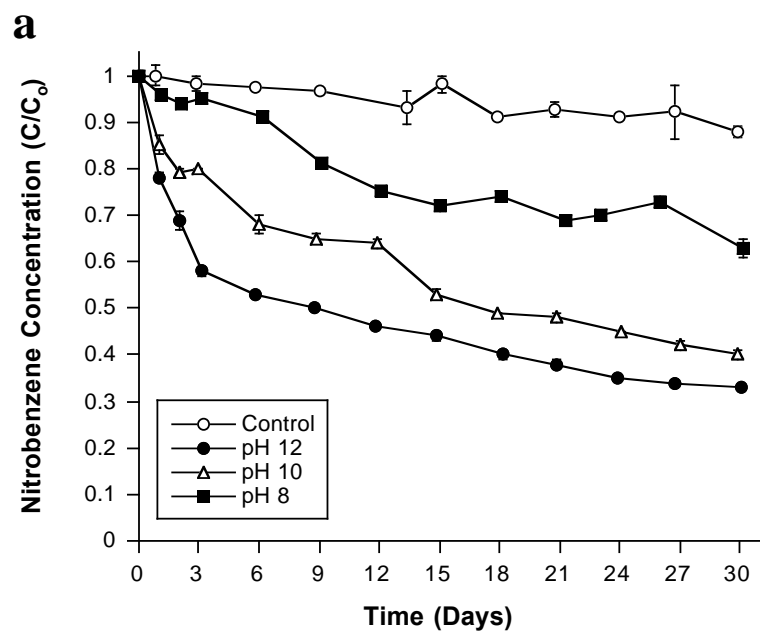


Figure 7.1.3.12. Hydroxyl radical generation quantified through nitrobenzene degradation in soil slurries KB1 (a) and KB2 (b). Time denotes days after the system reached the indicated pH and was spiked with nitrobenzene.

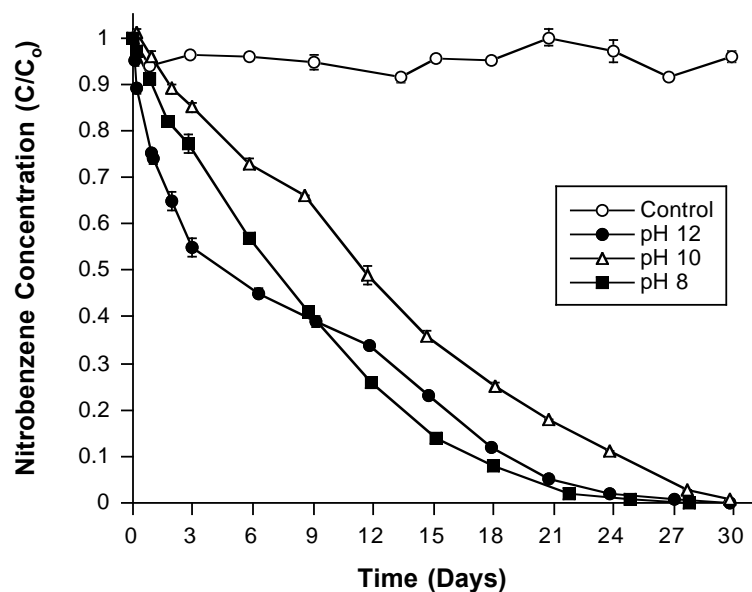
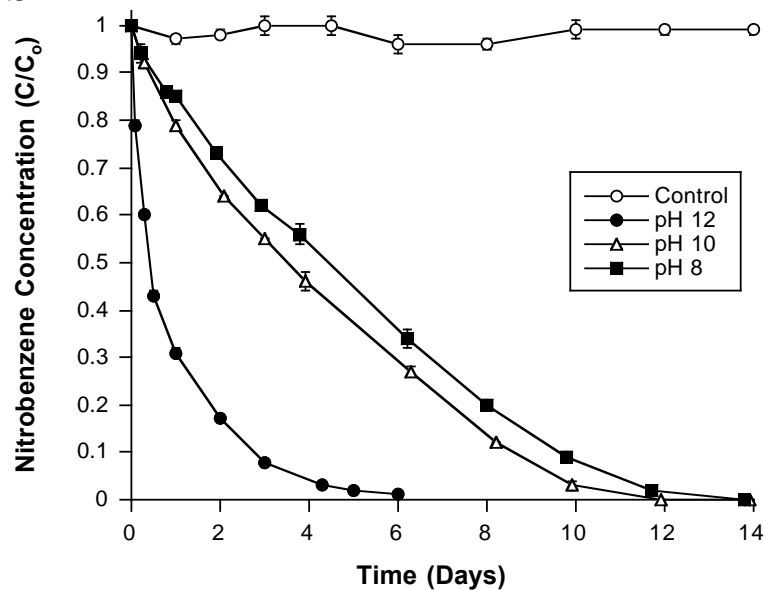
a**b**

Figure 7.1.3.13. Hydroxyl radical generation quantified through nitrobenzene degradation in soil slurries KB1-No SOM (a) and KB2-No SOM (b). Time denotes days after the system reached the indicated pH and was spiked with nitrobenzene.

Superoxide Radical and Reductant Generation as the pH Drifts to Circumneutral

Relative rates of superoxide radical and reductant generation were quantified by the reduction of hexachloroethane (HCA) as the pH drifted toward neutrality. HCA concentrations in the KB1 and KB2 slurries are shown in Figure 7.1.3.14a-b. HCA in the KB1 soil slurries was degraded to near-nondetectable concentrations after 2.5 d in the pH 12 system, 6 d in the pH 10 system, and 8 d in the pH 8 system. Reductant generation also occurred in parallel control systems with 62% HCA degradation after 8 d. The apparent reductant formation observed in the three soil slurries plus the control system indicate that SOM promoted reductive dechlorination in all four systems; SOM provides reducing conditions that likely degrade HCA by different pathways. Nevertheless, HCA degraded more rapidly in base-activated persulfate systems than in control systems.

HCA was degraded to nondetectable limits in the KB2 slurries after 5.5 d in the pH 12 system, and 8 d for both the pH 10 and pH 8 systems; 11% HCA degradation occurred in parallel control systems after 8 d. In general, reductant generation was greater in higher pH regimes for both the KB1 and KB2 soil systems. The pH 12 system of the KB1 soil slurries showed faster HCA degradation than the pH 12 system of the KB2 soil slurries with similar patterns for soil slurries in the pH 10 and pH 8 systems. Scavenging did not appear to affect the reductants as much as the oxidants; i.e., there was no significant difference in reductant formation between the KB1 and KB2 soils, with approximately 33% of the persulfate consumed before addition of the HCA probe.

Relative rates of reductant generation for the KB1-No SOM and KB2-No SOM slurries are shown in Figure 7.1.3.15a-b. HCA was degraded to nondetectable limits in the pH 12 system of the KB1-No SOM soil slurries after 6 d. HCA degradation of 90% occurred in the pH 10 system, and 25% in the pH 8 system after 8 d. HCA degradation in the KB2-No SOM soil slurries after 8 d was 83% in the pH 12 system, 27% in the pH 10 system, and 26% in the pH 8 system. Minimal HCA loss occurred in all parallel control systems. The pH 10 KB1-No SOM system showed significantly greater reductant generation than the parallel pH 10 KB2-No SOM system, which is likely due to slightly more organic matter remaining in the KB1-No SOM soil than the KB2-No SOM after the SOM removal procedure was completed. These results suggest that there is a minimum SOM concentration at which SOM can promote the generation of reductants.

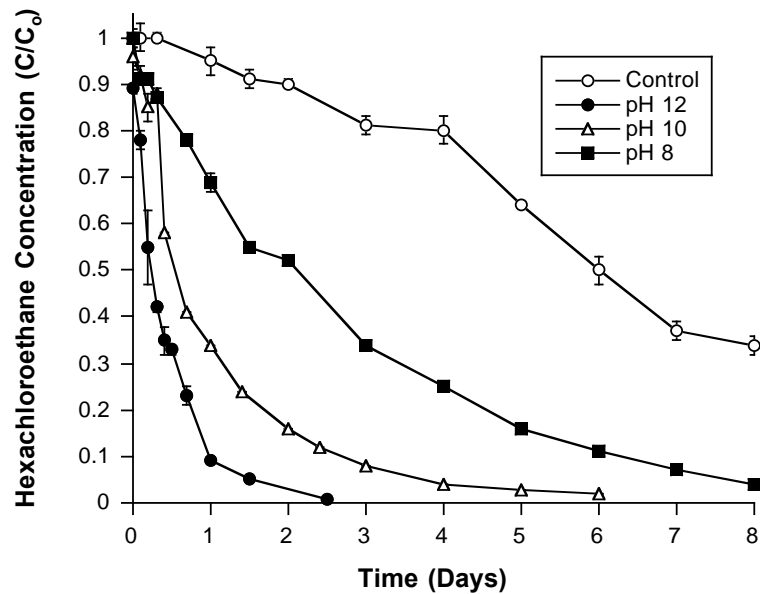
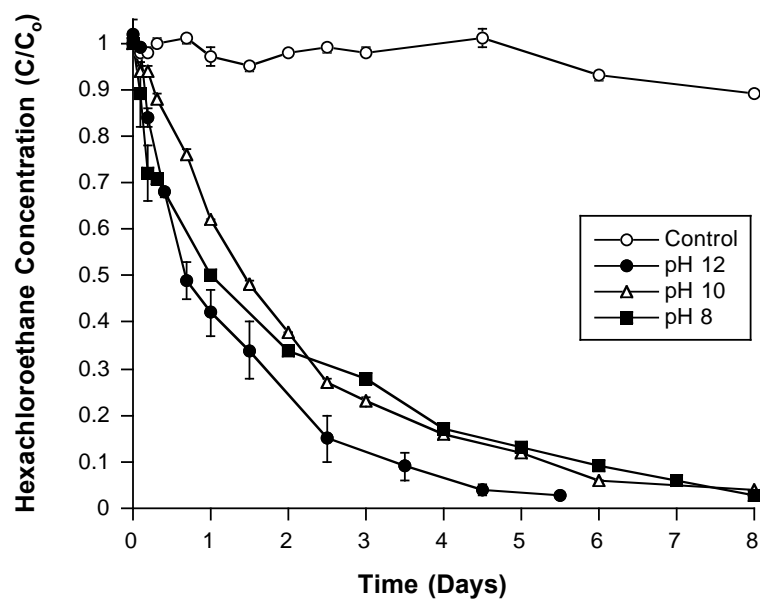
a**b**

Figure 7.1.3.14. Reductant generation quantified through hexachloroethane degradation in soil slurries KB1 (a) and KB2 (b). Time denotes days after the system reached the indicated pH and was spiked with hexachloroethane.

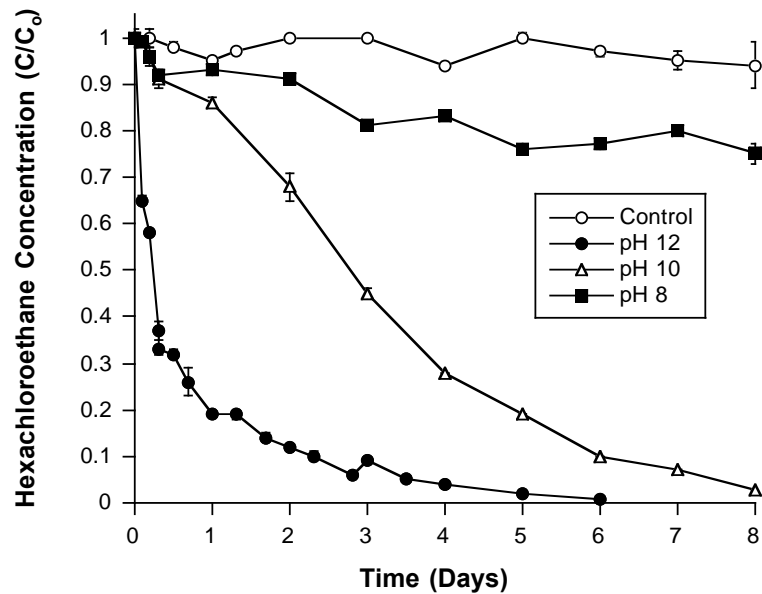
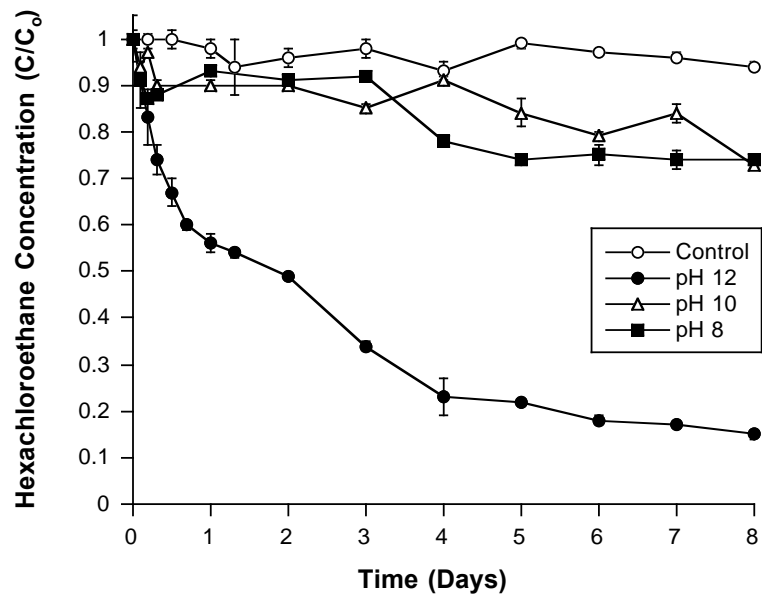
a**b**

Figure 7.1.3.15. Reductant generation quantified through hexachloroethane degradation in soil slurries KB1-No SOM (a) and KB2-No SOM (b). Time denotes days after the system reached the indicated pH and was spiked with hexachloroethane.

Conclusion

The potential for persulfate activation after base addition as the pH drifts from alkaline to circumneutral was investigated in four soil systems with varying SOM contents. Persulfate decomposition occurred most rapidly in the KB1 soil slurries due to the greater SOM content. Persulfate decomposition was minimal in the other slurries with the least occurring in the KB2-No SOM soil systems. pH drift was approximately parallel to persulfate decomposition in all four soil systems with the most rapid decline occurring in the presence of higher SOM.

In all soil slurries, hydroxyl radical and reductant formation occurred which was demonstrated by nitrobenzene and hexachloroethane degradation. In general, hydroxyl radical activity was greatest at higher pH systems, but still occurred in starting pH regimes of pH 10 and pH 8. Furthermore, greater rates of hydroxyl radical generation were found with decreasing SOM contents, which is likely due to a lower degree of hydroxyl scavenging by SOM.

Superoxide radical and reductant generation also occurred in all pH systems with lower generation rates as the pH drifted to circumneutral. In all pH systems, reductant generation was greatest in soil systems with greater SOM content. Considerably less reductant formation occurred for the systems at pH 10 and pH 8 once the SOM was removed, but reductants still formed.

The results of this research demonstrate that in the presence of subsurface solids, base-activated persulfate can generate reactive oxygen species in pH systems <10 ; these results differ from recent findings in which persulfate reactivity was negligible at pH <10 . SOM plays a significant role in this process by lowering net oxidant generation rates but promotes higher reductant activity. From a practical treatment perspective, application of base-activated persulfate in situ may potentially extend treatment longer than previously thought making it a more efficient ISCO technology.

7.1.4. Summary of Factors Controlling the Decomposition of Persulfate in the Subsurface

Table 7.1.4.1. Summary of factors controlling persulfate activation/decomposition

Factor	Comment
Major Subsurface Minerals	<ul style="list-style-type: none"> Persulfate decomposition rates were increased only slightly by iron and manganese oxides, and not at all by clays. In both high pH (> 12) and low pH (< 7) systems, the manganese oxide mineral birnessite was the most active initiator for generating additional oxidant flux, and the iron oxide mineral goethite was the most active initiator for generating reductants. The iron minerals ferrihydrite and hematite did not significantly activate persulfate at either pH regime. The clay minerals kaolinite and montmorillonite did not activate persulfate at either pH regime. The minerals present in a natural soil were not effective catalyzing persulfate to generate reactive oxygen species. The masses of crystalline Fe and Mn oxides typically found in soils are likely not sufficient to promote persulfate activation. However, the SOM of the natural soil was active in promoting reductant generation at high pH.
Trace Minerals	<ul style="list-style-type: none"> Persulfate decomposition was extremely rapid in the presence of cobaltite and pyrite; other trace minerals increased persulfate decomposition slightly and some not at all. Trace mineral-mediated decomposition of persulfate has varied consequences the in generation of reactive oxygen species, with some minerals increasing reactivity and others lowering reactivity.
Base-Activated Persulfate Treatment of Soils, with pH Drift	<ul style="list-style-type: none"> Greater persulfate decomposition occurred with higher SOM content. pH drift was approximately parallel to persulfate decomposition in all experimental soil systems, with the most rapid decomposition in presence of higher SOM. Hydroxyl radical activity was greatest in systems with an initial pH of 12, but was still significant when the initial pH was 10 and 8. Greater hydroxyl radical generation occurred with decreasing SOM content, likely due to decreased scavenging by SOM. Superoxide radical and reductant generation occurred in all pH systems, with decreased generation as pH drifted to circumneutral. Reductant generation was greater in soils with greater SOM content. Base-activated persulfate can generate reactive oxygen species even after the pH drifts below 10.

7.2. Persulfate Reactivity Under Different Conditions of Activation

7.2.1. Oxidative and Reductive Pathways in Iron-Ethylenediaminetetraacetic acid (EDTA) Activated Persulfate Systems

Persulfate Decomposition

The loss of persulfate in systems containing 2.5 mM, 5 mM, 10 mM, and 15 mM Na₂-EDTA, iron (II)-EDTA, and iron (III)-EDTA is shown in Figure 7.2.1.1a-d. Persulfate decomposition was minimal in the presence of 2.5 mM Na₂-EDTA, iron (II)-EDTA, and iron (III)-EDTA. However, persulfate decomposed 9% and 15% over 120 hr in the presence of 5 mM iron (II)-EDTA and iron (III)-EDTA, respectively. Persulfate decomposition with the addition of 5 mM Na₂-EDTA was not significantly different from persulfate decomposition in the deionized water control reactors. Addition of 10 mM iron (II)-EDTA and iron (III)-EDTA resulted in increased persulfate decomposition, with 22% loss in the presence of iron (II)-EDTA and 24% loss with iron (III)-EDTA. Persulfate loss in the system with 10 mM Na₂-EDTA was 4% relative to the control. The greatest persulfate loss occurred with the addition of 15 mM of the activators, with 25% persulfate decomposition in both the iron (II)-EDTA and iron (III)-EDTA systems. Systems containing 15 mM Na₂-EDTA showed less persulfate decomposition, with 12% persulfate loss relative to the control. The results of Figure 7.2.1.1 demonstrate that iron-EDTA chelates can decompose persulfate, and the rate of persulfate decomposition is proportional to the concentration of iron-EDTA. Such a trend is expected based on fundamental principles of catalysis; i.e., a higher turnover rate of substrate for higher concentrations of catalyst (Masel 2001). Furthermore, both iron (II) and iron (III) are similar in the promotion of persulfate decomposition when chelated with EDTA. The results of Figure 7.2.1.1 also document that Na₂-EDTA in the absence of iron also promotes some decomposition of persulfate, though to a lesser degree than iron-EDTA complexes. Ocampo (2009) reported that organic compounds such as phenoxides and keto acids can activate persulfate, and Na₂-EDTA may act similarly to decompose persulfate.

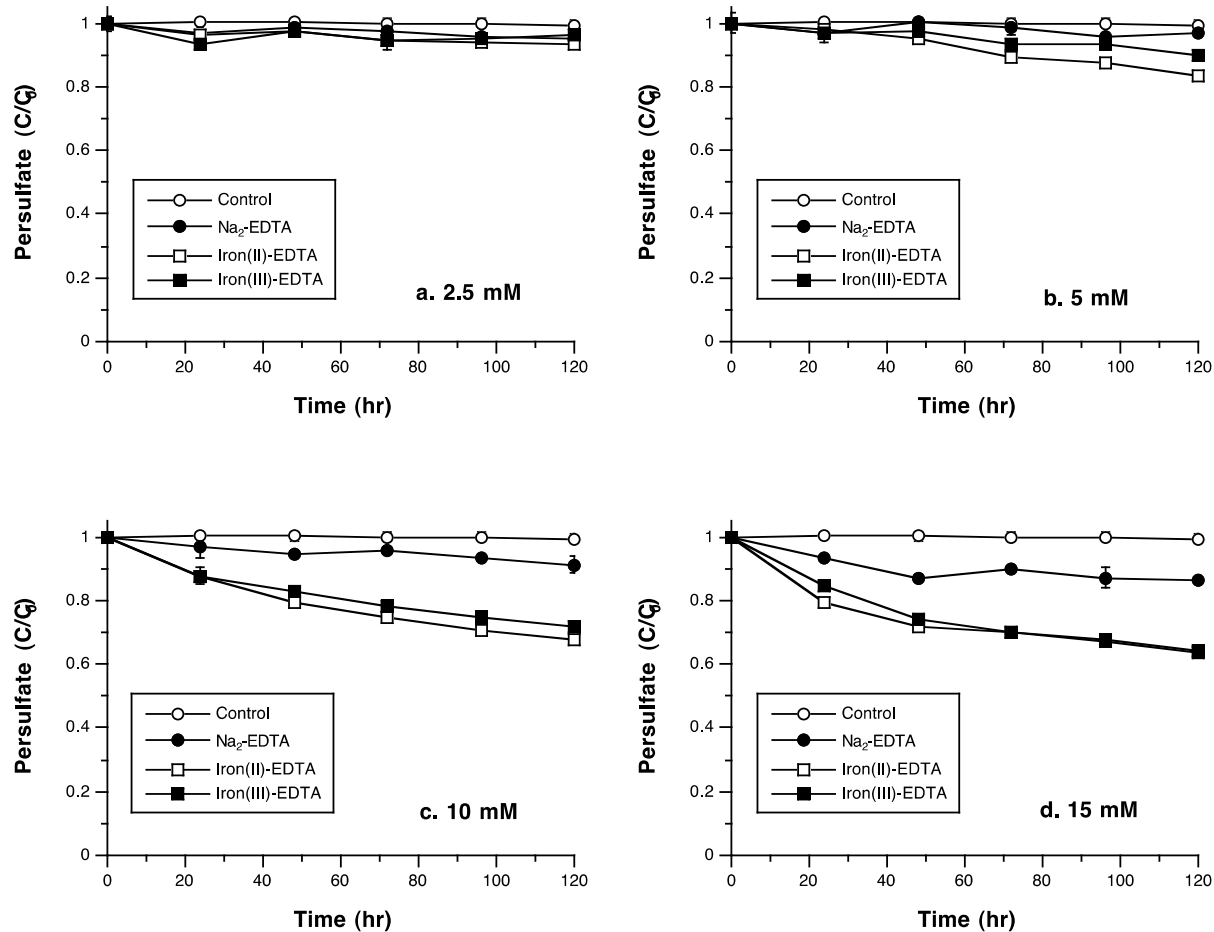


Figure 7.2.1.1. Persulfate decomposition in the presence of a) 2.5 mM; b) 5.0 mM; c) 10 mM; d) 15 mM of the activators $\text{Na}_2\text{-EDTA}$, iron (II)-EDTA, and iron (III)-EDTA.

Reactive Oxygen Species Generated in Iron-EDTA Activated Persulfate Systems

A suite of reactive oxygen species is often generated in base activated persulfate systems (Furman et al. 2010), and may also be generated in iron chelate activated persulfate systems. The cumulative generation of sulfate and hydroxyl radical in persulfate systems containing 10 mM Na₂-EDTA, iron (II)-EDTA, and iron (III)-EDTA, quantified by anisole loss, is shown in Figure 7.2.1.2. Persulfate systems in the presence of Na₂-EDTA promoted minimal loss of anisole over 2 hr relative to deionized water controls. In contrast, anisole loss was 88% over 2 hr in the iron (II)-EDTA system and > 99% over 25 min in the iron (III)-EDTA system. These results show that over the 2 hr reactions, Na₂-EDTA alone did not activate persulfate to generate sulfate or hydroxyl radical while the two iron EDTA chelates generated significant fluxes of sulfate and/or hydroxyl radical, with iron (III)-EDTA promoting a greater flux of radicals relative iron (II)-EDTA.

The generation of hydroxyl radical in persulfate systems containing 10 mM Na₂-EDTA, iron (II)-EDTA, and iron (III)-EDTA, quantified by nitrobenzene loss, is shown in Figure 7.2.1.3. Nitrobenzene loss in persulfate systems containing Na₂-EDTA was 51% over 80 hr relative to deionized water controls. Oxidation of nitrobenzene was 64% in the iron (II)-EDTA system and 86% in the iron (III)-EDTA system over 80 hr. These results demonstrate that iron (III)-EDTA activated persulfate promoted greater generation of hydroxyl radical compared to iron (II)-EDTA activated persulfate systems. Similar to the results of Figure 7.2.1.2, greater fluxes of hydroxyl radical were generated with iron (III)-EDTA compared to iron (II)-EDTA. However, nitrobenzene oxidation (Figure 7.2.1.3) was significantly slower than the rate of anisole oxidation (Figure 7.2.1.2). Nitrobenzene oxidation was likely slower because nitrobenzene reacts only with hydroxyl radical, whereas anisole reacts with both hydroxyl radical and sulfate radical; also, hydroxyl radical reacts slightly more rapidly with anisole ($k_{\text{OH}\cdot} = 5.4 \times 10^9 \text{ M}^{-1} \text{ sec}^{-1}$) than it does with nitrobenzene ($k_{\text{OH}\cdot} = 3.9 \times 10^9 \text{ M}^{-1} \text{ sec}^{-1}$).

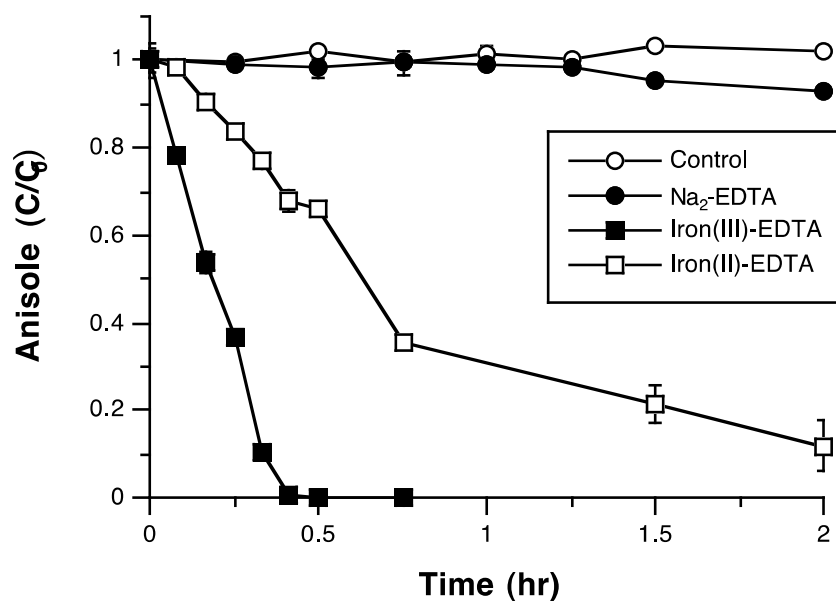


Figure 7.2.1.2. Degradation of the sulfate radical probe anisole in persulfate systems containing 10 mM Na₂-EDTA, iron (II)-EDTA, or iron (III)-EDTA.

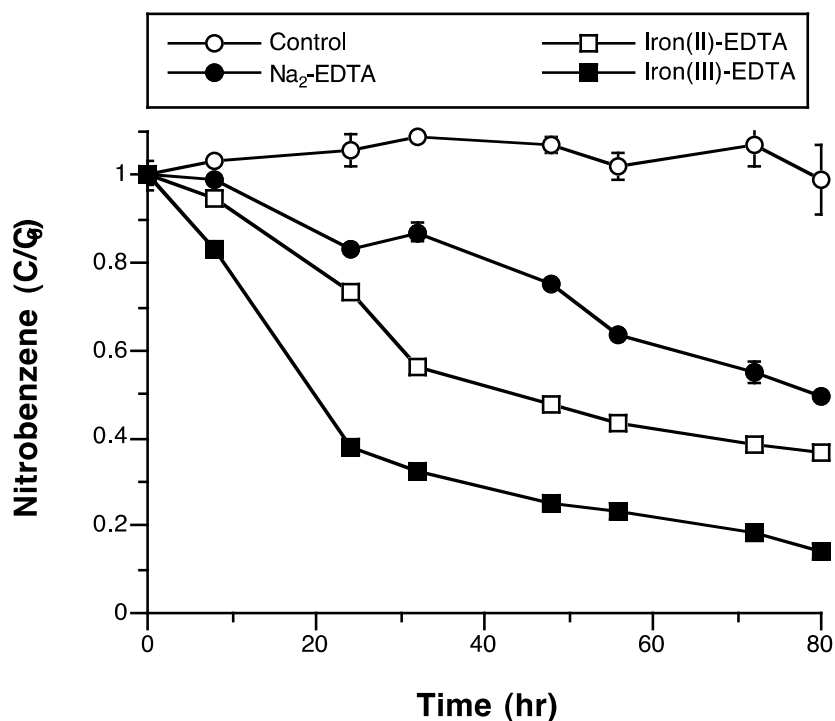


Figure 7.2.1.3. Degradation of the hydroxyl radical probe nitrobenzene in persulfate systems containing 10 mM Na₂-EDTA, iron (II)-EDTA, or iron (III)-EDTA.

The generation of reductants in the systems, quantified through HCA degradation, is shown in Figure 7.2.1.4. HCA degradation in $\text{Na}_2\text{-EDTA}$ persulfate systems was 22% over 80 hr relative to the deionized water control. In contrast, HCA degradation was 82% in the iron (II)-EDTA system and 80% in the iron (III)-EDTA system. Similar to the findings of Figures 7.2.1.2 and 7.2.1.3, these results demonstrate that iron-EDTA chelates are much more effective than $\text{Na}_2\text{-EDTA}$ alone in generating reductants from persulfate decomposition. However, unlike the results of Figures 7.2.1.2 and 7.2.1.3, iron (II) and iron (III) chelates appear to be equally effective in promoting reductant generation. Possible reductants in iron-EDTA activated persulfate systems include alkyl radicals, superoxide, or hydroperoxide (Smith et al. 2004). The potential to degrade highly oxidized organic contaminants greatly increases the effectiveness of activated persulfate ISCO applications.

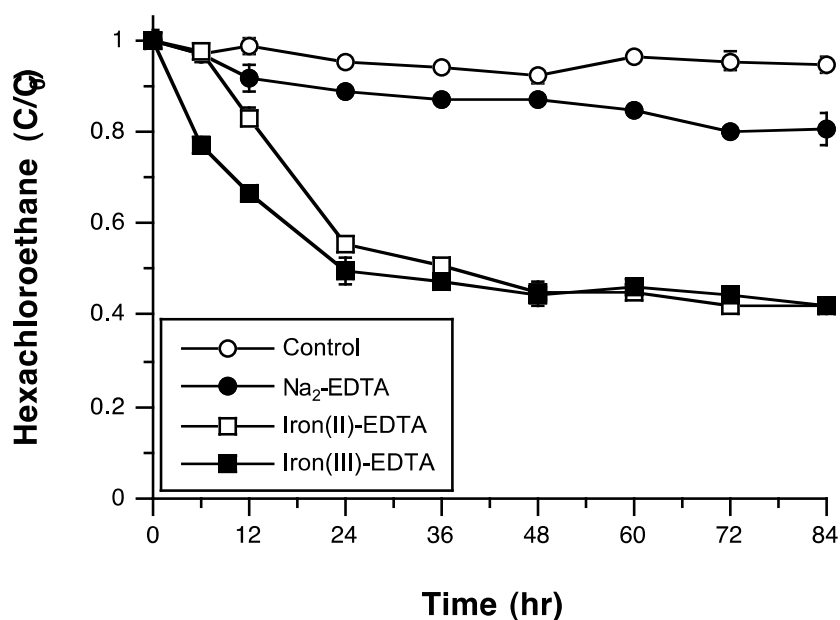


Figure 7.2.1.4. Degradation of the reductant probe hexachloroethane in persulfate systems containing 10 mM $\text{Na}_2\text{-EDTA}$, iron (II)-EDTA, or iron (III)-EDTA.

The results of Figures 7.2.1.2–4 demonstrate that both iron (II)-EDTA and iron (III)-EDTA activate persulfate, and that iron (III) activated persulfate promotes a greater flux of sulfate radical and hydroxyl radical compared to activation by iron (II)-EDTA. Unchelated iron (II) is well known as an activator of persulfate, but as it is oxidized to iron (III), persulfate activation stops (Liang et al. 2004). However, Liang et al. (2009) documented that iron (III)-EDTA is an effective activator of persulfate, and postulated that chelation by EDTA enhanced iron (II)–iron (III) cycling, allowing prolonged activation of persulfate. The results of Figures 7.2.1.2–4 are not only in agreement with the findings of Liang et al. (2009), but also show that iron (III)-EDTA is more effective than iron (II)-EDTA in promoting the generation of sulfate

radical and hydroxyl radical. A similar trend has been observed in CHP systems at hydrogen peroxide concentrations > 0.3 M; iron (III)-catalyzed decomposition of hydrogen peroxide promotes contaminant destruction much more effectively than iron (II)-catalyzed reactions (Watts and Dilly, 1996).

The results shown in Figures 7.2.1.2–4 indicate that a significant flux of sulfate radical, hydroxyl radical, and reductants is generated in iron (II)-EDTA and iron (III)-EDTA activated persulfate systems, with minimal persulfate decomposition over the same time period (Figure 7.2.1.1). The stoichiometry of radical generation in persulfate systems is significantly more efficient than in CHP systems, which is due to the large number of propagation reactions in these hydrogen peroxide based systems (Watts and Teel, 2005).

Scavenging of Reactive Oxygen Species

To elucidate the role of sulfate radical vs. hydroxyl radical in iron-EDTA activated persulfate systems, reactions with the probe compound anisole were repeated using the scavengers isopropanol and *tert*-butanol. Loss of the combined sulfate and hydroxyl radical probe anisole in iron (II)-EDTA activated persulfate systems in the presence of the combined sulfate and hydroxyl radical scavenger isopropanol and the hydroxyl radical scavenger *tert*-butanol is shown in Figure 7.2.1.5a. No measurable loss of anisole occurred over 2 hr in the presence of excess isopropanol, in contrast to the rapid degradation of anisole in the unscavenged persulfate system activated by iron (II)-EDTA. When hydroxyl radical alone was scavenged with the addition of excess *tert*-butanol, anisole loss was 22%, compared to 88% anisole loss with no scavenging. These results indicate that approximately 75% of the oxidation of anisole in iron (II)-EDTA activated persulfate systems was due to the activity of hydroxyl radical.

Loss of anisole using isopropanol and *tert*-butanol as scavengers in iron (III)-EDTA activated persulfate reactions is shown in Figure 7.2.1.5b. In the absence of the scavenger, anisole was oxidized to undetectable concentrations after 30 min. Similar to the results of Figure 7.2.1.5a, isopropanol scavenging resulted in anisole loss similar to the deionized water control, which demonstrates that sulfate radical and hydroxyl radical are the primary oxidants in iron (III)-EDTA activated persulfate systems. When hydroxyl radical was scavenged with excess *tert*-butanol, anisole was oxidized by 34% over 30 min, suggesting that approximately two-thirds of the anisole oxidation in iron (III)-EDTA activated persulfate systems is due to the activity of hydroxyl radical.

Sulfate radical is often presumed to be the dominant oxidant in activated persulfate systems at neutral pH (Couttenye et al., 2002, Huang et al., 2005). The results of Figure 7.2.1.5 show that hydroxyl radical is the predominant reactive oxygen species in both iron (II)-EDTA and iron (III)-EDTA activated persulfate systems at pH 5, and the ratio of sulfate radical to hydroxyl radical activity is similar in both systems. These findings suggest that the activity of hydroxyl radical may be more important than sulfate radical in iron-EDTA activated persulfate systems for ISCO. Similar results have been documented in base activated persulfate systems (Furman et al., 2010).

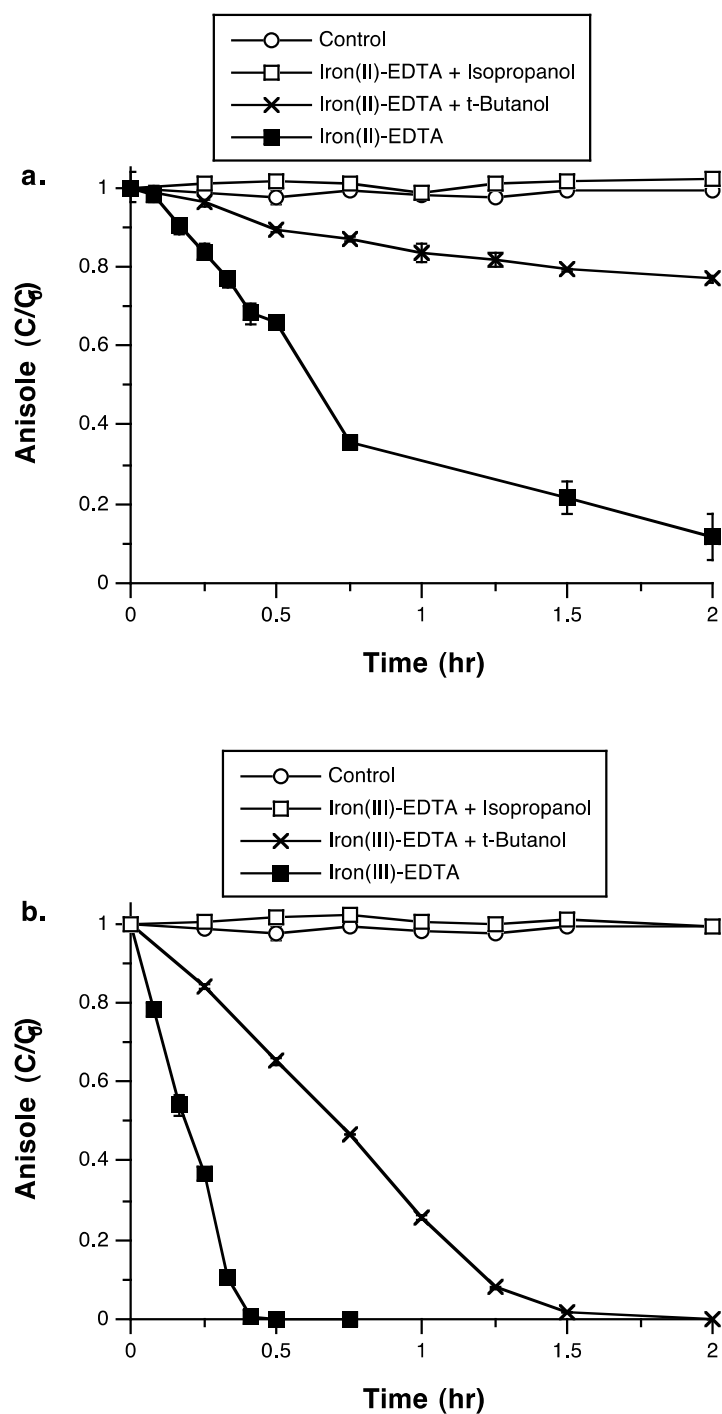


Figure 7.2.1.5. Scavenging of sulfate radicals and hydroxyl radicals using isopropanol and scavenging of of hydroxyl radicals using *tert*-butanol in persulfate systems activated by a) iron (II)-EDTA; b) iron (III)-EDTA.

Detection of Reactive Oxygen Species by ESR

The presence of hydroxyl and sulfate radicals in iron (II)-EDTA and iron (III)-EDTA activated persulfate reactions, previously detected using probe compounds, was confirmed by ESR using DMPO as a spin trapping agent (Figure 7.2.1.6a and b). A DMPO hydroxyl radical adduct with hyperfine splitting constants of $A_N = 14.96$ and $A_H = 14.78$ was observed with high intensity in the ESR spectra in both systems. A sulfate radical adduct with hyperfine splitting constants of $A_N = 13.51$, $A_H = 9.93$, $A^{\gamma_1}_H = 1.34$, and $A^{\gamma_2}_H = 0.88$ –gauss was observed in both systems but showed very low intensity compared to the hydroxyl radical adduct signal. The ESR spectra and hyperfine splitting constants are consistent with those reported for hydroxyl and sulfate radical in other studies (Kirino et al., 1981; Davies et al., 1992). No hydroxyl radical or sulfate radical adducts were observed in control reactions containing iron-EDTA and DMPO but no persulfate. These results, along with the data of Figure 7.2.1.5, show that hydroxyl radical is the predominant oxidant in iron-EDTA activated persulfate systems. Superoxide was not detected during the ESR analyses; the HCA degradation seen in Figure 7.2.1.4 may be due to organic radicals formed from the degradation of EDTA (Couttenye et al., 2002).

Degradation of a Model Groundwater Contaminant

TCE is one of the most commonly encountered groundwater contaminants, and has been used as a model contaminant in numerous activated persulfate studies (Liang et al. 2004; Dahmani et al. 2006; Liang et al. 2007; Liang and Lee 2008; Liang et al. 2008; Liang et al. 2009). Therefore, TCE was used as a model groundwater contaminant to confirm iron (II)-EDTA and iron (III)-EDTA activated persulfate reactivity, and to compare the results of this research to previous studies. Persulfate activated by iron (II)-EDTA resulted in 87% TCE degradation over 3 hr relative to deionized water controls (Figure 7.2.1.7a). Scavenging with the combined sulfate radical and hydroxyl radical scavenger isopropanol resulted in only 18% TCE loss, and scavenging with the hydroxyl radical scavenger *tert*-butanol resulted in 30% TCE loss. TCE degradation in iron (III)-EDTA activated persulfate systems was 98% over 3 hr relative to deionized water controls (Figure 7.2.1.7b). Scavenging with isopropanol resulted in only 16% TCE loss, and scavenging with the hydroxyl radical scavenger *tert*-butanol resulted in 23% TCE loss. The results suggest that iron (III)-EDTA may be a more effective activator than iron (II)-EDTA at pH 5, and confirm that hydroxyl radical has a major role and sulfate radical has only a minor role in degradation of contaminants in iron-EDTA activated persulfate systems. The small amount of TCE degradation that could not be eliminated by isopropanol scavenging was likely due to reductants in the system, as seen with HCA degradation (Figure 7.2.1.4). Although sulfate radical has traditionally been considered the primary reactive species in activated persulfate systems, the results of this research as well as other recent studies (Liang and Su, 2009; Furman et al., 2010) show that other reactive species are responsible for the degradation of contaminants, including TCE, in activated persulfate systems.

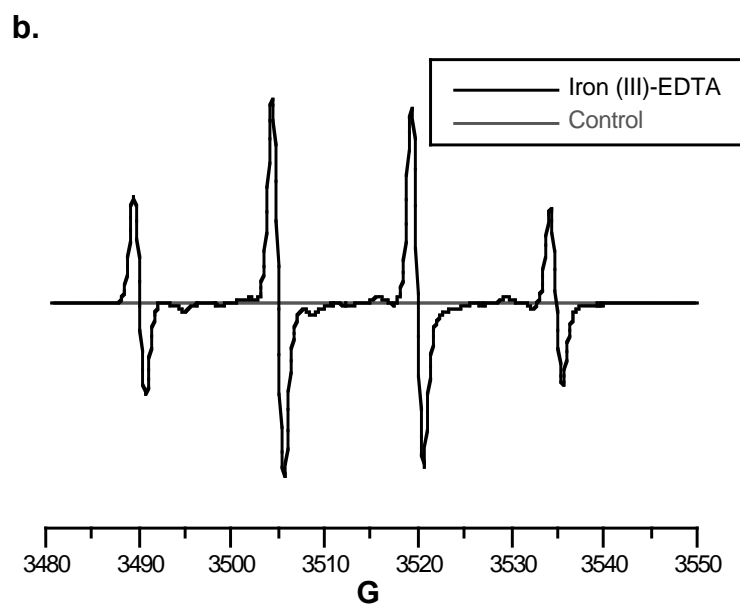
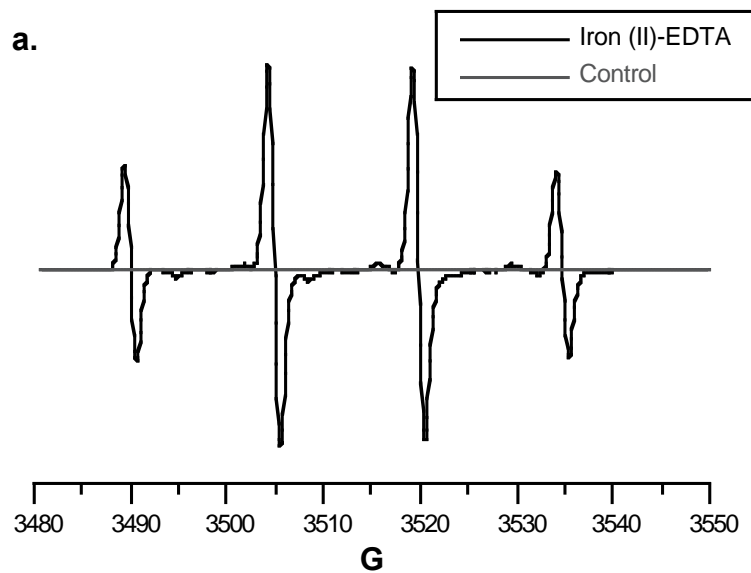


Figure 7.2.1.6. ESR spectra for a) iron (II)-EDTA and b) iron (III)-EDTA activated persulfate systems.

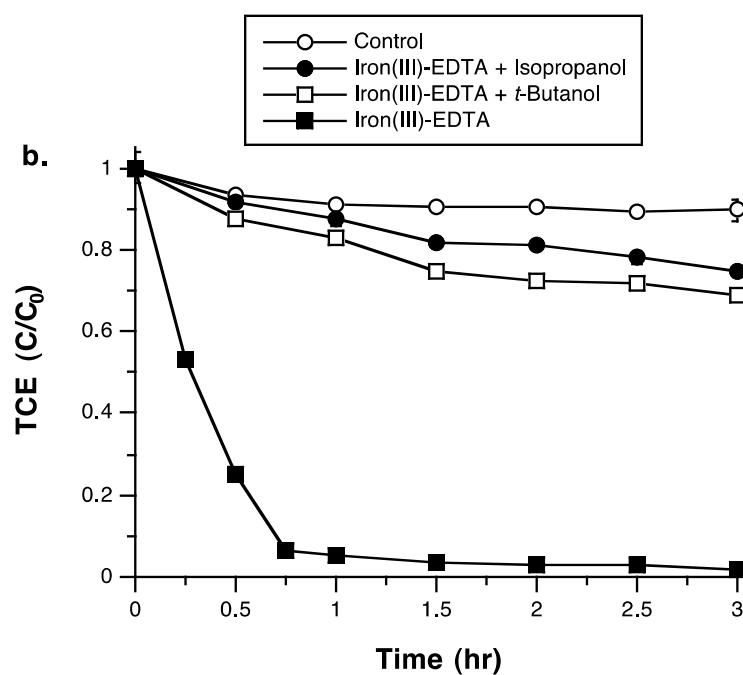
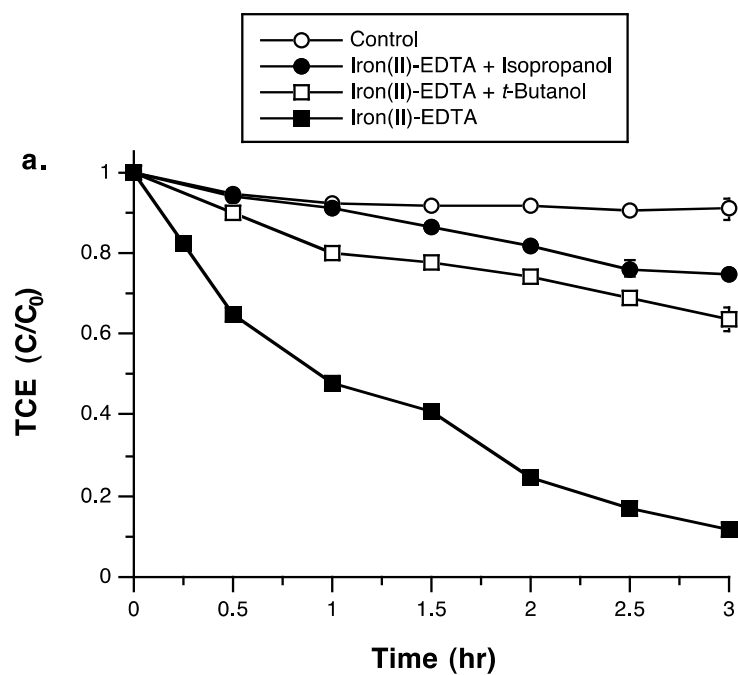


Figure 7.2.1.7. Degradation of the model groundwater pollutant TCE with scavenging by isopropanol and *tert*-butanol in persulfate systems activated by a) iron (II)-EDTA; b) iron (III)-EDTA.

Conclusion

Iron (II)-EDTA and iron (III)-EDTA were investigated for their potential to activate persulfate at circumneutral pH compared to $\text{Na}_2\text{-EDTA}$ alone. Although some persulfate decomposition occurred in the presence of $\text{Na}_2\text{-EDTA}$, both iron (II)-EDTA and iron (III)-EDTA decomposed persulfate more rapidly than $\text{Na}_2\text{-EDTA}$. The persulfate systems were investigated for their ability to generate sulfate radical, hydroxyl radical, and reductants using reaction-specific probe compounds. Along with these probes, scavengers were also used to isolate the relative roles of hydroxyl radical and sulfate radical, and the presence of hydroxyl radical in the reactions was confirmed using ESR. The results demonstrate that both iron (II)-EDTA and iron (III)-EDTA were effective for activating persulfate decomposition and generating reductants, while iron (III)-EDTA was somewhat more effective than iron (II)-EDTA in generating sulfate radical and hydroxyl radical. Furthermore, the dominant oxidant in the iron-EDTA activated persulfate systems was hydroxyl radical, rather than sulfate radical. Both iron (II)-EDTA and iron (III)-EDTA activation of persulfate were effective for the treatment of the model groundwater contaminant TCE. The results of this research show that iron (II)-EDTA and iron (III)-EDTA activated persulfate at circumneutral pH effectively generate sulfate radical, hydroxyl radical, and reductants. These reactive species have the potential to rapidly and effectively treat TCE and potentially other biorefractory contaminants.

7.2.2. Effect of Basicity on Persulfate Reactivity

Effect of pH on the generation of reactive oxygen species

The probe compound anisole is highly reactive with both sulfate radical and hydroxyl radical (O'Neill et al., 1975; Buxton et al., 1988); it was used because no compounds are available that react solely with sulfate radical. The combined generation of sulfate radical and hydroxyl radical in 0.5 M persulfate systems at pH 2, 7, and 12, measured by anisole degradation, is shown in Figure 7.2.2.1a. The system pH had a significant effect on the generation of sulfate radical and/or hydroxyl radical. Anisole oxidation was minimal at pH 2 and pH 7, indicating that sulfate radical and hydroxyl radical generation rates are very low at these pH regimes. In contrast, >99% of the anisole was oxidized over 30 min at pH 12, indicating that significant fluxes of sulfate radical, hydroxyl radical, or both are generated at pH 12. These data are in agreement with the results of Block (2004), who found that persulfate is highly reactive in basic systems.

The generation of hydroxyl radical in persulfate systems at pH 2, 7, and 12, measured by nitrobenzene loss, is shown in Figure 7.2.2.1b. Nitrobenzene degradation at pH 2 and 7 was similar to the rates in parallel control systems; however, > 60% oxidation of nitrobenzene occurred over 10 hr at pH 12. These results suggest that hydroxyl radical is an important reactive oxygen species in base-activated persulfate systems. Liang and Su (2009) also found that hydroxyl radical is a dominant reactive species in thermally activated persulfate systems at pH 12.

In addition to oxidants, base-activated persulfate systems may potentially generate reducing species. Hexachloroethane, a highly oxidized compound, was used to detect reducing species (Smith et al., 2004). Hexachloroethane degradation over the 96 hr reaction time was not significantly different from controls at pH 2 and pH 7 ($p > 0.05$), while 8% of the hexachloroethane was lost relative to the control at pH 12 over 96 hr ($p < 0.05$) (Figure 7.2.2.1c). These data show that reductants were generated only slowly or not at all at the three pH regimes.

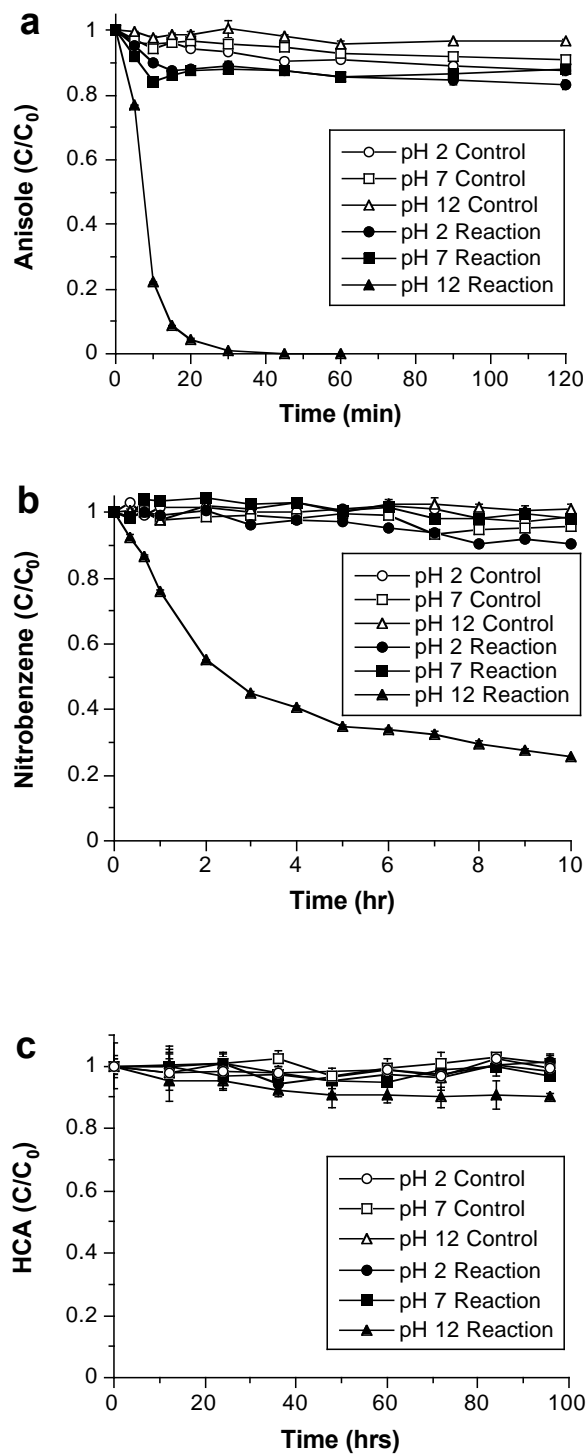


Figure 7.2.2.1. Activity of hydroxyl radical and reductants in persulfate systems at pH 2, 7, and 12. a) Sulfate and hydroxyl radical activity measured by anisole loss; b) Hydroxyl radical activity measured by nitrobenzene loss; c) Reductant activity measured by hexachloroethane loss.

The mechanism of base-activated persulfate has not been elucidated, but may involve the base-catalyzed hydrolysis of persulfate; the hydroperoxide formed through hydrolysis may then initiate propagation reactions that generate sulfate radical, hydroxyl radical, and superoxide radical anion. The activity of hydroxyl radical in 0.5 M persulfate systems at pH 12 was further investigated using anisole as a probe compound in conjunction with the hydroxyl radical scavenger *tert*-butyl alcohol and the hydroxyl radical/sulfate radical scavenger isopropyl alcohol (Figure 7.2.2.2a). Anisole loss in systems with no scavenging was > 99% in 30 min; however, scavenging of hydroxyl radical with *tert*-butyl alcohol resulted in only 12% loss of anisole, and scavenging of both hydroxyl radical and sulfate radical with isopropyl alcohol resulted in only 5% loss of anisole. These results demonstrate that the majority of oxidation in base-activated persulfate systems is the result of hydroxyl radical activity. To confirm the results shown in Figure 7.2.2.2a, the experiment was repeated with the hydroxyl radical probe nitrobenzene (Figure 7.2.2.2b). Minimal loss of nitrobenzene occurred in the presence of both isopropyl alcohol and *tert*-butyl alcohol after 10 hr, compared to 68% loss without scavengers, confirming that hydroxyl radical is a dominant oxidant in base-activated persulfate systems at pH 12.

The pathway by which hydroxyl radical is generated in base-activated persulfate systems is likely an electron transfer reaction with sulfate radical (Kolthoff and Miller 1951):



This pathway appears to be dominant in base-activated persulfate systems and results in widespread contaminant destruction. Sulfate radical is a relatively specific oxidant; it does not react rapidly with oxidized organic compounds such as those with a high degree of chlorine and nitrate substitution (Neta et al., 1977). The results of Figure 7.2.2.2a–b demonstrate that the dominant oxidative pathway of base-activated persulfate formulations is via hydroxyl radical, a strong, relatively nonspecific oxidant that reacts rapidly with > 95% of organic priority pollutants (Haag and Yao 1992). Because hydroxyl radical is the dominant reactive oxygen species in base-activated persulfate systems, subsequent experiments used only the hydroxyl radical probe nitrobenzene.

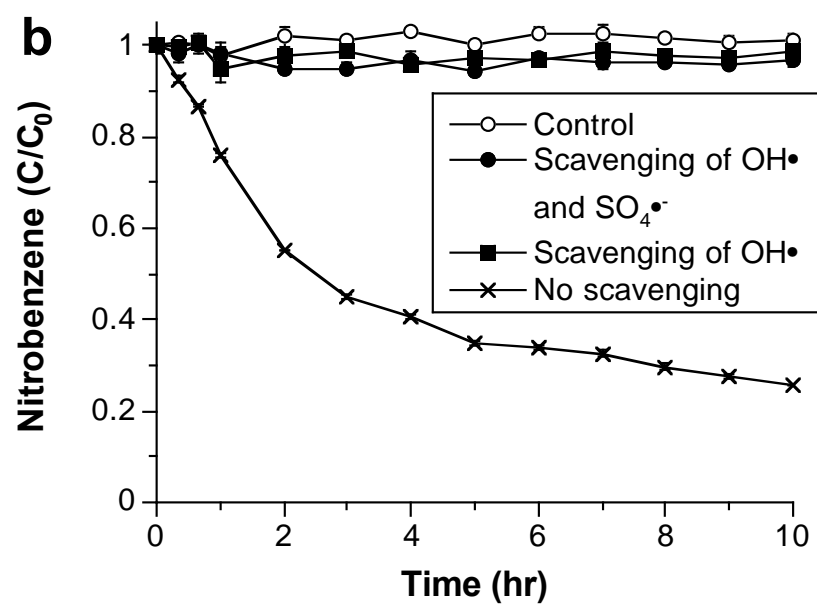
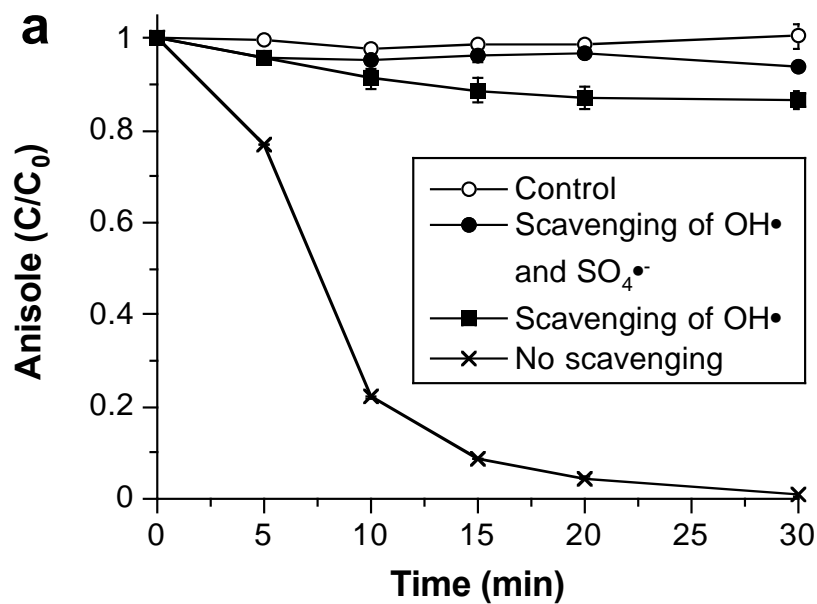


Figure 7.2.2.2. Activity of hydroxyl radical in the presence of a hydroxyl radical scavenger (*tert*-butyl alcohol) and a sulfate/hydroxyl radical scavenger (isopropyl alcohol) measured by a) anisole loss and b) nitrobenzene loss.

Effect of Persulfate Concentration on the Generation of Reactive Oxygen Species

The effect of persulfate concentration on the generation of hydroxyl radical at pH 12 is shown in Figure 7.2.2.3a. Increasing persulfate concentrations at pH 12 resulted in a greater flux of hydroxyl radical, as quantified by the degradation of nitrobenzene. Loss of nitrobenzene was negligible in 0.025 M and 0.05 M persulfate systems, while 42% and 68% of the nitrobenzene was lost over 10 hr with 0.25 M and 0.5 M persulfate, respectively. These results are consistent with other findings that higher concentrations of an oxidant source drive free radical generation (Watts and Teel, 2006). Generation of reductants, quantified by hexachloroethane degradation, with varying persulfate concentrations is shown in Figure 7.2.2.3b. Hexachloroethane degradation was negligible relative to the control for all four persulfate concentrations. These results confirm that in persulfate systems at pH 12, there is minimal generation of reducing species capable of degrading highly oxidized organic compounds. The data of Figure 7.2.2.3a–b demonstrate that higher persulfate concentrations in systems at pH 12 promoted increased oxidation through hydroxyl radical, but did not increase the degradation rate of highly oxidized compounds, such as hexachloroethane. These results are in agreement with those of Liang et al. (2003, 2004a, 2004b) and Huang et al. (2002, 2005), who also found greater contaminant oxidation rates with higher persulfate concentrations in heat- and Fe(II)-activated persulfate systems. Negligible carbon tetrachloride degradation in a heat-activated persulfate system was also observed by Huang et al. (2005).

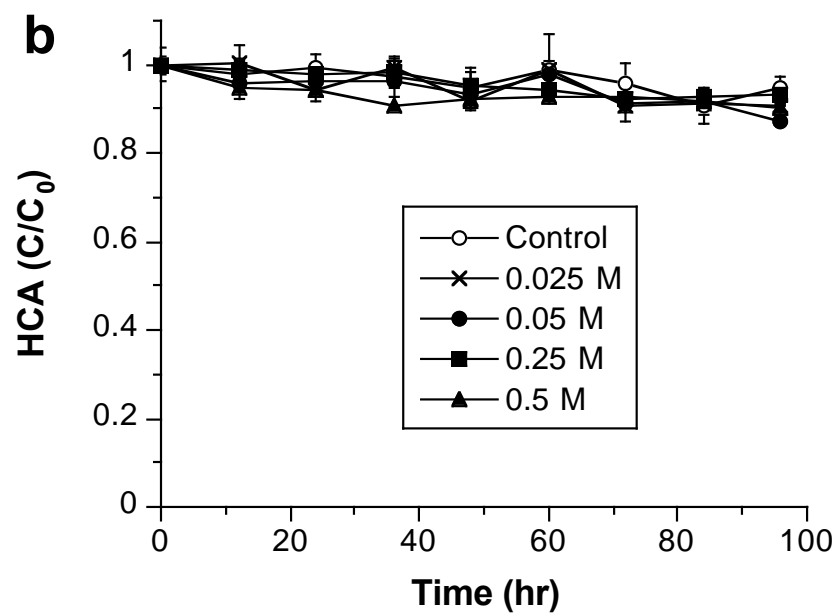
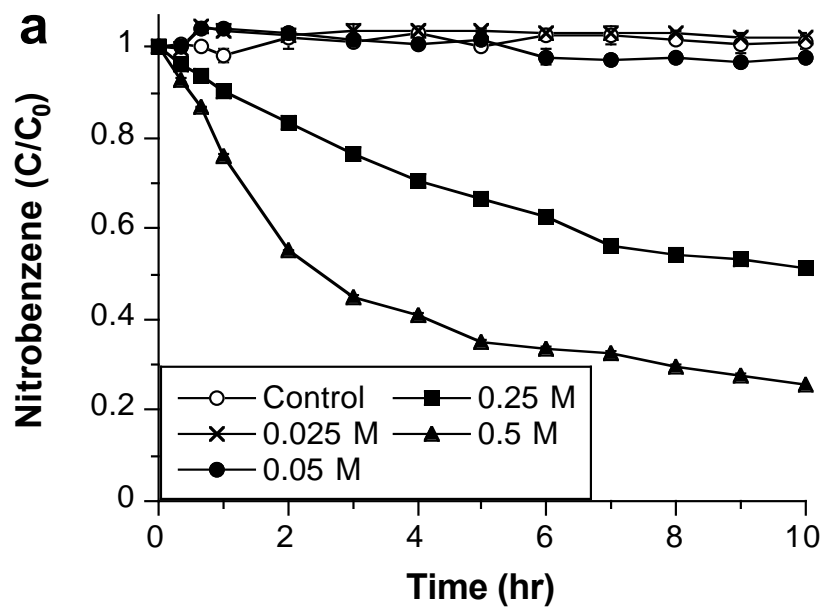


Figure 7.2.2.3. Activity of hydroxyl radical and reductants in systems with four different persulfate concentrations. a) Hydroxyl radical activity measured by nitrobenzene loss; b) Reductant activity measured by hexachloroethane loss.

Relative rates of reactive oxygen species generation at high base:persulfate ratios

Persulfate solutions adjusted to pH 12 resulted in effective hydroxyl radical generation but minimal reductant generation. However, base-activated persulfate systems at pH 12 contained a relatively low concentration of base, with a base:persulfate molar ratio of 0.04:1. Therefore, higher base:persulfate ratios were investigated to determine if greater reactivity could be achieved. An additional benefit of higher base:persulfate ratios is the potential of a lesser pH drop as the persulfate decomposes to sulfuric acid. The relative rate of hydroxyl radical generation in base-activated persulfate (0.5 M) systems containing 0.2:1, 0.5:1, 1:1, 2:1, and 3:1 base:persulfate molar ratios, quantified through the degradation of nitrobenzene, is shown in Figure 7.2.2.4a. There was no significant difference in nitrobenzene degradation between all five base:persulfate ratios; $\geq 90\%$ of the nitrobenzene was degraded in approximately 12 hr in all of these systems. These results indicate that increasing the base:persulfate ratios up to 3:1 does not significantly affect hydroxyl radical generation, which may be due to near-equal rates of base-catalyzed hydrolysis of persulfate at these molar ratios. Nitrobenzene loss for each of the five base:persulfate molar ratios was characterized by a sigmoidal trend. Liang and Bruell (2008) found a fractional reaction order with respect to persulfate in thermally activated persulfate systems; such a fractional reaction order may be characteristic of the base-activated system shown in Figure 7.2.2.4a, and the reaction order may change as the reaction proceeds.

Relative rates of hydroxyl radical generation, quantified through nitrobenzene loss, for base:persulfate molar ratios of 4:1, 5:1, and 6:1 are shown in Figure 7.2.2.4b. The trends in nitrobenzene loss in Figure 7.2.2.4b are different from the trends in Figure 7.2.2.4a in two ways: 1) the rate of nitrobenzene loss was exponential rather than sigmoidal, and 2) the rate of nitrobenzene loss increased with increasing hydroxide concentrations. These trends may be due to the increased rates of initiation provided by the high concentrations of hydroxide, which may promote the exponential loss of nitrobenzene, indicating a high flux of hydroxyl radical.

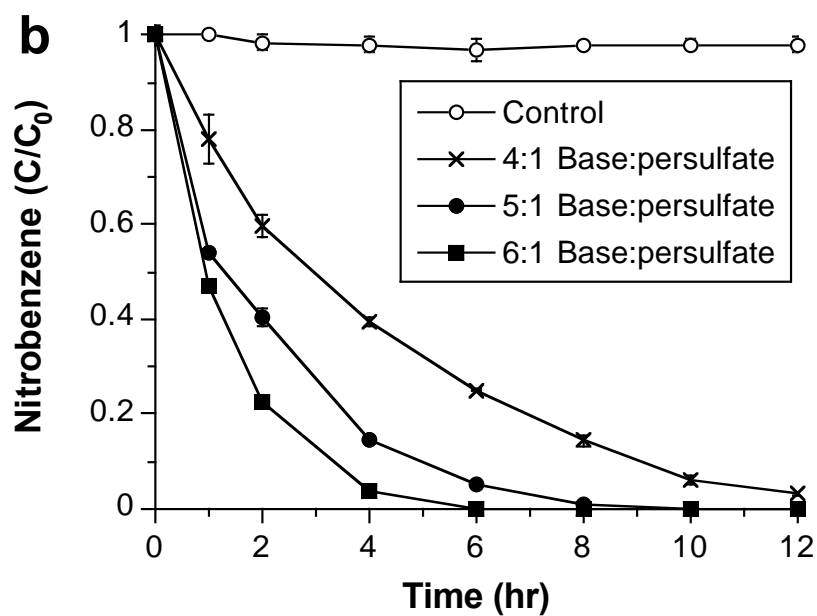
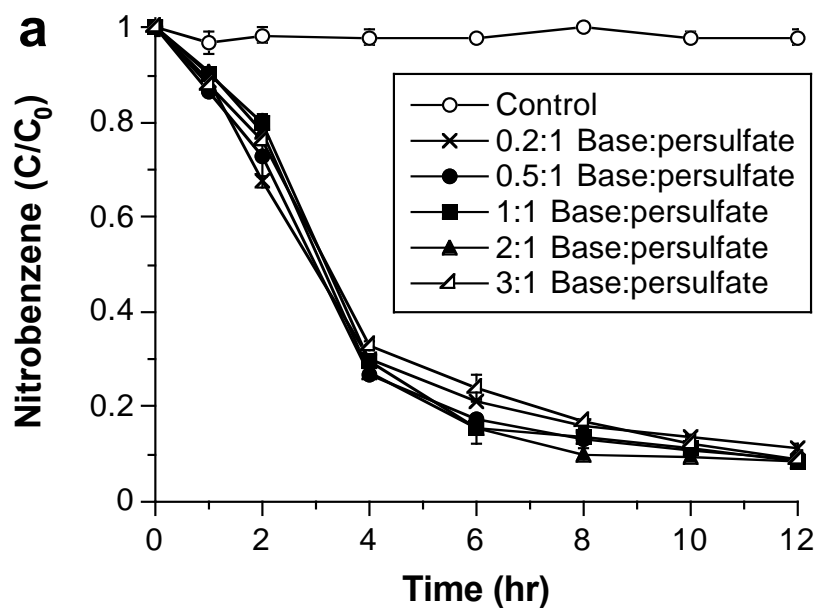


Figure 7.2.2.4. Activity of hydroxyl radical in persulfate systems containing varying molar ratios of base:persulfate measured by nitrobenzene loss. a) Base:persulfate ratios from 0.2:1 to 3:1; b) Base:persulfate ratios from 4:1 to 6:1.

Relative rates of reductant generation for persulfate formulations containing 0.5 M persulfate activated by hydroxide in molar ratios ranging from 1:1 to 6:1 base:persulfate are shown in Figure 7.2.2.5a–f. In contrast to the minimal reductant activity at pH 12 (Figures 7.2.2.1c and 7.2.2.3b), succeeding higher rates of reductant generation were observed with increasing basicity beyond a 1:1 base:persulfate molar ratio. Hexachloroethane concentrations in the control systems decreased succeeding faster at higher hydroxide dosages, which was likely due to the base-catalyzed hydrolysis of hexachloroethane (Larson and Weber, 1994); nonetheless, net reductant generation rates relative to the controls increased with higher base:persulfate ratios. The increase in reductant generation may be the result of an increased rate of base-catalyzed hydrolysis of persulfate resulting in the generation of hydroperoxide anion and superoxide anion. The data shown in Figures 7.2.2.4–5 demonstrate that higher molar ratios of base:persulfate result in a change in degradation pathways compared to systems that are simply adjusted to pH 12. While the activity of hydroxyl radical predominates in pH 12 reactions, increasing the hydroxide concentration results in increased reductant activity. An additional advantage of using higher base dosages than that required for the simple adjustment to pH 12 is related to the drop in pH that occurs as persulfate decomposes. Decomposition of one mole of persulfate generates two moles of sulfuric acid, so a base:persulfate molar ratio of 2:1 would result in near-neutral pH after the reaction is complete. In contrast, the small mass of base required to adjust the pH to 12 would be rapidly overcome by the large mass of sulfuric acid formed, resulting in acidic pH conditions when the reaction is complete.

The results of this research demonstrate that base-activated persulfate is characterized by varied reactivity under different conditions of basicity. When the pH is simply adjusted to pH 12, a significant flux of hydroxyl radical is generated, with minimal activity of reducing species. However, when increasingly higher concentrations of base were used in persulfate systems, rates of reductant generation increased in proportion to the molar ratio of base added to the persulfate formulations. In summary, increased concentrations of base in persulfate formulations, particularly above a base:persulfate molar ratio of 3:1, increased the oxidant and reductant reactivity of the system. These results demonstrate that base-activated persulfate using high base:persulfate ratios can be an important process condition for the ISCO treatment of contaminated soils and groundwater.

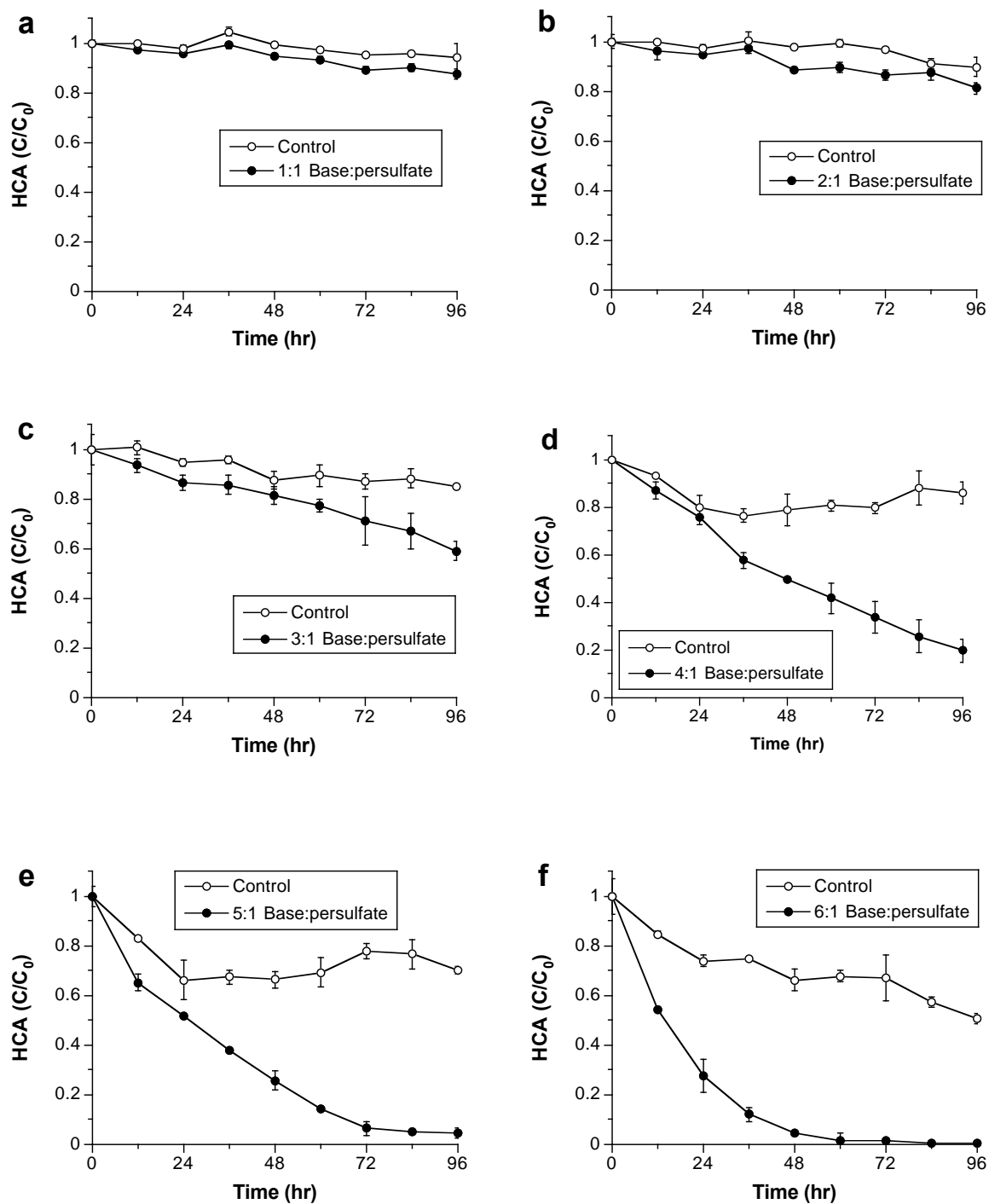


Figure 7.2.2.5. Activity of reductants in persulfate systems containing varying molar ratios of base:persulfate measured by hexachloroethane loss. a) Base:persulfate ratio of 1:1; b) Base:persulfate ratio of 2:1; c) Base:persulfate ratio of 3:1; d) Base:persulfate ratio of 4:1; e) Base:persulfate ratio of 5:1; f) Base:persulfate ratio of 6:1.

Conclusion

The reactive species generated in persulfate solutions at pH 2 and pH 7 and in base-activated persulfate systems were investigated as a basis for evaluating persulfate reactivity for ISCO applications. Using probe compounds of specific reactivity with sulfate radical, hydroxyl radical, and reductants, persulfate-driven oxidation was more rapid at pH 12 than at lower pH regimes, but only slightly effective at generating reductants at pH 12. The hydroxyl radical scavenger *tert*-butyl alcohol and the sulfate and hydroxyl radical scavenger isopropyl alcohol were used to further isolate the primary oxidative pathway at pH 12; hydroxyl radical was found to be the dominant oxidative species in base-activated persulfate systems. Increasing the molar ratio of base:persulfate increased the rate of hydroxyl radical generation slightly beyond that seen at pH 12, but no significant differences in hydroxyl radical generation were found at molar ratios between 0.2:1 and 3:1. However, succeeding higher hydroxyl radical generation rates were found at base:persulfate molar ratios of 4:1, 5:1, and 6:1. Reductant generation increased above base:persulfate molar ratios of 1:1, with increasing rates of reductant generation occurring with increasing molar ratios. These results demonstrate that base-activated persulfate systems become increasingly reactive with higher base:persulfate molar ratios.

7.2.3. Mechanism of Base Activation of Persulfate

Base-Activated Persulfate Decomposition Kinetics

The pseudo-first order loss of persulfate in solutions with a range of base:persulfate molar ratios is shown in Figure 7.2.3.1a. Persulfate decomposition rates increased with increasing concentrations of NaOH, demonstrating that the rate of persulfate decomposition is a function of basicity. Therefore, the relationship between the first-order persulfate decomposition rate and NaOH concentration was evaluated to determine the reaction order with respect to NaOH. When $\ln[\text{NaOH}]$ was plotted as a function of $\ln[\text{persulfate}]$ (Figure 7.2.3.1b), the slope was 2.2, which indicates a second order reaction with respect to NaOH (Houston, 2006).

The results of Figure 7.2.3.1 suggest that the base-catalyzed hydrolysis of persulfate is the first step in the activation of persulfate under alkaline conditions (Mabey and Mill, 1978). To confirm the base-catalyzed hydrolysis of persulfate, persulfate decomposition reactions were conducted in D_2O vs. H_2O . The results of Figure 7.2.3.2 show greater persulfate decomposition in D_2O , with $k_{\text{D}_2\text{O}}/k_{\text{H}_2\text{O}} = 1.3$; these results are consistent with the kinetics of base-catalyzed hydrolysis of esters and amides (Marlier et al., 1999; Slebocka-Tilk et al., 2003). Because the $\text{D}_2\text{O}/\text{DO}^-$ system provides stronger nucleophilic activity than the $\text{H}_2\text{O}/\text{HO}^-$ system (Slebocka-Tilk et al., 2003), the inverse deuterium kinetic isotope experimental value of 1.3 derived from Figure 7.2.3.2 confirms a hydroxide-catalyzed direct nucleophilic attack on persulfate.

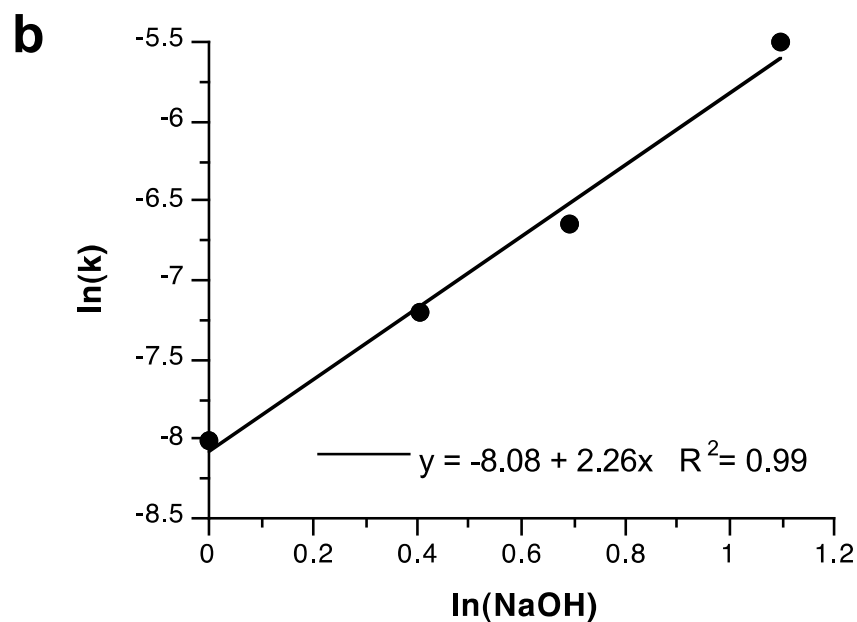
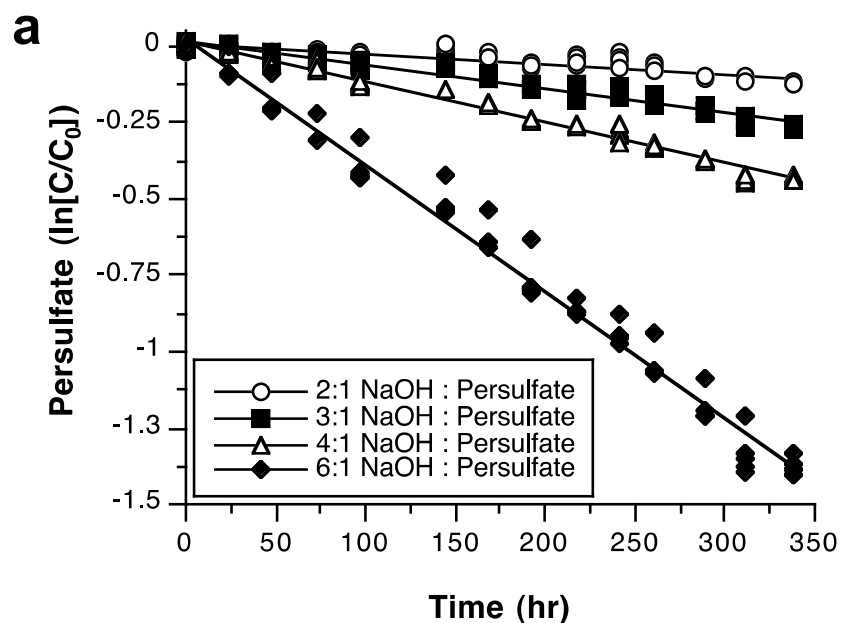


Figure 7.2.3.1. a) First order decomposition of base-activated persulfate with varying molar ratios of NaOH:persulfate (reactors: 0.5 M persulfate, 1 M, 1.5 M, 2 M, or 3 M NaOH; 20 mL total volume; $T = 20 \pm 2^\circ\text{C}$). b) First order rate constants for persulfate decomposition in base-activated systems as a function of initial NaOH concentration.

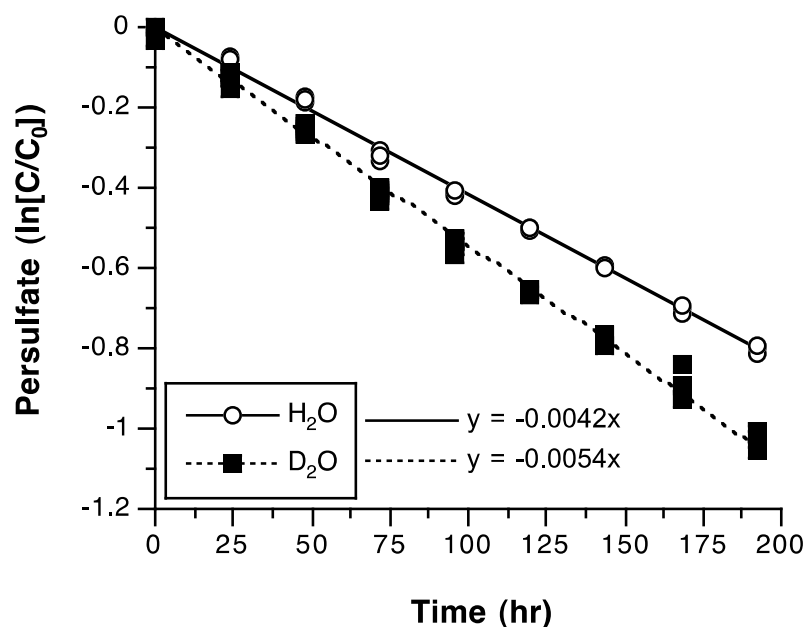


Figure 7.2.3.2. First order decomposition of base-activated persulfate in D₂O vs. H₂O (reactors: 0.5 M persulfate and 3 M NaOH in 20 mL total volume of D₂O or H₂O; T = 20 ± 2°C).

In addition, the effect of ionic strength on the rate of persulfate decomposition was investigated in base-activated persulfate systems; persulfate decomposition rates increased as a function of ionic strength (Figure 7.2.3.3). These results are in agreement with the Debye-Hückel-Bronsted theory and demonstrate a positive electrolyte effect, which indicates that the rate-determining step is a reaction between two negatively charged ions (i.e., persulfate and hydroxide) (Singh and Venkatarao, 1976).

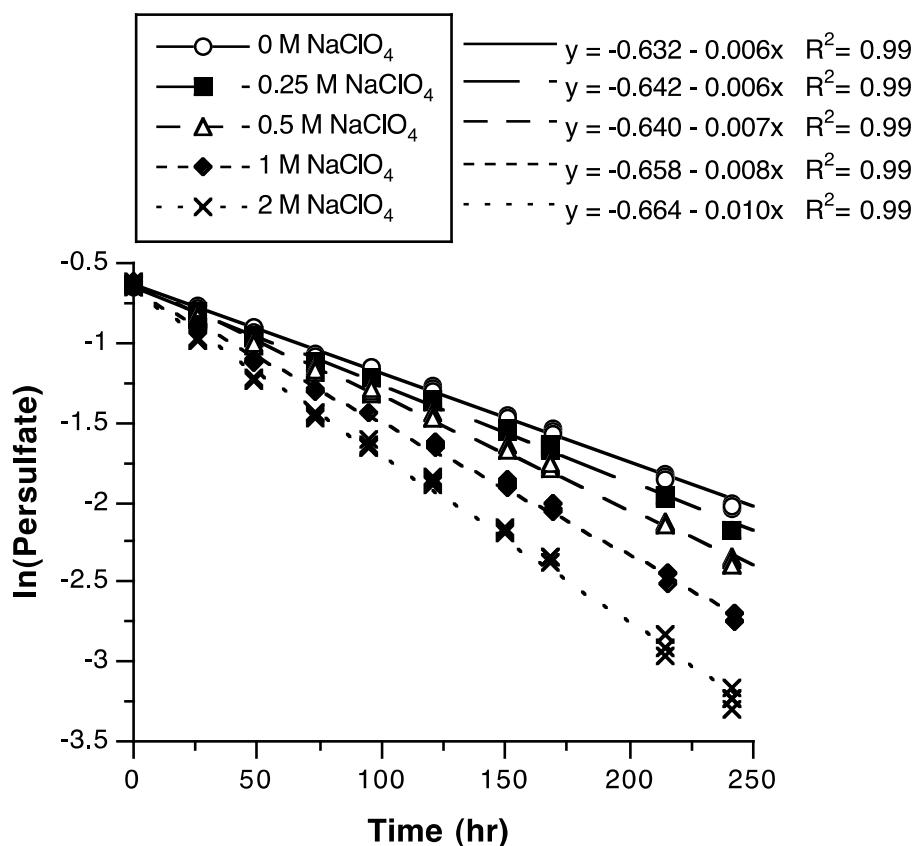
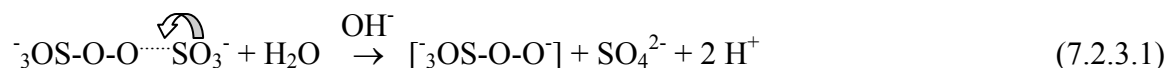


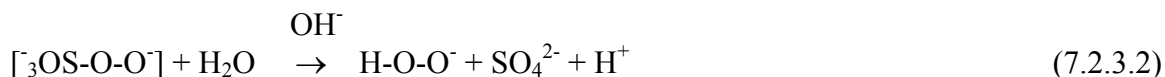
Figure 7.2.3.3. Effect of ionic strength on persulfate degradation rate (reactors: 0.5 M persulfate, 3 M NaOH, 0–2 M NaClO₄; 20 mL total volume; T = 20 ± 2°C). Error bars represent the standard error of the mean.

Proposed Mechanism

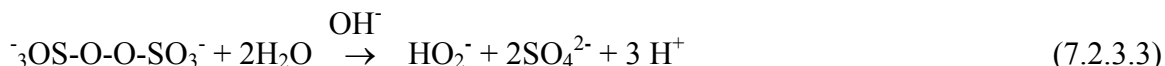
Based on the results of Figures 7.2.3.1 and 7.2.3.2, the initial step of the proposed mechanism is the base-catalyzed hydrolysis of persulfate (S₂O₈²⁻) to peroxomonosulfate (SO₅²⁻) and sulfate (SO₄²⁻). Persulfate likely forms an activated complex with hydroxide that weakens the S—O bond:



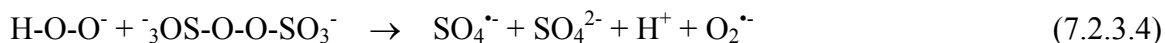
As a result, the S—O bond undergoes fission. A similar fission of the remaining S—O bond in peroxomonosulfate results in the formation of sulfate and hydroperoxide (HO₂⁻), the conjugate base of hydrogen peroxide:



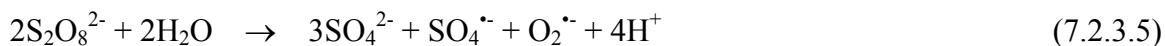
In reaction 7.2.3.1, peroxomonosulfate would be formed as a transient intermediate during the base-catalyzed hydrolysis of persulfate; however, it was not detected by ion chromatography in solutions containing persulfate and any of numerous NaOH concentrations. Peroxomonosulfate undergoes rapid decomposition to hydroperoxide and sulfate at basic pH (Ball and Edwards, 1956; Koubek et al., 1964; Lunenok-Burmakina and Aleeva, 1972); therefore, no detectable peroxomonosulfate is expected in base-activated persulfate systems. Reactions 7.2.3.1 and 7.2.3.2 can be summed to provide the following net reaction for the base-catalyzed hydrolysis of persulfate:



Preliminary experiments using HCA as a superoxide probe (Furman et al., 2009; Furman et al., 2010) showed the presence of superoxide in base-activated persulfate systems, which suggests that superoxide may be generated as a result of persulfate activation. In the proposed mechanism, the hydroperoxide formed from the hydrolysis of one persulfate molecule then reduces another persulfate molecule, generating sulfate radical ($\text{SO}_4^{\bullet-}$) and sulfate anion, while hydroperoxide is oxidized to superoxide ($\text{O}_2^{\bullet-}$):



Reduction and initiation of an oxidant by hydroperoxide is not without precedent; Staehelin and Hoigné (1982) documented the reduction of ozone by hydroperoxide in ozone/ H_2O_2 advanced oxidation processes. Summing reactions 7.2.3.3 and 7.2.3.4 yields the following net reaction for persulfate activation under basic conditions:



Furthermore, in highly alkaline conditions, sulfate radical reacts with hydroxide to form hydroxyl radical (OH^\bullet) (Hayon et al., 1972):



To confirm the proposed mechanism described in reactions 7.2.3.4–6, the reduction of persulfate by hydroperoxide, the generation of superoxide, and the stoichiometric evolution of oxygen were evaluated in base-activated persulfate systems.

Reduction of Persulfate by Hydroperoxide Anion

In the proposed mechanism, hydroperoxide is generated through reaction 7.2.3.2; however, hydroperoxide was non-detectable by Ti (IV) sulfate complexation or ion chromatography (Eisenberg, 1943). Other methods typically used to detect $\text{H}_2\text{O}_2 + \text{HO}_2^-$, such as iodometric titration or catalase, could not be used because of positive interference from

persulfate. Persulfate decomposes relatively slowly, with a rate of $\sim 3.3 \times 10^{-3}$ mM/min in a solution of 0.5 M persulfate and 3 M NaOH (Figure 7.2.3.1). Therefore, hydroperoxide would be generated through reaction 7.2.3.2 at approximately the same low rate; because hydroperoxide is likely consumed by reduction of persulfate at a rate significantly more rapid than its production, it is undetectable in base-activated persulfate systems. To confirm the rapid rate of reaction of hydroperoxide, 3.3×10^{-3} mM $\text{H}_2\text{O}_2 + \text{HO}_2^-$ was added to a basic persulfate system (0.5 M persulfate and 3 M NaOH) and was assayed with titanium sulfate complexation; no $\text{H}_2\text{O}_2 + \text{HO}_2^-$ was detected.

To evaluate the fate of hydroperoxide generated through the base-catalyzed hydrolysis of persulfate, external hydroperoxide addition was investigated from two perspectives: 1) the fate of $\text{H}_2\text{O}_2 + \text{HO}_2^-$ after its addition to basic persulfate systems, and 2) the effect of adding excess $\text{H}_2\text{O}_2 + \text{HO}_2^-$ on the generation of superoxide. $\text{H}_2\text{O}_2 + \text{HO}_2^-$ concentrations decreased rapidly when hydrogen peroxide was added to basic persulfate solutions (Figure 7.2.3.4) with 95% loss after 15 min, confirming that hydroperoxide reacts rapidly with persulfate. Furthermore, both persulfate and $\text{H}_2\text{O}_2 + \text{HO}_2^-$ decomposed at the same rate, with $> 98\%$ degradation by 180 min; because the starting masses were equivalent, the degradation stoichiometry of hydroperoxide:persulfate was 1:1. The rate of persulfate decomposition in the presence of added $\text{H}_2\text{O}_2 + \text{HO}_2^-$ in Figure 7.2.3.4 was significantly faster than that shown in Figure 7.2.3.1a, which is expected based on reaction 7.2.3.4 of the proposed mechanism in which hydroperoxide rapidly reduces persulfate. In addition, rates of $\text{H}_2\text{O}_2 + \text{HO}_2^-$ decomposition increased with increasing NaOH concentrations (Figure 7.2.3.5), which is likely due to a higher proportion of hydroperoxide at higher pH regimes.

The stoichiometry of the reaction of hydroperoxide with persulfate was further investigated (Figure 7.2.3.6). When 0.5 M $\text{H}_2\text{O}_2 + \text{HO}_2^-$ was added to 0.5 M persulfate, nearly all of the $\text{H}_2\text{O}_2 + \text{HO}_2^-$ was consumed over 30 min, confirming the results of Figure 7.2.3.4. However, when 1 M $\text{H}_2\text{O}_2 + \text{HO}_2^-$ was added to 0.5 M persulfate, the reaction stalled after 3 min when ~ 0.5 M $\text{H}_2\text{O}_2 + \text{HO}_2^-$ was consumed. These results confirm a molar ratio of 1:1 for the reaction of hydroperoxide with persulfate.

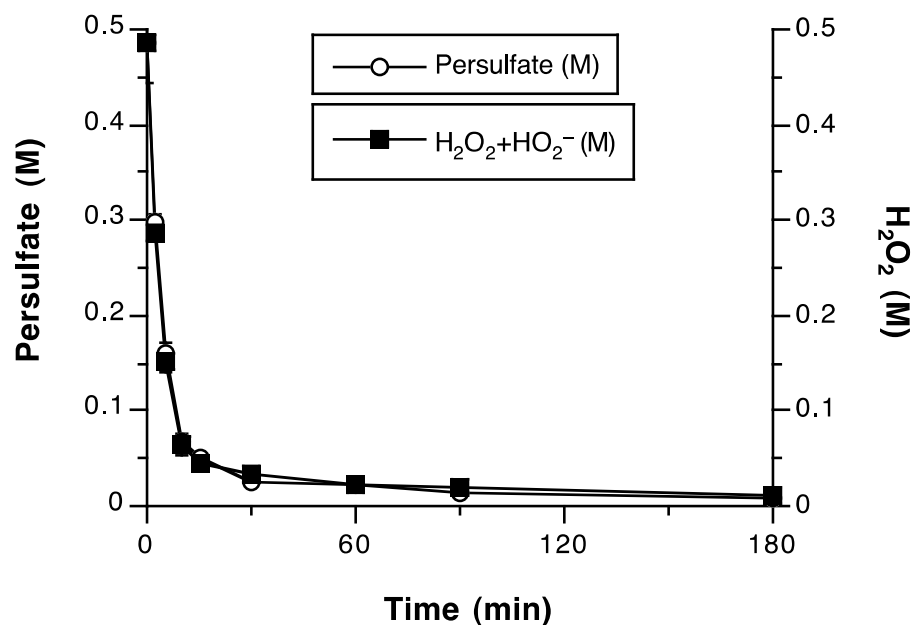


Figure 7.2.3.4. Decomposition of persulfate and hydrogen peroxide in a 1:1 persulfate:H₂O₂ system (reactors: 0.5 M persulfate, 0.5 M H₂O₂, 1.5 M NaOH; 20 mL total volume; T = 20 ± 2 °C). Error bars represent the standard error of the mean.

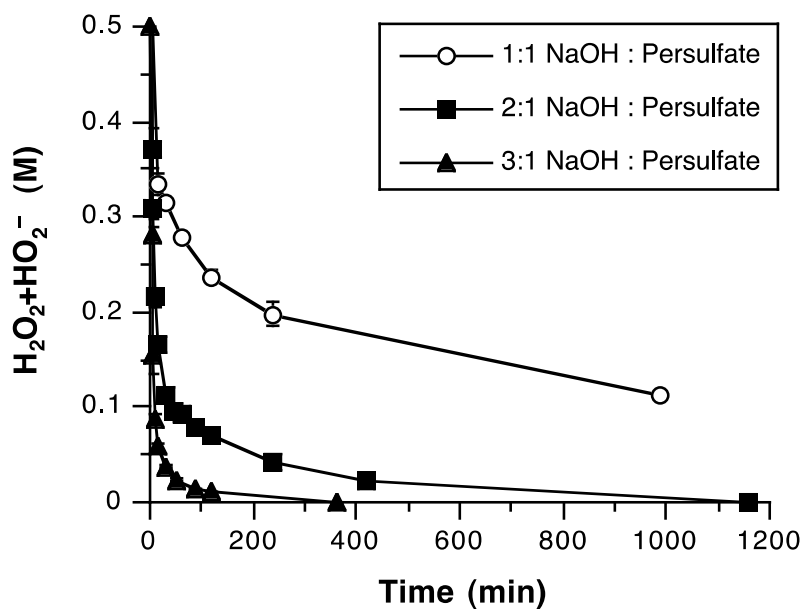


Figure 7.2.3.5. Effect of varying base:persulfate ratio on the degradation rate of added H₂O₂+HO₂⁻ (reactors: 0.5 M persulfate, 0.5 M H₂O₂, and 0.5 M, 1.0 M, or 1.5 M NaOH; 20 mL total volume; T = 20 ± 2 °C). Error bars represent the standard error of the mean.

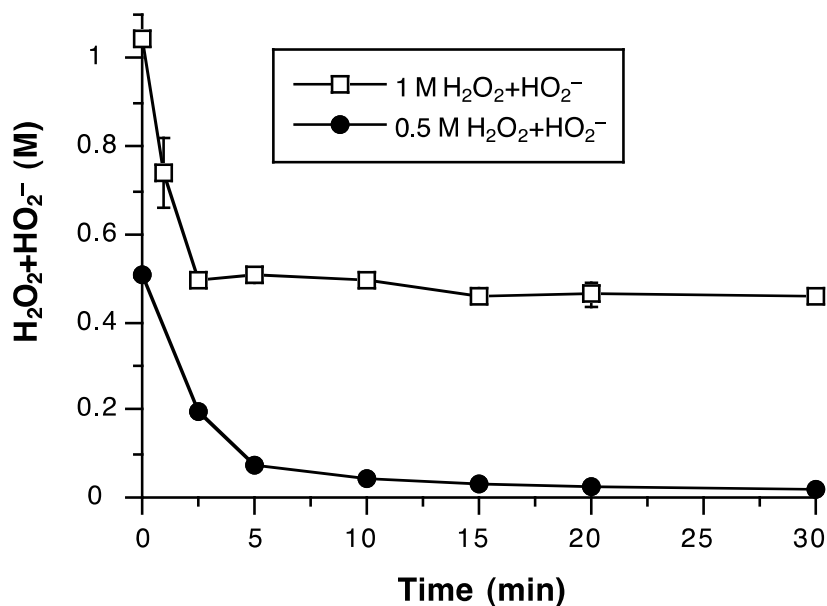


Figure 7.2.3.6. Stoichiometry for the degradation of added hydroperoxide in base-activated persulfate systems (reactors: 0.5 M persulfate, 1.5 M NaOH, 0.5 M or 1 M H_2O_2 ; 20 mL total volume; $T = 20 \pm 2^\circ\text{C}$). Error bars represent the standard error of the mean.

Generation of Superoxide Anion

The effect of increasing $\text{H}_2\text{O}_2 + \text{HO}_2^-$ concentrations on degradation of the superoxide probe HCA in base-activated persulfate systems is shown in Figure 7.2.3.7. (Hydroperoxide reacts at a negligible rate with HCA; the loss of HCA in the presence of hydroperoxide was no different than in deionized water control systems (Furman et al., 2009)). As the concentration of added $\text{H}_2\text{O}_2 + \text{HO}_2^-$ increased, HCA degradation increased proportionately. These results are consistent with the proposed mechanism of the oxidation of hydroperoxide to superoxide as persulfate is reduced to sulfate anion and sulfate radical; i.e., HCA degradation by superoxide proceeds in proportion to the mass of hydroperoxide added to the system.

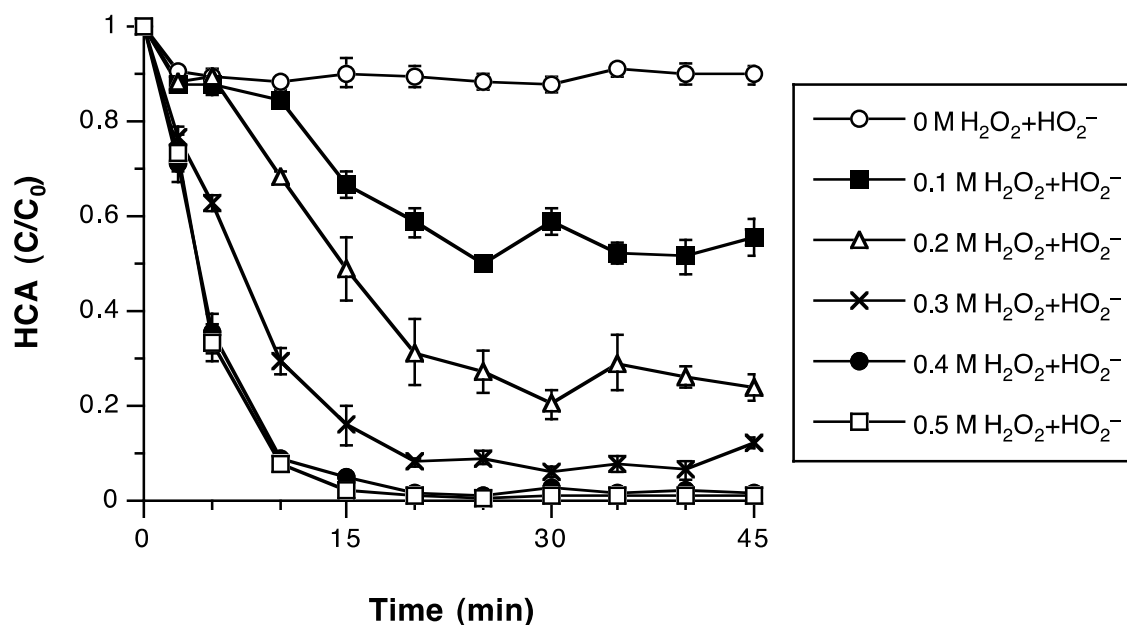


Figure 7.2.3.7. Relative rates of superoxide generation measured by the probe molecule hexachloroethane with varying masses of $\text{H}_2\text{O}_2 + \text{HO}_2^-$ added to base-activated persulfate systems (reactors: 0.5 M persulfate, 1 M NaOH, 0–0.5 M $\text{H}_2\text{O}_2 + \text{HO}_2^-$, 2 μM HCA; 20 mL total volume; $T = 20 \pm 2^\circ\text{C}$). Error bars represent the standard error of the mean.

To distinguish between reduction of HCA by superoxide and reduction of HCA by any alkyl radicals that might be formed in the system, copper (II) was used to dismutate superoxide formed in reaction 7.2.3.4 (Piechowski et al., 1993; Zafiriou et al., 1998) (Figure 7.2.3.8). Without copper addition, the superoxide probe HCA degraded 70% within 5 min. However, when 2 μM Cu (II) was added to the system, HCA degradation was only 15% after 5 min, and was similar to control reactions without the addition of hydrogen peroxide. These results provide additional support that superoxide is formed in reaction 7.2.3.4.

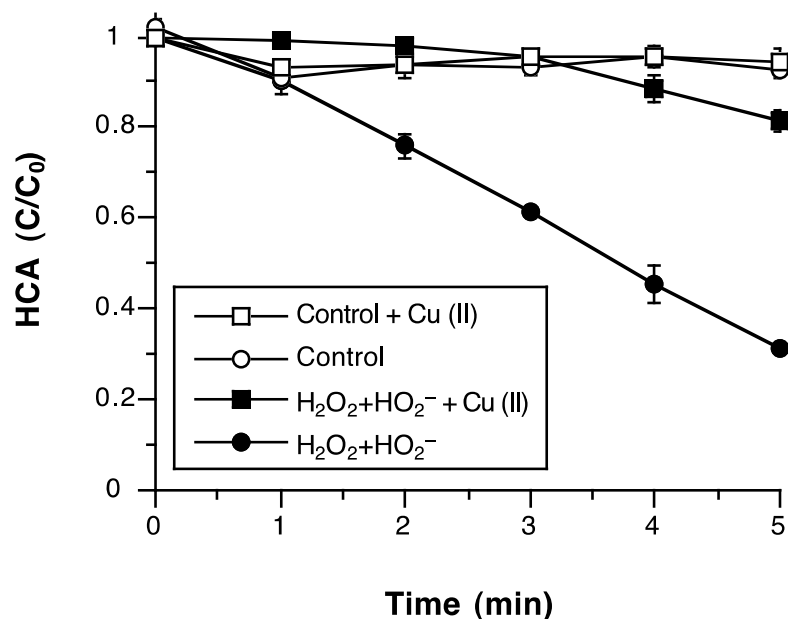


Figure 7.2.3.8. Effect of copper (II) scavenging of superoxide on HCA degradation in base-activated persulfate systems with added $\text{H}_2\text{O}_2+\text{HO}_2^-$ (reactors: 0.5 M persulfate, 1 M NaOH, 0.5 M $\text{H}_2\text{O}_2+\text{HO}_2^-$, 2 μM HCA, 0 and 2 μM Cu (II); 20 ml total volume; controls: $\text{H}_2\text{O}_2+\text{HO}_2^-$ replaced by deionized water; $T=20 \pm 2^\circ \text{C}$). Error bars represent the standard error of the mean.

To confirm the identity of the reactive species generated in reaction 7.2.3.4 as well as reaction 7.2.3.6, ESR spectroscopy was used with DMPO as a spin trap agent to identify the radicals present in base-activated persulfate systems containing a 1:1 ratio of $\text{H}_2\text{O}_2+\text{HO}_2^-$:persulfate. A peak for hydroxyl radical was evident in the ESR spectra (Figure 7.2.3.9); however, the presence of sulfate radical and superoxide was difficult to determine, likely due to low fluxes of these radicals in the system. Detection of superoxide in the system by ESR is also further limited by its low rate of reaction with DMPO ($k = 10\text{--}18 \text{ M}^{-1}\text{s}^{-1}$) (Finkelstein et al., 1980; Keszler et al., 2003). Therefore, the software WinSim 2002 was used to analyze the ESR spectra. The simulated ESR spectra that fit the actual spectra best, with a Spearman's rank correlation coefficient of $R = 0.97$, included all three predicted reactive oxygen species: hydroxyl radical, sulfate radical, and superoxide. On the basis of the hyperfine splitting constant values obtained by the simulation, adducts were identified as DMPO-OH ($A_N = 15.21$, $A_H = 15.77$ gauss), DMPO-SO₄ ($A_N = 13.97$, $A_H = 9.94$, $A_H^{\text{N}} = 1.44$, and $A_H^{\text{S}} = 0.79$ -gauss), and DMPO-OOH ($A_N = 14.49$, $A_H^{\beta} = 10.83$, $A_H^{\alpha} = 1.31$ -gauss). These results are consistent with ESR spectra and

hyperfine splitting constants reported for hydroxyl radical, sulfate radical, and superoxide in other studies (Kirino et al., 1981; Davies et al., 1992) and are consistent with the proposed mechanism.

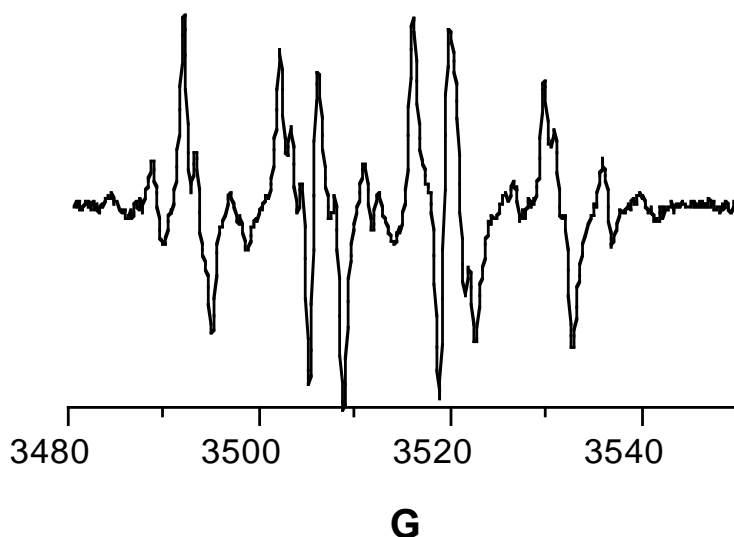


Figure 7.2.3.9. ESR spectrum for a base-activated persulfate system with added $\text{H}_2\text{O}_2 + \text{HO}_2^-$ (reactors: 0.05 M persulfate, 0.1 M NaOH, 0.05 M $\text{H}_2\text{O}_2 + \text{HO}_2^-$, and 0.09 M DMPO; $T = 20 \pm 2^\circ \text{C}$).

Stoichiometric Oxygen Evolution

The final step in confirming the proposed mechanism was to quantify the stoichiometry of molecular oxygen generated from the decomposition of base-activated persulfate. The sulfate radical, superoxide, and hydroxyl radical generated in reactions 7.2.3.4 and 7.2.3.6 proceed through propagation and scavenging reactions in base-activated persulfate systems, resulting in the generation of molecular oxygen:



Superoxide is likely scavenged by hydroxyl radical through reaction 7.2.3.7, as well as by sulfate radical in reaction 7.2.3.8, resulting in the generation of one mole of molecular oxygen per mole of superoxide decomposed. Because the superoxide generated through reaction 7.2.3.5 eventually collapses to molecular oxygen, the mass of oxygen evolved would be expected to follow the stoichiometry:



To investigate the stoichiometry of oxygen evolution during base-activated persulfate decomposition, oxygen evolution was measured in reactions with a 6:1 molar ratio of base:persulfate (Figure 7.2.3.10). Persulfate decomposition was also quantified in the reactions, and the predicted oxygen evolution based on the persulfate loss is also shown in Figure 7.2.3.10. The actual oxygen evolution correlated highly with the predicted evolution of 2 moles of oxygen per mole of persulfate decomposed ($R_{\text{Pearson}} = 0.99$). The results of Figure 7.2.3.10 provide additional confirmation of the proposed mechanism.

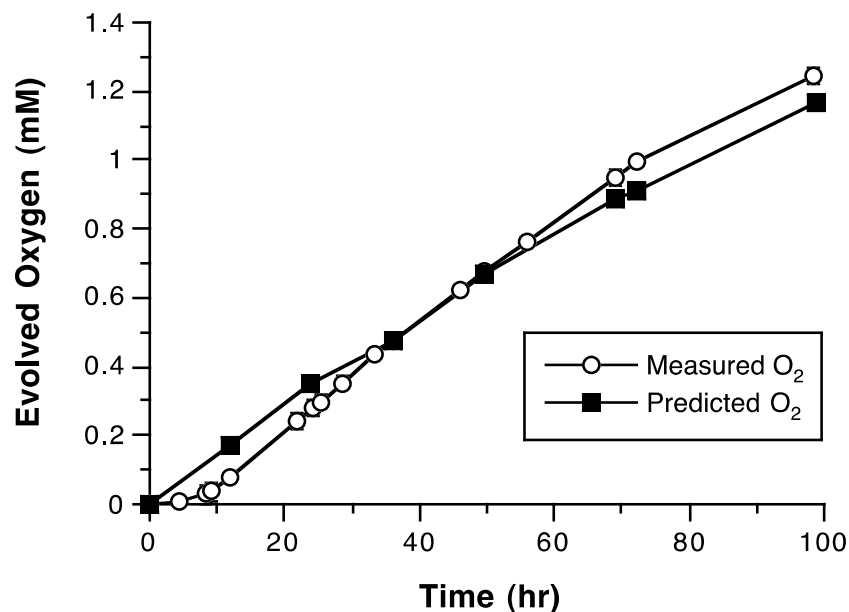


Figure 7.2.3.10. Measured vs. predicted oxygen evolution in persulfate-NaOH reactions (reactors: 0.5 M persulfate and 3 M NaOH; 12 ml total volume; $T = 20 \pm 2^\circ\text{C}$). Error bars represent the standard error of the mean.

The results of this research provide data that are consistent with a mechanism for the base activation of persulfate in which 1) persulfate decomposes to hydroperoxide through base-catalyzed hydrolysis, and 2) hydroperoxide reduces another persulfate molecule resulting in the formation of sulfate radical and sulfate while the hydroperoxide is oxidized to superoxide. Sulfate radical then oxidizes hydroxide, resulting in the formation of hydroxyl radical. Kinetic

analyses of persulfate decomposition are consistent with its base-catalyzed hydrolysis, and hydroperoxide decomposition dynamics are also consistent with the proposed mechanism. Probe compound and scavenging studies supported the generation of superoxide in base-activated persulfate reactions, and ESR spectroscopy confirmed the presence of all three predicted species: sulfate radical, hydroxyl radical, and superoxide. One half mole of molecular oxygen was produced per mole of persulfate decomposed, which is consistent with the stoichiometry of the proposed mechanism.

Base-activated persulfate is now used extensively for the ISCO remediation of contaminated soils and groundwater. Recent findings have documented that base-activated persulfate can destroy not only compounds that react with sulfate radical and hydroxyl radical (e.g., alkenes and aromatic compounds), but highly oxidized perhalogenated compounds as well (e.g., carbon tetrachloride) (Huang et al., 2005; Furman et al., 2010). The mechanism proposed in this study explains the widespread reactivity of base-activated persulfate, and will aid in the design of base-activated persulfate remediation systems.

7.2.4. Persulfate Activation By Phenoxide Derivatives

Detection of Hydroxyl and Sulfate Radicals

For all experiments using different phenoxides to activate persulfate, the change in persulfate concentration over time was negligible ($\alpha = 0.05$) (Figure 7.2.4.1). This may reflect the fact that only a small amount of persulfate is needed to promote the generation of reactive species.

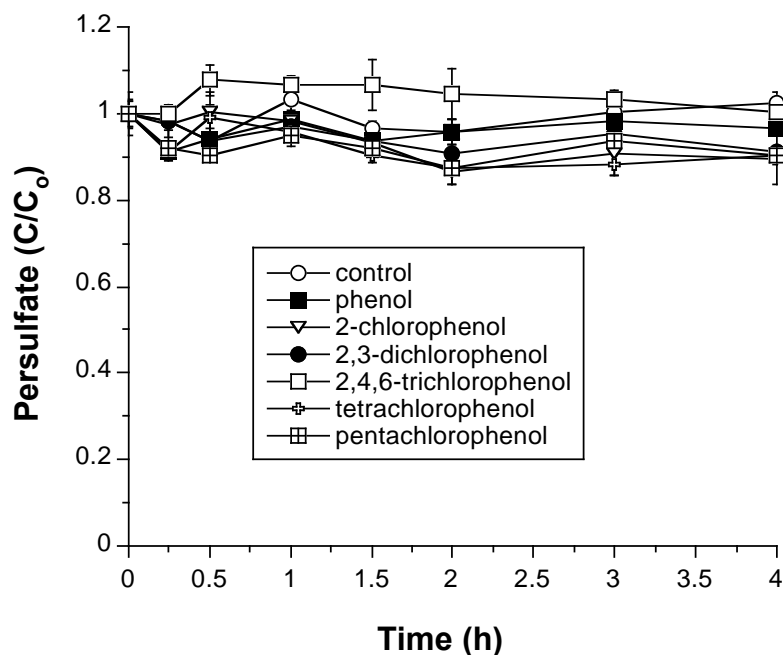


Figure 7.2.4.1. Persulfate decomposition in phenoxides activated persulfate systems at basic pH: 0.5 M sodium persulfate, 2M NaOH, 2 mM phenoxide, and 2 μ M hexachloroethane; 20 mL total volume. Error bars represent the standard error of the mean for three replicates.

The loss of hexachloroethane in phenoxide activated persulfate systems at basic pH is shown in Figure 7.2.4.2. Loss of hexachloroethane indicates the generation of reductants as a result of propagation reactions from persulfate activation. The data demonstrate that all of the phenoxides used in this study activate persulfate. Furthermore, a more reduced compound such as phenol activates persulfate more effectively than a highly chlorinated or more highly oxidized compound, such as pentachlorophenol. Activation using pentachlorophenol resulted in a 40% loss of hexachloroethane in 4 h, compared with > 99.9% when phenol was used as an activator. Hexachloroethane was degraded most rapidly when catechol was used as the activator, with

>99.9% hexachloroethane loss in less than an hour. This is likely due to catechol being a stronger reducing agent than the other phenols. Controls without added phenoxide showed no degradation of hexachloroethane. When hexachloroethane was used as a probe, the results show that persulfate activation by phenoxides in a basic environment generates primarily reductants. Experimental results also demonstrate that without phenoxide in the system, no degradation of hexachloroethane was observed.

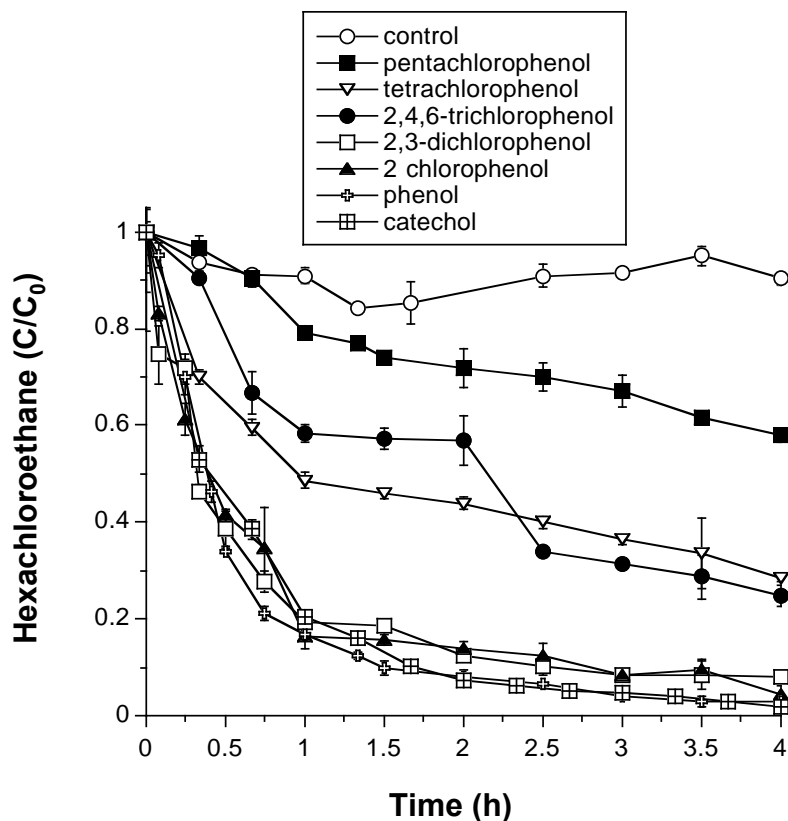


Figure 7.2.4.2. Degradation of hexachloroethane in phenoxide-activated persulfate systems at basic pH: 0.5 M sodium persulfate, 2M NaOH, 2 mM phenoxide, and 2 μ M hexachloroethane; 20 mL total volume. Error bars represent the standard error of the mean for three replicates.

Nitrobenzene degradation was measured to detect hydroxyl radical during persulfate activation. As with hexachloroethane experiments, the persulfate concentrations remained relatively constant during the course of the reaction ($\alpha = 0.05$) (Figure 7.2.4.3). The loss of nitrobenzene in phenoxide activated persulfate systems at basic pH, shown in Figure 7.2.4.4, indicates that persulfate activation using phenoxides generates hydroxyl radical. The relative capacities of the phenoxides to activate persulfate were similar to that seen with

hexachloroethane, with pentachlorophenol promoting a slower degradation rate and the more reduced compounds (e.g., catechol, phenol) causing faster nitrobenzene degradation.

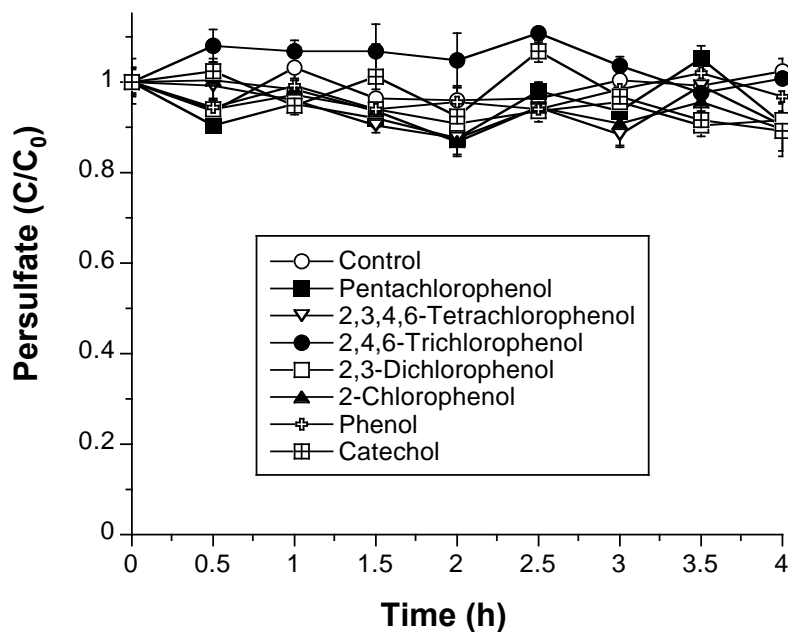


Figure 7.2.4.3. Persulfate decomposition in phenoxid-activated persulfate systems at basic pH: 0.5 M sodium persulfate, 2 M NaOH, 2 mM phenoxide, and 1 mM nitrobenzene; 15 mL total volume. Error bars represent the standard error of the mean for three replicates.

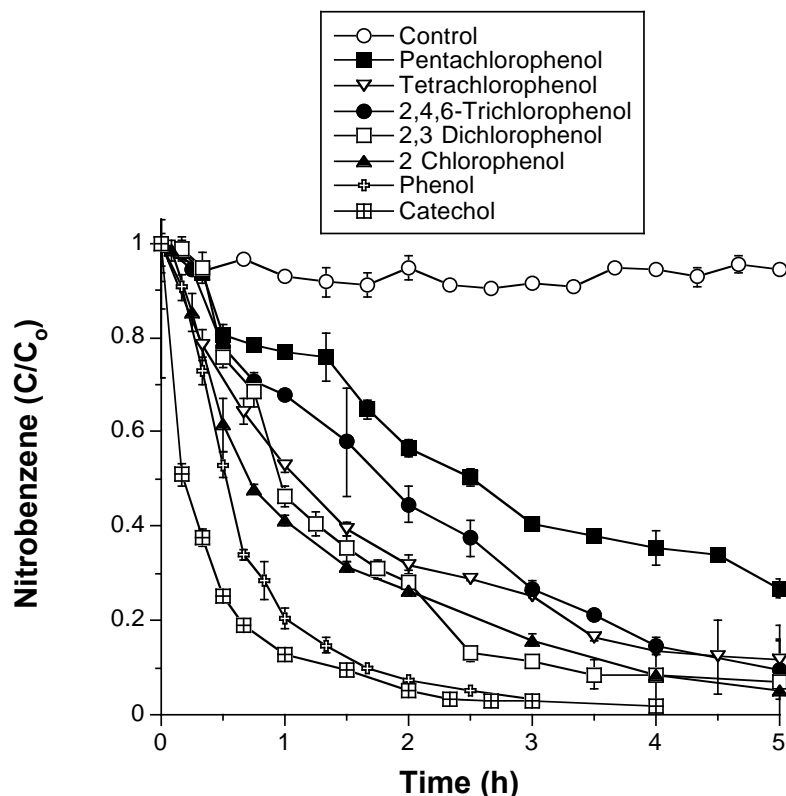


Figure 7.2.4.4. Degradation of nitrobenzene in phenoxide-activated persulfate systems at basic pH: 0.5 M sodium persulfate, 2 M NaOH, 2 mM phenoxide, and 1 mM nitrobenzene; 15 mL total volume. Error bars represent the standard error of the mean for three replicates.

Scavenging of Hydroxyl Radicals

An excess of *t*-butyl alcohol was added to scavenge hydroxyl radical and isopropanol to scavenge both hydroxyl radical and sulfate radical (Anipsitakis et al., 2004). Anisole analyses show a loss of approximately 78% with activation by pentachlorophenol (Figure 7.2.4.5). However, anisole degradation in the presence of the two scavengers was less than that of the positive control. These data provide evidence that sulfate radical and hydroxyl radical are generated during the activation of persulfate by phenoxide.

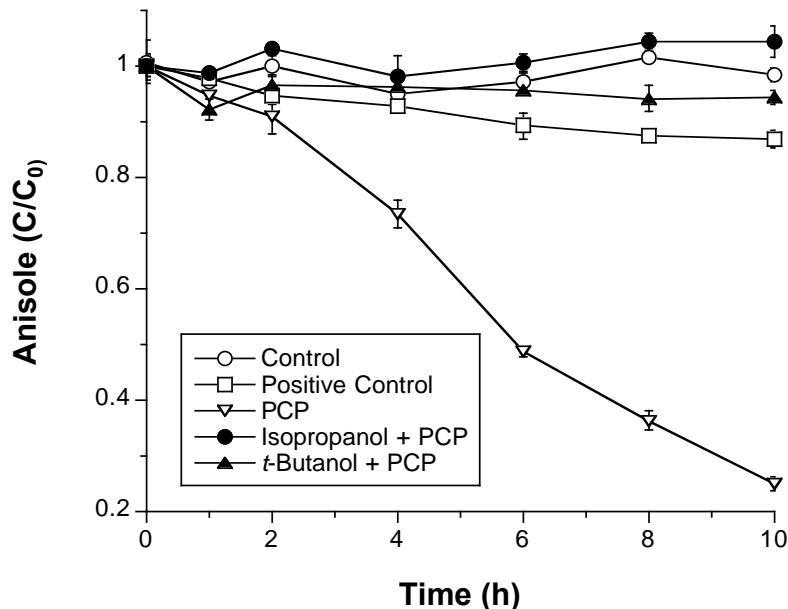


Figure 7.2.4.5. Scavenging of hydroxyl radicals in phenoxide-activated persulfate systems at basic pH: 0.5 M sodium persulfate, 2 M NaOH, 2 mM phenoxide, and 1 mM nitrobenzene; 15 mL total volume, the molar ratio of anisole to *t*-butyl alcohol was 1:1000. Error bars represent the standard error of the mean for three replicates.

Influence of pH

The anionic (i.e. phenoxide) form of phenols is likely the activating species in persulfate systems; to evaluate this hypothesis; the effect of pH on persulfate activation by phenoxides was investigated. The degradation of anisole by pentachlorophenol-activated persulfate at pH ranging from 3 to 8 over 6 hr is shown in Figure 7.2.4.6. These results indicate that when pentachlorophenol was primarily in the anionic form (PhO^-) (at a pH above its pK_a of 4.5; Watts, 1998), the phenoxide activation of persulfate increased. Minimal anisole degradation was observed at pH 3, indicating less activation of persulfate and subsequent formation of hydroxyl and sulfate radicals. These data are consistent with the activation of persulfate primarily by the phenoxide ion. Furthermore, these results indicate the importance of hydroxyl radicals in a system where persulfate is activated by organic compounds. Lipczynska-Kochany (1992) found that neutral forms of phenols are more susceptible to the electrophilic attack from hydroxyl radicals than the phenolate forms.

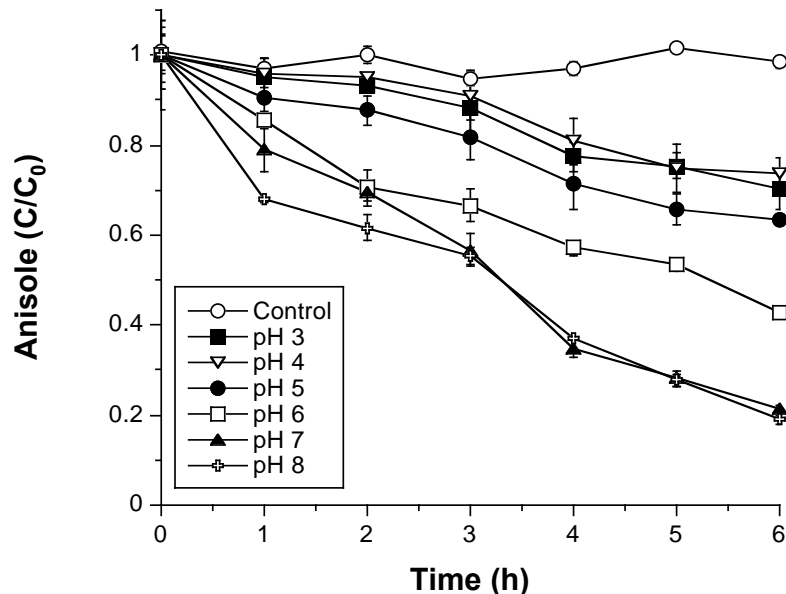
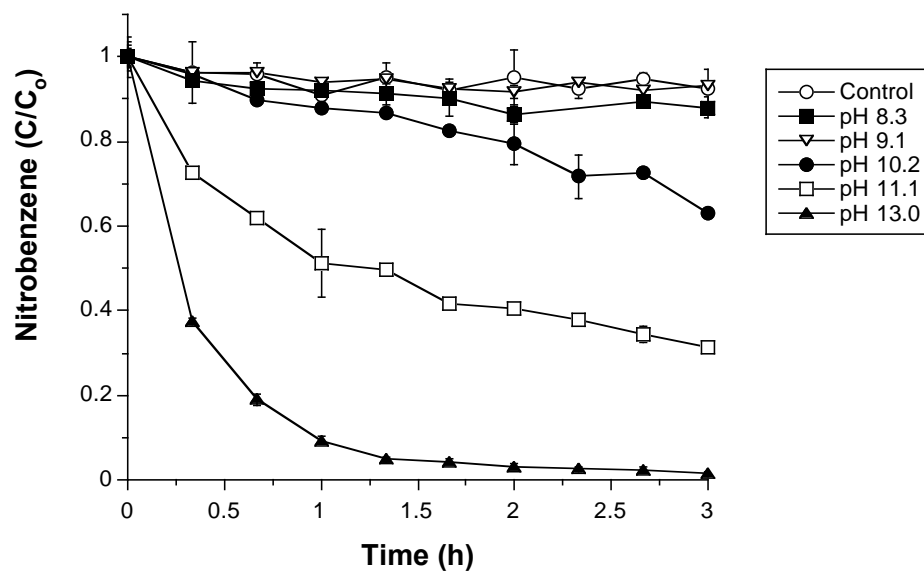


Figure 7.2.4.6. Degradation of anisole in phenol activated persulfate system at different pH regimes: 0.5 M sodium persulfate, 2 mM phenol, and 1 mM anisole; 15 mL total volume at pH 3–8. Error bars represent the standard error of the mean for three replicates.

The effect of pH on the activation of persulfate by another reduced compound, catechol ($pK_a = 9.34$; Linde, 2009), is shown in Figure 7.2.4.7. As with phenol, the rates of nitrobenzene degradation were markedly greater at higher pH (Figure 7.2.4.7a), achieving near complete loss of nitrobenzene at pH 13.0. HCA loss exhibited a similar pattern (Figure 7.2.4.7b), suggesting that a similar reaction pathway is involved in both oxidant and reductant generation.

a.



b.

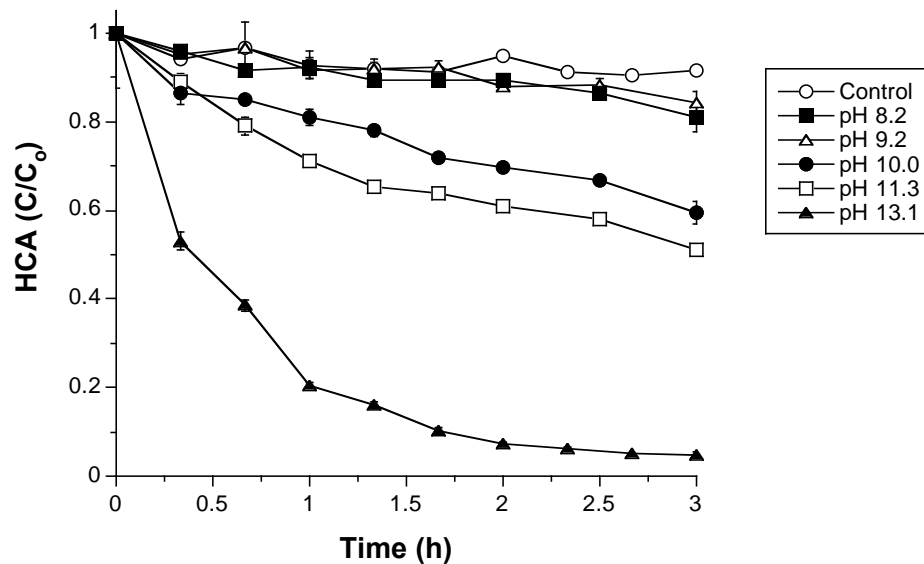


Figure 7.2.4.7. Degradation of probe compounds in catechol activated persulfate system at different pH regimes: 0.5 M sodium persulfate, 2 mM catechol, at 8, 9, 10, 11, and 13 pH values. Error bars represent the standard error of the mean for three replicates (a) Degradation of nitrobenzene (1 mM nitrobenzene, 15 mL total volume) (b) Degradation of hexachloroethane (2 μ M HCA, 20 mL total volume).

Effects of Phenol Concentrations

Persulfate activation was evaluated at several phenol concentrations (0.01 to 10 mM) with a fixed NaOH:persulfate molar ratio of 4:1. The reactions were conducted at pH > 13, which is 3 pH units greater than the pK_a of phenol; therefore 99.9% of the phenol is in the phenoxide form. Figure 7.2.4.8 shows that the rates of hydroxyl radical generation as indicated by nitrobenzene loss are faster as the phenol concentration increases. These results suggest a zero order phenomenon in hydroxyl radical generation with respect to phenoxide concentration.

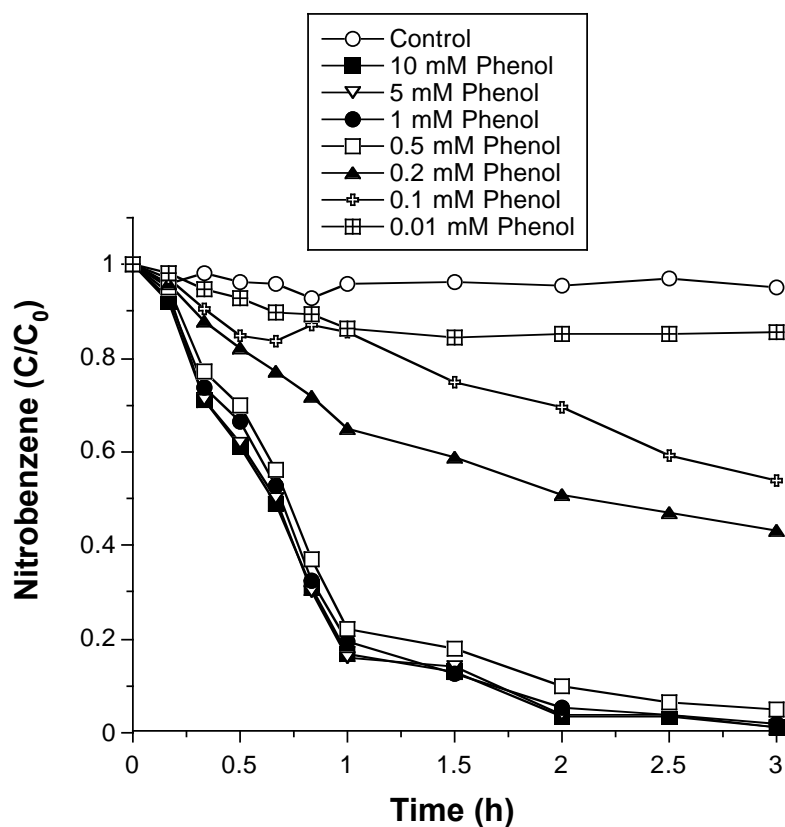
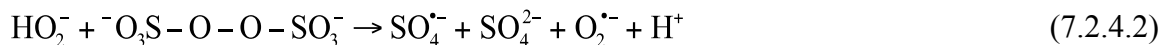


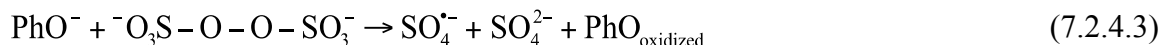
Figure 7.2.4.8. Degradation of nitrobenzene in phenol activated persulfate system at basic pH: 0.5 M sodium persulfate, 2 M NaOH, 1 mM nitrobenzene, and different phenol concentrations ranging from 0.01 to 10 mM; 15 mL total volume. Error bars represent the standard error of the mean for three replicates.

Mechanism of Persulfate Activation

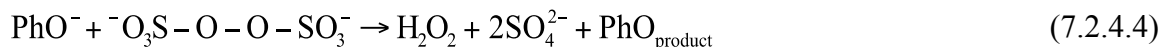
The two-step base activation of persulfate described by Furman et al. (2010) would be occurring at basic pH in addition to phenoxide activation:



Two possible mechanisms are possible for the phenoxide activation of persulfate. One possible mechanism is the reduction of persulfate by the phenoxide with subsequent generation of sulfate radical; the phenoxide would then be oxidized.



The second possible mechanism is the nucleophilic attack of the phenoxide on persulfate, generating hydroperoxide:



Evaluation of the mechanism occurring was based on two fundamental concepts. First, only hydroperoxide (i.e., not hydrogen peroxide) and the phenoxide (i.e., not the phenol) activate persulfate. Secondly, the pK_a of pentachlorophenol is 4.5, and the pK_a of hydrogen peroxide is 11.8. To elucidate which mechanism is occurring, pentachlorophenoxide-activated persulfate reactions were conducted at pH 8 to provide a pH regime at which a phenoxide is present, but hydroperoxide is not. If the reduction mechanism (Eq. 7.2.4.3) is occurring, sulfate (and its propagation product, hydroxyl radical) would be formed. If the nucleophilic activation mechanism is occurring, hydrogen peroxide should be detected.

When the pentachlorophenoxide-activated reaction was conducted at pH 8, no hydroperoxide was formed, which suggests that the reductive activation step is the mechanism of activation. When the pentachlorophenoxide reaction was conducted in systems containing the hydroxyl radical probe nitrobenzene, the probe was degraded (Figure 7.2.4.9). Furthermore, no loss of the reductant probe HCA occurred in the pentachlorophenoxide system at pH 8 (Figure 7.2.4.10). These results provide strong evidence that the mechanism for phenoxide activation of persulfate is through a one-electron reduction of persulfate by the phenoxide, similar to initiation by a reduced metal (e.g., iron (III)).

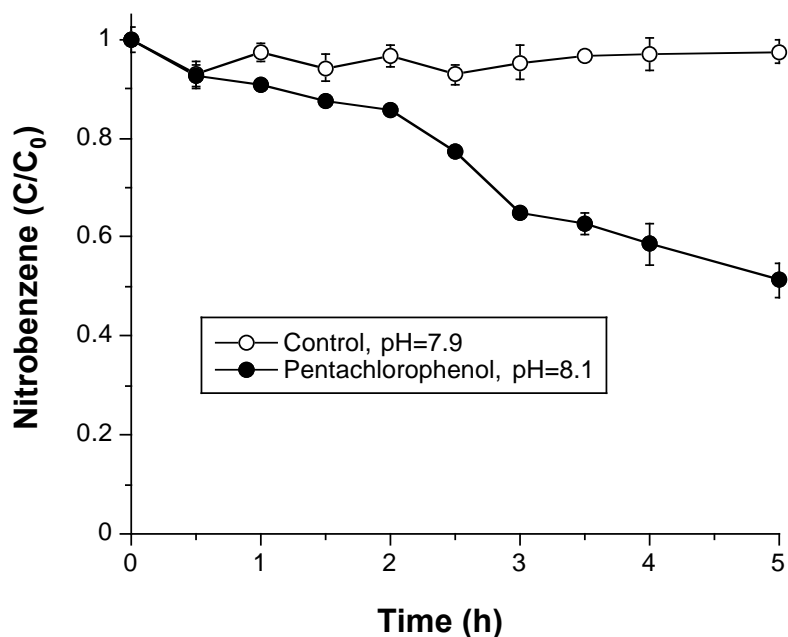


Figure 7.2.4.9. Degradation of nitrobenzene in pentachlorophenolate activated persulfate system at pH 8.0: 0.5 M sodium persulfate, 2 mM pentachlorophenol and 1 mM nitrobenzene; 15 mL total volume. Error bars represent the standard error of the mean for three replicates.

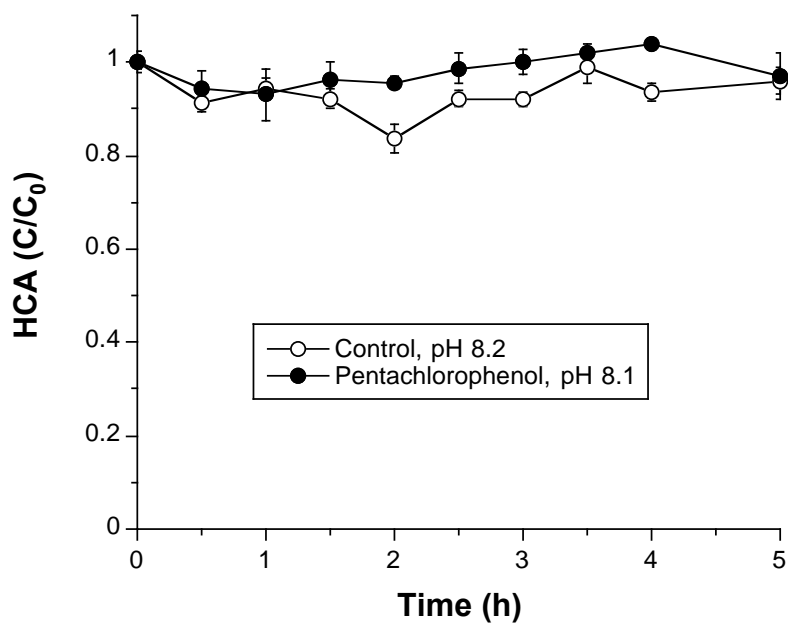


Figure 7.2.4.10. Degradation of hexachloroethane in pentachlorophenolate activated persulfate system at pH 8: 0.5 M sodium persulfate, 2 mM pentachlorophenol, and 2 μ M hexachloroethane; 20 mL total volume. Error bars represent the standard error of the mean for three replicates.

Degradation of pentachlorophenoxide generated hydroquinone byproducts, as predicted by the oxidation of pentachlorophenol (Merz and Waters, 1949). The most relevant compounds produced were tetrachloride-hydroquinone, 3,4,6-trichloro-pyrocatechol, and 3,4-dichloro-2,5-furandione. These hydroquinone products have primarily *ortho* and *para* orientation of the OH groups, which is typical of electrophilic substitution in benzene rings (Metelitsa, 1971). The formation of furandione may indicate the production of chlorophenoxy radicals (Sommeling et al., 1993).

Conclusion

The results of the study demonstrate that phenoxides promote persulfate oxidation at basic pH, resulting in the rapid oxidation of the hydroxyl radical probe nitrobenzene and loss of the reductant probe hexachloroethane. Phenoxides decomposed along with the probe compound. Rates of loss of both nitrobenzene and hexachloroethane were inversely proportional to the degree of chlorine substitution on the phenol used for activation.

Reactions conducted at different pH regimes confirmed that only the phenoxide forms of the phenols promote the activation of persulfate. Because persulfate can be activated by both hydroperoxide and phenoxides at pH > 12, the activation of persulfate by a phenoxide was evaluated using pentachlorophenol at pH 8, a pH regime at which hydroperoxide existed in the protonated form of hydrogen peroxide. The results obtained are in agreement with a reductive pathway in the activation of persulfate by phenoxides.

The results of this research demonstrate that when persulfate treatment is implemented in the presence of phenols, such as those present in soil organic matter, persulfate activation by organic compounds can be a significant pathway for contaminant degradation. Therefore, the soil organic carbon content should be considered in process screening and treatability testing for persulfate ISCO.

7.2.5. Persulfate Activation by Alcohols, Aldehydes, Ketones, Organic Acids, and Keto Acids

Ketones

The potential for ketones to activate persulfate was studied using acetone, 2-butanone, 2-pentanone, and 2-heptanone. Hexachloroethane was used as a probe compound to evaluate the generation of reductants in basic persulfate systems. The relative generation rates of reductants by ketone-activated persulfate over 3 hr are shown in Figure 7.2.5.1. Hexachloroethane was degraded most rapidly with acetone as the activator, with >99% degradation over 3 hr, compared with 20% degradation when 2-heptanone was the activator. In the control system, the 8% loss of hexachloroethane was likely due to volatilization. The results demonstrate that ketones activate persulfate, and that the relative generation of reductants in ketone-activated persulfate systems decreased as the number of carbons that are bound to the carbonyl group (C=O) of the ketone increased.

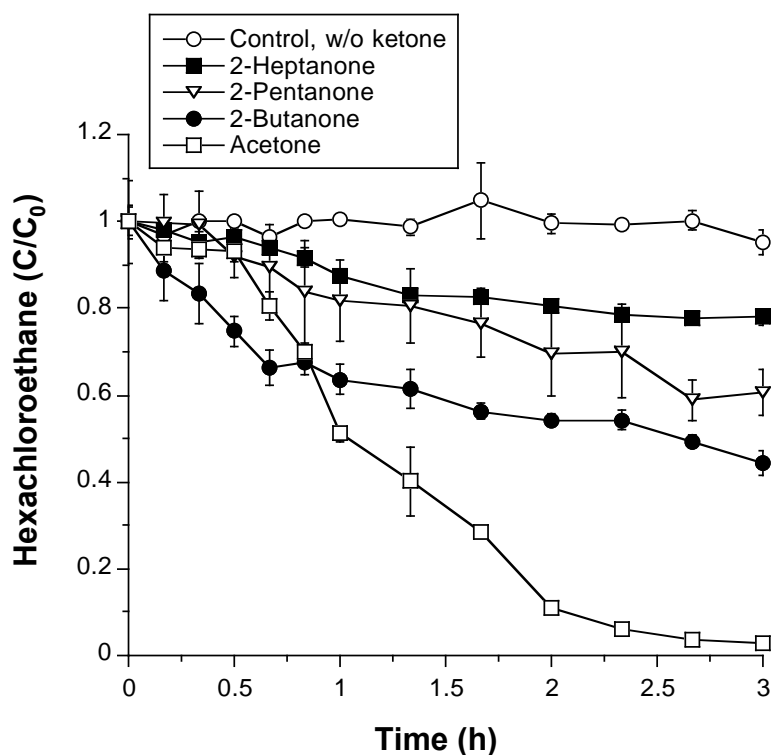


Figure 7.2.5.1. Degradation of hexachloroethane in ketones activated persulfate systems at basic pH: 0.5 M sodium persulfate, 2 M NaOH, 10 mM ketone, and 2 μ M hexachloroethane; 20 mL total volume. Error bars represent the standard error of the mean for three replicates.

Hydroxyl radical generation in the basic ketone-activated persulfate systems was studied using nitrobenzene as a probe (Figure 7.2.5.2). The destruction of nitrobenzene over time exhibited a similar pattern to the hexachloroethane results for all ketones. Acetone was the most effective activator of persulfate with 93% nitrobenzene loss over 3 hr, while 2-heptanone was the least effective activator with 20% nitrobenzene loss. In the control systems containing no ketones, no measurable loss of nitrobenzene was observed during the 3 hr experiment.

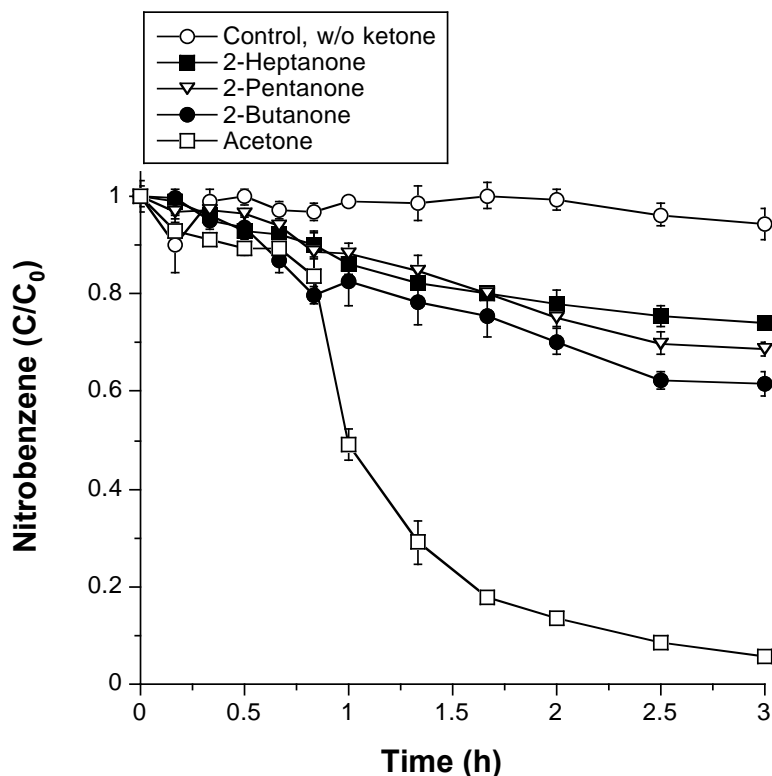


Figure 7.2.5.2. Degradation of nitrobenzene in ketones activated persulfate systems at basic pH: 0.5 M sodium persulfate, 2 M NaOH, 10 mM ketone, and 1 mM nitrobenzene; 15 mL total volume. Error bars represent the standard error of the mean for three replicates.

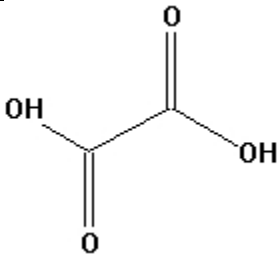
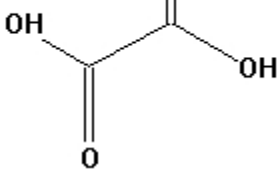
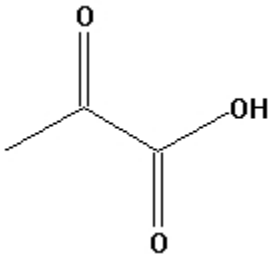
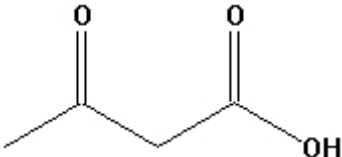
The behavior of acetone indicates that the two methyl substituents adjacent to the carbonyl carbon increased the reactivity of persulfate activation. The degradation rate of both probes, hexachloroethane and nitrobenzene, was inversely proportional to the length of the alkyl group linked to the carbonyl carbon. For example, 2-heptanone activated persulfate to a lesser degree than 2-butanone. Therefore, the size of the relative substituent to the ketone group affects the activation rate. These results are similar to those of Selvararani et al. (2005), who studied the ketone-catalyzed decomposition of peroxomonosulfate (SO_5^{2-}) in aqueous alkaline medium. They found that the nucleophilic addition of SO_5^{2-} ion at the carbonyl carbon in the ketone leads

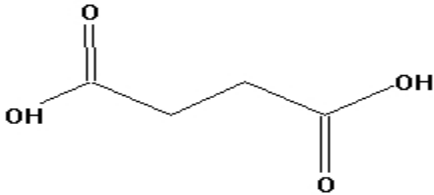
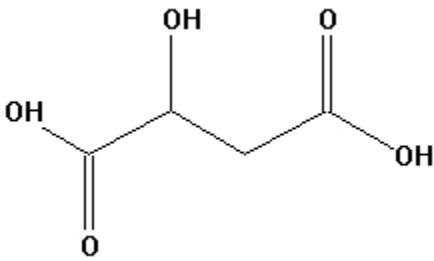
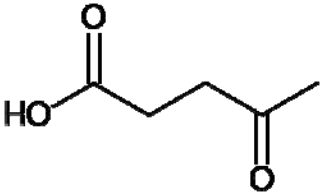
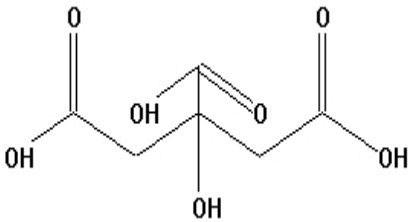
to the formation of the oxirane, and the rate constant of that reaction is inversely proportional to the size of the substituents of the carbonyl group.

Krebs Cycle Compounds

The Krebs cycle compounds were classified into three categories: keto acids, alcohol acids, and dicarboxylic acids. The keto acids included pyruvic acid, the main substrate for the Krebs cycle, acetoacetic acid, and levulinic acid. Alcohol acids included malic and citric acid. Dicarboxylic acids were represented by oxalic acid and succinic acid. The relative proportion of the acid form and the ionized salt for the Krebs cycle compounds, as a function of pH, is shown in Table 7.2.5.1. Persulfate activation by these organic compounds was studied in a basic environment at a pH above 12; therefore, all the Krebs cycle compounds used were in their ionized form.

Table 7.2.5.1. Values of pK_a for ketones and krebs cycle compounds.

Compound	Molecular Formula	Chemical Structure	Step of the Dissociation Constant	pK_a
Oxalic Acid	$C_2H_2O_4$		1	1.25^1
			2	3.81^1
Pyruvic Acid	$C_3H_4O_3$			2.39^1
Acetoacetic Acid	$C_4H_6O_3$			3.6^1

Compound	Molecular Formula	Chemical Structure	Step of the Dissociation Constant	pK _a
Succinic Acid	C ₄ H ₆ O ₄		1	4.21 ¹
			2	5.64 ¹
Malic Acid	C ₄ H ₆ O ₅		1	3.40 ¹
			2	5.11 ¹
Levulinic Acid	C ₅ H ₈ O ₃			4.62
Citric Acid	C ₆ H ₈ O ₇		1	3.13 ¹
			2	4.76 ¹
			3	6.40 ¹

⁽¹⁾Lide, 2008-2009.

The generation of reductants in the basic Krebs cycle compounds-activated persulfate systems is shown in Figure 7.2.5.3. The most rapid degradation of hexachloroethane was accomplished by the keto acids (Figure 7.2.5.3a). In particular, levulinic acid, which has the ketone group located at the third carbon from the carboxylic group (Table 1), was the compound that most effectively activated persulfate to generate reductants. In contrast, complete

degradation of hexachloroethane was achieved in the presence of alcohol acids (Figure 7.2.5.3b) but at a slower rate compared with the keto acids. Greater than 99% hexachloroethane degradation was accomplished in just 0.4 hours when keto acids were the activators in the persulfate system, compared to 1 hour when alcoholic acids were the selected organic activators. Dicarboxylic acids (Figure 7.2.5.3c) promoted the least degradation of hexachloroethane (< 20%) of all the Krebs cycle compounds evaluated.

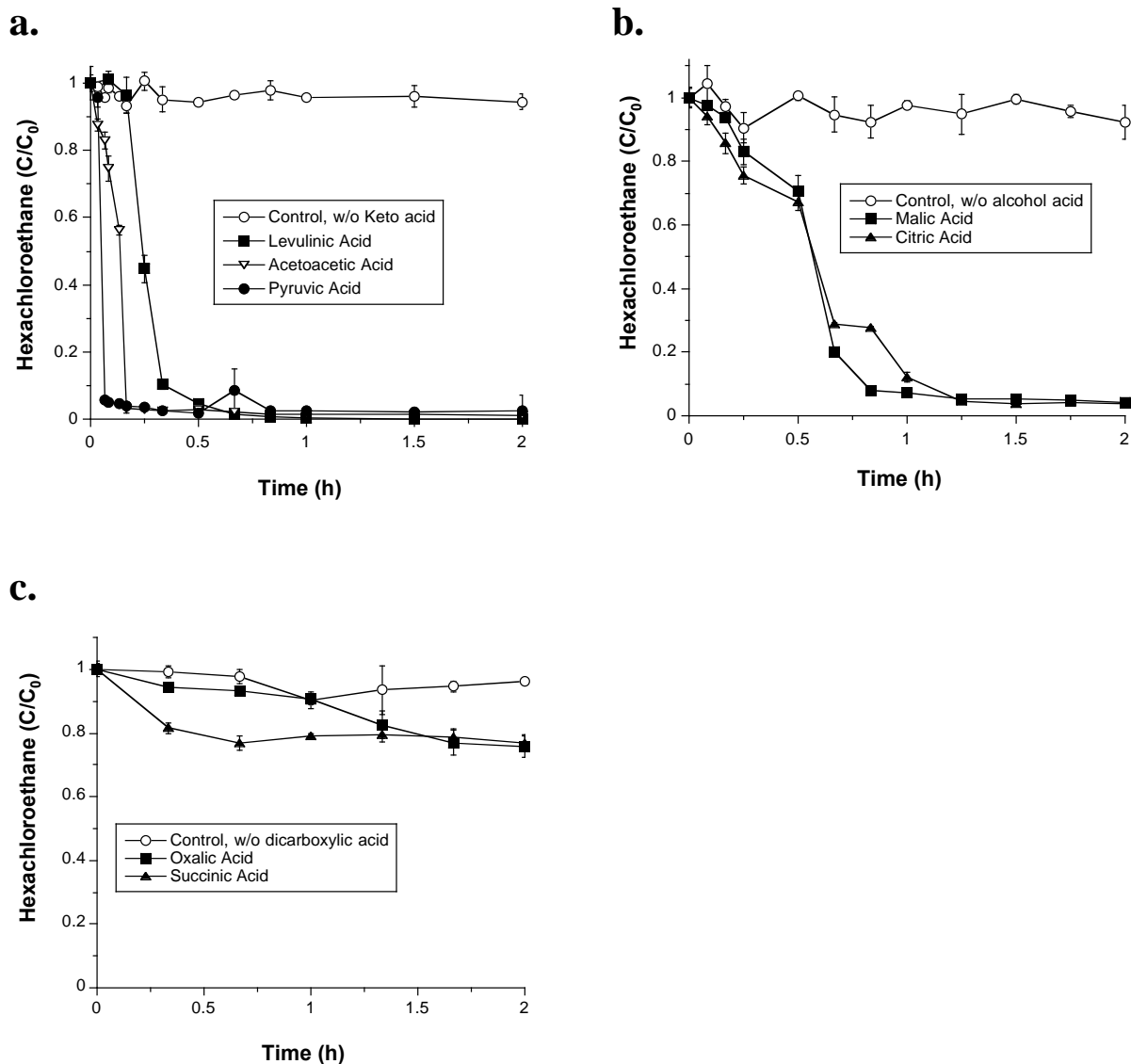


Figure 7.2.5.3. Degradation of hexachloroethane in Krebs cycle-activated persulfate systems at basic pH: 0.5 M sodium persulfate, 2 M NaOH, 10 mM Krebs cycle compound, and 2 μ M hexachloroethane; 20 mL total volume. Error bars represent the standard error of the mean for three replicates. (a) Keto acids; (b) Alcohol acids; (c) Dicarboxylic acids.

The generation of hydroxyl radicals in the basic Krebs cycle intermediates-activated persulfate systems is shown in Figure 7.2.5.4. After the 2 hr reaction time, total degradation of nitrobenzene was not achieved in the alcohol acids system (Figure 7.2.5.4b), but >99% degradation occurred in the presence of keto acids (Figure 7.2.5.4a). For the two alcohol acids used as activators, the nitrobenzene degradation was 80% in the presence of malic acid and 40% in the presence of citric acid, which could be attributed to citric acid being a ternary alcohol and malic acid a secondary alcohol, thereby increasing its reactivity and potential as an activator for persulfate (Bernthsen, 1933). On the other hand, both dicarboxylic acids used, oxalic acid and succinic acid, showed minimal nitrobenzene degradation (< 10%) during the reaction period of 2 hr (Figure 7.2.5.4c).

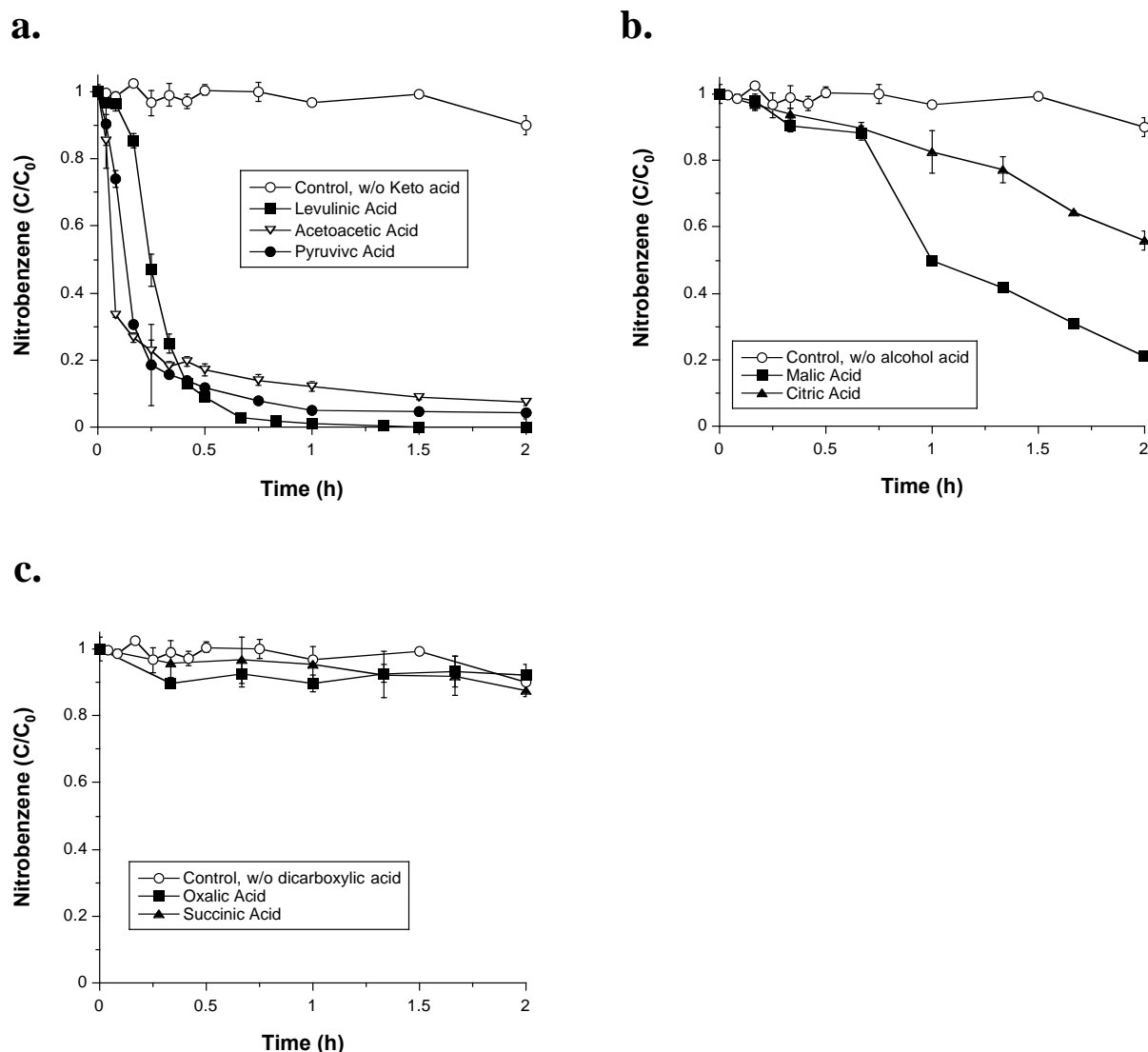


Figure 7.2.5.4. Degradation of nitrobenzene in Krebs cycle-activated persulfate systems at basic pH: 0.5 M sodium persulfate, 2 M NaOH, 10 mM Krebs cycle compound, and 1 mM nitrobenzene; 15 mL total volume. Error bars represent the standard error of the mean for three replicates. (a) Keto acids; (b) Alcohol acids; (c) Dicarboxylic acids.

Moreover, dicarboxylic acids did not promote either reductant or hydroxyl radical generation. The presence of organic compounds with two carboxyl groups may scavenge the hydroxyl radical or inhibit hydroxyl radical generation. It may also promote minimal generation of reductants.

In general, these data show that in basic systems, Krebs cycle keto acids are the compounds with the greatest persulfate activation. Therefore, a ketone functional group results in more activation of persulfate to generate hydroxyl radicals and reductants in the system compared to a carboxylic acid group. It also shows that when the organic compound contains a carboxylic group in its structure the activation of persulfate is slow or insignificant. A possible explanation for this behavior is that an electron is generally needed to activate persulfate, and the activation is coming from the oxidation of a reduced organic compound, therefore a ketone group can activate persulfate much more effectively than a carboxylic group.

Alcohols

This segment of the research focused on the activation of persulfate by primary, secondary, and tertiary alcohols. The isomers of the alcohols used are listed in Table 2. The pK_a values of these alcohols range from 15 to 17 (Perrin et al., 1981); therefore, dissociation of the alcohols would be minimal at the pH of the experiments.

Different isomers of alcohol were screened to determine their effectiveness for activating persulfate based on the position of the hydroxyl group in the alcohols. Maruthamuthu and Neta (1977) reported the rate constant for the reaction between sulfate radicals and some alcohols such as methanol, ethanol, 2-propanol and *t*-butyl alcohol. Their results indicated that the rate constants for the primary and secondary alcohols are the same order of magnitude, but the rate constant values for the tertiary alcohols are two orders of magnitude lower.

Table 7.2.5.2. Isomers of the alcohols used in the study to activate persulfate.

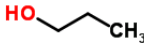
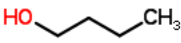
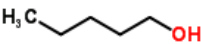
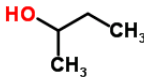
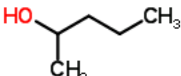
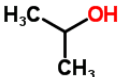
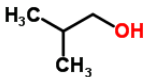
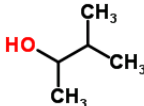
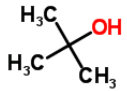
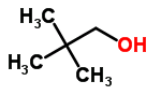
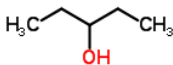
Position Isomer	Alcohol Compound	Molecular Formula	Chemical Structure
Primary Alcohols	<i>n</i> -propanol	C ₃ H ₈ O	
	<i>n</i> -butanol	C ₄ H ₁₀ O	
	<i>n</i> -pentanol	C ₅ H ₁₂ O	
Secondary Alcohols (Straight chain)	sec-butanol	C ₄ H ₁₀ O	
	2-pentanol	C ₅ H ₁₂ O	
Secondary Alcohols (Isomers)	2-propanol	C ₃ H ₈ O	
	isobutanol	C ₄ H ₁₀ O	
	3-methyl-2-butanol	C ₅ H ₁₂ O	

Table 7.2.5.2. continued

Position Isomer	Alcohol Compound	Molecular Formula	Chemical Structure
Ternary Alcohols	<i>t</i> -butyl alcohol	C ₄ H ₁₀ O	
	neopentyl alcohol	C ₅ H ₁₂ O	
	3-pentanol	C ₅ H ₁₂ O	

Relative rates of reductant generation, as measured through the oxidation of hexachloroethane over a 9 h period, in a basic persulfate system in the presence of alcohols, are shown in Figure 7.2.5.5. The highest relative rates of reductant generation occurred in the presence of the three primary alcohols: *n*-propanol, *n*-butanol and *n*-pentanol (>99%). The slowest rate generation of reductants was found with the ternary alcohol *t*-butyl, which showed a 20% degradation of hexachloroethane. Alcohol-free controls showed no degradation of hexachloroethane.

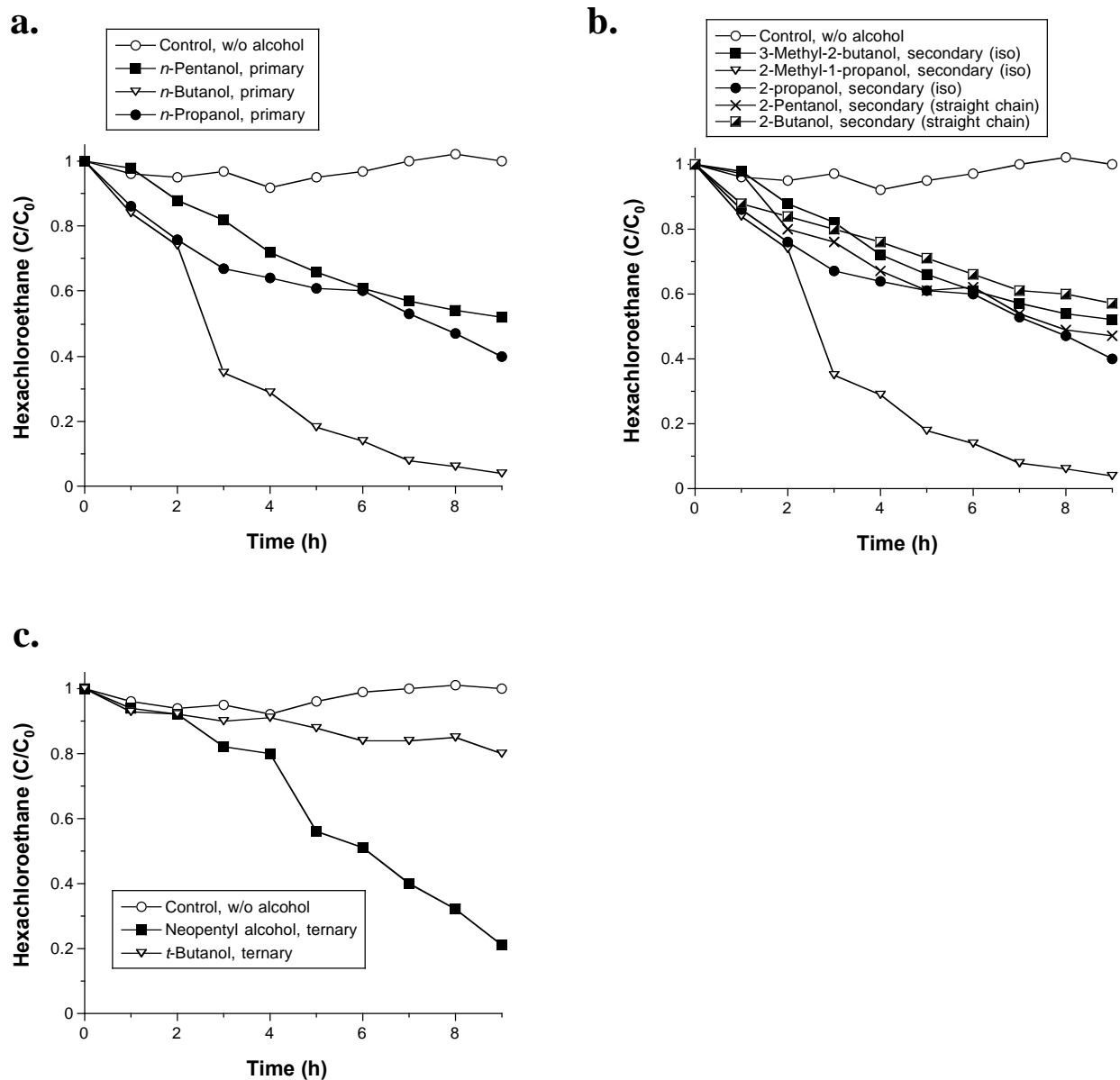


Figure 7.2.5.5. Degradation of hexachloroethane in alcohols activated persulfate systems at basic pH: 0.5 M sodium persulfate, 2 M NaOH, 10 mM alcohol, and 2 μ M hexachloroethane; 20 mL total volume. Error bars represent the standard error of the mean for three replicates. (a) Primary alcohols; (b) Secondary alcohols; (c) Ternary alcohols.

Relative rates of hydroxyl radical generation, measured through the degradation of nitrobenzene over a 9 h period, in basic systems in the presence of alcohols are shown in Figure 7.2.5.6. The behavior of the alcohols in the generation of hydroxyl radicals is similar to the results for the generation of reductants. Based on the batch experimental results, the alcohol with the highest degradation rate for nitrobenzene was *n*-propanol (>99%). Only minimal

nitrobenzene degradation (< 16 %) was observed for the three ternary alcohols, neopentyl, *t*-butyl and 3-pentanol.

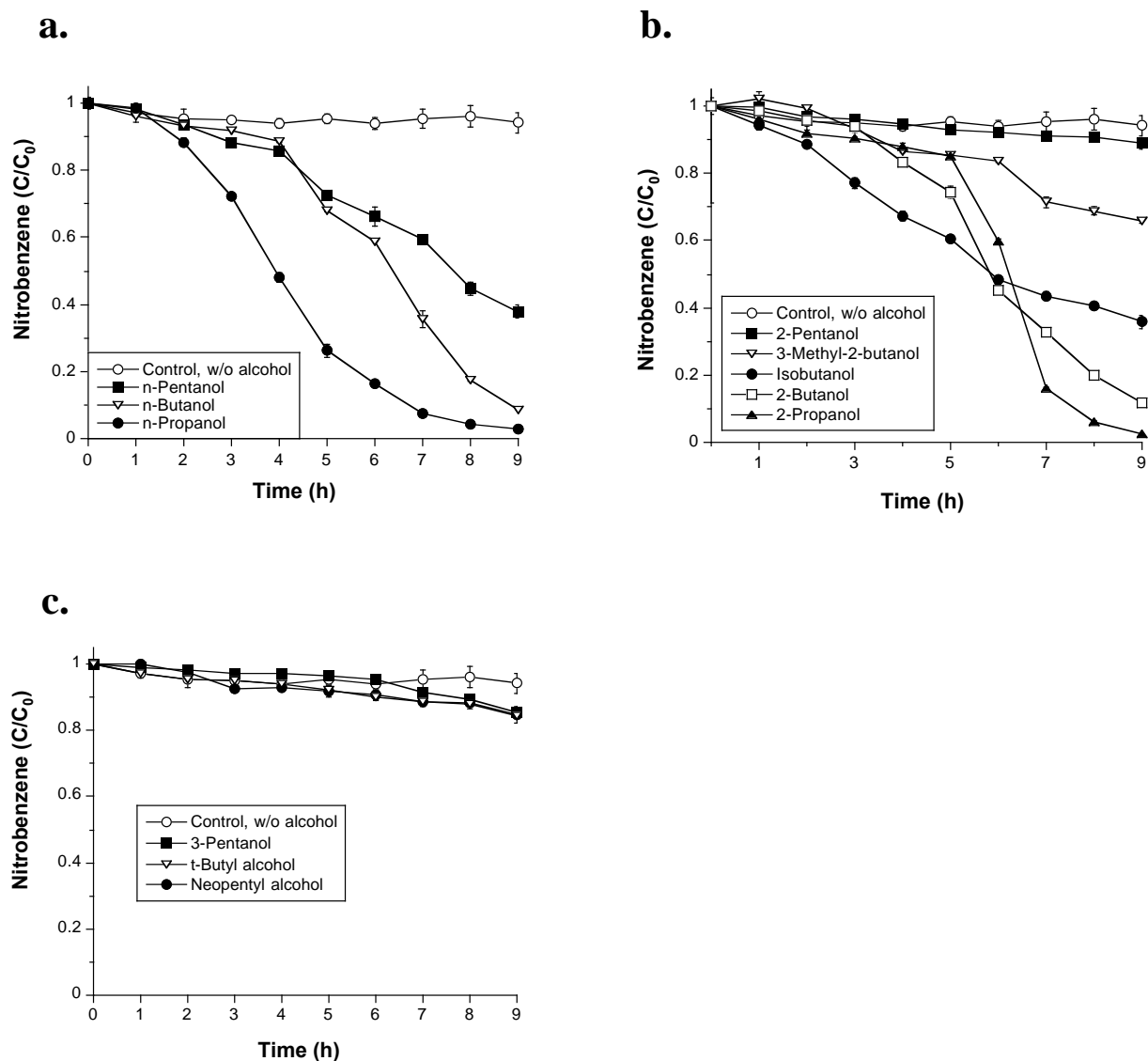


Figure 7.2.5.6. Degradation of nitrobenzene in alcohols activated persulfate systems at basic pH: 0.5 M sodium persulfate, 2 M NaOH, 10 mM alcohol, and 1 mM nitrobenzene; 15 mL total volume. Error bars represent the standard error of the mean for three replicates. (a) Primary alcohols; (b) Secondary alcohols; (c) Ternary alcohols.

The results of Figures 7.2.5.5 and 7.2.5.6 indicate that the position of the OH group in the alcohol plays an important role in its potential to activate persulfate. The alcohols that provided the greatest persulfate activation were the primary alcohols, and the alcohols with the least activation capacity were the tertiary alcohols. Furthermore, the number of carbons in the alcohol affected its potential to activate persulfate. For example, in the case of the primary alcohols, *n*-propanol provided the highest activation of persulfate and *n*-pentanol provided the lowest (Figure 7.2.5.6a). The same effect is observed in the case of the secondary alcohols (Figure 7.2.5.6b), where the alcohol with the least activation of persulfate was 3-methyl-2-butanol, which also had the slowest degradation rate for nitrobenzene.

In general, the potential of primary alcohols to activate persulfate was lower than that of the other activators tested, such as acetone or ketoacids. The primary alcohols required 9 hours to degrade either of the probe compounds, compared with 3 hr for acetone and only 1 hr for the keto acid compounds.

Aldehydes

Formaldehyde, acetaldehyde, propionaldehyde, and butyraldehyde were used to identify the potential for an aldehyde functional group to activate persulfate. The pK_a value of the aldehydes is 17 (Perrin et al., 1981); consequently they are characterized by minimal dissociation at the pH at which the basic persulfate reactions were conducted.

The loss of hexachloroethane in aldehyde activated persulfate systems at basic pH is shown in Figure 7.2.5.7. The data demonstrate that all the aldehydes used in this study activate persulfate. However, the rate of degradation differed depending on the structure of the functional group attached to the aldehyde group. For example, the use of propionaldehyde as the organic activator resulted in a > 99 % loss of hexachloroethane in 3 hr, compared to 30% when formaldehyde was used. In the control system without aldehydes, the degradation of hexachloroethane was insignificant and likely due to volatilization.

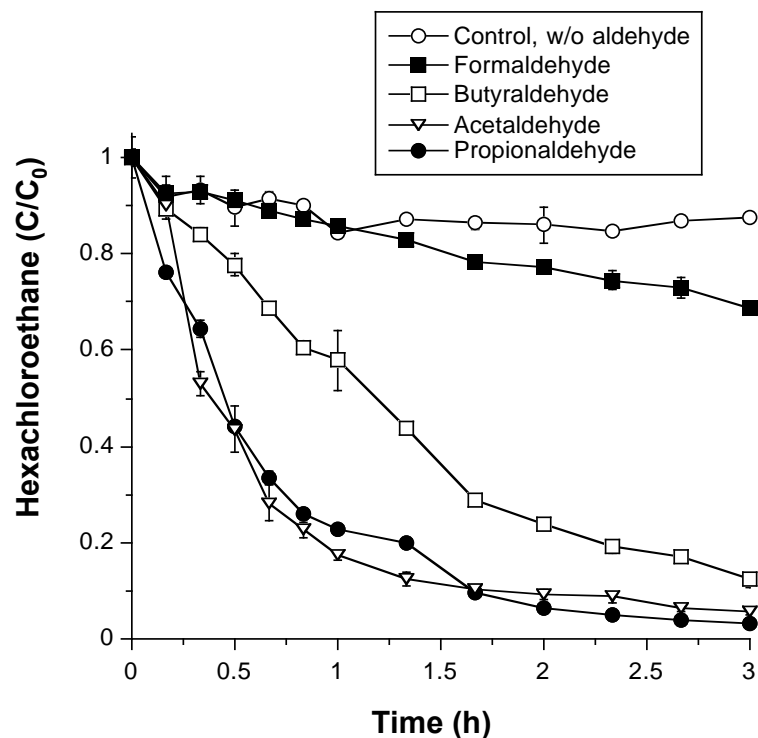


Figure 7.2.5.7. Degradation of hexachloroethane in aldehydes activated persulfate systems at basic pH: 0.5 M sodium persulfate, 2 M NaOH, 10 mM aldehyde, and 2 μ M hexachloroethane; 20 mL total volume. Error bars represent the standard error of the mean for three replicates.

Nitrobenzene degradation was measured to evaluate the generation of hydroxyl radical during persulfate activation by aldehydes. The loss of nitrobenzene in aldehyde activated persulfate systems at basic pH is shown in Figure 7.2.5.8. The data indicate that persulfate activation using most of the aldehydes investigated generates hydroxyl radical, but at a relatively slower rate than for reductants. For example, in propionaldehyde activated persulfate systems, hexachloroethane degradation was near-complete in 3 h, compared with the 9 h that were needed for the nitrobenzene degradation.

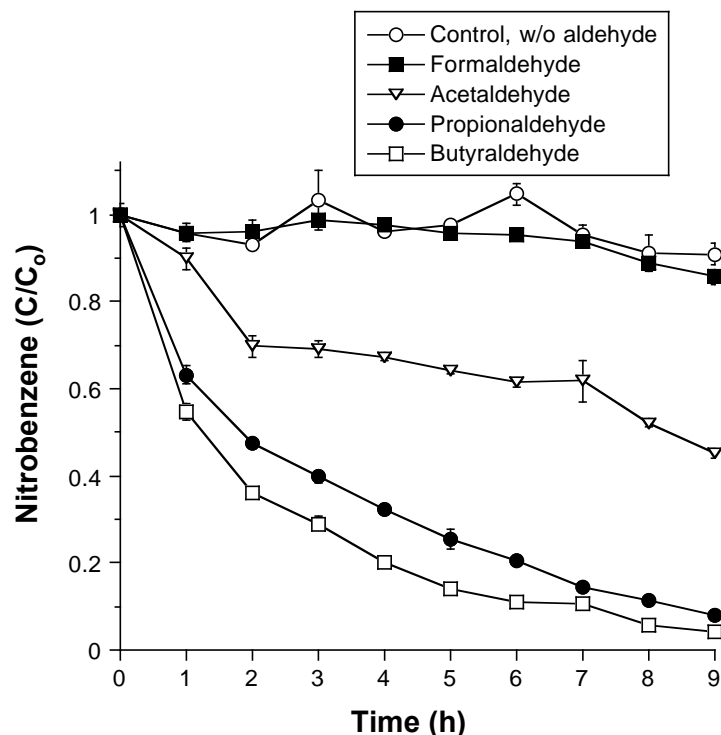


Figure 7.2.5.8. Degradation of nitrobenzene in aldehydes activated persulfate systems at basic pH: 0.5 M sodium persulfate, 2 M NaOH, 10 mM aldehyde, and 1 mM nitrobenzene; 15 mL total volume. Error bars represent the standard error of the mean for three replicates. (a) Primary alcohols (b) Secondary alcohols (c) Ternary alcohols.

The pattern between the different aldehydes was not the same for reductant generation using hexachloroethane and a probe and hydroxyl radical generation using nitrobenzene as a probe as it was for other functional groups such as ketones and alcohols. Acetaldehyde, for example, was one of the fastest activators for hexachloroethane degradation, but fairly slow for nitrobenzene. Nitrobenzene and hexachloroethane react at completely different rates with hydroxyl radicals and reductants, respectively. However, the principal use of the probe compounds is to compare relative rates for a given species (such as the hydroxyl radical) rather than to compare rates between hydroxyl radicals and reductants.

Scavenging of Hydroxyl Radical

An excess of *t*-butyl alcohol was added to scavenge hydroxyl radical (Anipsitakis et al., 2004). The organic compounds used to evaluate the degradation of nitrobenzene in the presence of the hydroxyl radical scavenger *t*-butyl alcohol were acetone, pyruvic acid, *n*-propanol, and

propionaldehyde. These four compounds were used because they promoted the greatest activation of persulfate in each functional group evaluated. A common characteristic of these compounds is that they have a similar molecular formula, with 3 carbons in the main chain. In the absence of the scavenger, >99% of the nitrobenzene was lost with acetone, pyruvic acid, *n*-propanol, and propionaldehyde activation. Nitrobenzene was extensively degraded due to the ready availability of hydroxyl radicals (Figure 7.2.5.9). However, when *t*-butyl alcohol was added, nitrobenzene was not significantly degraded by persulfate activation through addition of acetone, pyruvic acid, and *n*-propanol. For propionaldehyde the degradation was less than 40%. Therefore, hydroxyl radical is the dominant oxidant in persulfate systems at pH 12 when the activation is carried out by organic compounds such as ketones, alcohols, aldehydes, and Krebs cycle compounds.

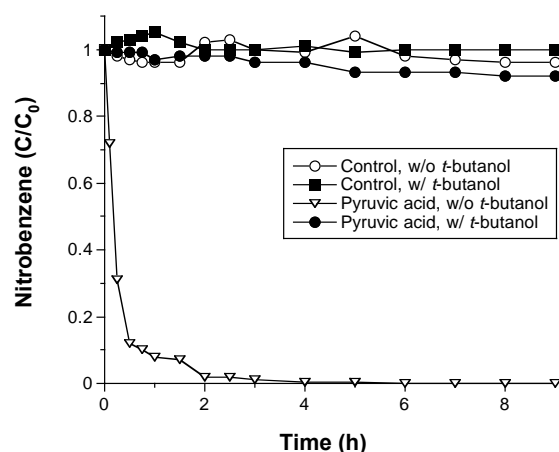
Conclusions

The results of this study demonstrate that many naturally-occurring organic compounds promote persulfate activation at basic pH. These organic compounds may be found as degradation products of contaminants, or as compounds that can be produced by native microbes. All of the four classes of organic compounds that were selected for this study activated persulfate at pH > 12. The organic groups included ketones, Krebs cycle compounds, alcohols, and aldehydes.

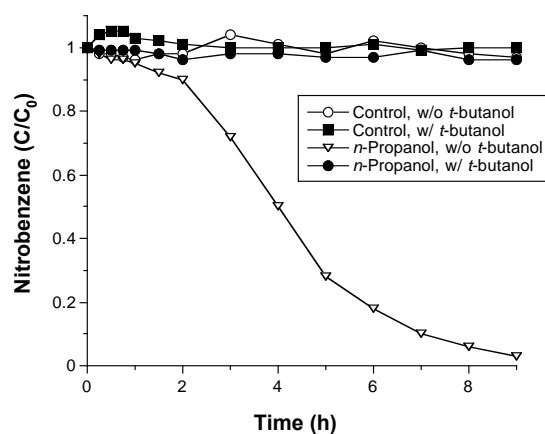
The degree of activation was related to the functional group in the organic compound and its position in the structure. For example, when carboxylic acids were the only functional group in the structure of the organic compound, the activation of persulfate was insignificant, as was the case with oxalic and succinic acid. In contrast, when the carboxylic acid was combined with other functional group such as an alcohol, the rate of persulfate activation increased as with malic and citric acid. The reactivity of the carboxylic acids also increased when a ketone was present in the structure of the organic compound as was the case with keto acids. Similarly, the alcohol group plays an important role in alcohol activation of persulfate. However, the degree of activation depends on the orientation of the OH group in the structure. For example, primary alcohols were more effective activators compared to ternary alcohols.

Ketones, alcohols and aldehydes were not completely in their ionized form during the experiments, since their pK_a values were above 12. The only group that was fully ionized during the experiments were the Krebs cycle compounds, with pK_a values ranging from 1–6. The results indicate that the organic group with the highest degree of persulfate activation was the ketoacid, which confirms that the ionized forms of the organic compounds are important to promote the activation of persulfate.

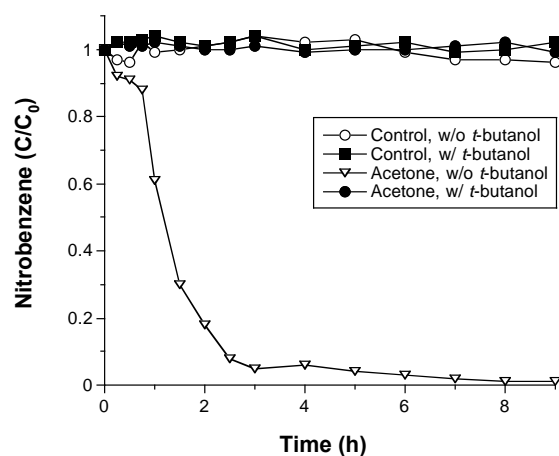
a.



b.



c.



d.

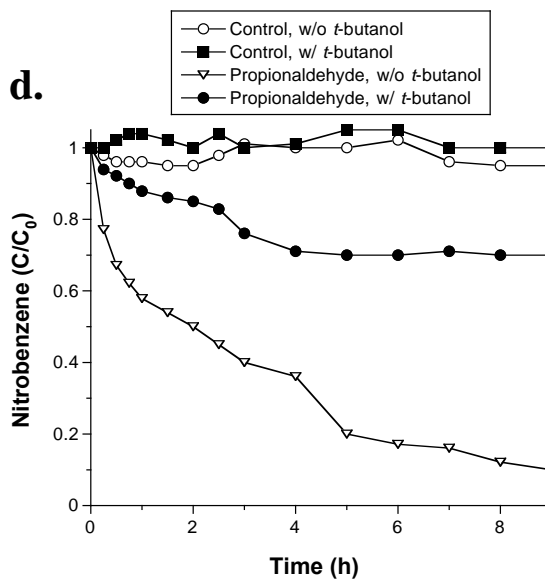


Figure 7.2.5.9. Scavenging of hydroxyl radicals in persulfate activation by selected organic compounds: 0.5 M sodium persulfate, 2 M NaOH, 10 mM organic compound, and 1 mM nitrobenzene; 15 mL total volume; the molar ratio of nitrobenzene to *t*-butyl alcohol was 1:1000. Error bars represent the standard error of the mean for three replicates. (a) acetone (C_3H_6O); (b) pyruvic acid ($C_3H_4O_3$); (c) *n*-propanol (C_3H_8O); (d) propionaldehyde (C_3H_6O).

7.2.6. Persulfate Activation by Soil Organic Matter

Generation of hydroxyl radical

Using nitrobenzene as a hydroxyl radical probe, the relative rates of hydroxyl radical generation in the Carson Valley Soils 1–4 are shown in Figures 7.2.6.1–4, respectively. Nitrobenzene loss was undetectable in the deionized water control and basic persulfate positive control in all four systems. However, nitrobenzene degradation was approximately 80% in all four soils with soil organic matter contents varying from 2000 mg/kg to 16,000 mg/kg. These results are in agreement with the findings of Ocampo (2009), who found that phenoxides activate persulfate. Soil organic matter contains phenolic moieties that likely activate persulfate when the pH is sufficiently high to deprotonate the hydroxyl groups.

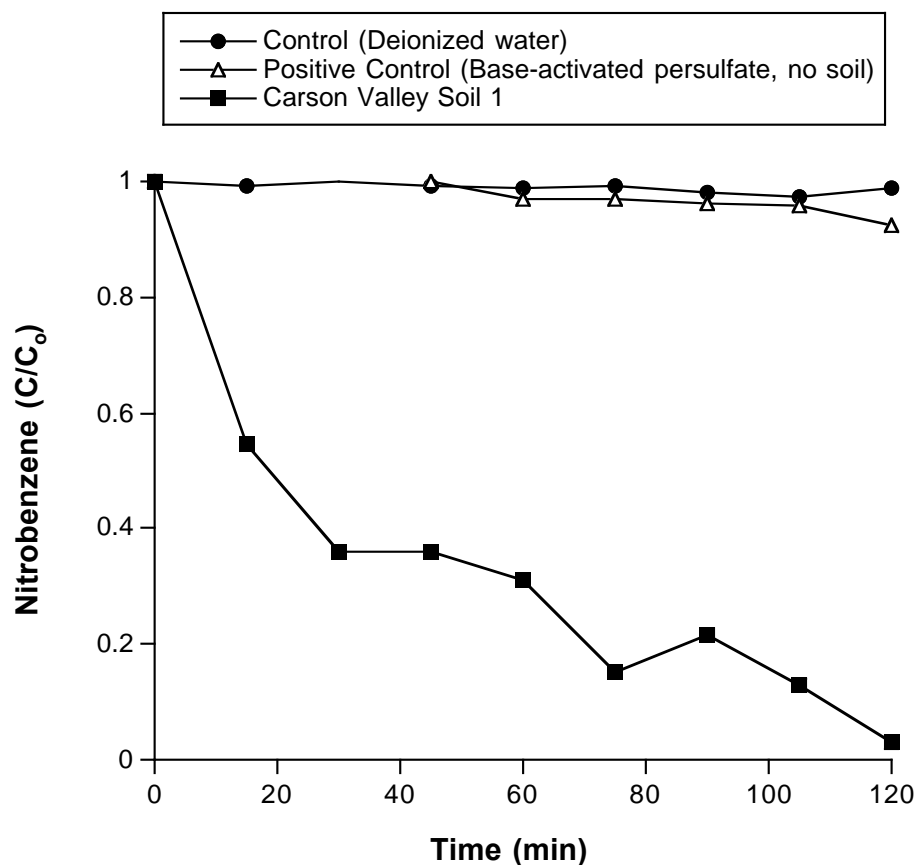


Figure 7.2.6.1. Relative hydroxyl radical generation, as quantified by nitrobenzene degradation, in persulfate systems containing the Carson Valley Soil 1.

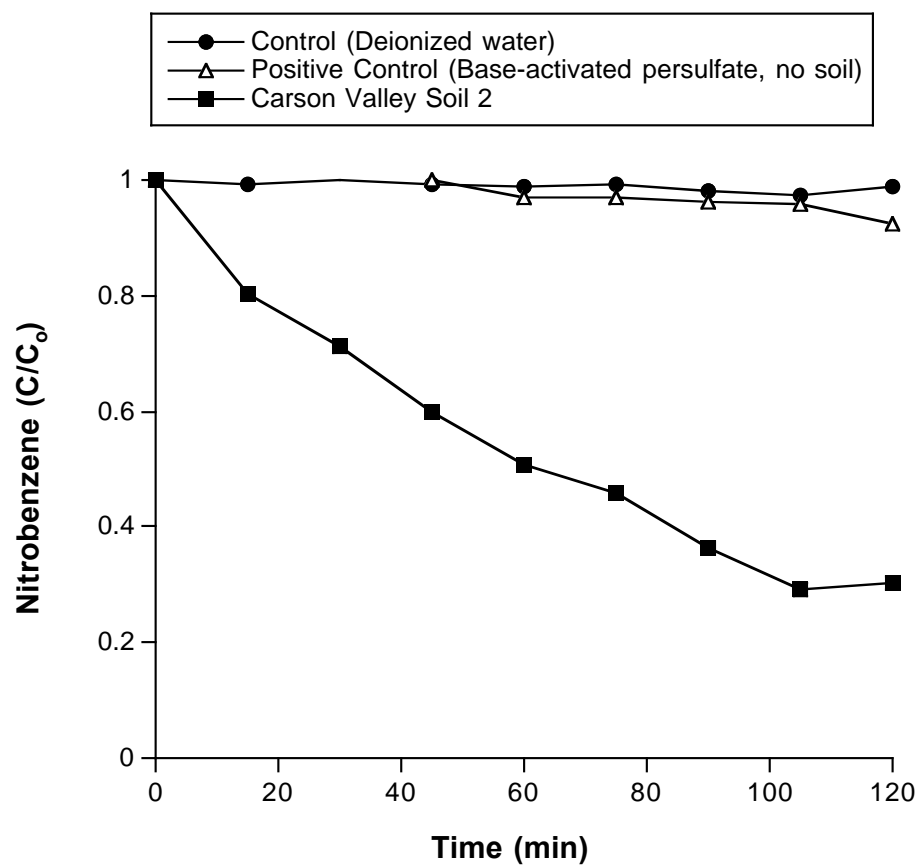


Figure 7.2.6.2. Relative hydroxyl radical generation, as quantified by nitrobenzene degradation, in persulfate systems containing the Carson Valley Soil 2.

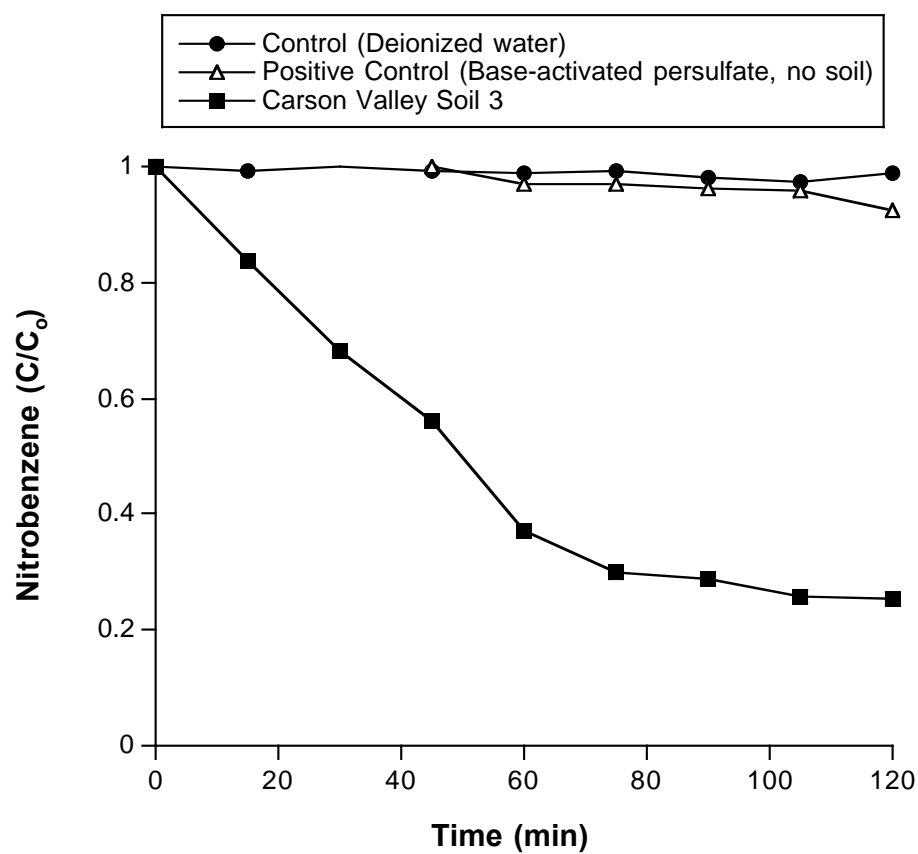


Figure 7.2.6.3. Relative hydroxyl radical generation, as quantified by nitrobenzene degradation, in persulfate systems containing the Carson Valley Soil 3.

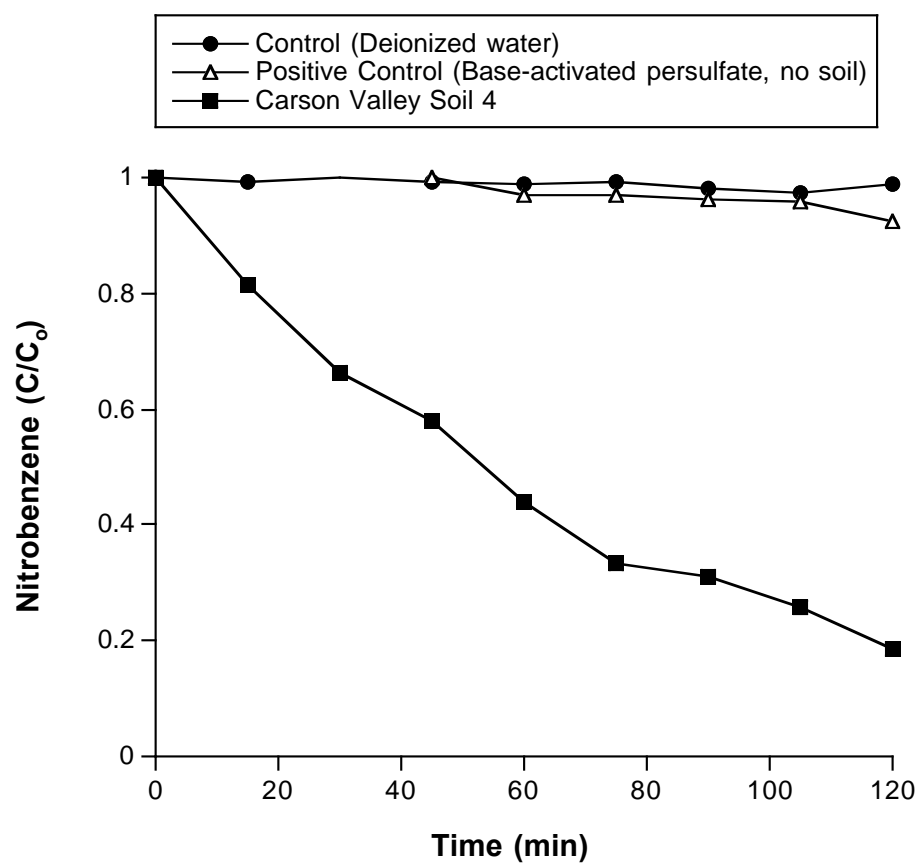


Figure 7.2.6.4. Relative hydroxyl radical generation, as quantified by nitrobenzene degradation, in persulfate systems containing the Carson Valley Soil 4.

To confirm that soil organic matter is activating persulfate, soil organic matter was removed, and the relative rates of hydroxyl radical generation were evaluated in the presence of the mineral fraction, but without SOM. The loss of nitrobenzene in these soil mineral-only systems was no different from that of deionized water controls or positive controls containing aqueous basic persulfate (Figures 7.2.6.5–8). These results confirm that soil organic matter activates persulfate to generate hydroxyl radical.

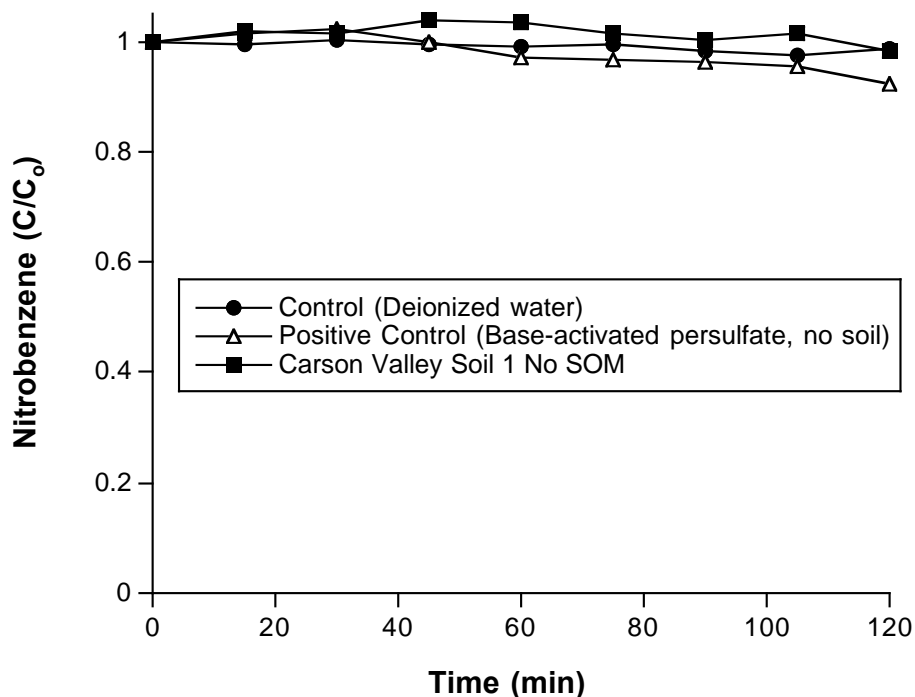


Figure 7.2.6.5. Relative hydroxyl radical generation, as quantified by nitrobenzene degradation, in persulfate systems containing the Carson Valley Soil 1 with soil organic matter removed.

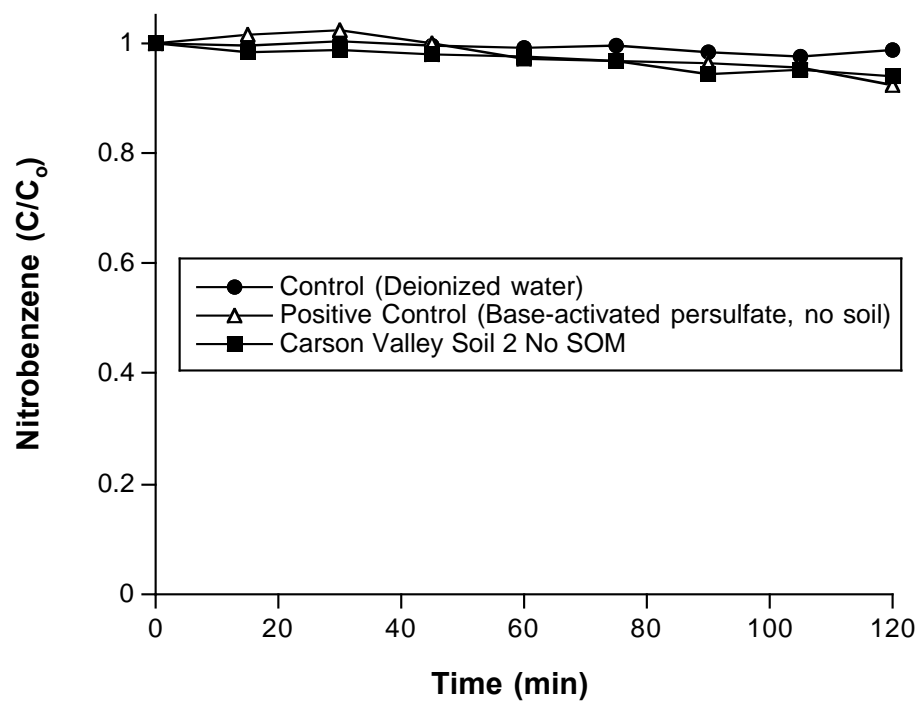


Figure 7.2.6.6. Relative hydroxyl radical generation, as quantified by nitrobenzene degradation, in persulfate systems containing the Carson Valley Soil 2 with soil organic matter removed.

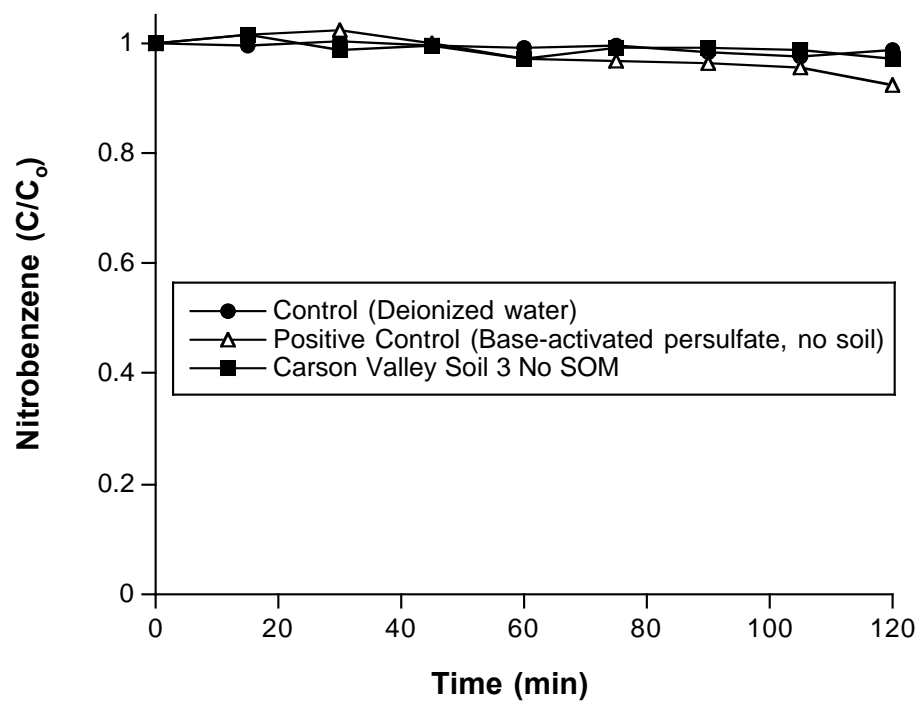


Figure 7.2.6.7. Relative hydroxyl radical generation, as quantified by nitrobenzene degradation, in persulfate systems containing the Carson Valley Soil 3 with soil organic matter removed.

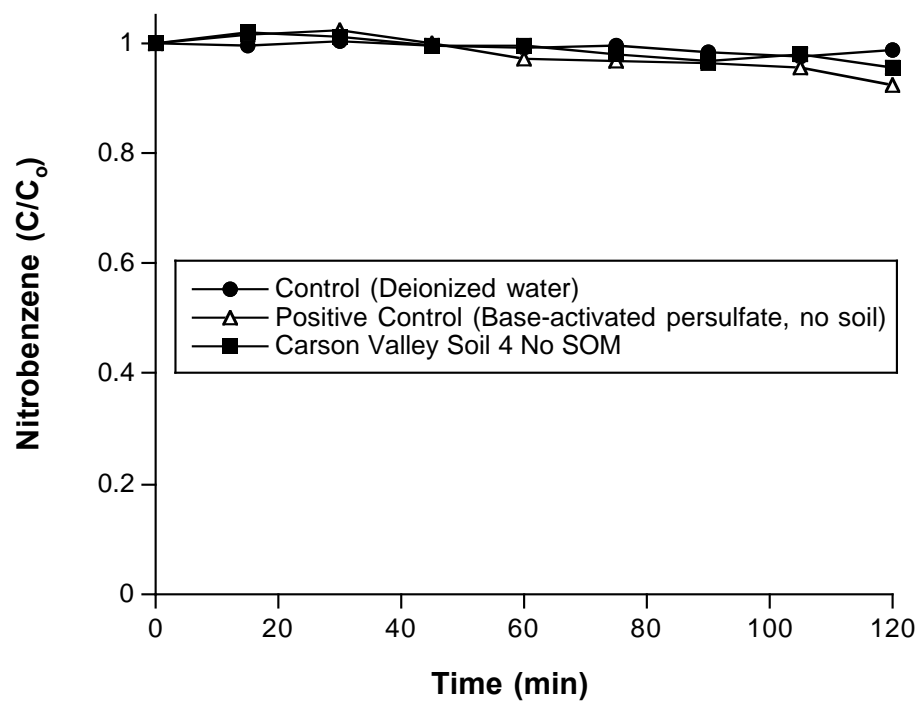


Figure 7.2.6.8. Relative hydroxyl radical generation, as quantified by nitrobenzene degradation, in persulfate systems containing the Carson Valley Soil 4 with soil organic matter removed.

Generation of reductants

The relative rates of reductant generation in the Carson Valley Soils 1–4 using HCA as a reductant probe are shown in Figures 7.2.6.9–12. No measurable HCA loss occurred in the deionized water controls or aqueous basic persulfate positive controls. Similar to the results of Figures 7.2.6.1–4, reductant generation was significant in all four soils with approximately 95% HCA loss over 2 hr. The reductants generated by the SOM-activation of persulfate are likely alkyl radicals, but could include other reactive species, such as superoxide or solvated electrons.

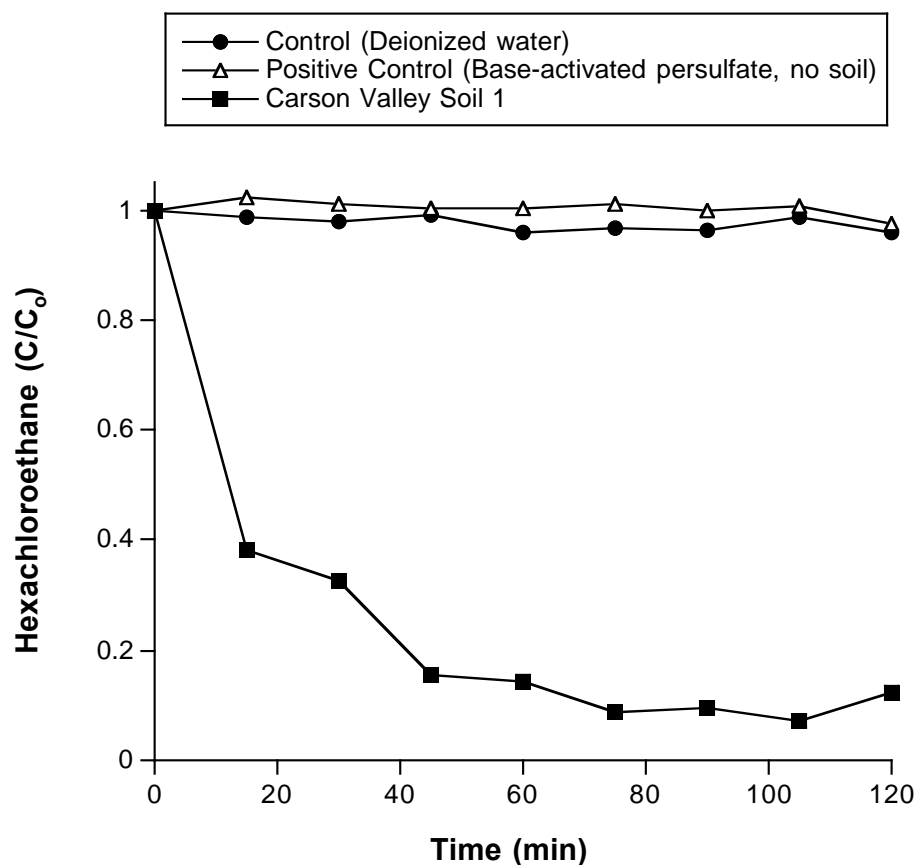


Figure 7.2.6.9. Relative reductant generation, as quantified by hexachloroethane degradation, in persulfate systems containing the Carson Valley Soil 1.

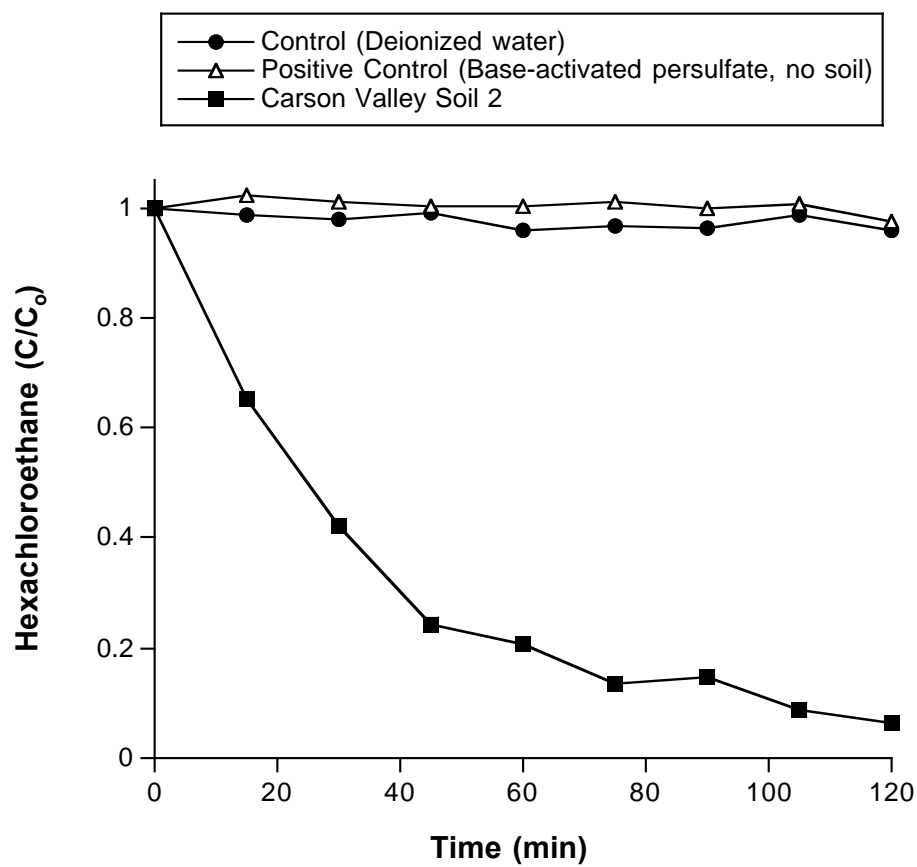


Figure 7.2.6.10. Relative reductant generation, as quantified by hexachloroethane degradation, in persulfate systems containing the Carson Valley Soil 2.

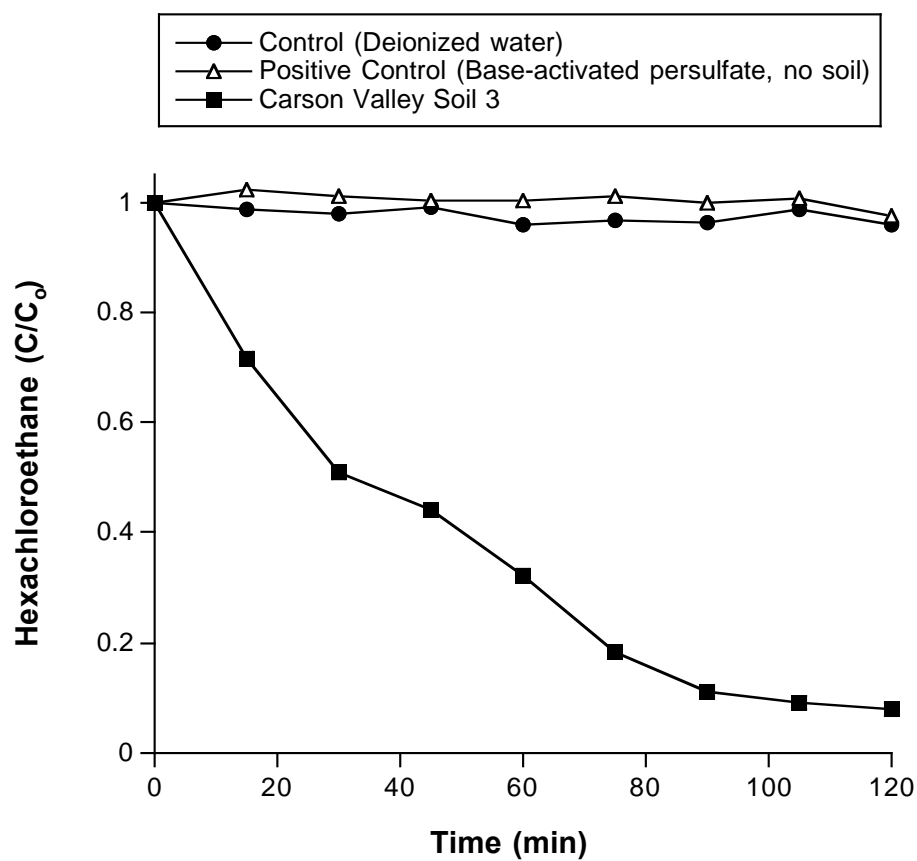


Figure 7.2.6.11. Relative reductant generation, as quantified by hexachloroethane degradation, in persulfate systems containing the Carson Valley Soil 3.

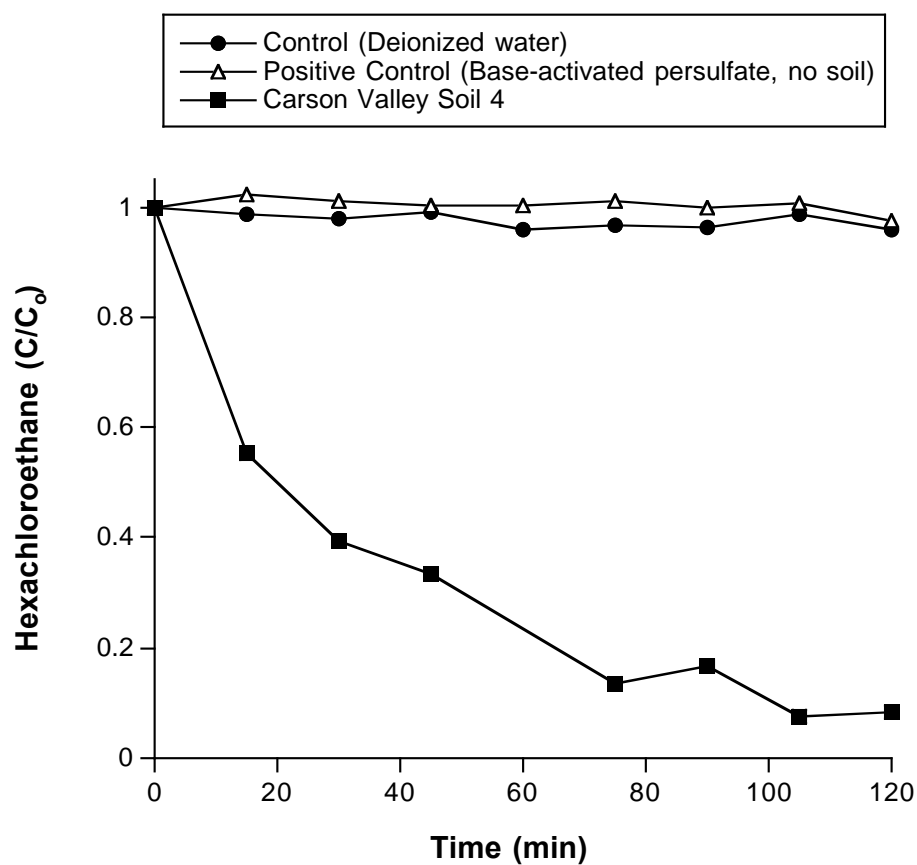


Figure 7.2.6.12. Relative reductant generation, as quantified by hexachloroethane degradation, in persulfate systems containing the Carson Valley Soil 4.

To confirm the role of soil organic matter in the generation of reductants, the reactions were repeated using HCA as a probe, but with the soil organic matter removed. No measurable generation of reductants was observed relative to deionized water controls or positive controls consisting of aqueous basic persulfate (Figures 7.2.6.13–16). These results confirm the role of soil organic matter.

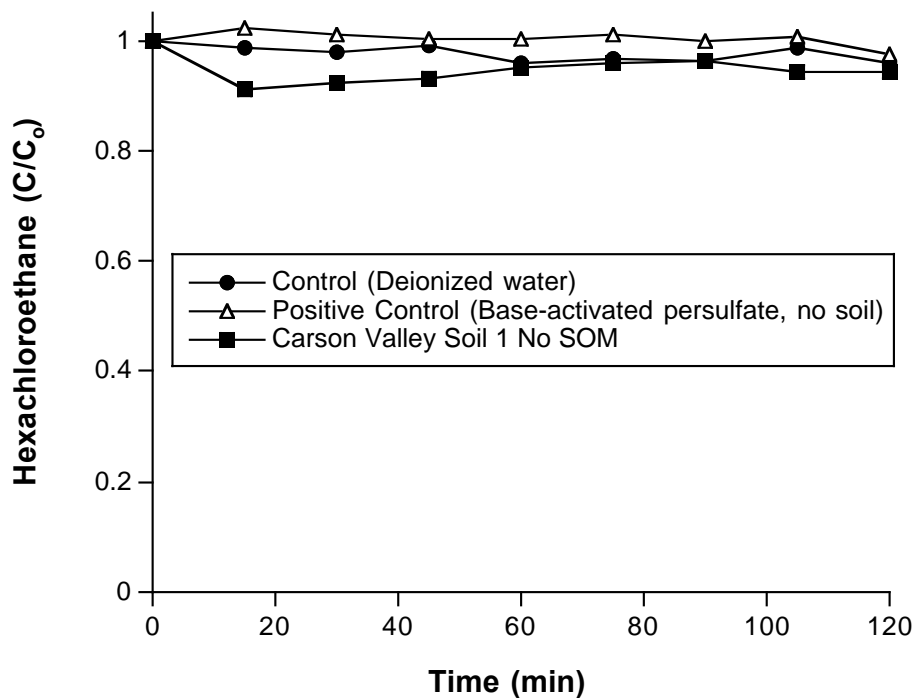


Figure 7.2.6.13. Relative reductant generation, as quantified by hexachloroethane degradation, in persulfate systems containing the Carson Valley Soil 1 with soil organic matter removed.

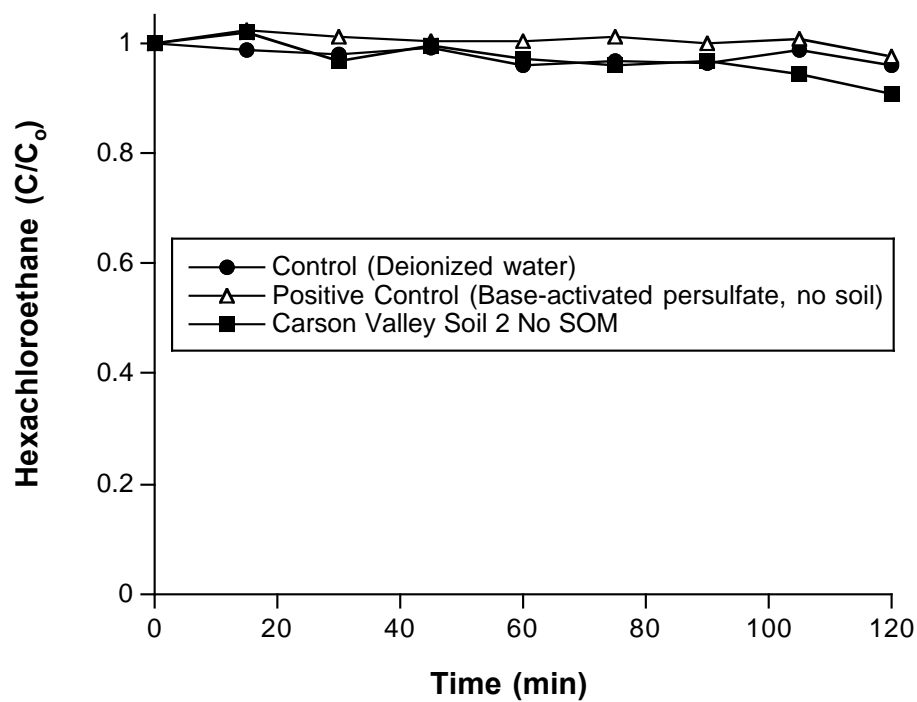


Figure 7.2.6.14. Relative reductant generation, as quantified by hexachloroethane degradation, in persulfate systems containing the Carson Valley Soil 2 with soil organic matter removed.

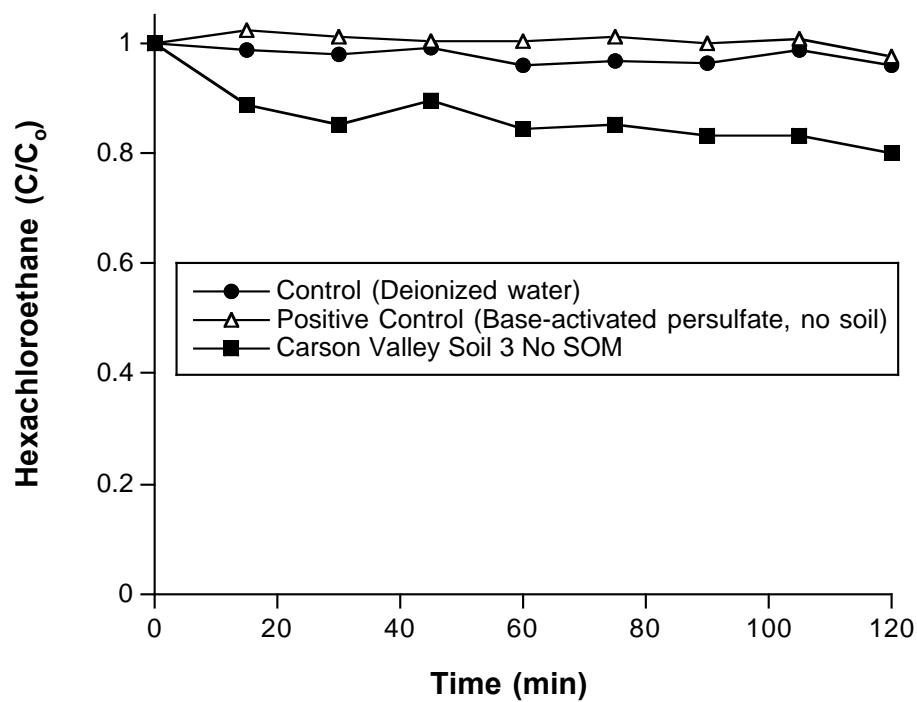


Figure 7.2.6.15. Relative reductant generation, as quantified by hexachloroethane degradation, in persulfate systems containing the Carson Valley Soil 3 with soil organic matter removed.

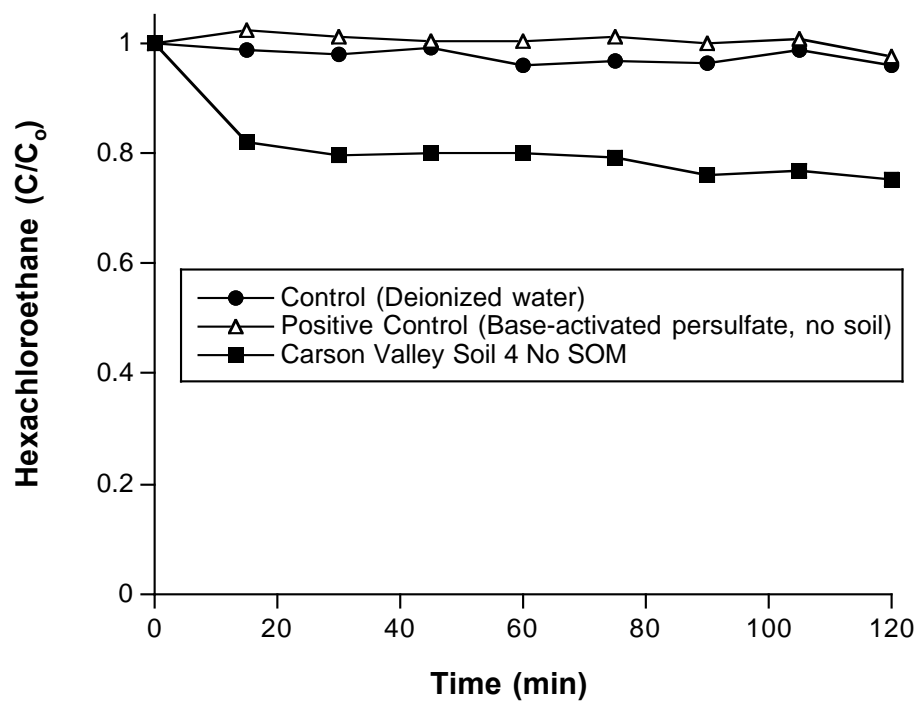


Figure 7.2.6.16. Relative reductant generation, as quantified by hexachloroethane degradation, in persulfate systems containing the Carson Valley Soil 4 with soil organic matter removed.

Persulfate activation with minimal soil organic matter

All of the soil organic matter contents of the Carson Valley Soils promoted equal relative rates of hydroxyl radical and reductant generation. To evaluate rates of soil organic matter activation at lower soil organic matter levels, the Carson Valley Soil 1 was mixed with Carson Valley Soil 1 from which the organic matter had been removed, to provide organic carbon contents of 500 mg/kg and 1000 mg/kg. The results, shown in Figure 17, demonstrate that the soil with 1000 mg/kg organic carbon still promoted effective hydroxyl radical generation. However, 500 mg/kg organic carbon provided minimal hydroxyl radical generation. These results suggest a zero order phenomenon of persulfate activation with respect to soil organic carbon contents. Minimal organic carbon appears to be required to activate persulfate, and then the rate of activation reaches a maximum very rapidly.

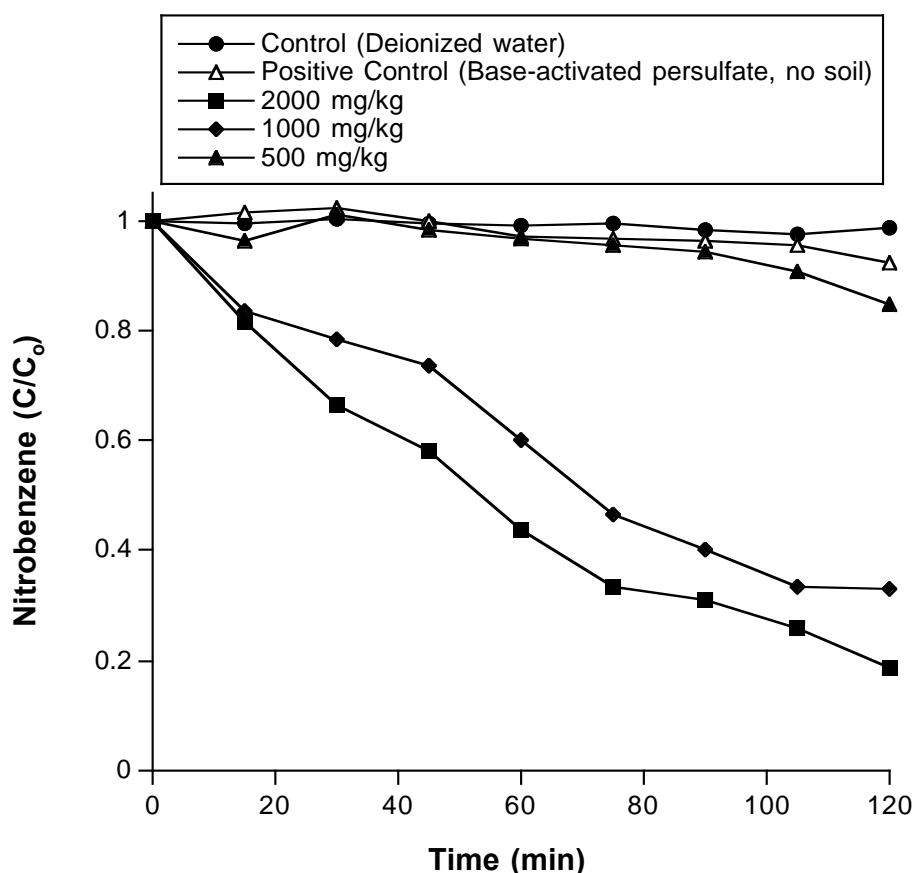


Figure 7.2.6.17. Relative hydroxyl radical generation, as quantified by nitrobenzene degradation, in persulfate systems containing Carson Valley Soil 1 with varying concentrations of soil organic matter.

Conclusion

The results of this research demonstrate that soil organic matter activates persulfate under alkaline conditions to generate both oxidants and reductants. The activation is likely provided by phenoxide moieties associated with the soil organic matter. This pathway of persulfate activation is likely a dominant mechanism for contaminant destruction in soils and the subsurface.

7.2.7. Model Contaminants

Degradation of the seven model contaminants will be discussed in three groups of structurally similar compounds: 1) TCE and PCE, 2) DCA and TCA, and 3) CB, DCB, and anisole.

TCE and PCE

The degradation of TCE and PCE using base to persulfate molar ratios of 1:1, 2:1, and 3:1 is shown in Figures 7.2.7.1 and 7.2.7.2. TCE degradation was fastest with a 3:1 base to persulfate molar ratio. These results are expected because higher base concentrations promote more rapid base-catalyzed hydrolysis of persulfate and therefore faster rates of initiation of radical-based pathways (Furman et al., 2010). Rates of PCE degradation were significantly slower than rates of PCE degradation. Persulfate initiation rates are likely equal in the presence of both contaminants; the slower rate of PCE degradation may be due to the low reactivity of sulfate radical with PCE.

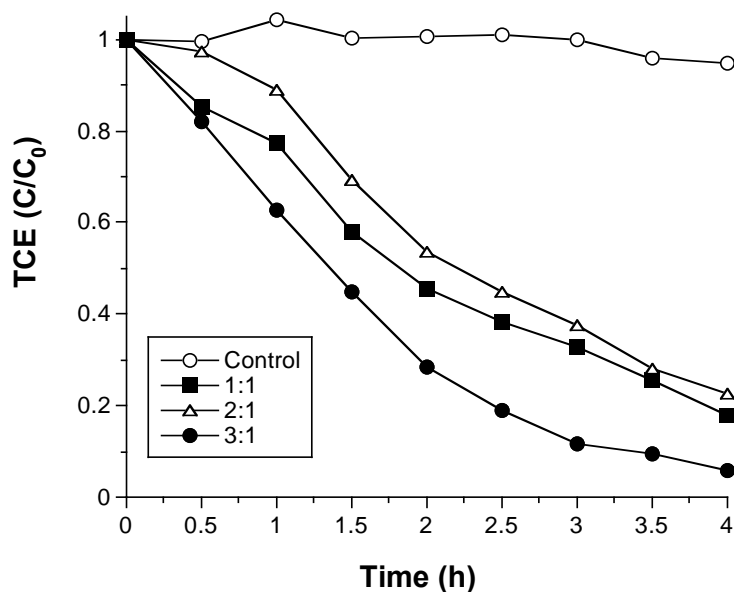


Figure 7.2.7.1. TCE degradation in base-activated persulfate systems containing base to persulfate molar ratios of 1:1, 2:1, and 3:1. Controls: base and persulfate substituted with deionized water.

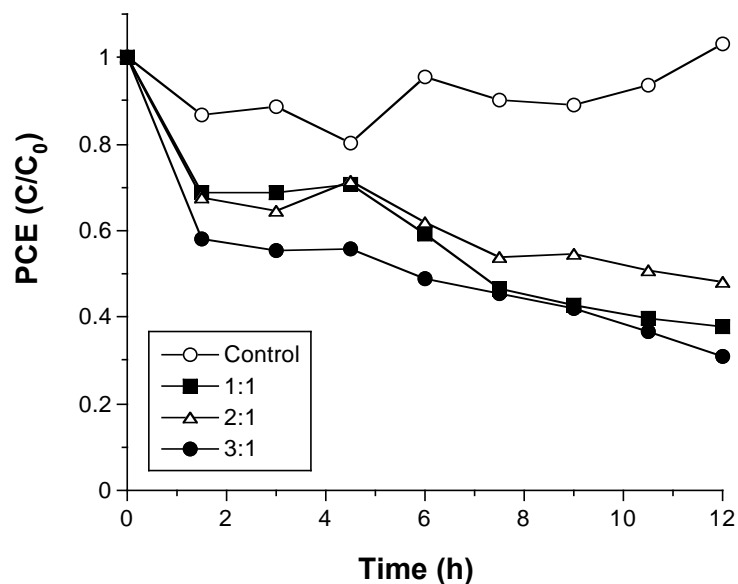


Figure 7.2.7.2. PCE degradation in base-activated persulfate systems containing base to persulfate molar ratios of 1:1, 2:1, and 3:1. Controls: base and persulfate substituted with deionized water.

DCA and TCA

The degradation of DCA and TCA is shown in Figures 7.2.7.3 and 7.2.7.4, respectively. The degradation of DCA was faster with increasing basicity, while basicity had minimal effect on TCA degradation. Because of the difference in chlorination of these two alkanes, they may degrade by different pathways in base-activated persulfate systems. TCA likely degrades through a reaction with superoxide (Furman et al., 2010). DCA may degrade through reactions with both superoxide and hydroxyl radical, which may explain the difference in reactivity trends between the two contaminants.

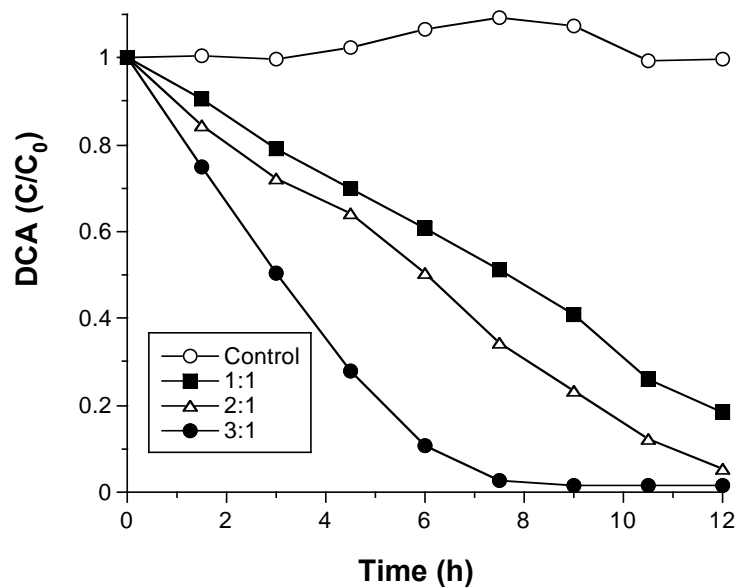


Figure 7.2.7.3. DCA degradation in base-activated persulfate systems containing base to persulfate molar ratios of 1:1, 2:1, and 3:1. Controls: base and persulfate substituted with deionized water.

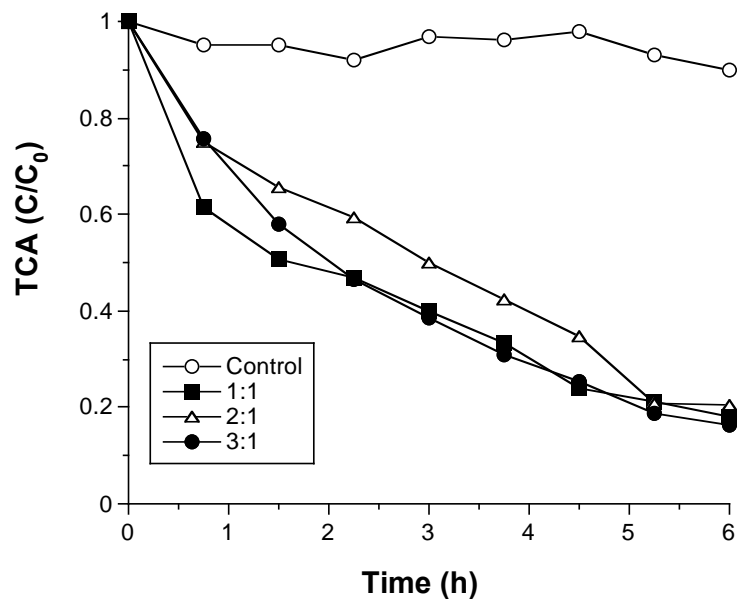


Figure 7.2.7.4. TCA degradation in base-activated persulfate systems containing base to persulfate molar ratios of 1:1, 2:1, and 3:1. Controls: base and persulfate substituted with deionized water.

Aromatic Contaminants

The degradation of the aromatic compounds CB, DCB, and anisole is shown in Figures 7.2.7.5, 7.2.7.6, and 7.2.7.7, respectively. CB degraded more rapidly than DCB, and the basicity of the persulfate formulations had minimal effect on the rate of degradation. Because hydroxyl radical reacts with CB and DCB at the same rate, the involvement of another reactive oxygen species, such as sulfate radical, is likely the cause in the difference in degradation rates between CB and DCB. The rate of anisole degradation was significantly different from that of the six other model contaminants. Anisole degradation was slow for 2 hr, but then its rate of degradation increased significantly over the following 2 hr. The increase in anisole degradation may be due to its oxidation to a phenolic compound, which then activates persulfate, increasing the reactivity of the persulfate system (Ocampo, 2009).

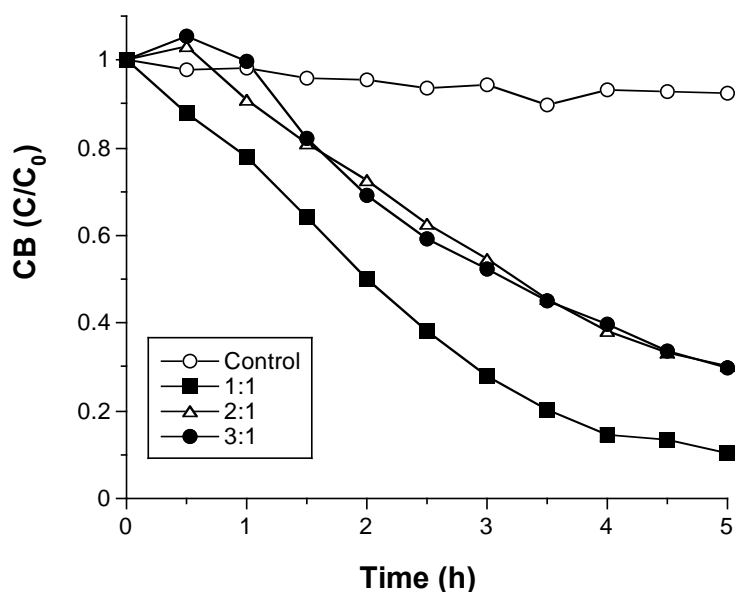


Figure 7.2.7.5. CB degradation in base-activated persulfate systems containing base to persulfate molar ratios of 1:1, 2:1, and 3:1. Controls: base and persulfate substituted with deionized water.

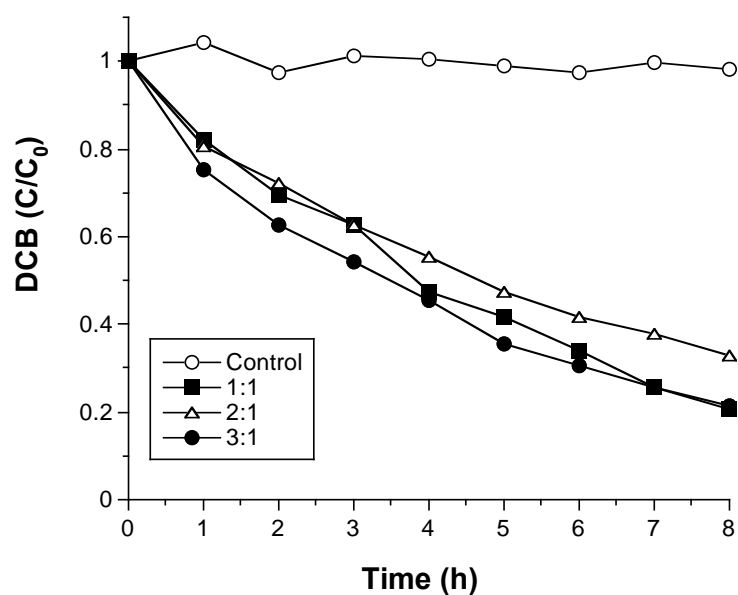


Figure 7.2.7.6. DCB degradation in base-activated persulfate systems containing base to persulfate molar ratios of 1:1, 2:1, and 3:1. Controls: base and persulfate substituted with deionized water.

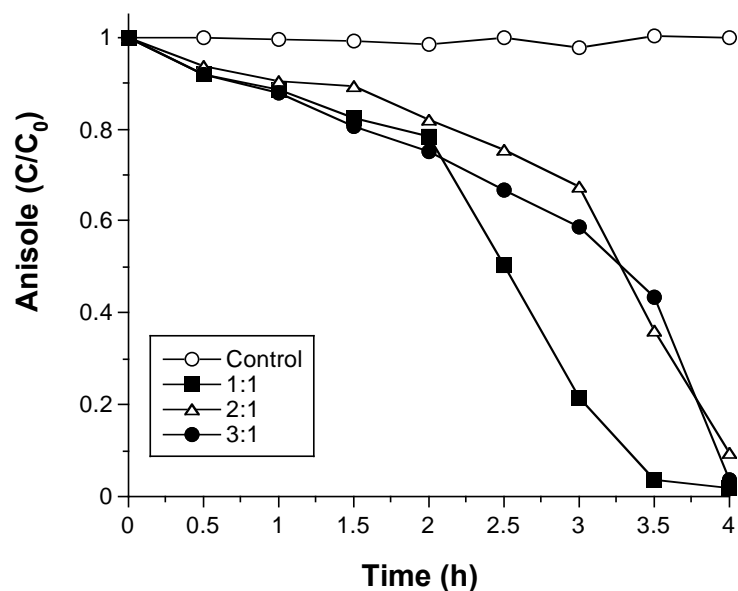


Figure 7.2.7.7. Anisole degradation in base-activated persulfate systems containing base to persulfate molar ratios of 1:1, 2:1, and 3:1. Controls: base and persulfate substituted with deionized water.

Conclusion

The results of this research demonstrate that all seven model contaminants were degraded by activated persulfate. The molar ratio of base to persulfate had an effect on the degradation rate of two of the contaminants: DCA and TCE. The two more highly chlorinated aliphatic compounds, TCA and PCE, degraded at equal rates regardless of the basicity of the persulfate formulation. Anisole degradation increased after 2 hr, likely due to the oxidation of anisole to a phenolic derivative. The results of this research show that numerous classes of contaminants are effectively degraded by activated persulfate, although the reaction pathway may differ for each.

7.2.8. Effect of Sorption on Contaminant Oxidation in Activated Persulfate Systems

CHP Treatment of Sorbed PCE

The enhanced treatment of PCE sorbed on a surface soil by CHP was documented by Watts et. al. (1999); however, the use of diatomaceous earth as a sorbent may provide different desorption-CHP degradation dynamics compared to a natural soil. Diatomaceous earth has a large surface area, negligible amounts of organic matter, and has different mineralogy than a natural soil. The degradation of PCE sorbed to the diatomaceous earth by CHP in relation to gas-purge desorption is shown in Figure 7.2.8.1. PCE desorbed in the gas-purge reactors within 60 min. PCE destruction in CHP reactions using 0.6 M hydrogen peroxide was slightly slower than the rate of gas-purge desorption, and was similar to gas-purge desorption in 1.8 M hydrogen peroxide reactions. However, rates of PCE destruction in reactions containing 3.6 and 5.4 M hydrogen peroxide were significantly greater than the corresponding rate of gas-purge desorption, with the PCE treated to undetectable concentrations within 20 min. These results are consistent with previously published results documenting the enhanced treatment of sorbed contaminants by CHP (Watts et al., 2002; Watts et al., 1999; Watts and Stanton, 1999); in particular, PCE degradation rates were similar in the diatomaceous earth (Figure 7.2.8.1) and in a natural surface soil (Watts et al., 1999). However, the rate of gas-purge desorption of PCE shown in Figure 7.2.8.1 was significantly more rapid than in a surface soil (Watts et al., 1999). The likely reason for the more rapid rate of PCE desorption in diatomaceous earth is the absence of soil organic matter, which serves as the primary sorbent in most soils (Watts, 1998).

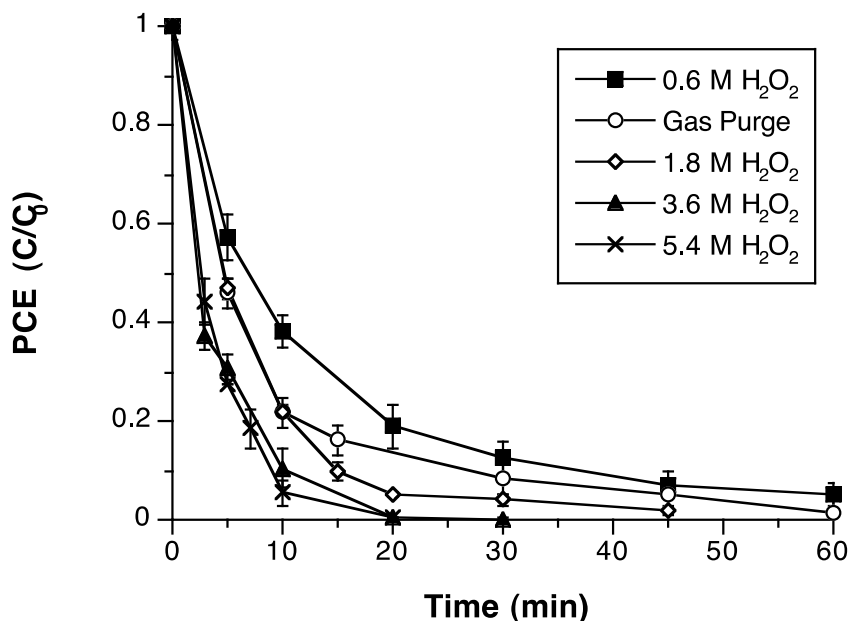


Figure 7.2.8.1. CHP treatment of PCE sorbed on diatomaceous earth in relation to its rate of gas purge desorption.

Activated Persulfate Treatment of Sorbed PCE

The concentration of PCE sorbed onto diatomaceous earth during treatment with iron (II)–citrate-activated persulfate compared to gas-purge desorption is shown in Figure 7.2.8.2. Desorption of PCE by gas purging was > 99% over 60 minutes. All three concentrations of activator (5 mM, 10 mM, and 20 mM citrate-iron (II) chelate) with 1 M persulfate degraded PCE at approximately the same rate as gas purge desorption. The results of Figure 7.2.8.2 demonstrate that iron citrate-activated persulfate systems degrade PCE as quickly as it desorbs, but do not provide enhanced contaminant desorption of PCE relative to its maximum natural rate of desorption as measured by gas-purge methodology.

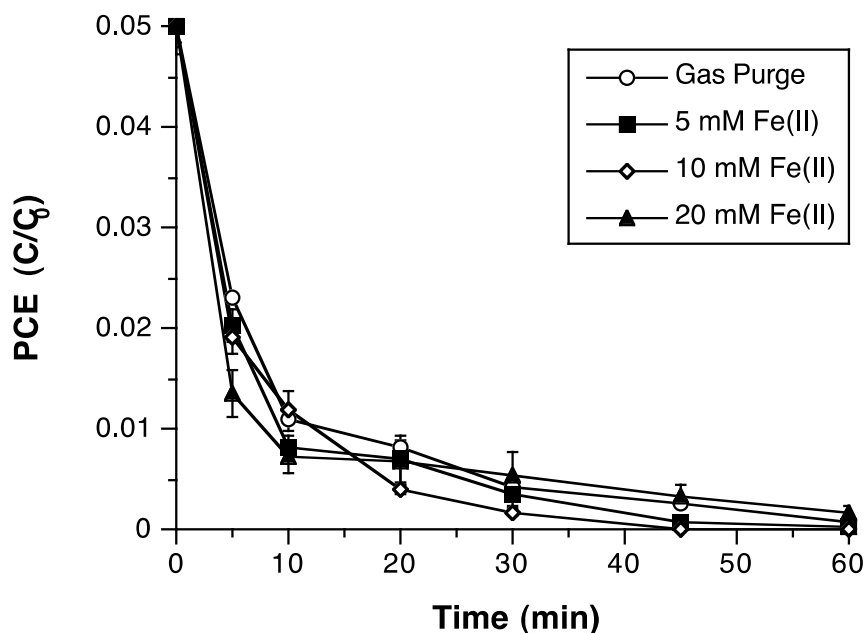


Figure 7.2.8.2. Iron (II)–citrate-activated persulfate treatment of PCE sorbed on diatomaceous earth by in relation to its rate of gas purge desorption.

Base-activated persulfate (2:1 molar ratio of sodium hydroxide:persulfate) treatment of PCE sorbed on diatomaceous earth in relation to gas purge desorption is shown in Figure 7.2.8.3. With 0.1 M persulfate, 76% of the PCE degraded over 60 min, which was significantly slower than the rate of gas purge desorption. The rate of base-activated destruction of PCE increased with the dosage of persulfate, with 92% persulfate loss in the 1 M persulfate system. However, PCE degradation in all of the base-activated persulfate systems was less than the loss in the gas-purge system. The results of Figure 7.2.8.3 demonstrate that base-activated persulfate can destroy PCE, but not more rapidly than its corresponding rate of gas-purge desorption.

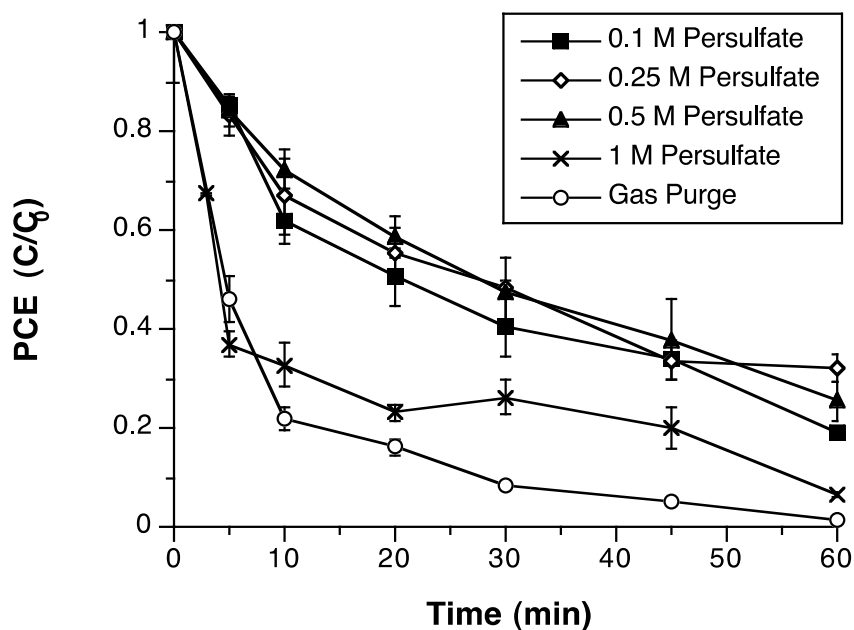


Figure 7.2.8.3. Base-activated persulfate treatment of PCE sorbed on diatomaceous earth in relation to its rate of gas purge desorption.

CHP Treatment of Sorbed HCCP

There was no evidence of enhanced treatment of sorbed PCE by activated persulfate formulations; therefore, the more hydrophobic probe compound HCCP was used to detect potential enhanced treatment of sorbed contaminants. The enhanced treatment of HCCP sorbed on diatomaceous earth by CHP in relation to gas-purge desorption is shown in Figure 7.2.8.4. Desorption of HCCP was minimal in gas-purge systems over 120 min. In contrast, loss of HCCP was greater than gas-purge desorption in CHP reactions containing 2, 5, and 10 M hydrogen peroxide. HCCP destruction increased with increasing hydrogen peroxide concentrations in the three CHP systems, with 70% HCCP destruction after 120 min in the 10 M hydrogen peroxide reaction.

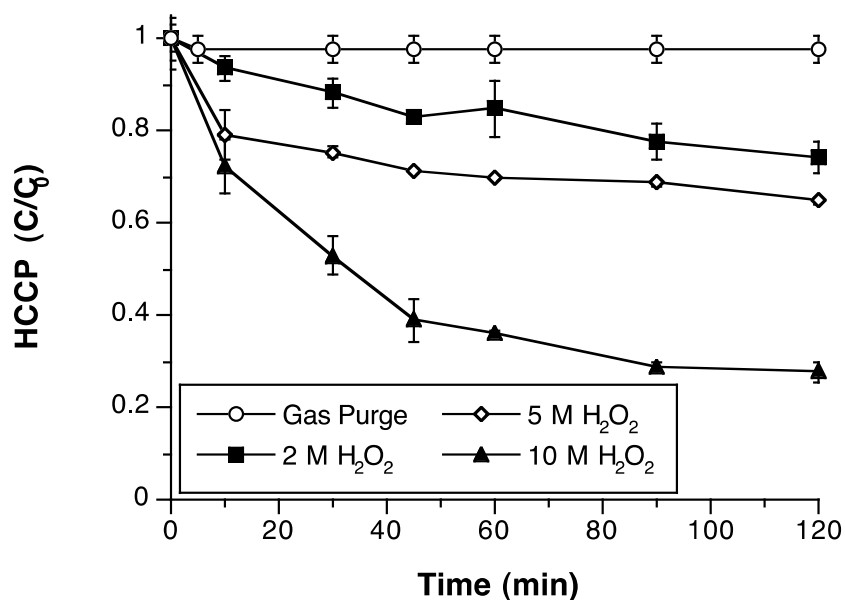


Figure 7.2.8.4. CHP treatment of HCCP sorbed on diatomaceous earth in relation to its rate of gas purge desorption.

Activated Persulfate Treatment of Sorbed HCCP

The iron (II)-citrate-activated treatment of HCCP sorbed on diatomaceous earth in relation to its gas-purge desorption is shown in Figure 7.2.8.5. Iron (II)-citrate-activated persulfate treatment resulted in no measurable HCCP degradation at any of the activator concentrations over the 120 min reaction time. These data are consistent with the results with PCE (Figure 7.2.8.2) and demonstrate that iron (II)-citrate-activated persulfate does not treat sorbed contaminants more rapidly than their maximum natural rate of desorption.

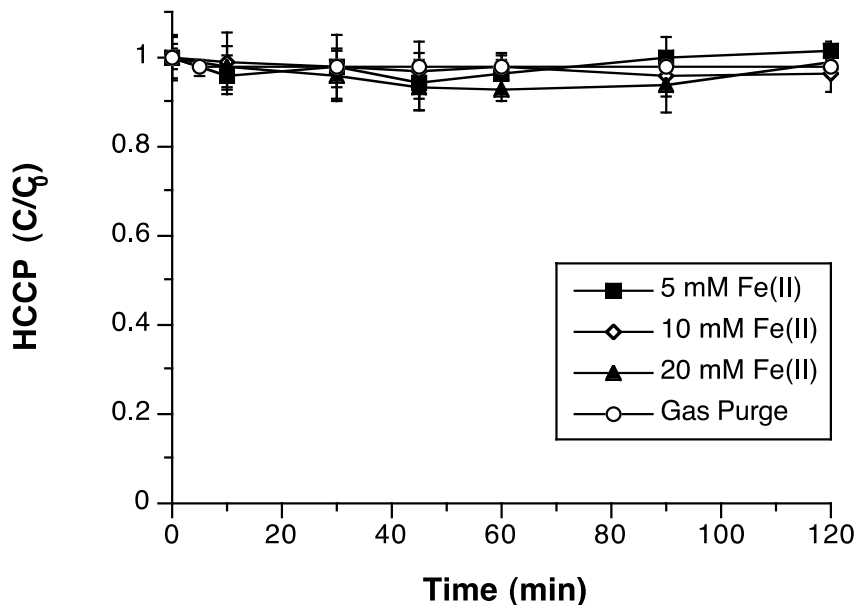


Figure 7.2.8.5. Iron (II)–citrate-activated persulfate treatment of HCCP sorbed on diatomaceous earth in relation to its rate of gas purge desorption.

The base activated treatment of HCCP sorbed on diatomaceous earth is shown in Figure 7.2.8.6. Similar to the data in Figure 7.2.8.5, gas-purge desorption was negligible and the base-activated persulfate degradation of HCCP was undetectable over the 120 min reaction time. The data of Figures 7.2.8.5 and 7.2.8.6 confirm the results shown in Figures 7.2.8.2 and 7.2.8.3 for the activated persulfate treatment of PCE. In neither formulation of activated persulfate and for neither probe compound was the rate of probe compound destruction greater than the maximum natural rate of desorption. These data document that iron (II)–citrate- and base-activated persulfate do not promote the enhanced treatment of sorbed PCE and HCCP, and likely do not provide enhanced treatment of other hydrophobic compounds sorbed to solids.

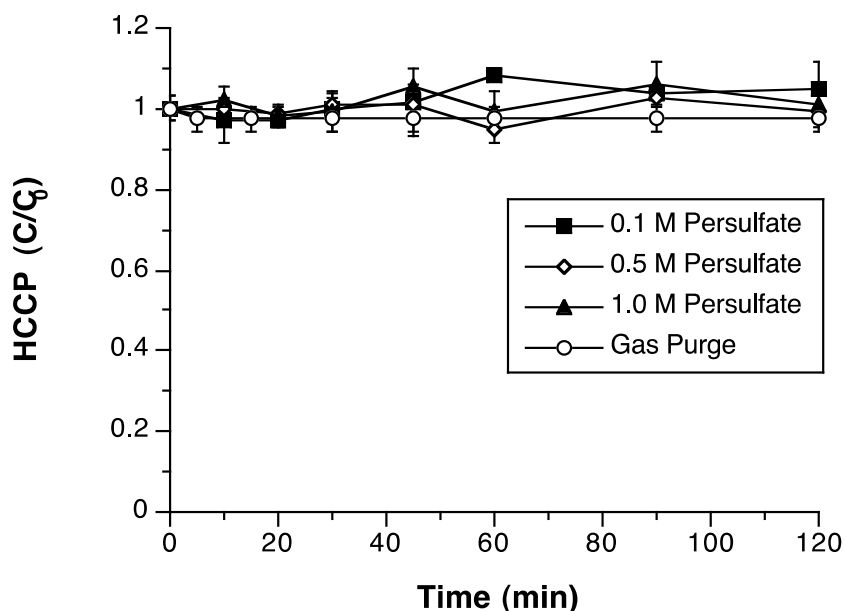


Figure 7.2.8.6. Base-activated persulfate treatment of HCCP sorbed on diatomaceous earth in relation to its rate of gas purge desorption.

Most remediation processes are limited by rates of desorption (Watts, 1998). For example, bioremediation, reactions with hydroxyl radicals, and reactions with reductants such as dithionite, occur in the aqueous phase (Sedlak and Andren, 1994; Ogram et al., 1985). Sorbed contaminants must desorb into the aqueous phase where they are degraded; a concentration gradient is then established, resulting in subsequent desorption to the aqueous phase with continued contaminant degradation. If the contaminant is degraded instantaneously after desorption, then the rate of contaminant degradation is equal to the rate of gas purge desorption. Such a phenomenon is evident in Figure 7.2.8.2 for the iron (II)–citrate-activated persulfate treatment of sorbed PCE. If the rate of sorbed contaminant destruction is greater than the rate of gas-purge desorption, then some mechanism of enhanced desorption is likely taking place. This phenomenon has been documented in CHP systems and is also evident in the data for the enhanced destruction of sorbed PCE by CHP shown in Figure 7.2.8.1.

The results of this research demonstrate that activated persulfate does not provide enhanced treatment of sorbed contaminants, may not be the treatment of choice for highly hydrophobic compounds sorbed in the subsurface. However, many common groundwater contaminants (e.g. trichloroethylene [TCE], PCE, and 1,1,1-trichloroethane [1,1,1-TCA]) are not strongly sorbed in subsurface systems and therefore their treatment by persulfate would be more rapid. Therefore, activated persulfate, which may not be effective for the highly hydrophobic contaminants found in surface soils, should be effective for the treatment of many common groundwater contaminants.

Conclusion

The effectiveness of two activated persulfate formulations in treating sorbed contaminants was compared to CHP treatment using two model compounds sorbed on diatomaceous earth. The probe compounds used were PCE, a common groundwater contaminant that is not strongly sorbed, and HCCP, a hydrophobic pollutant that readily sorbs to soils and subsurface solids. Persulfate formulations were activated by iron (II)-citrate and sodium hydroxide, a base. All activated persulfate and CHP conditions were compared to the rate of gas-purge desorption, which represents the maximum natural rate of contaminant desorption from diatomaceous earth. Unlike the CHP system, neither activated persulfate formulation promoted rates of PCE and HCCP destruction greater than that of gas-purge desorption. However, while activated persulfate may not be effective for hydrophobic contaminants that are highly sorbed to subsurface soils, it can be effective for compounds that are not limited by desorption.

7.2.9. Summary of Persulfate Activation Conditions

Table 7.2.9.1. Summary of Persulfate Activation

Activation Condition	Comments
EDTA	<ul style="list-style-type: none"> Iron (II)-EDTA and iron (III)-EDTA activated persulfate at circumneutral pH effectively generate sulfate radical, hydroxyl radical, and reductants with potential to rapidly and effectively treat TCE and potentially other biorefractory contaminants.
Effect of Basicity	<ul style="list-style-type: none"> Hydroxyl radical was the dominant oxidative species in base-activated persulfate systems at lower base:persulfate molar ratios. Base-activated persulfate systems become increasingly reactive and begin to generate reductants at higher base:persulfate molar ratios, with a 6:1 base:persulfate ratio the most effective.
Mechanism of Base Activation	<ul style="list-style-type: none"> Persulfate decomposes to hydroperoxide through base-catalyzed hydrolysis. Hydroperoxide reduces another persulfate molecule, resulting in formation of sulfate radical and sulfate, while hydroperoxide is oxidized to superoxide. Sulfate radical then oxidizes hydroxide, resulting in formation of hydroxyl radical.
Phenoxide Derivatives	<ul style="list-style-type: none"> Phenoxides activate persulfate at basic pH. Persulfate activation by phenolic compounds in soil organic matter may be significant pathway for contaminant degradation. Soil organic carbon content should be considered in process screening and treatability testing
Alcohols, Aldehydes, Ketones, Organic Acids, Keto Acids	<ul style="list-style-type: none"> Ketones, Krebs cycle compounds, alcohols, and aldehydes activated persulfate at pH>12. Persulfate activation was highest with the ketoacid, confirming that ionized forms of organic compounds are important to promote persulfate activation. Naturally-occurring organic compounds found as degradation products of contaminants, or as compounds produced by native microbes, can promote persulfate activation at basic pH.
Soil Organic Matter	<ul style="list-style-type: none"> SOM activates persulfate under alkaline conditions to generate both oxidants and reductants. Activation likely occurs through phenoxide moieties associated with SOM. This activation pathway is likely a dominant mechanism for contaminant destruction.
Model Contaminants	<ul style="list-style-type: none"> All 7 model contaminants (TCE, PCE, DCA, TCA, CB, DCB, anisole) were degraded by base-activated persulfate. The molar ratio of base:persulfate affected the degradation rates of DCA and TCE. In contrast, the more highly chlorinated TCA and PCE were degraded at equal rates regardless of the basicity of the persulfate formulation. Anisole degradation increased after 2 hr, likely due to oxidation of anisole to phenolic derivative that then further activated persulfate.
Effects of Sorption	<ul style="list-style-type: none"> Activated persulfate may not be effective for highly sorbed hydrophobic contaminants. Activated persulfate can be effective for compounds that are not limited by desorption (e.g., PCE).

7.3. Effect of Persulfate on Subsurface Characteristics

7.3.1. Effect of Persulfate Formulations on Soil Mineralogy

X-Ray diffraction

X-ray diffraction (XRD) scans for the three persulfate process conditions and the control for goethite for 15, 30 and 45 days are shown in Figures 7.3.1.1-4. Parallel scans for hematite are shown in Figures 7.3.1.5-8, for ferrihydrite in Figures 7.3.1.9-12, and for birnessite in Figures 7.3.1.13-16. For the clay minerals, XRD scans for kaolinite are shown in Figures 7.3.1.17-20 and those for montmorillonite are shown in Figures 7.3.1.21-24. No changes in mineralogy were observed for kaolinite, hematite, and goethite in any of the persulfate systems.

In contrast, changes in mineralogy were found for ferrihydrite in all persulfate systems with the exception of unactivated persulfate, in which no change in mineralogy occurred. The iron oxide ferrihydrite (2-line) matured from an amorphous habit into more ordered structures such as goethite and hematite. Treatment of ferrihydrite with deionized water resulted in the formation of hematite in just 15 days. Non-activated persulfate appears to have prevented the formation of a more crystalline habit, possibly due to the low pH regime in the solution and the presence of high sodium and sulfate concentrations. The treatment of ferrihydrite with base-activated persulfate resulted in a rapid transformation to goethite in less than 15 days. It was visually observed (through color changes) that this transformation occurred in less than two days. Ferrihydrite in the iron-EDTA-activated persulfate system appeared to change very slowly, with a very minor degree of change to goethite at 45 days.

Mineral structural changes also occurred in one of the birnessite-persulfate systems. The manganese oxide birnessite did not transform in the presence of deionized water, unactivated persulfate, or base-activated persulfate, but did transform in the presence of iron-EDTA-activated persulfate. After 30 days, birnessite in the presence of iron-EDTA-activated persulfate had begun a transformation to the manganese mineral vernadite [δ - MnO_2 ; $(\text{Mn}^{4+}, \text{Fe}^{3+}, \text{Ca}, \text{Na})(\text{O}, \text{OH})_2 \cdot n\text{H}_2\text{O}$]. At 45 days, the x-ray diffraction pattern showed a clear intergrade between birnessite and vernadite, which appeared to be a result of Fe (III) substituting for Mn (IV) in the structure.

Persulfate concentrations in persulfate-mineral systems

Persulfate concentrations in the mineral–persulfate systems, quantified over 45 days, are shown in Figures 7.3.1.25-31. Relative to controls, persulfate concentration remained constant for kaolinite and goethite. Persulfate concentrations in base-activated systems containing hematite and birnessite decreased relative to the persulfate controls containing no minerals. The presence of montmorillonite in base-activated persulfate and iron (III)-EDTA-activated persulfate systems resulted in lower rates of persulfate decomposition relative to persulfate controls containing no minerals; i.e. it appears that montmorillonite may have stabilized persulfate relative to the control.

pH changes in persulfate-mineral systems

The solution pH in mineral–persulfate systems was also monitored over 45 days (Figures 7.3.1.32-38). No differences in pH relative to control systems were observed for kaolinite,

hematite, and goethite. However, pH increased slightly relative to controls for iron-EDTA-activated persulfate systems containing montmorillonite and ferrihydrite. Furthermore, the pH of base-activated persulfate systems containing birnessite decreased substantially relative to persulfate controls containing no minerals.

Mineral surface areas

Mineral specific surface areas, measured using the BET method at the end of the 45 days of the experiment, are listed in Table 7.3.1.1. Hematite, goethite, and kaolinite showed minimal changes. Ferrihydrite showed a decrease in surface area, which was expected as it transformed from an amorphous high surface mineral to a more crystalline species. Birnessite surface area decreased slightly, which is expected when a synthetic mineral is placed into more oxidizing conditions and becomes more crystalline. Montmorillonite showed significant decreases (20-60 m²/g) in surface areas in all treatments except for deionized-mineral treatment. This is most likely due to the interlayer collapse of the mineral structure, which would decrease the mineral surface edge surface area and might also prevent nitrogen gas from penetrating into the interlayer structure during BET testing.

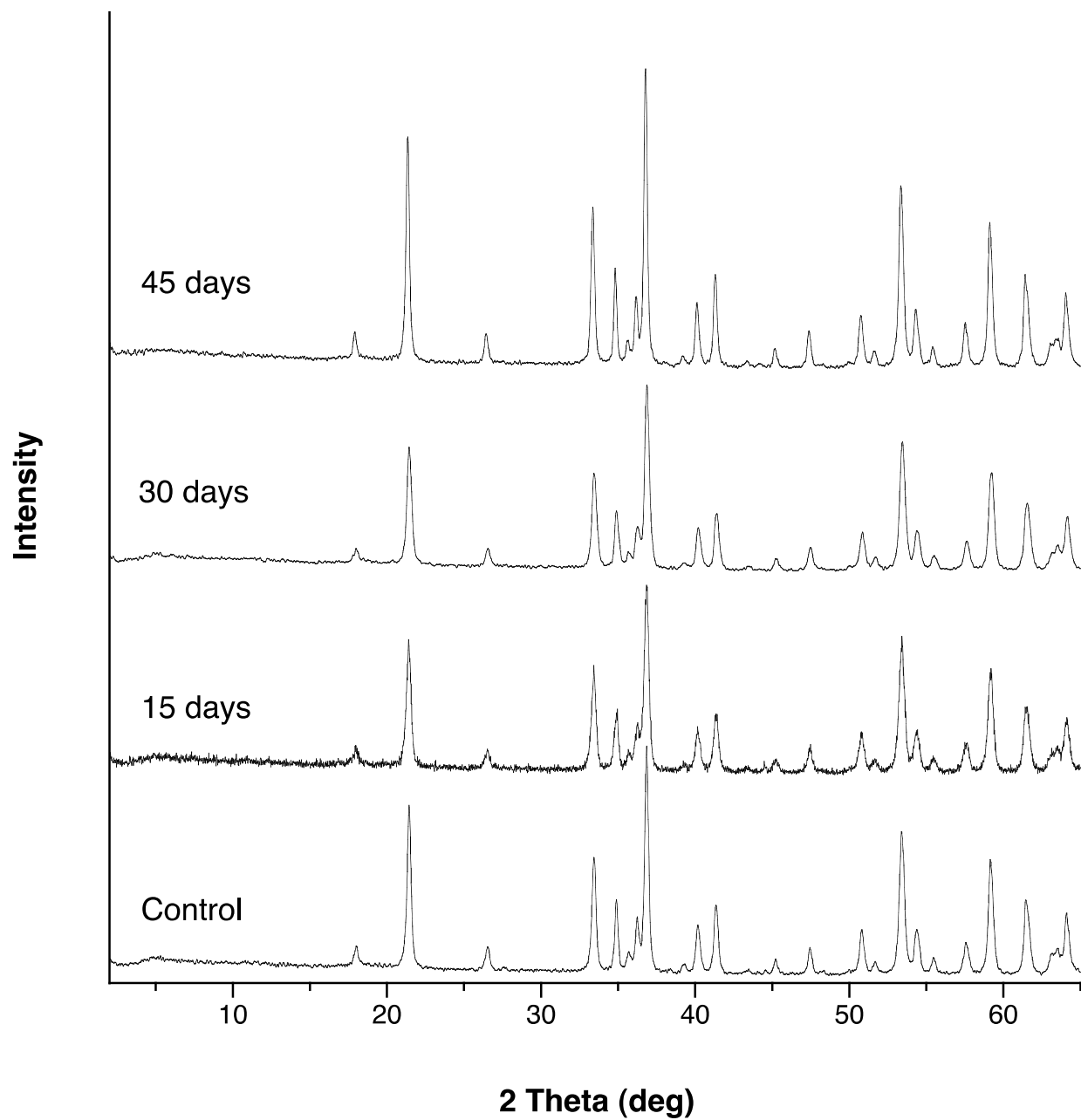


Figure 7.3.1.1. XRD spectra for goethite treated with deionized water over 45 days.

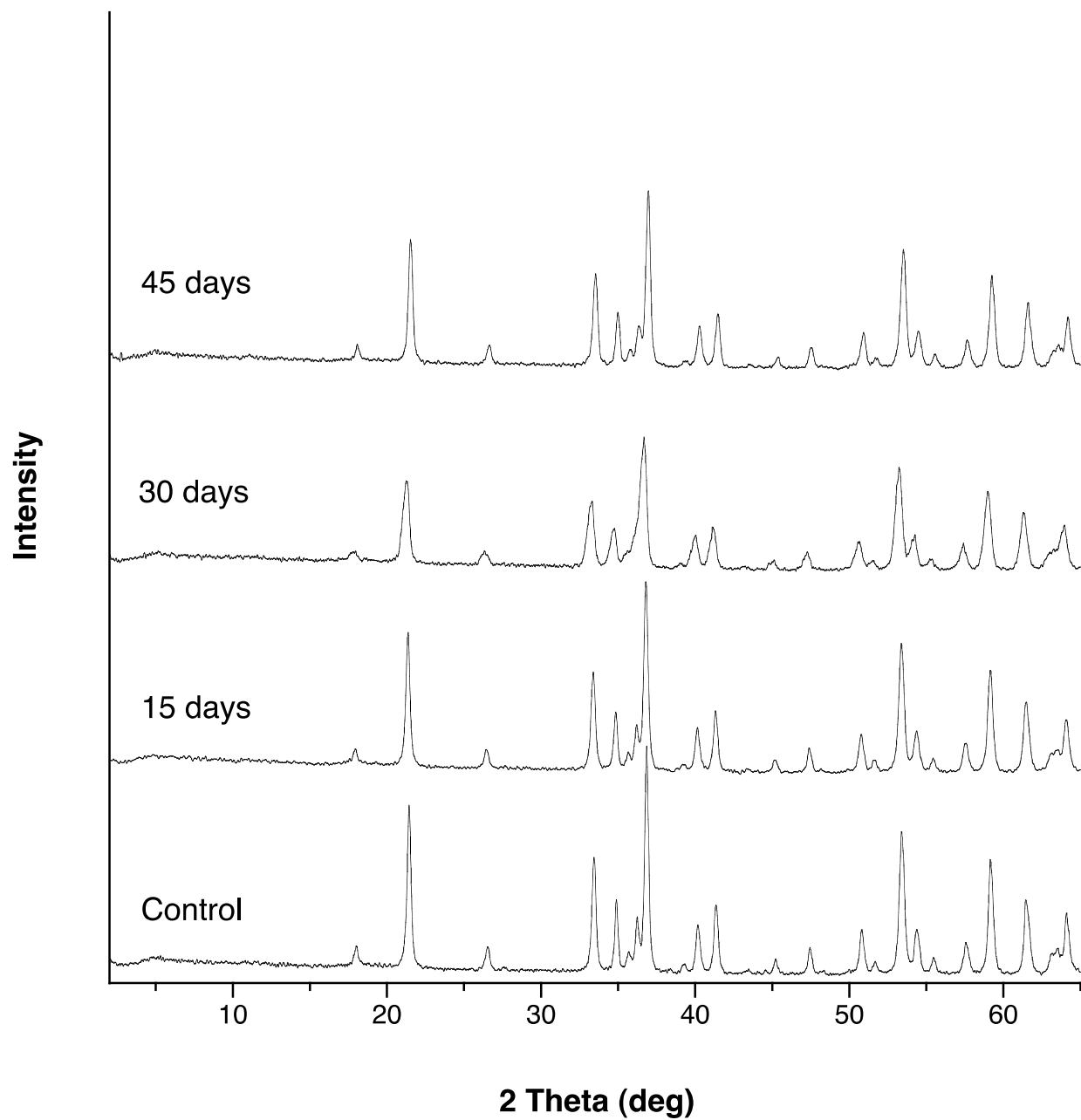


Figure 7.3.1.2. XRD spectra for goethite treated with persulfate over 45 days.

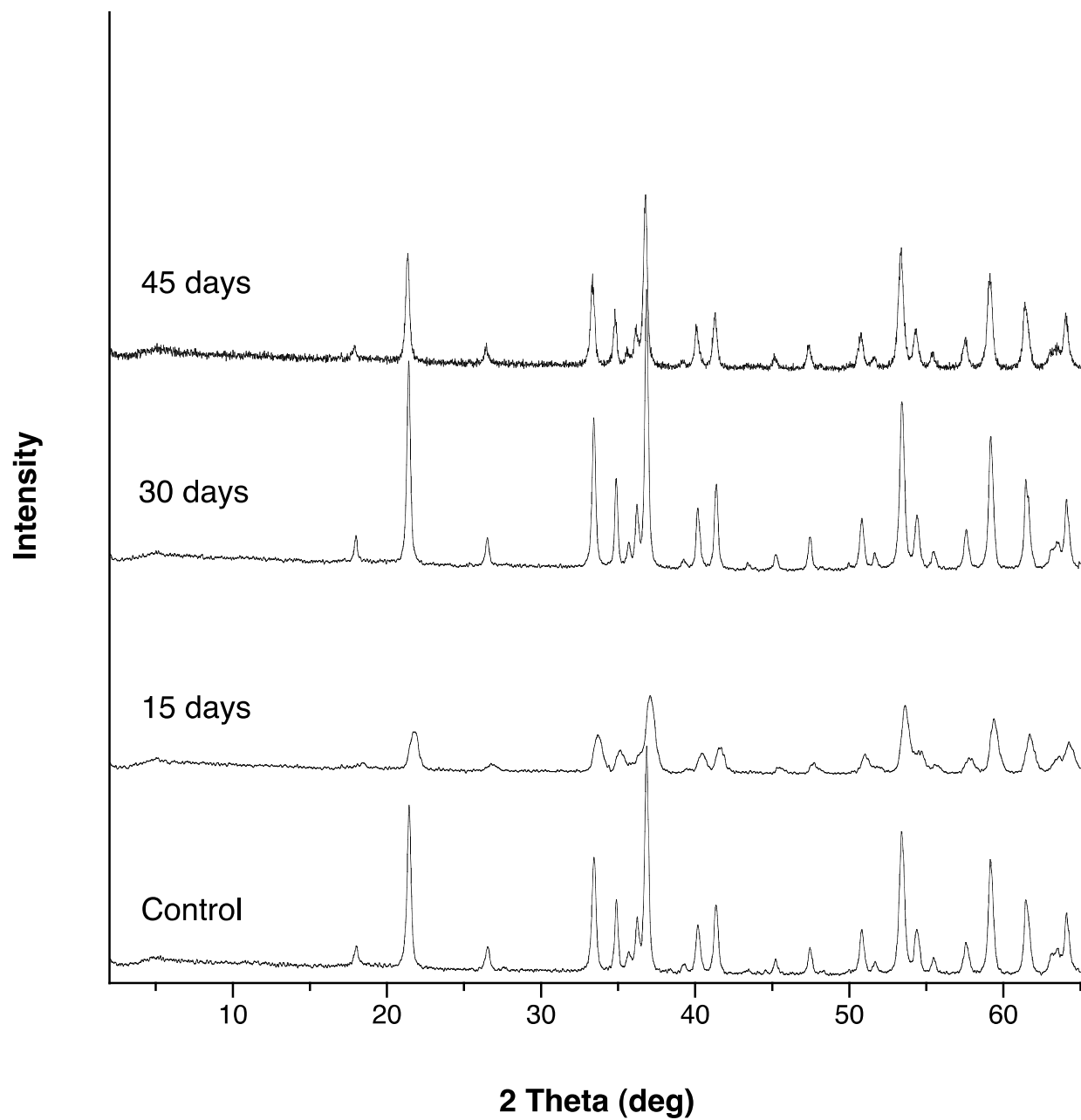


Figure 7.3.1.3. XRD spectra for goethite treated with iron (III)–EDTA-activated persulfate over 45 days.

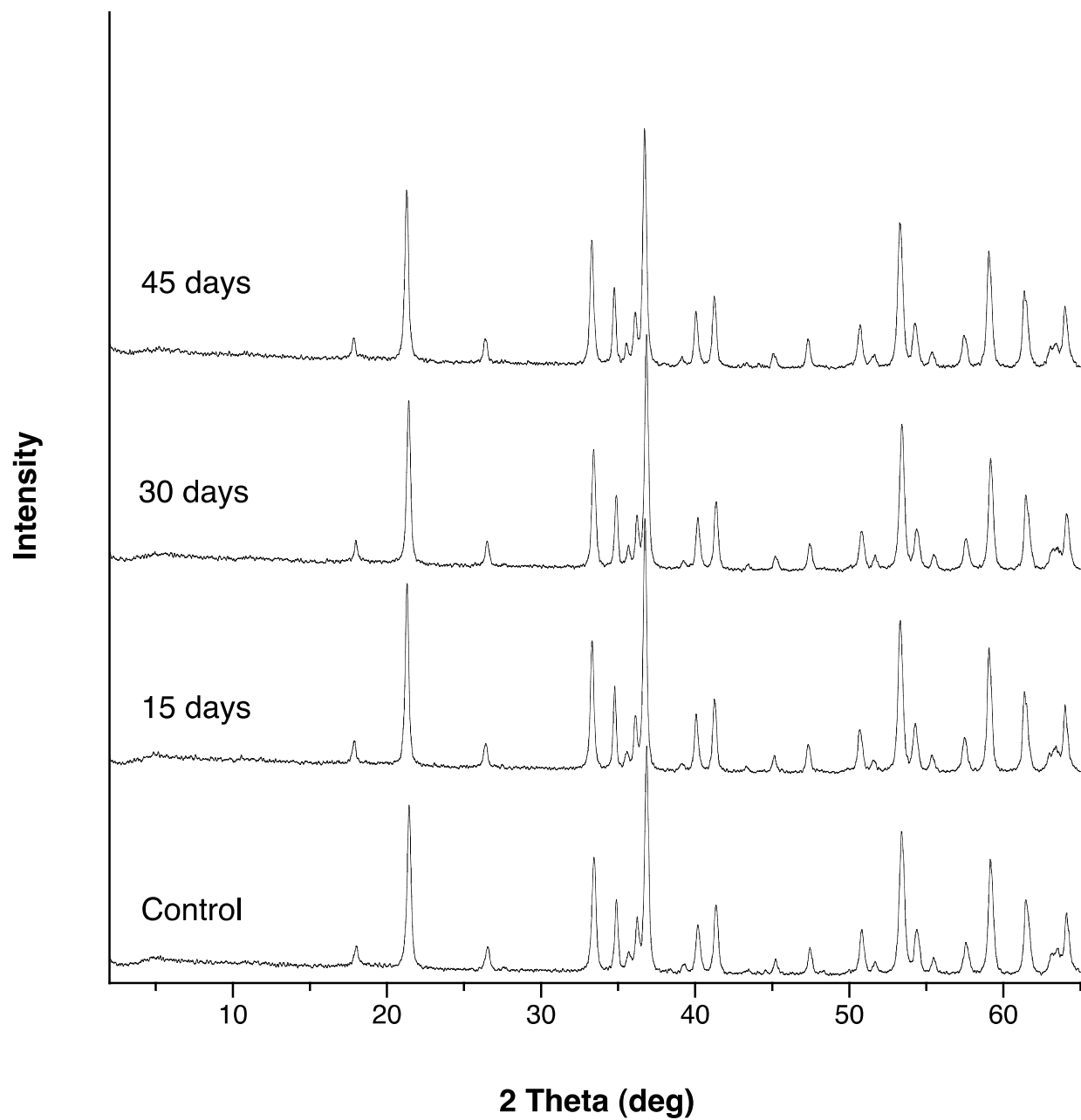


Figure 7.3.1.4. XRD spectra for goethite treated with base-activated persulfate (2:1 molar ratio of NaOH to persulfate) over 45 days.

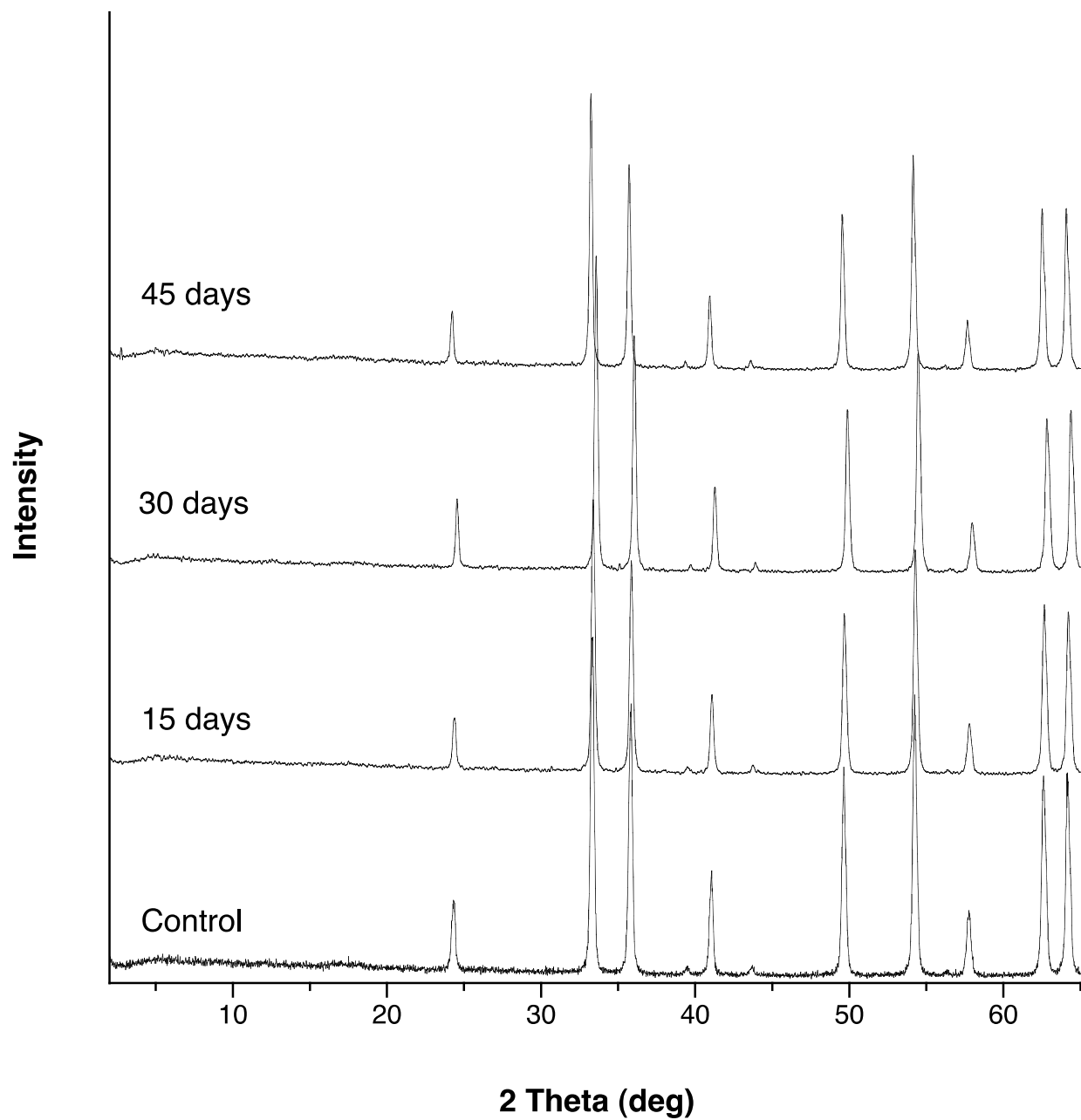


Figure 7.3.1.5. XRD spectra for hematite treated with deionized water over 45 days.

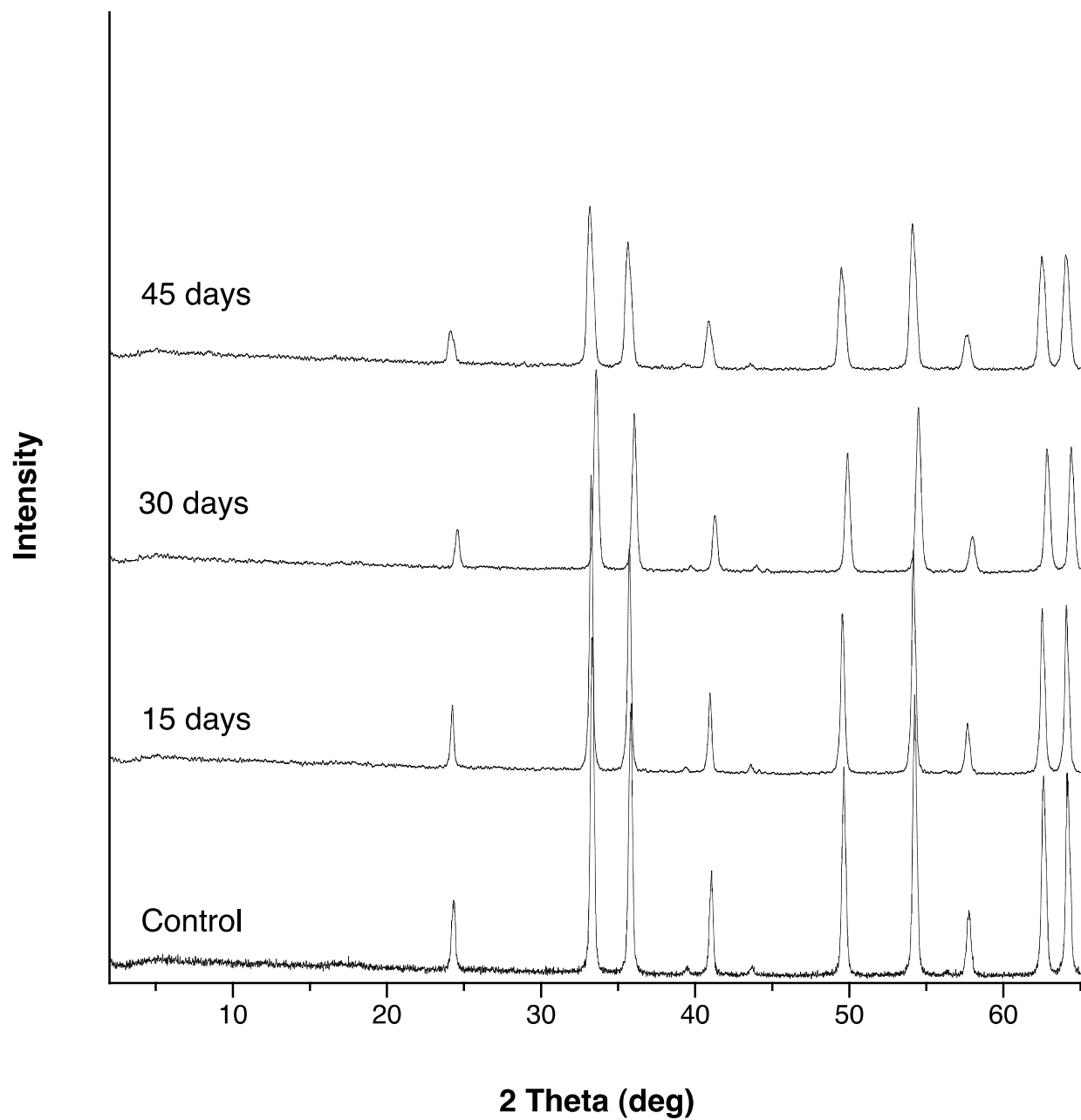


Figure 7.3.1.6. XRD spectra for hematite treated with persulfate over 45 days.

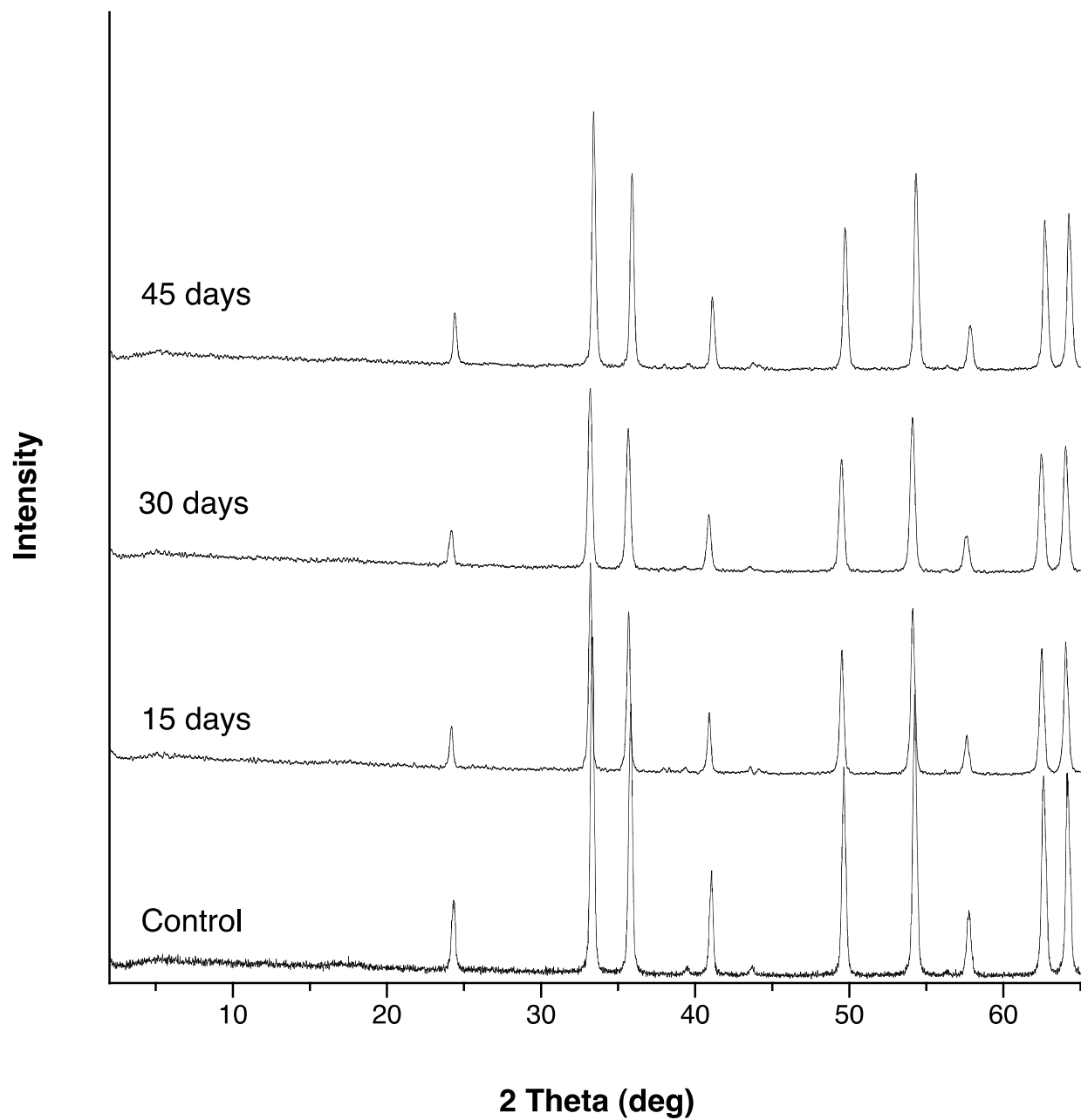


Figure 7.3.1.7. XRD spectra for hematite treated with iron (III)–EDTA-activated persulfate over 45 days.

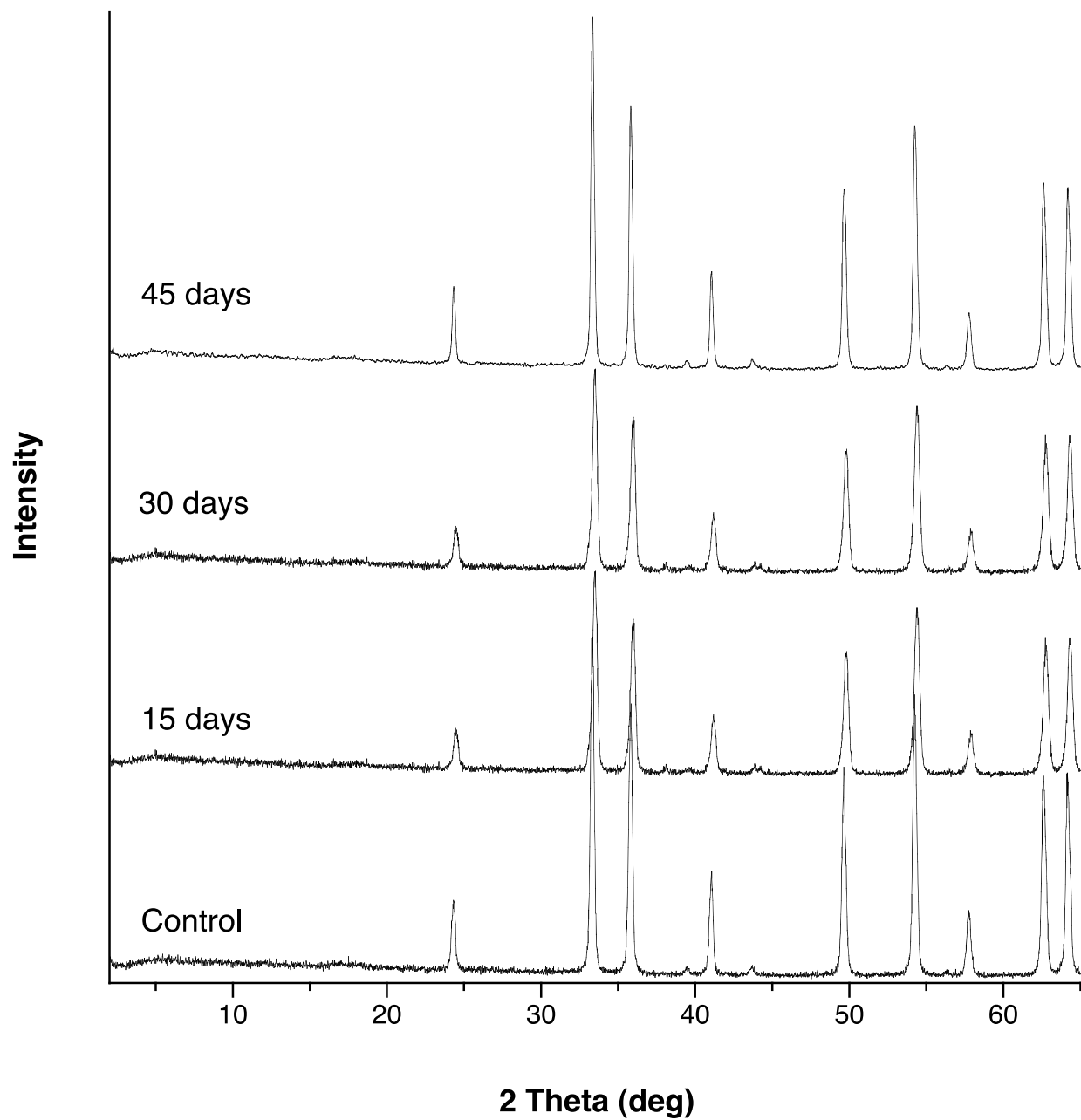


Figure 7.3.1.8. XRD spectra for hematite treated with base-activated persulfate (2:1 molar ratio of NaOH to persulfate) over 45 days.

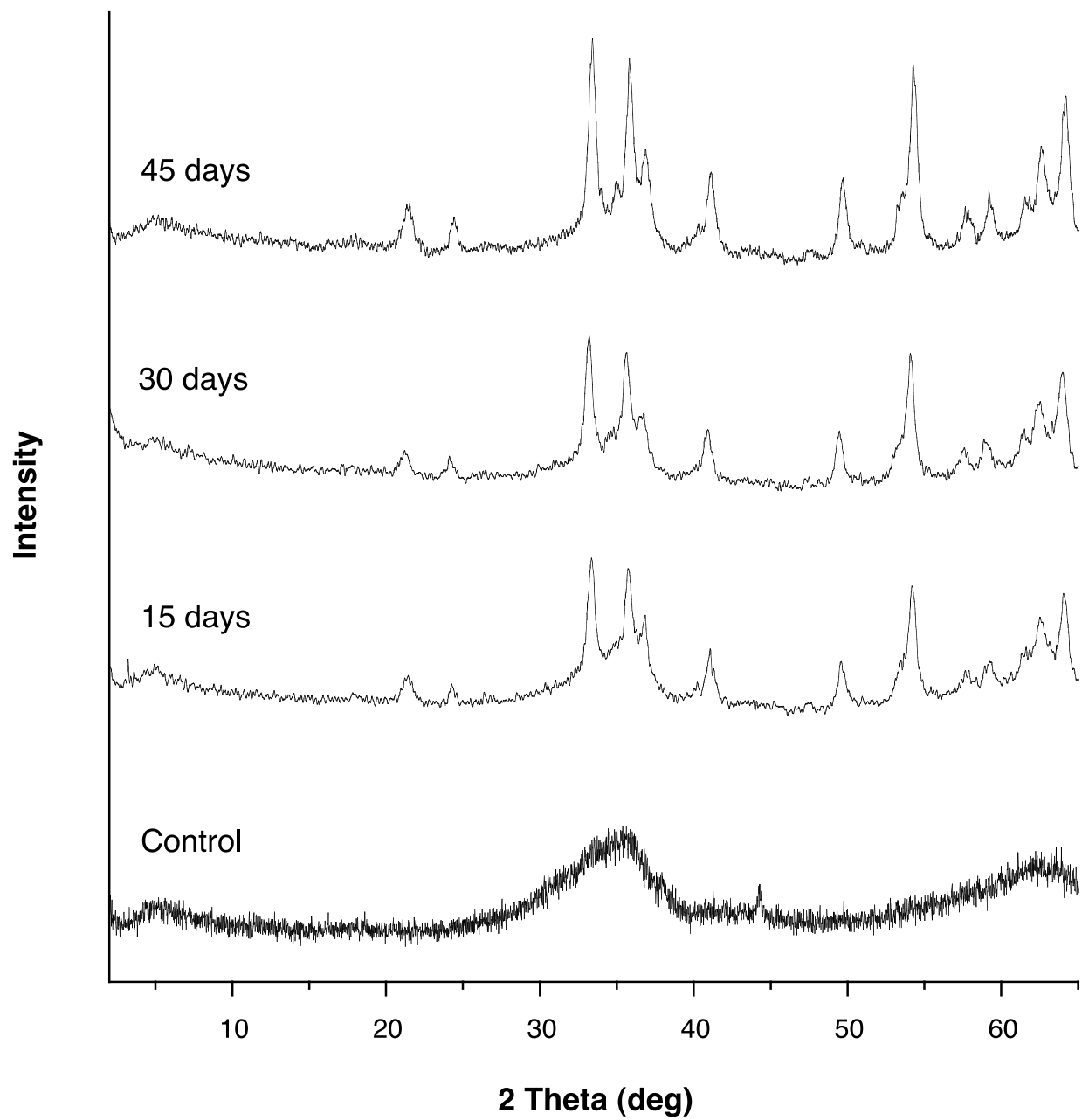


Figure 7.3.1.9. XRD spectra for ferrihydrite treated with deionized water over 45 days.

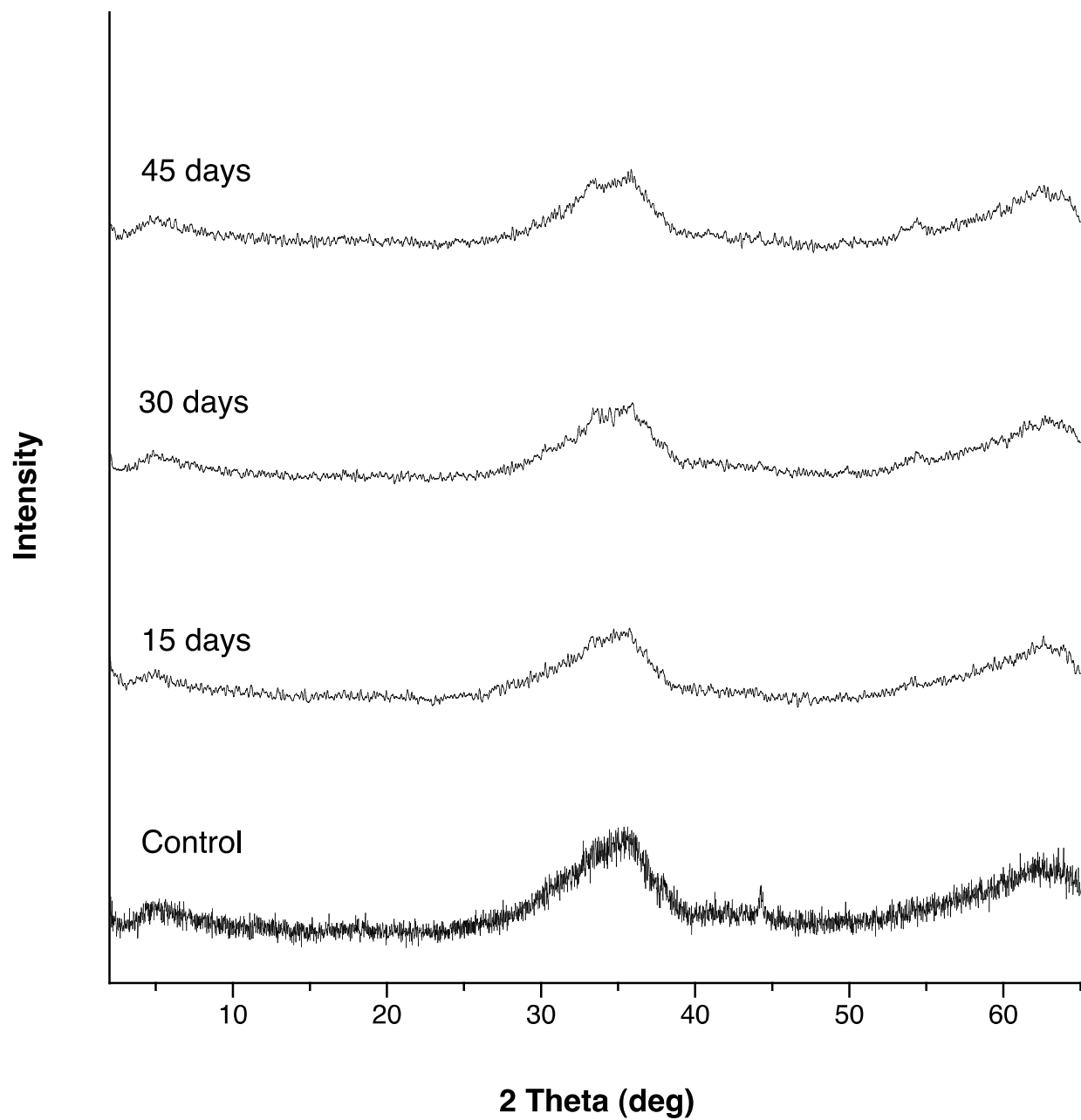


Figure 7.3.1.10. XRD spectra for ferrihydrite treated with persulfate over 45 days.

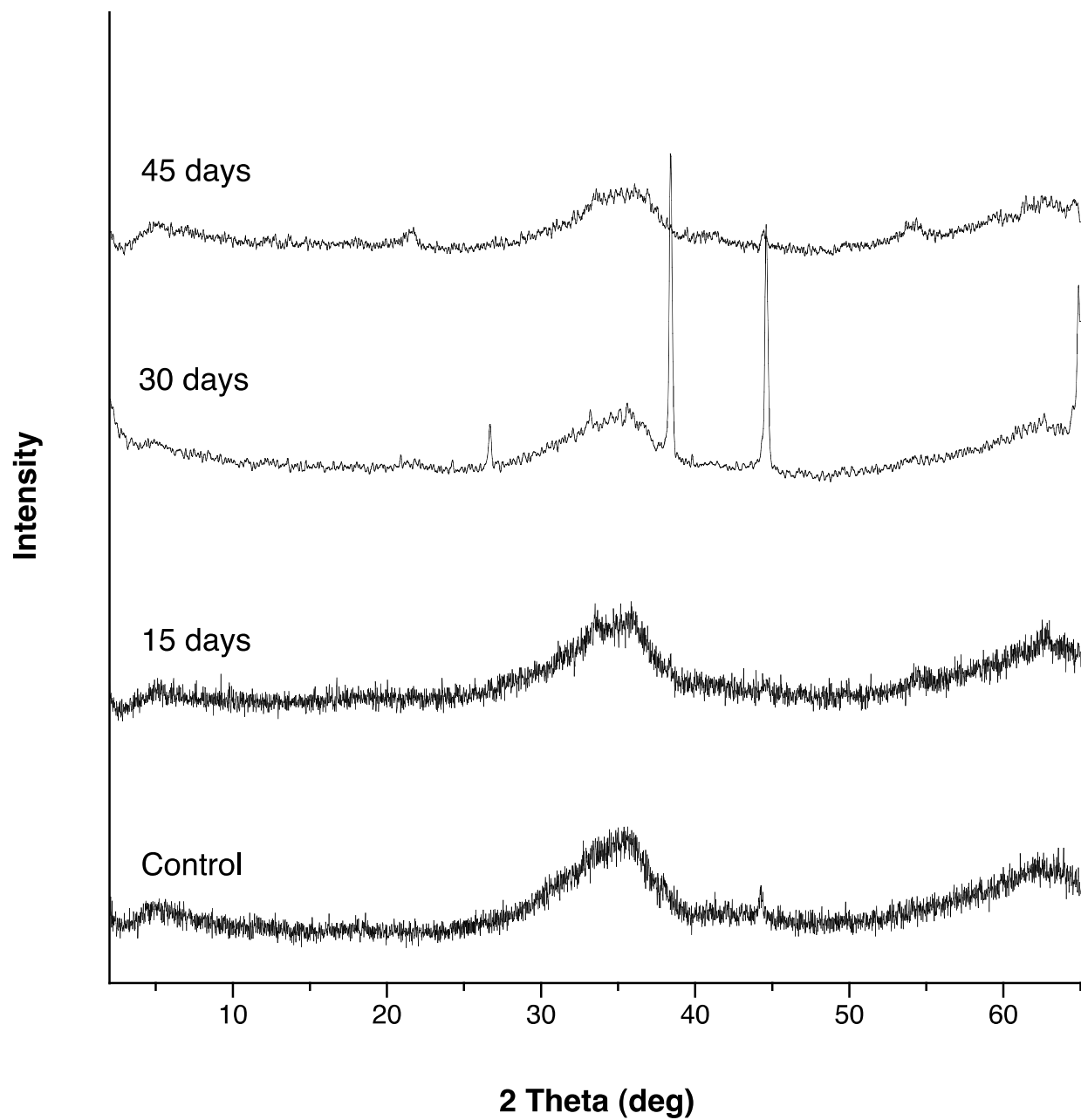


Figure 7.3.1.11. XRD spectra for ferrihydrite treated with iron (III)–EDTA-activated persulfate over 45 days.

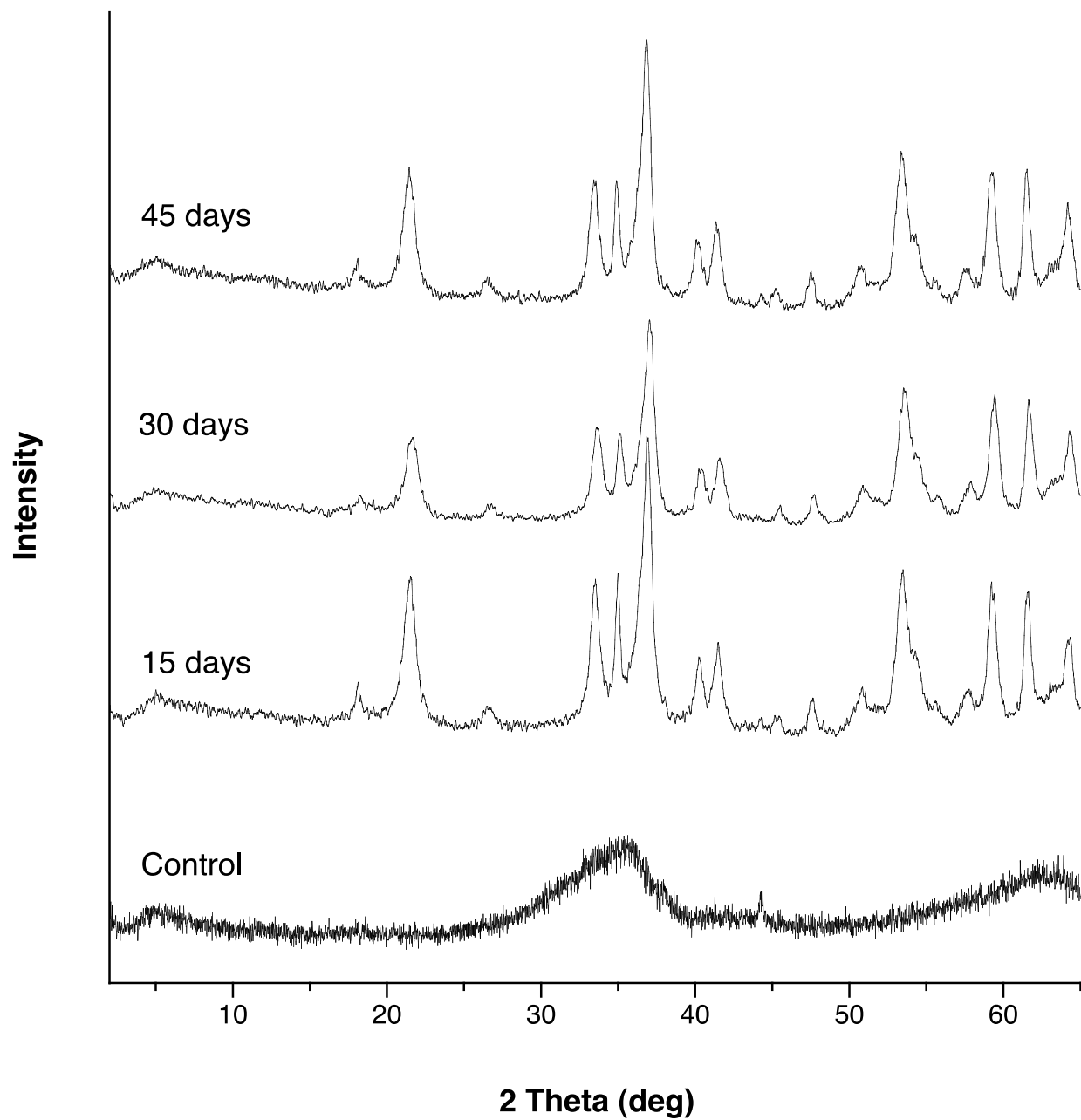


Figure 7.3.1.12. XRD spectra for ferrihydrite treated with base-activated persulfate (2:1 molar ratio of NaOH to persulfate) over 45 days.

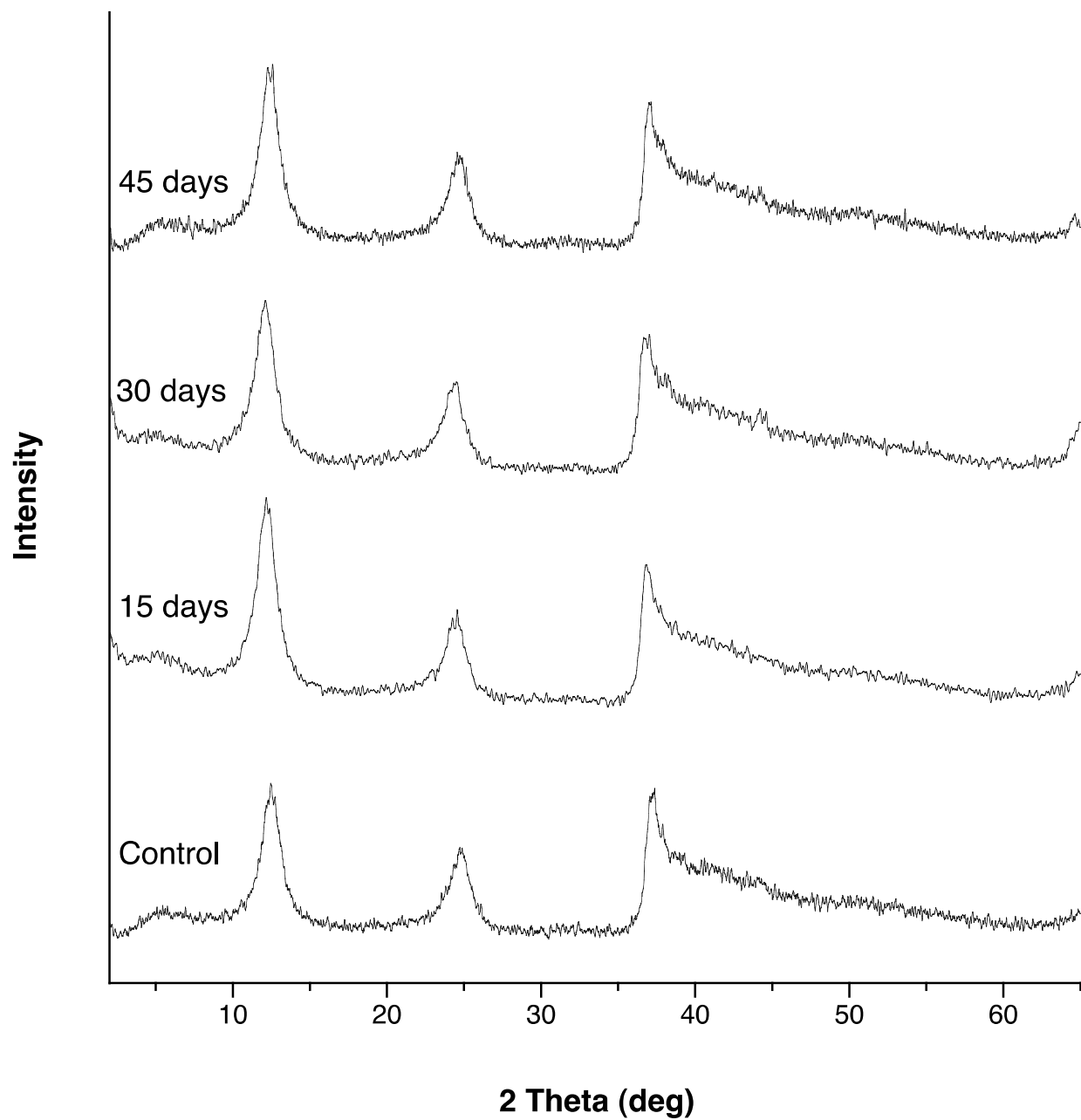


Figure 7.3.1.13. XRD spectra for birnessite treated with deionized water over 45 days.

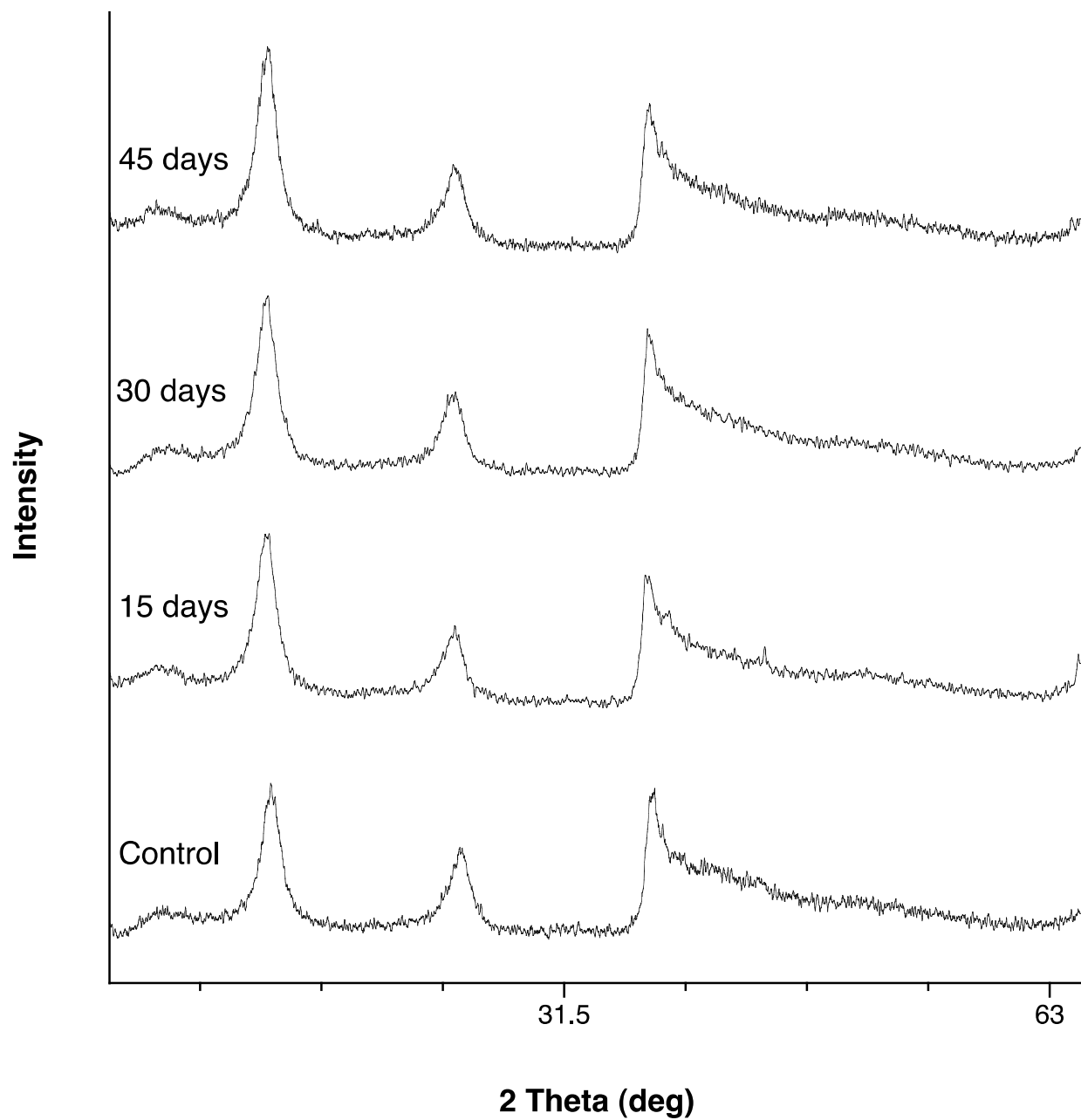


Figure 7.3.1.14. XRD spectra for birnessite treated with persulfate over 45 days.

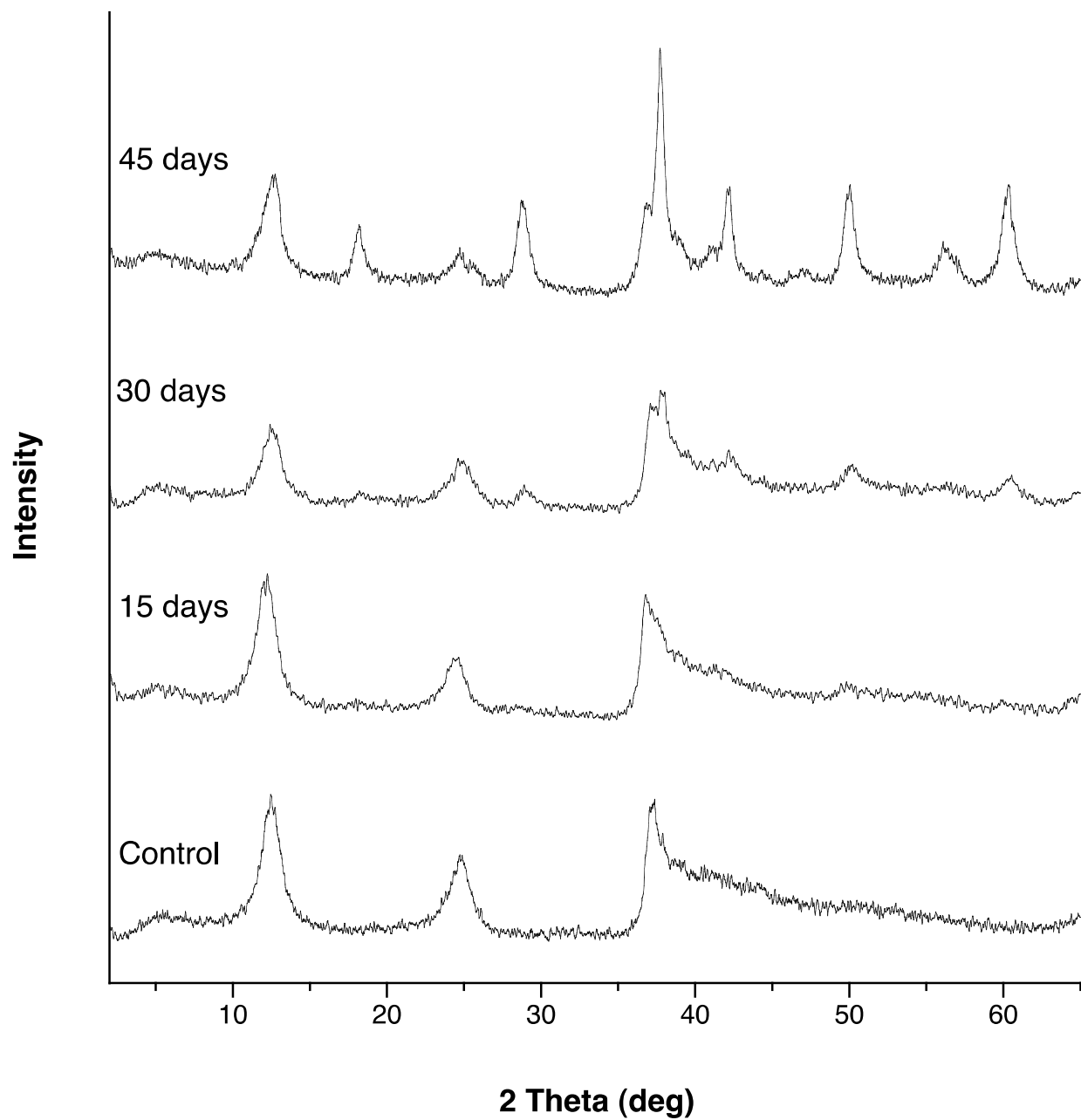


Figure 7.3.1.15. XRD spectra for birnessite treated with iron (III)–EDTA-activated persulfate over 45 days.

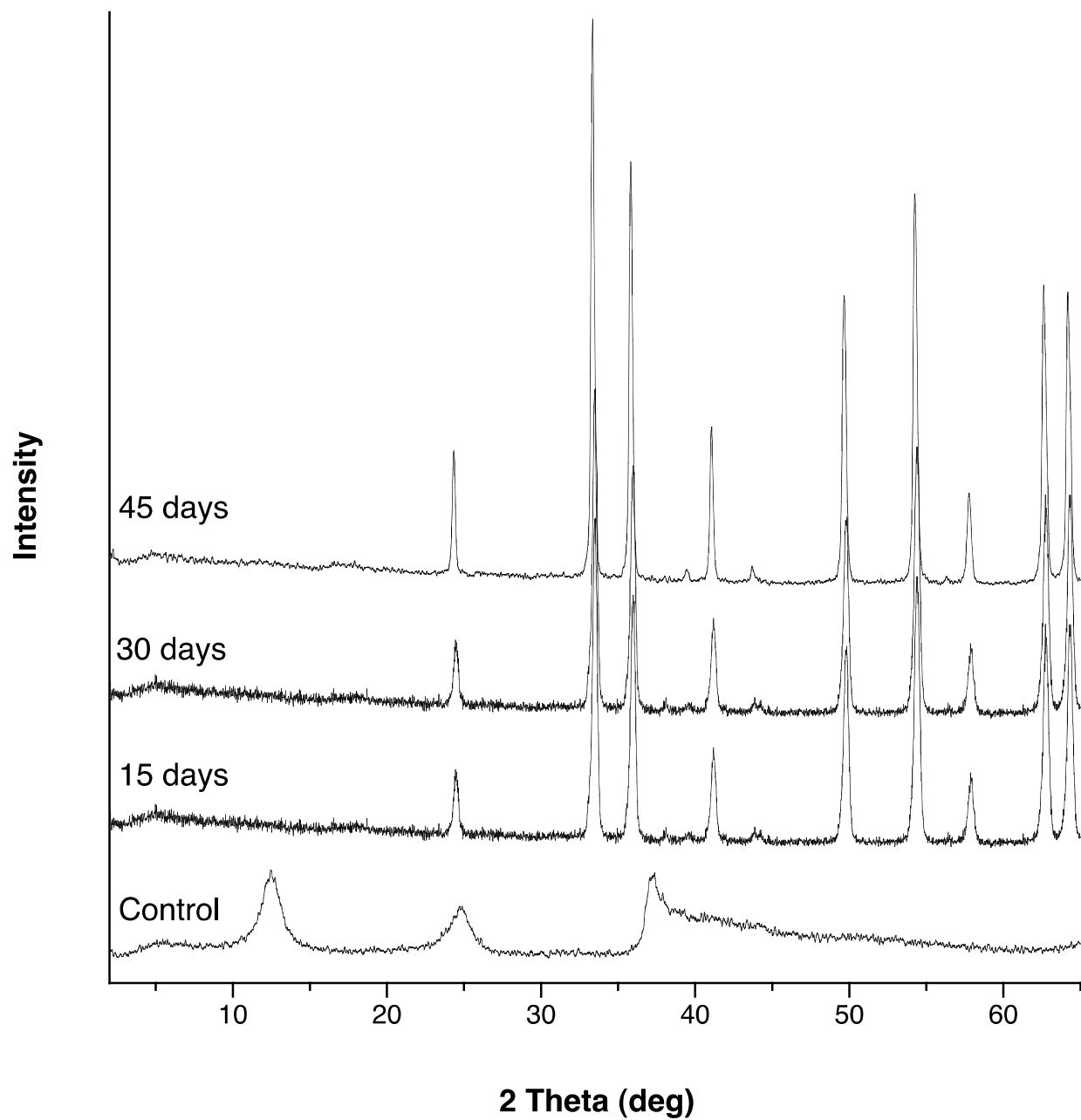


Figure 7.3.1.16. XRD spectra for birnessite treated with base-activated persulfate (2:1 molar ratio of NaOH to persulfate) over 45 days.

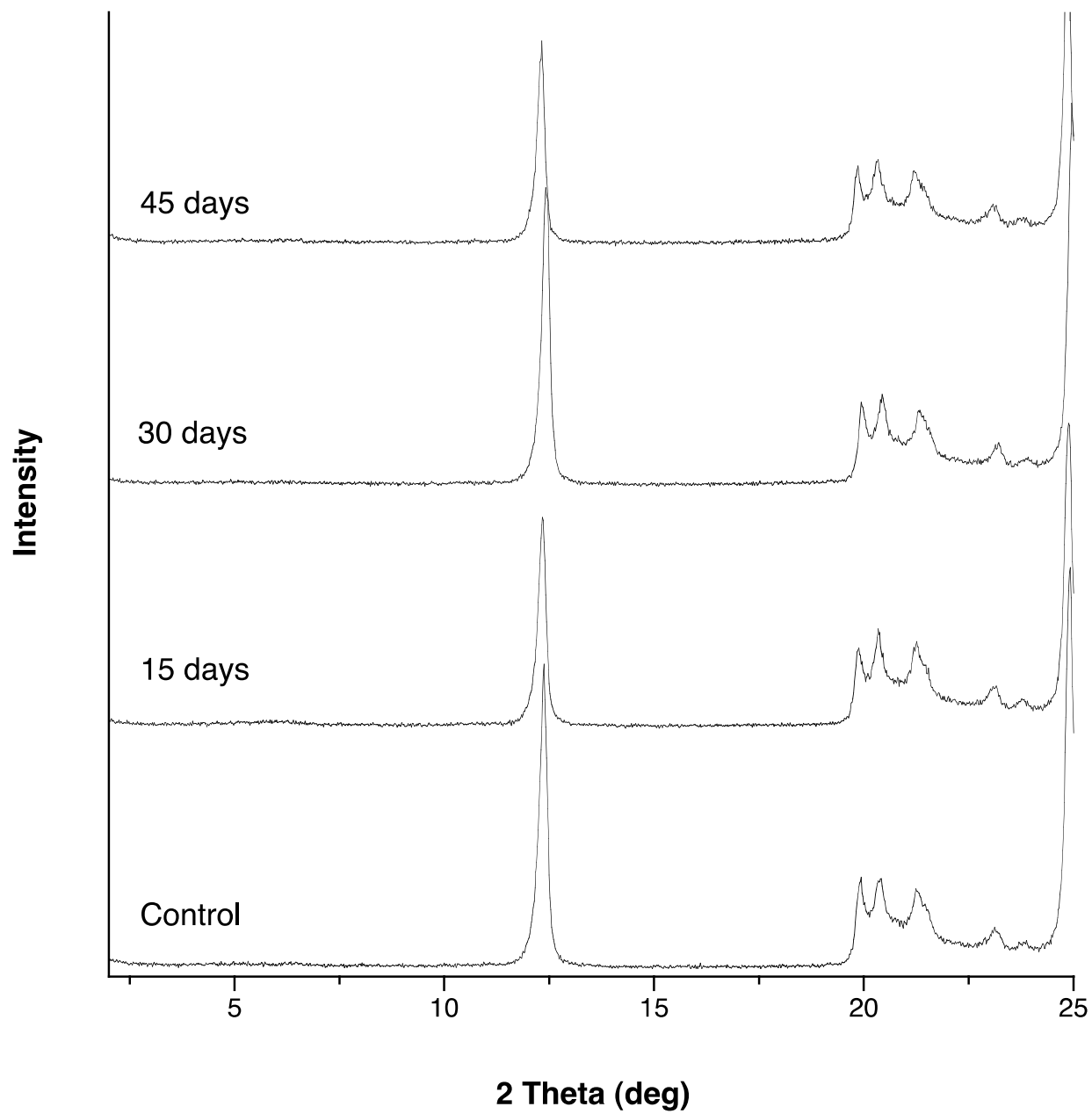


Figure 7.3.1.17. XRD spectra for kaolinite treated with deionized water over 45 days.

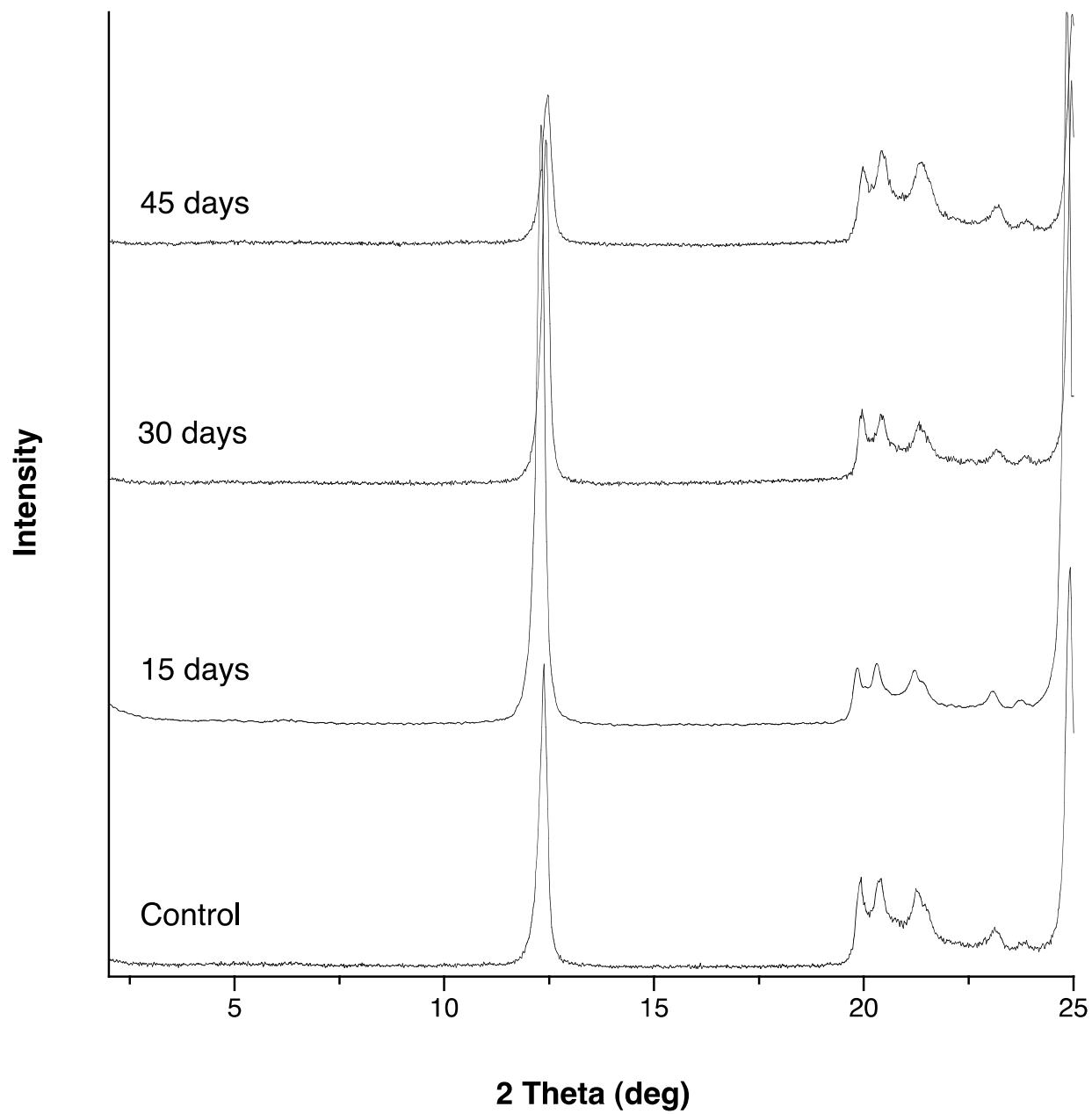


Figure 7.3.1.18. XRD spectra for kaolinite treated with persulfate over 45 days.

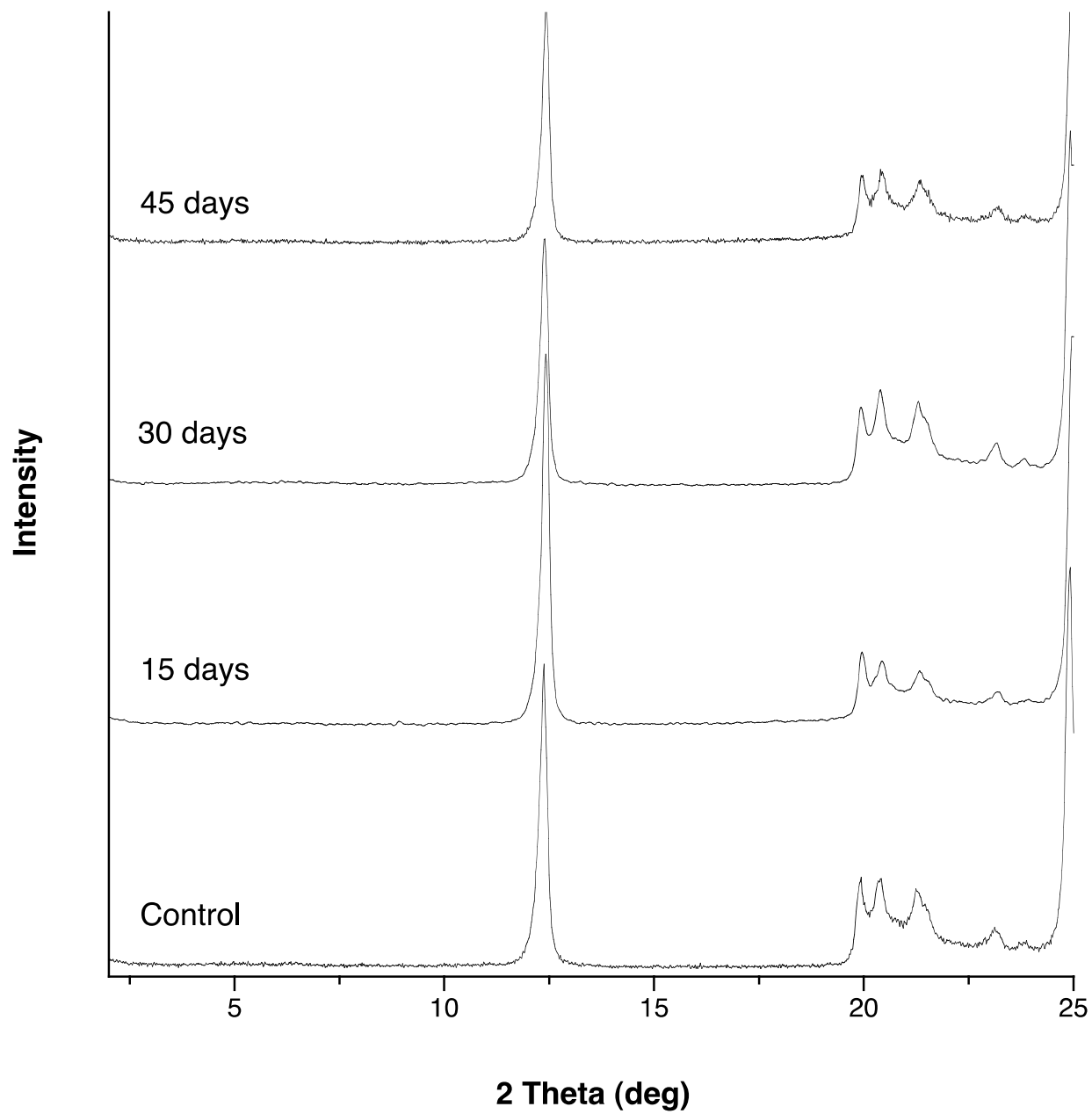


Figure 7.3.1.19. XRD spectra for kaolinite treated with iron (III)–EDTA-activated persulfate over 45 days.

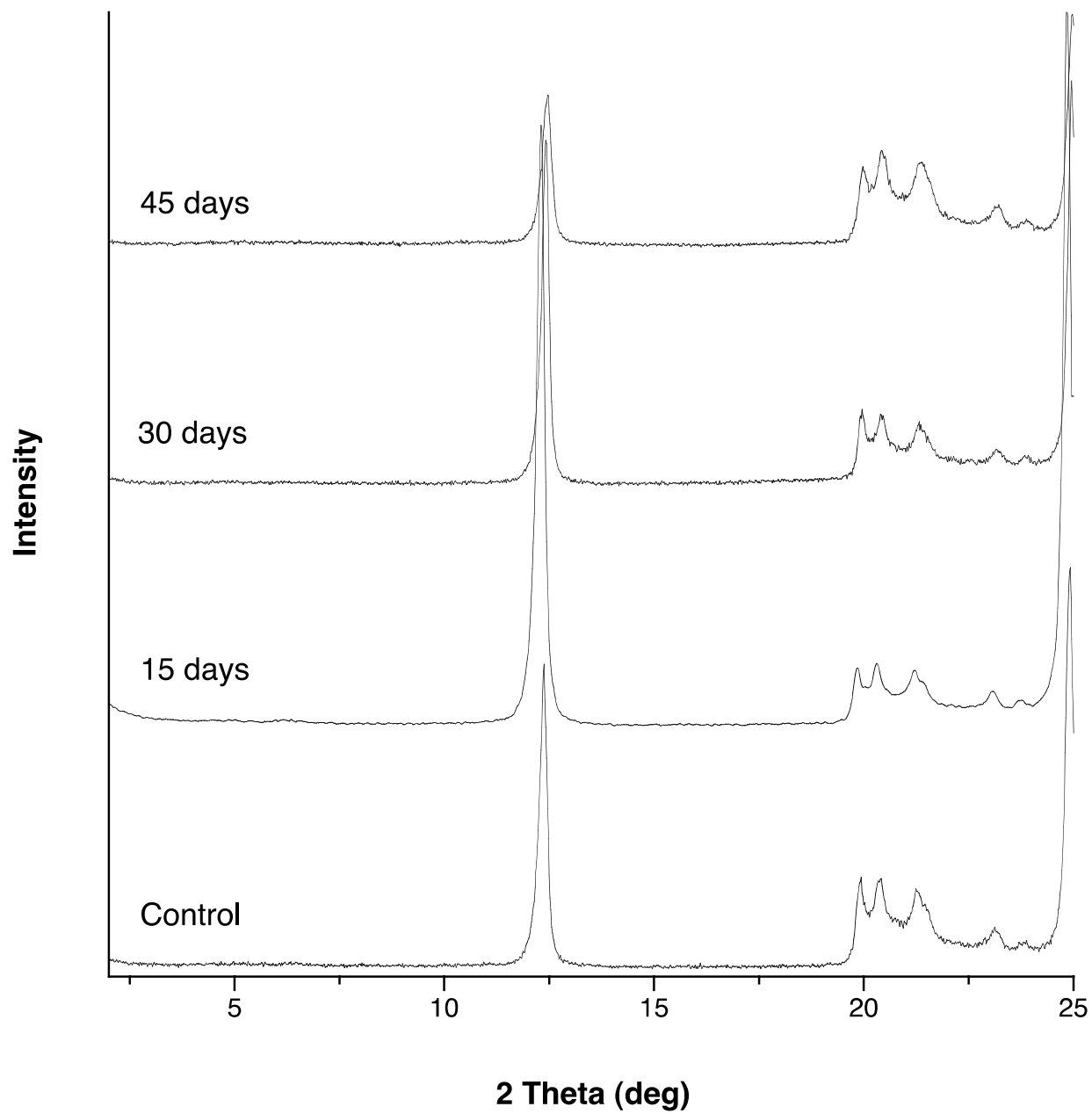


Figure 7.3.1.20. XRD spectra for kaolinite treated with base-activated persulfate (2:1 molar ratio of NaOH to persulfate) over 45 days.

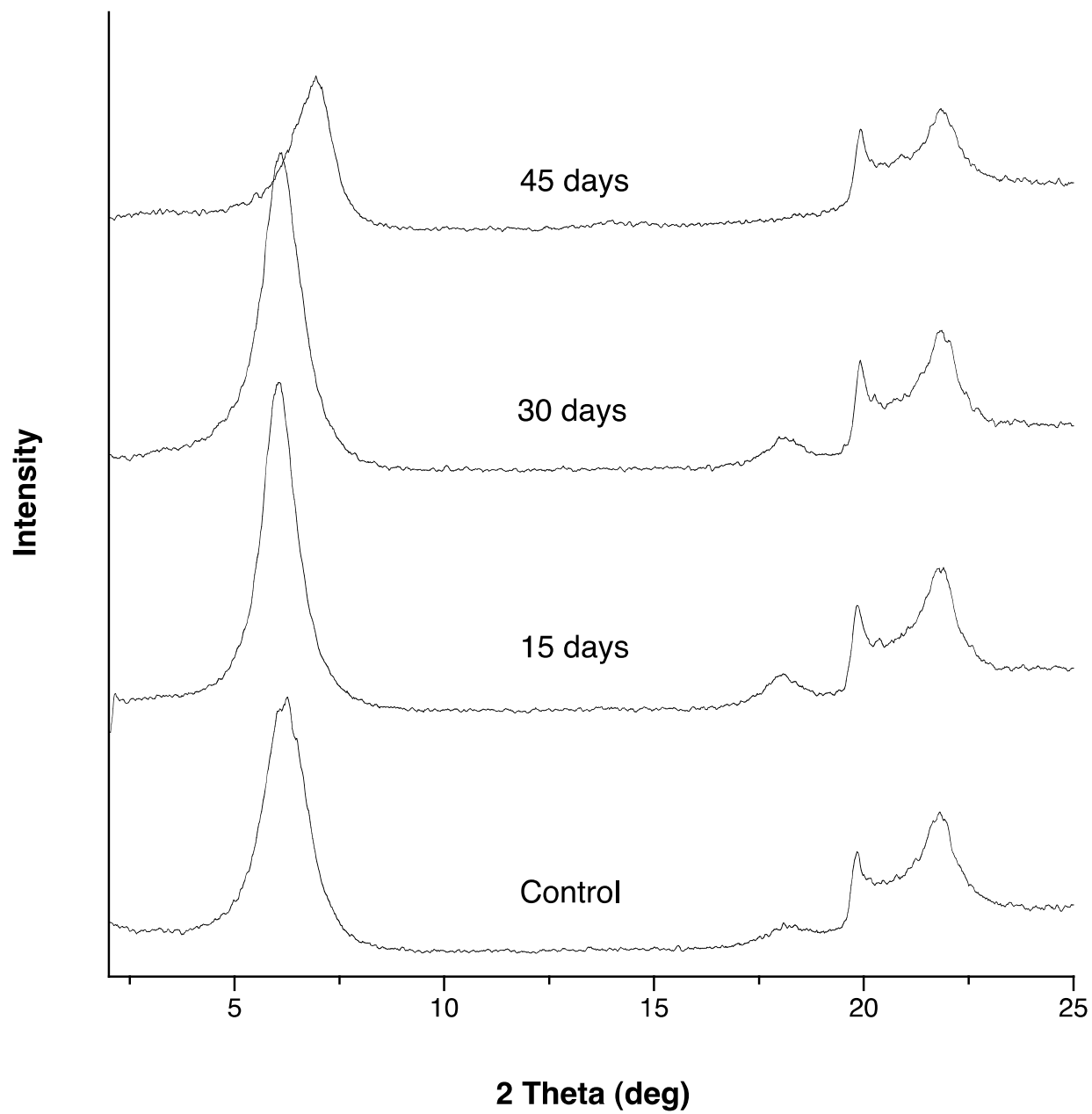


Figure 7.3.1.21. XRD spectra for montmorillonite treated with deionized water over 45 days.

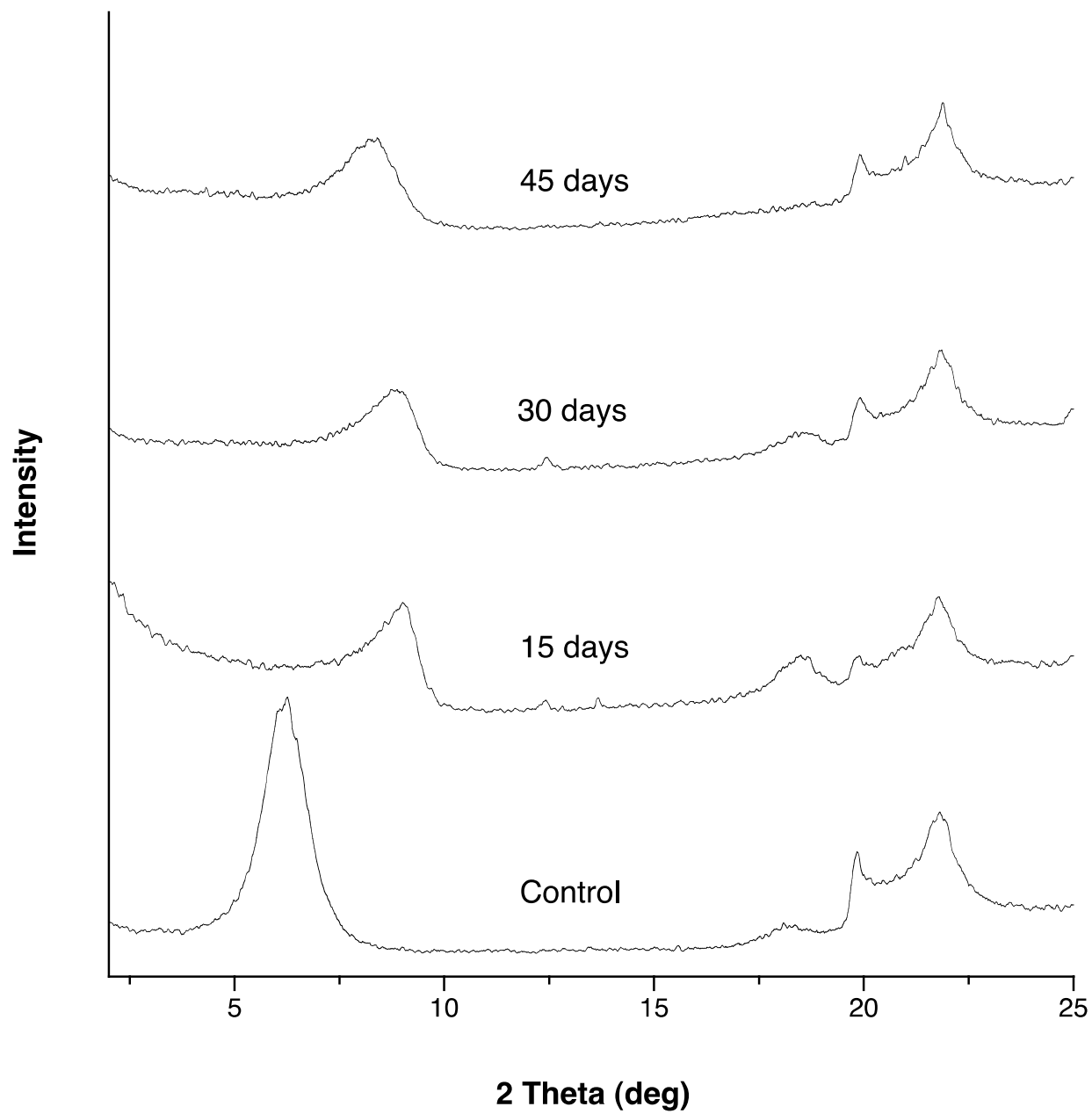


Figure 7.3.1.22. XRD spectra for montmorillonite treated with persulfate over 45 days.

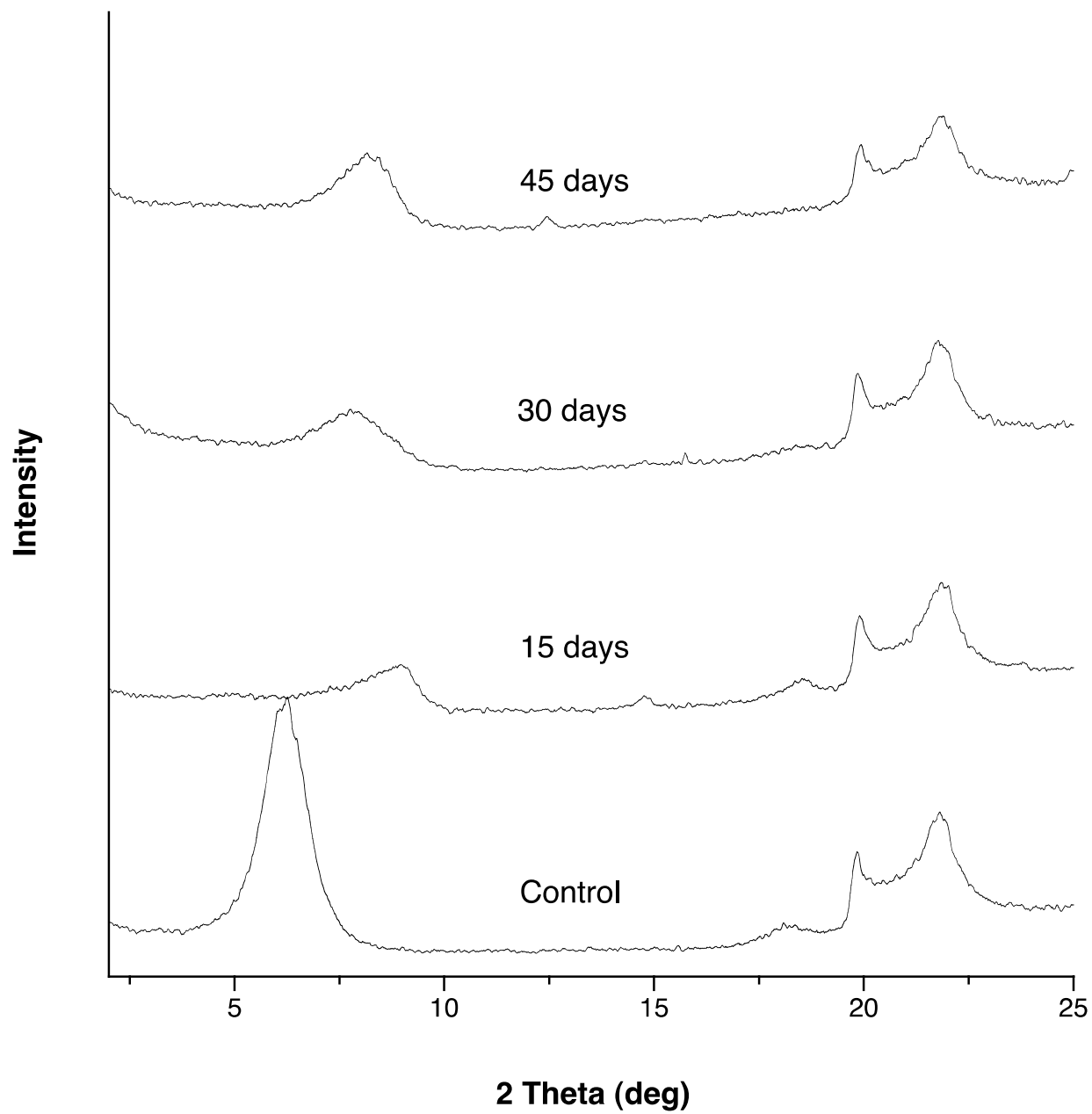


Figure 7.3.1.23. XRD spectra for montmorillonite treated with iron (III)–EDTA-activated persulfate over 45 days.

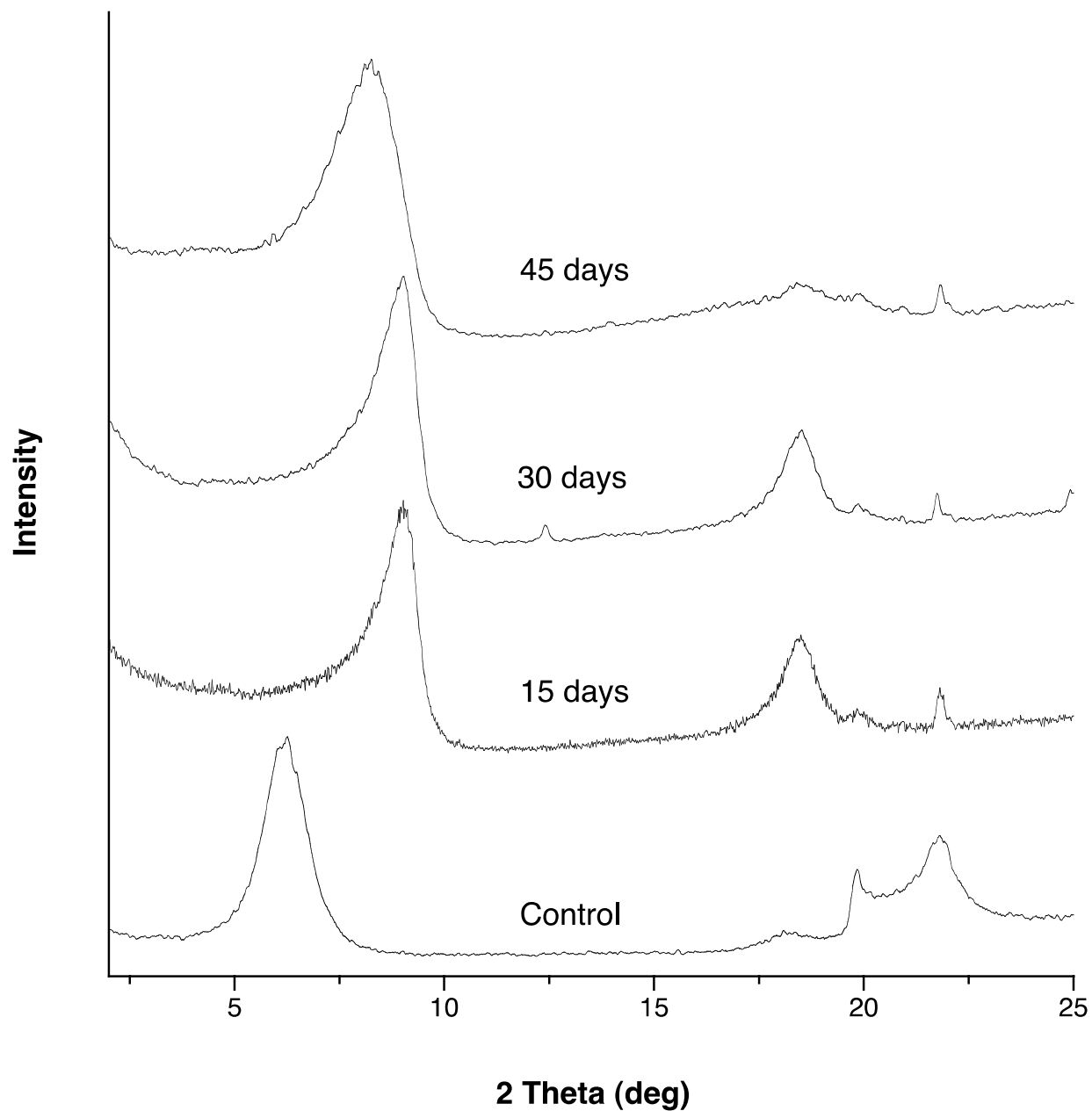


Figure 7.3.1.24. XRD spectra for montmorillonite treated with base-activated persulfate (2:1 molar ratio of NaOH to persulfate) over 45 days.

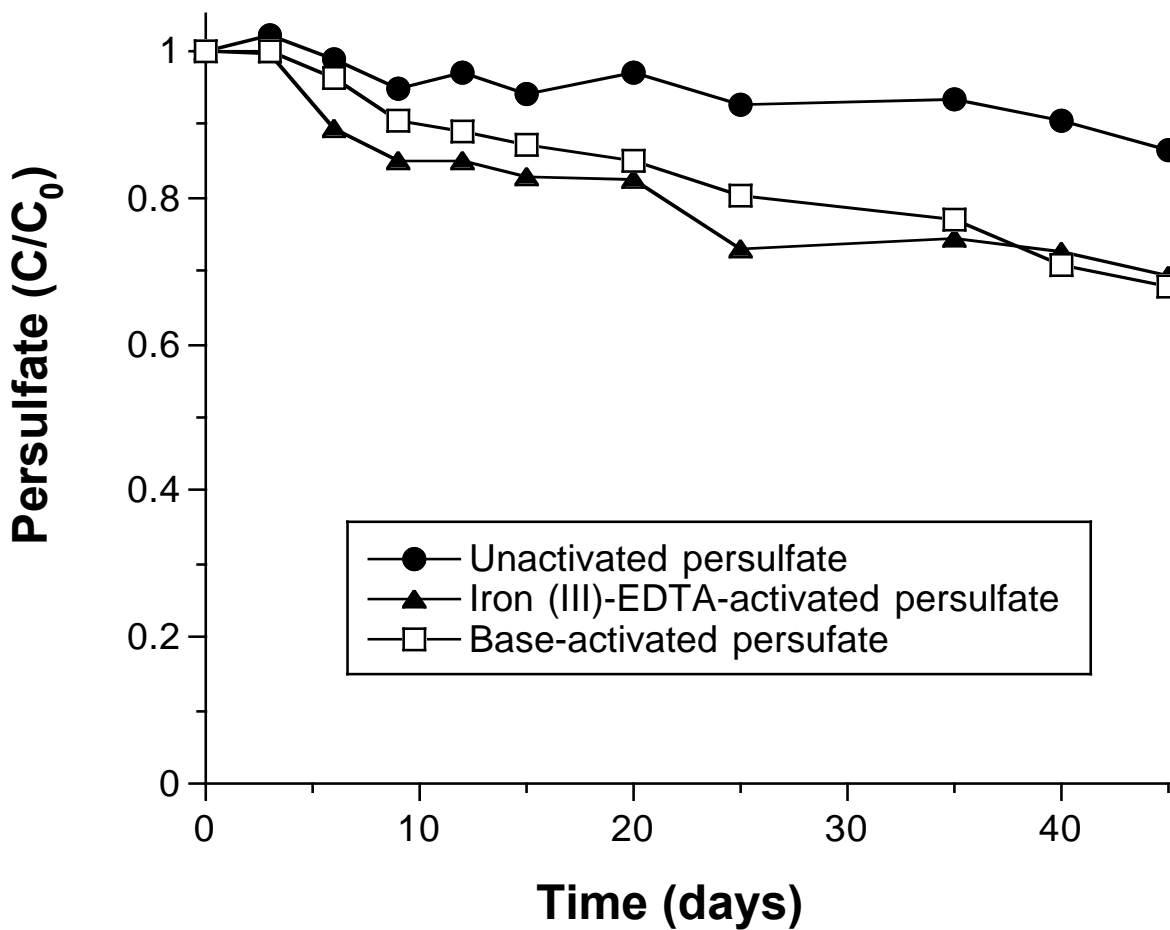


Figure 7.3.1.25. Persulfate concentrations over time in control solutions with no minerals containing persulfate alone (unactivated), iron (III)-EDTA-activated persulfate, or base-activated persulfate (with a 2:1 ratio of base to persulfate).

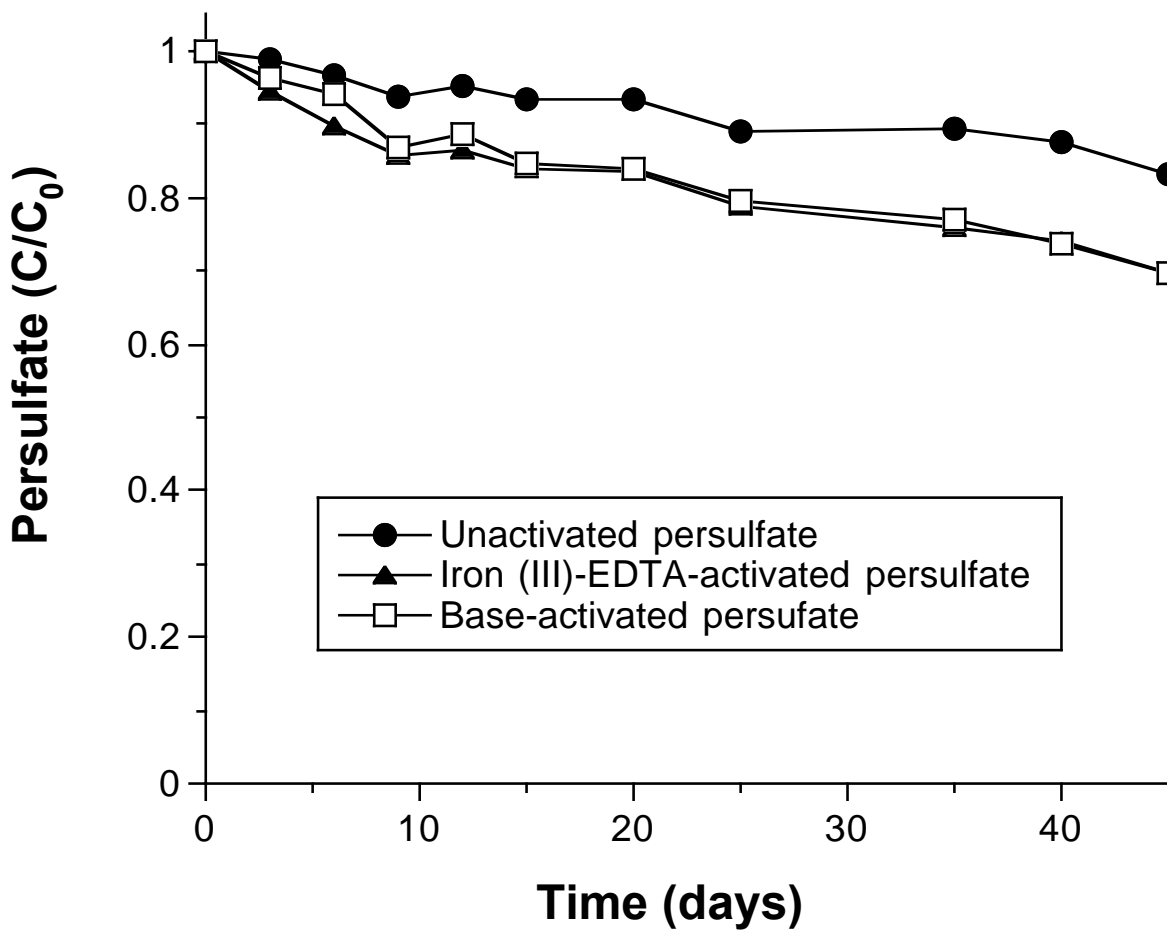


Figure 7.3.1.26. Persulfate concentrations over time in goethite systems containing persulfate alone (unactivated), iron (III)-EDTA-activated persulfate, or base-activated persulfate (with a 2:1 ratio of base to persulfate).

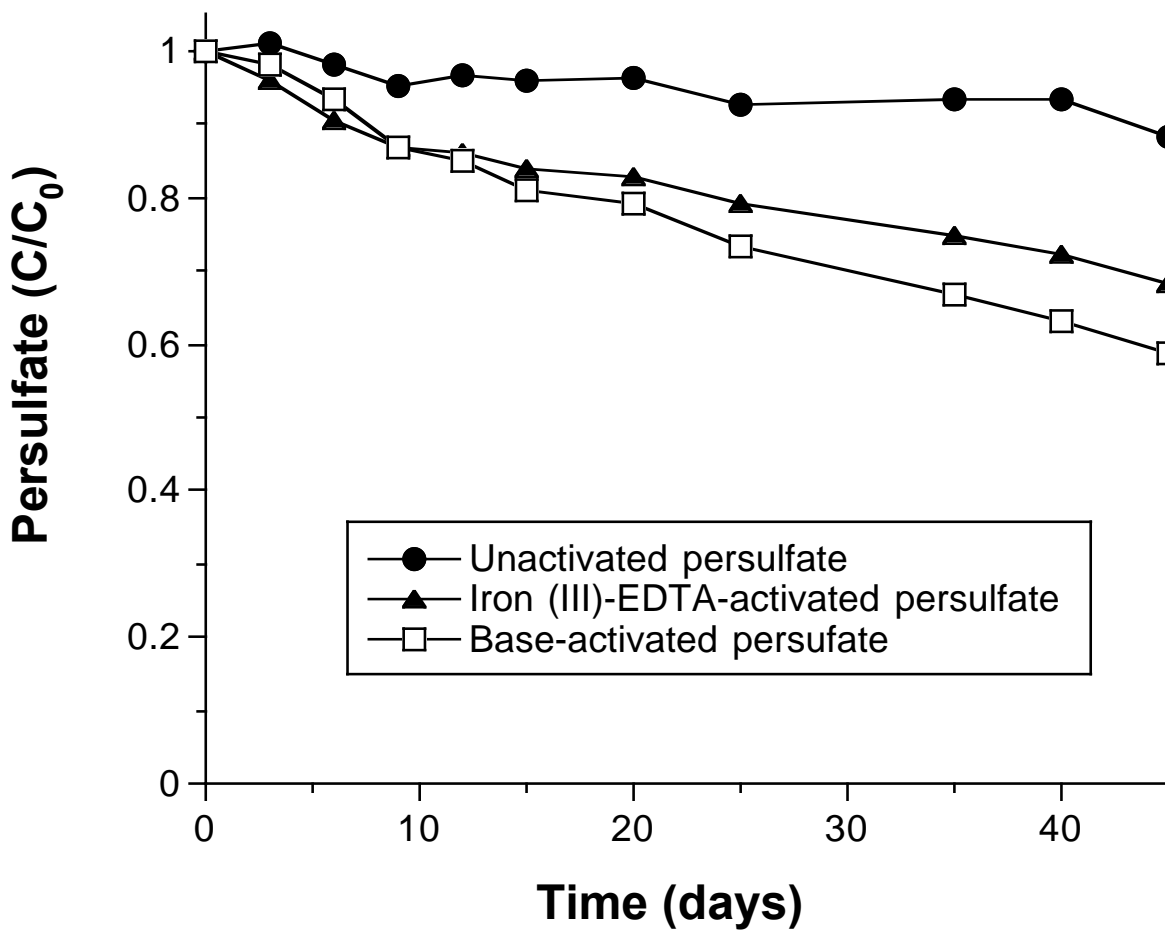


Figure 7.3.1.27. Persulfate concentrations over time in hematite systems containing persulfate alone (unactivated), iron (III)-EDTA-activated persulfate, or base-activated persulfate (with a 2:1 ratio of base to persulfate).

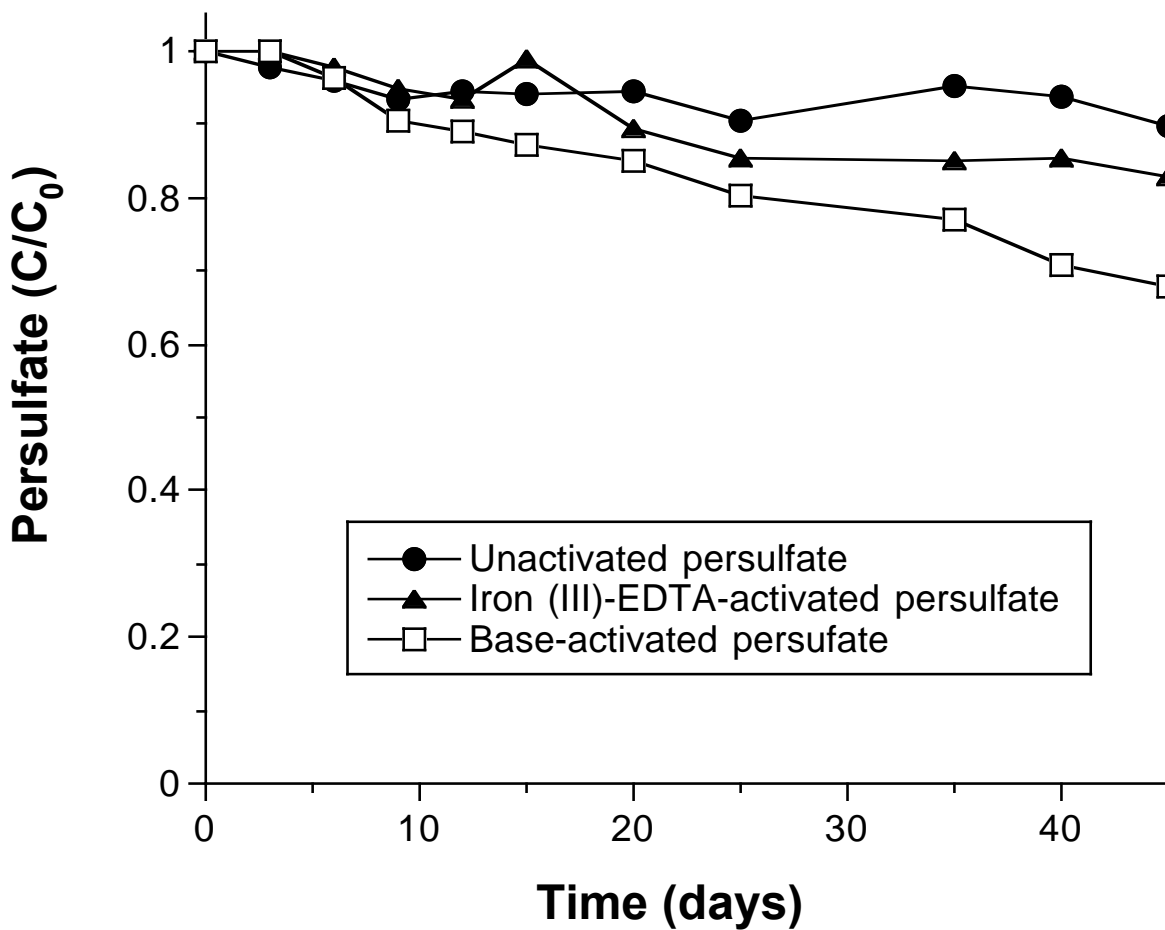


Figure 7.3.1.28. Persulfate concentrations over time in ferrihydrite systems containing persulfate alone (unactivated), iron (III)-EDTA-activated persulfate, or base-activated persulfate (with a 2:1 ratio of base to persulfate).

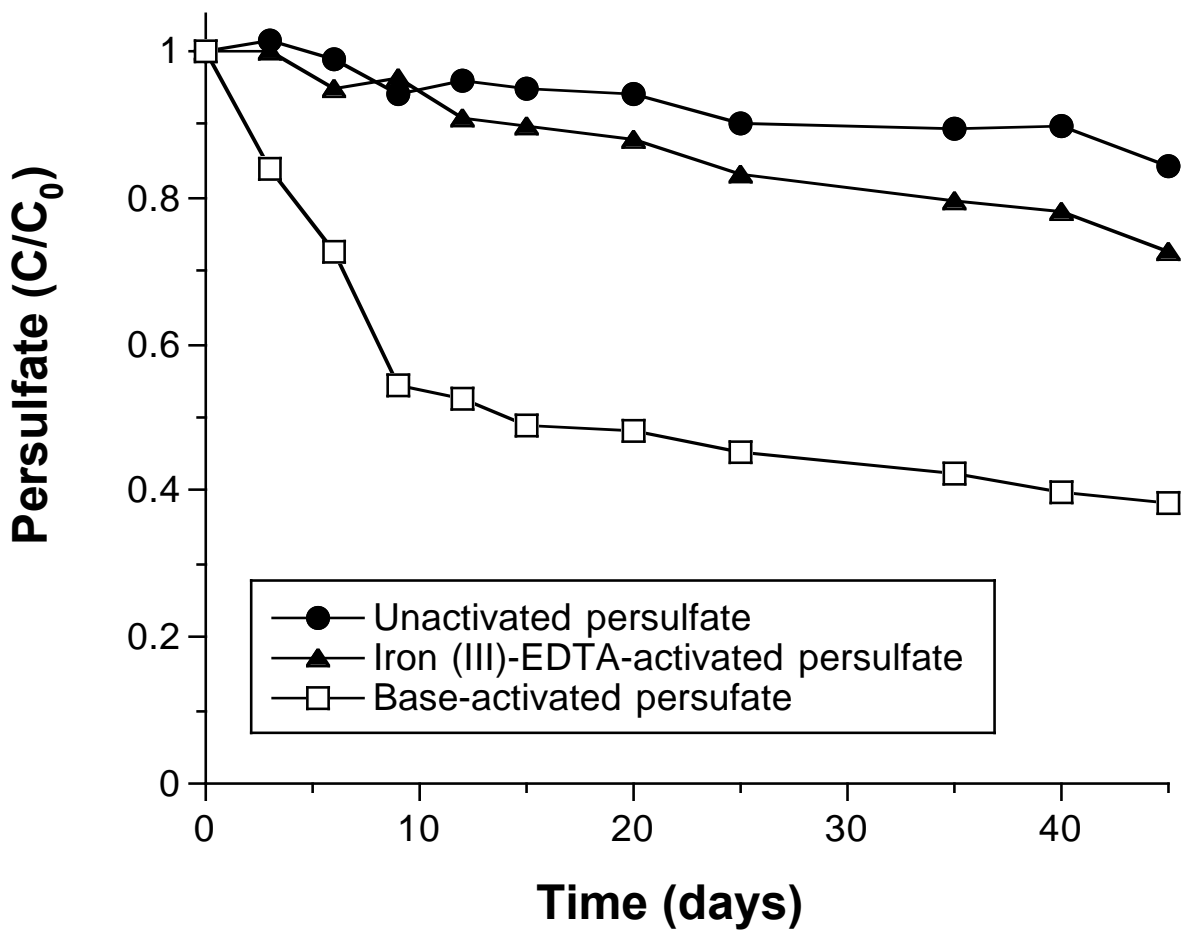


Figure 7.3.1.29. Persulfate concentrations over time in birnessite systems containing persulfate alone (unactivated), iron (III)-EDTA-activated persulfate, or base-activated persulfate (with a 2:1 ratio of base to persulfate).

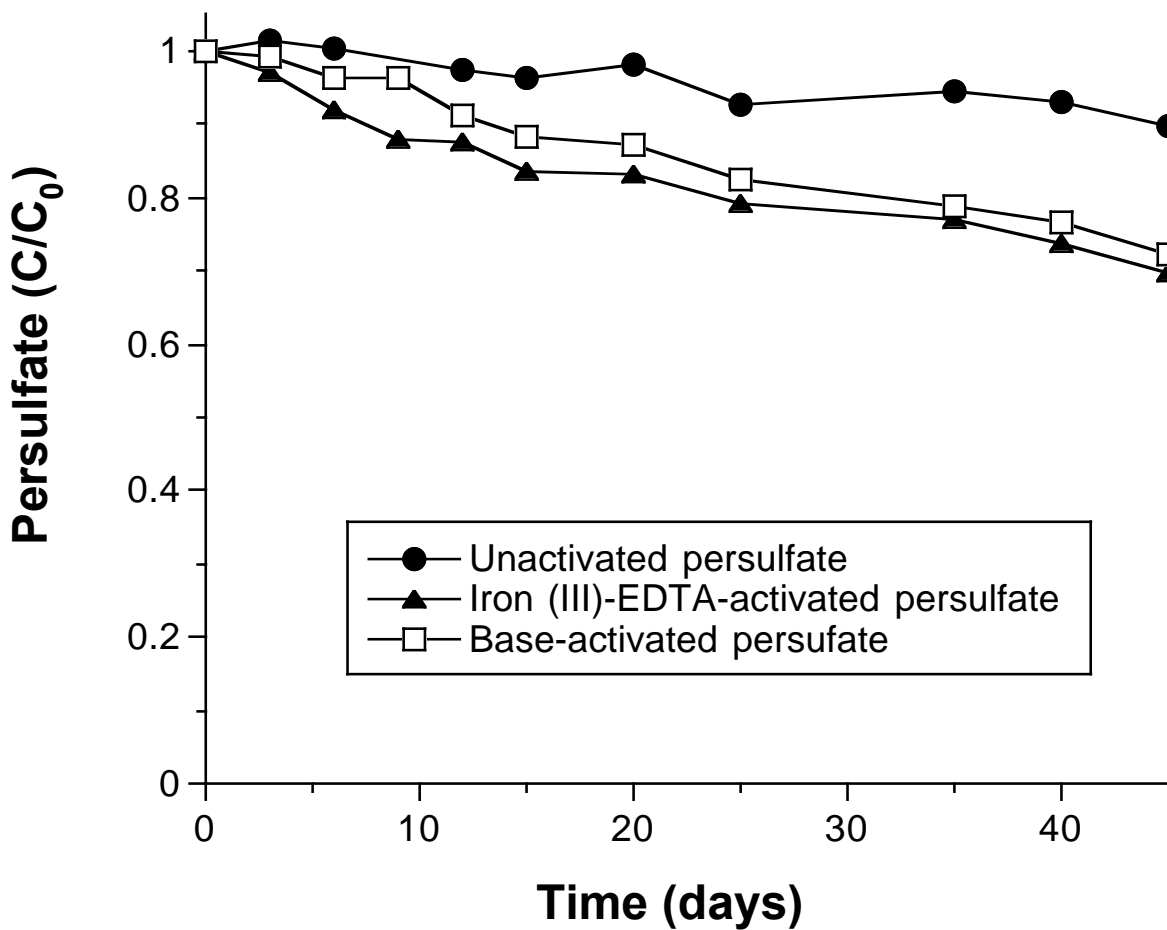


Figure 7.3.1.30. Persulfate concentrations over time kaolinite systems containing persulfate alone (unactivated), iron (III)-EDTA-activated persulfate, or base-activated persulfate (with a 2:1 ratio of base to persulfate).

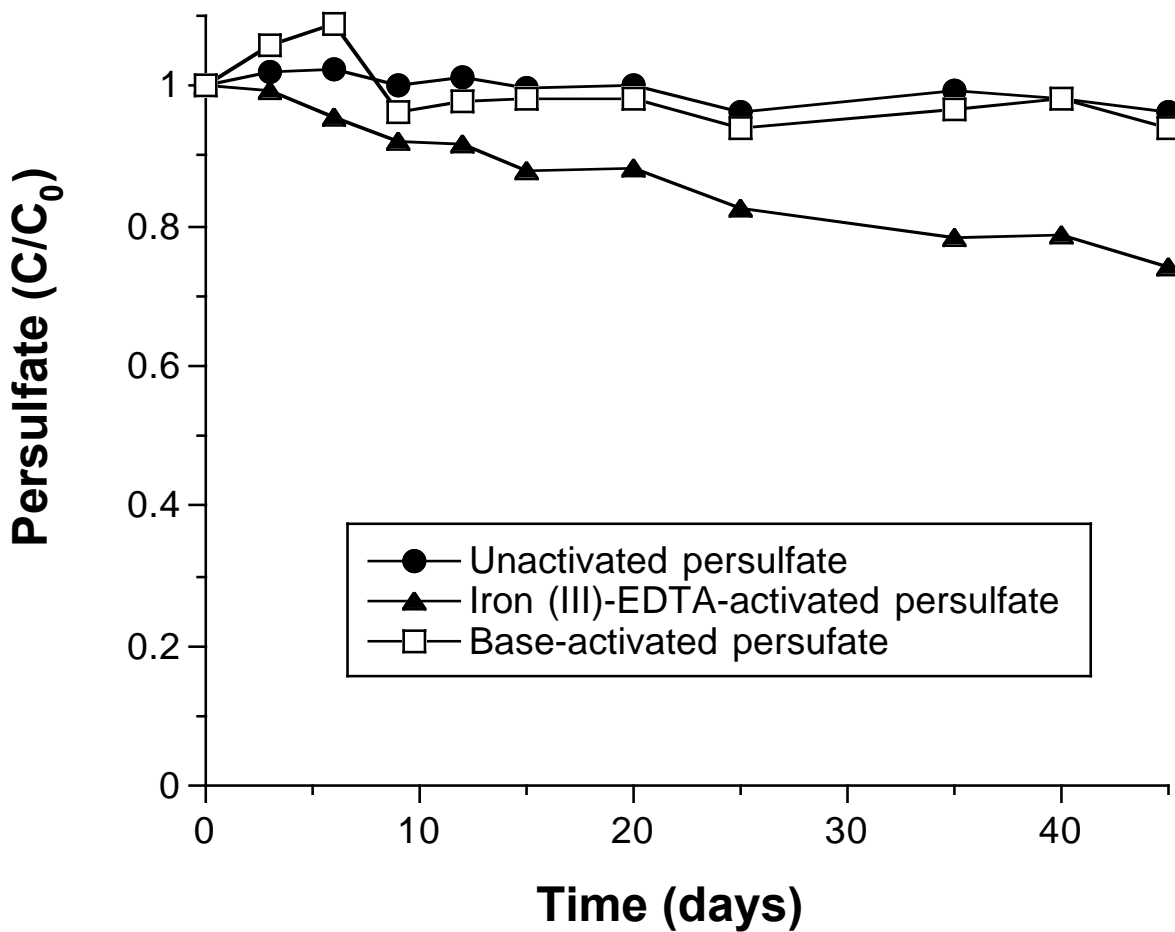


Figure 7.3.1.31. Persulfate concentrations over time montmorillonite systems containing persulfate alone (unactivated), iron (III)-EDTA-activated persulfate, or base-activated persulfate (with a 2:1 ratio of base to persulfate).

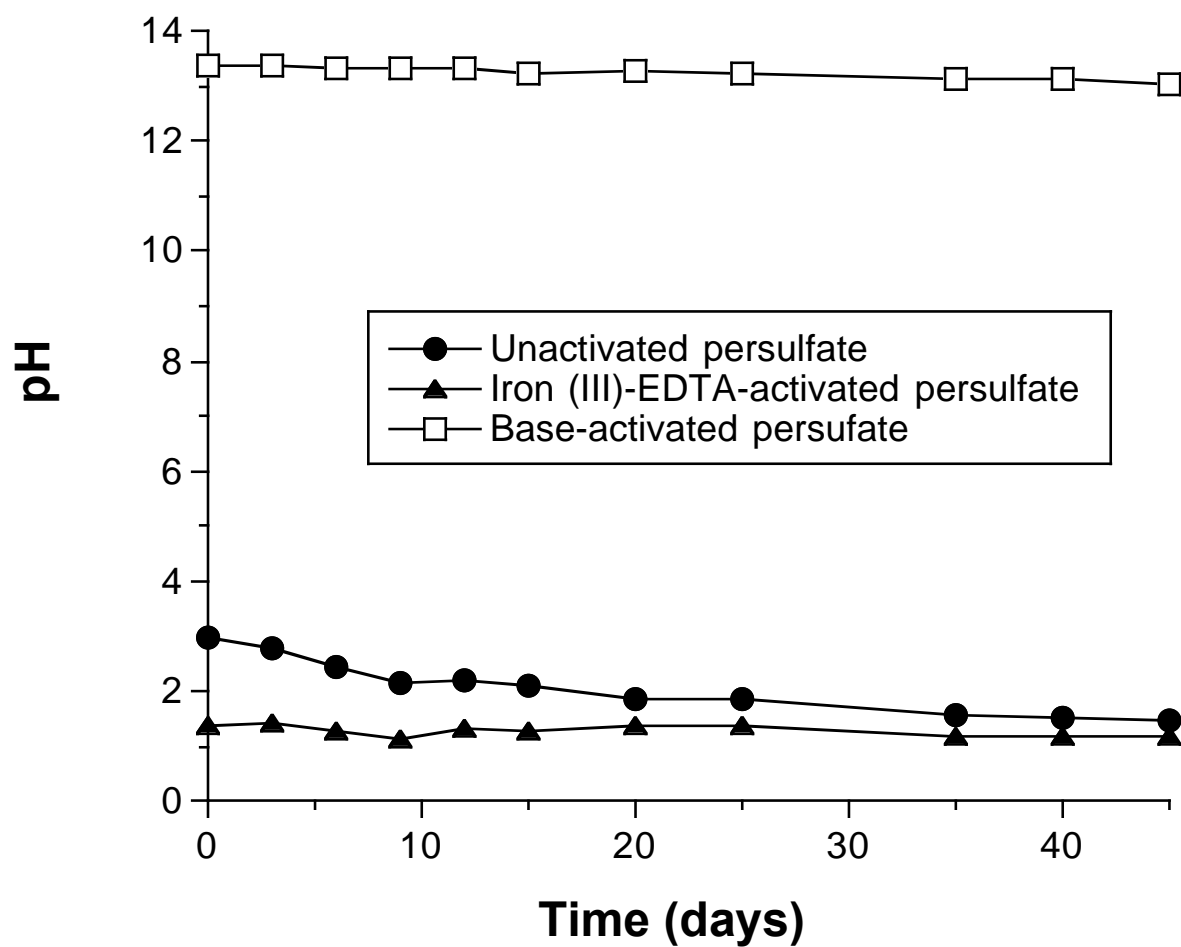


Figure 7.3.1.32. pH over time in control solutions with no minerals containing persulfate alone (unactivated), iron (III)-EDTA-activated persulfate, or base-activated persulfate (with a 2:1 ratio of base to persulfate).

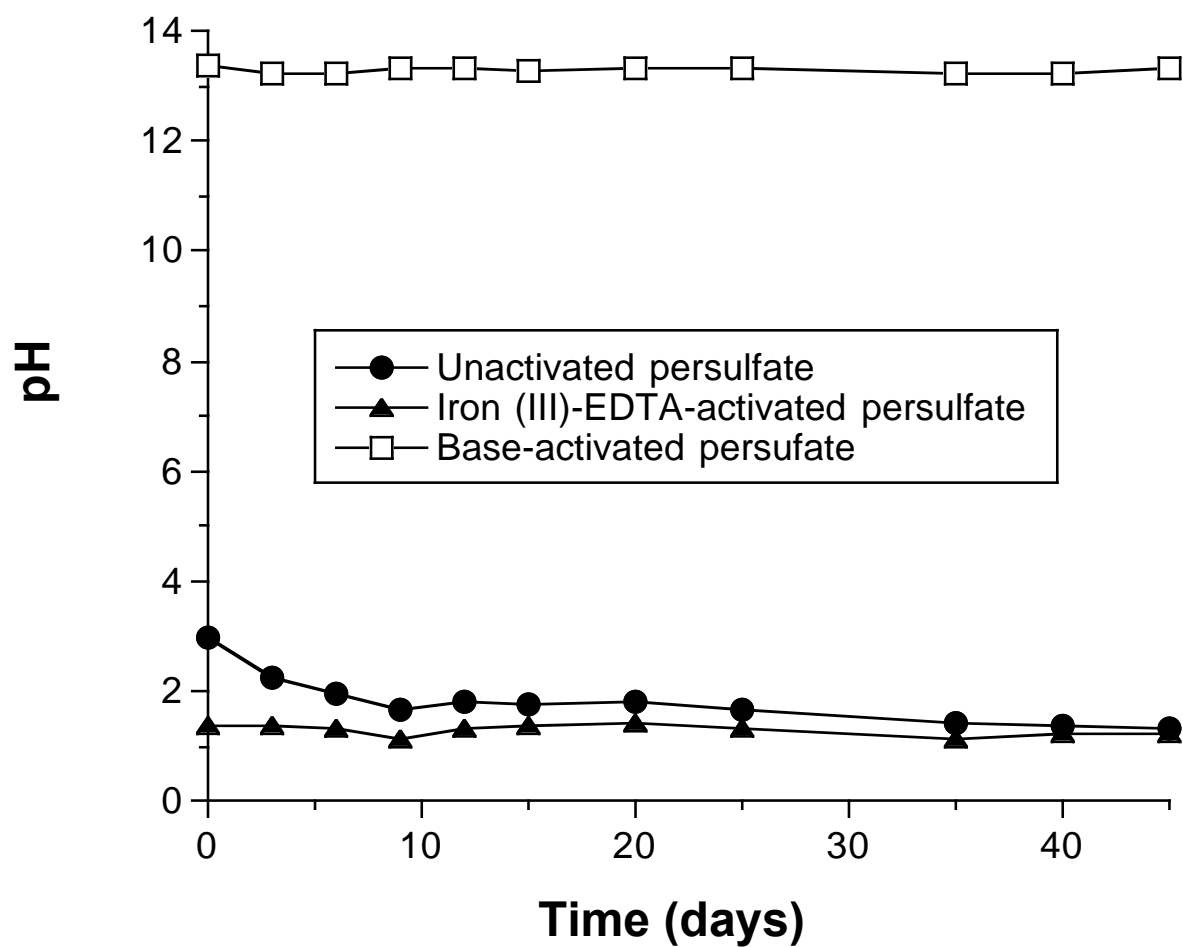


Figure 7.3.1.33. pH over time in goethite systems containing persulfate alone (unactivated), iron (III)-EDTA-activated persulfate, or base-activated persulfate (with a 2:1 ratio of base to persulfate).

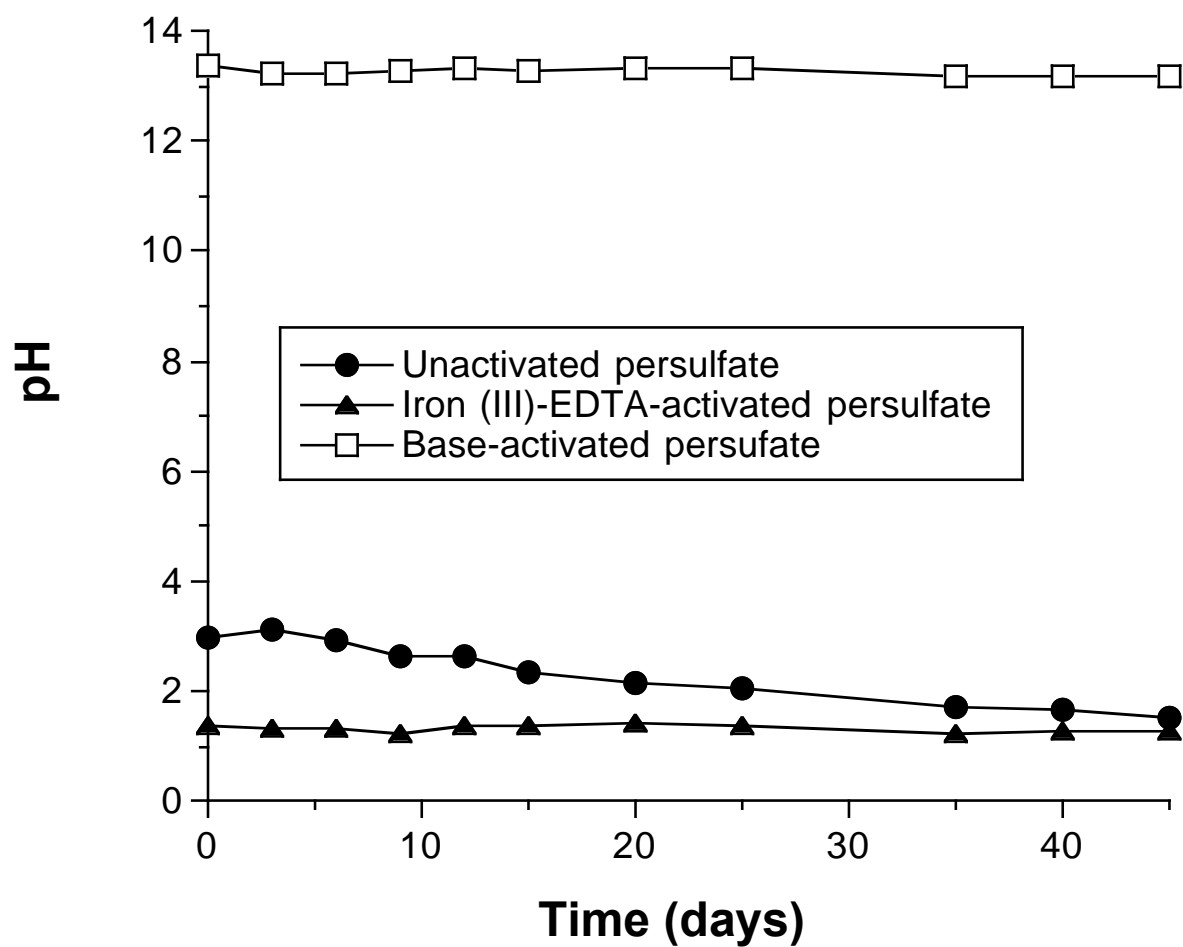


Figure 7.3.1.34. pH over time in hematite systems containing persulfate alone (unactivated), iron (III)-EDTA-activated persulfate, or base-activated persulfate (with a 2:1 ratio of base to persulfate).

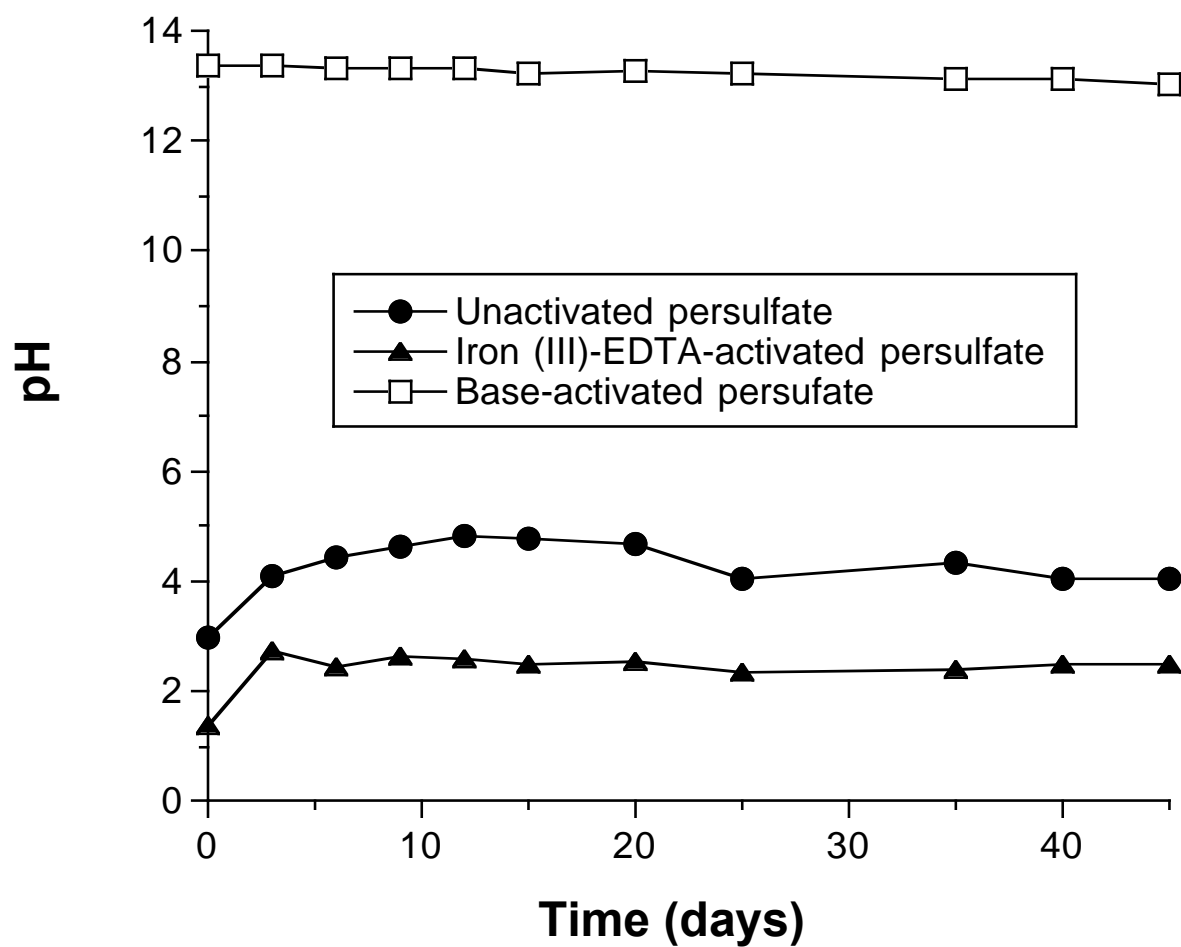


Figure 7.3.1.35. pH over time in ferrihydrite systems containing persulfate alone (unactivated), iron (III)-EDTA-activated persulfate, or base-activated persulfate (with a 2:1 ratio of base to persulfate).

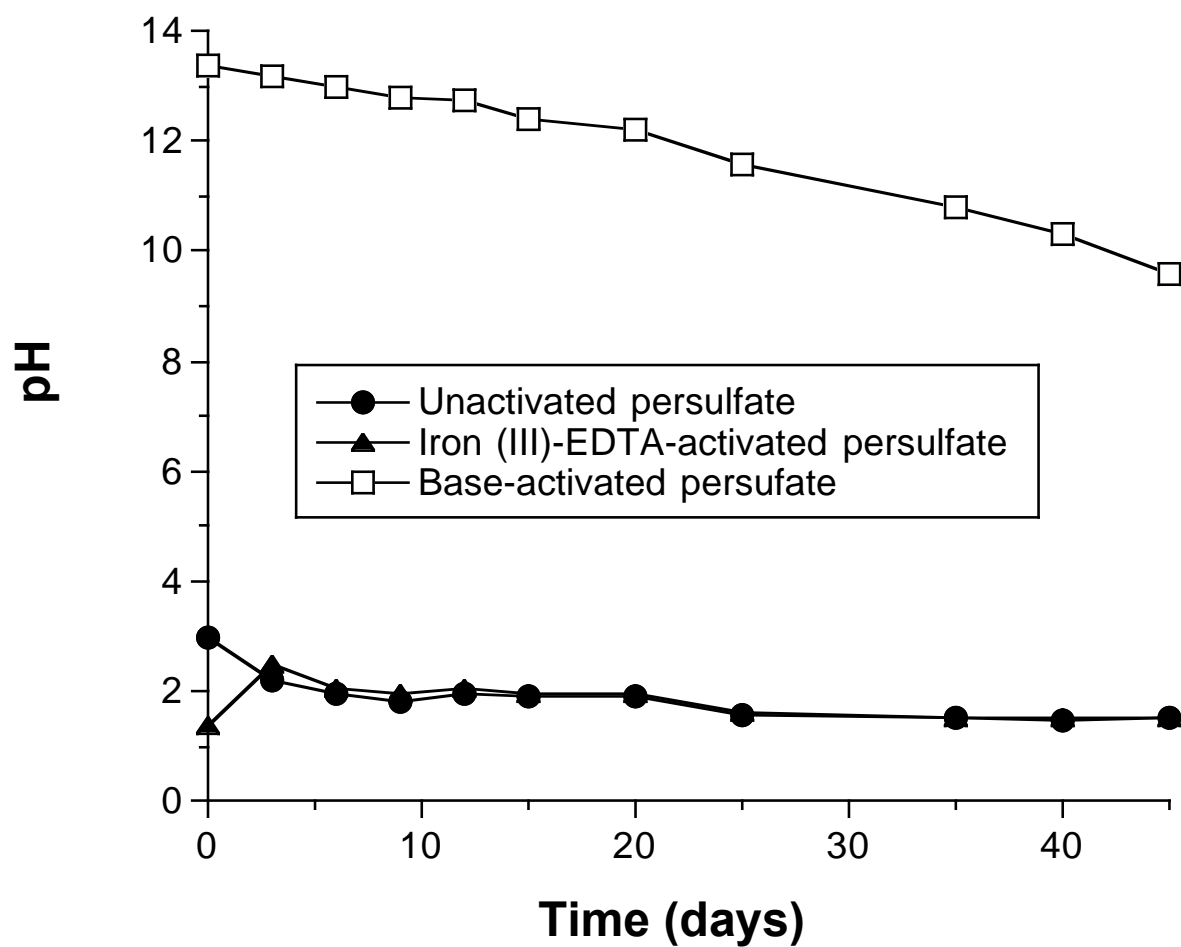


Figure 7.3.1.36. pH over time in birnessite systems containing persulfate alone (unactivated), iron (III)-EDTA-activated persulfate, or base-activated persulfate (with a 2:1 ratio of base to persulfate).

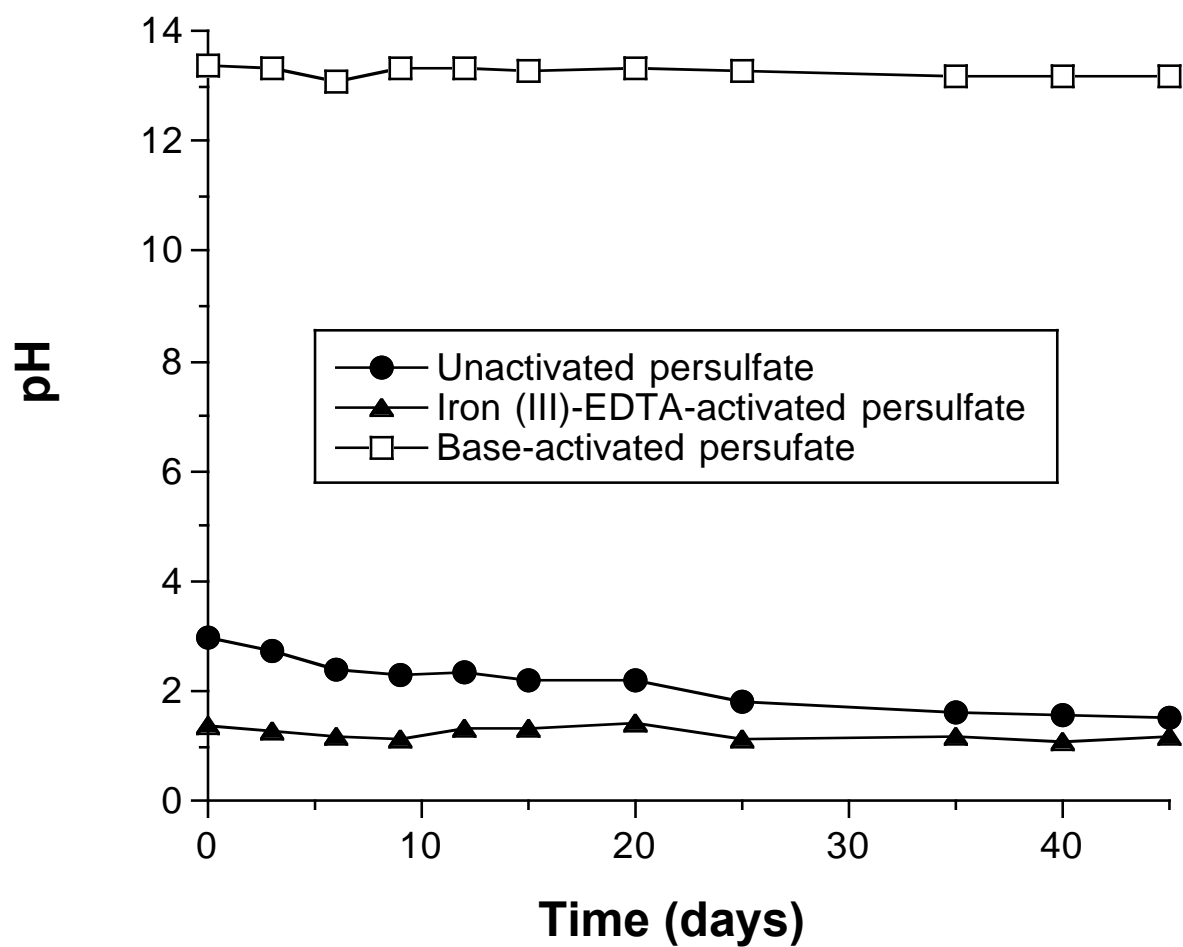


Figure 7.3.1.37. pH over time in kaolinite systems containing persulfate alone (unactivated), iron (III)-EDTA-activated persulfate, or base-activated persulfate (with a 2:1 ratio of base to persulfate).

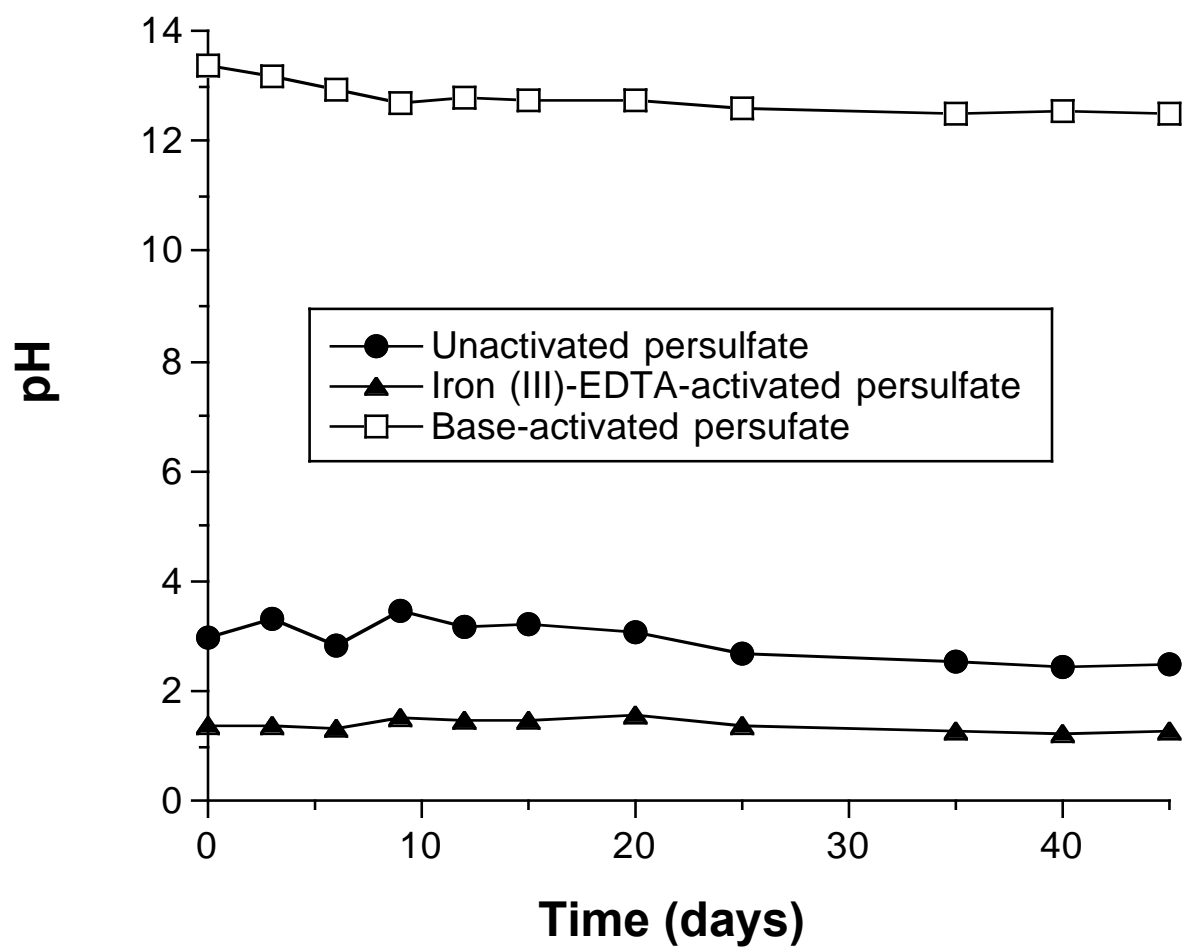


Figure 7.3.1.38. pH over time in montmorillonite systems containing persulfate alone (unactivated), iron (III)-EDTA-activated persulfate, or base-activated persulfate (with a 2:1 ratio of base to persulfate).

Table 7.3.1.1. Surface area of minerals after treatment with different persulfate systems.

	Treatment time (days)	BET surface area (m ² /g)			
		Deionized water	Unactivated persulfate	Iron (III)-EDTA-activated persulfate	Base-activated persulfate
Goethite	0	18.9	18.9	18.9	18.9
	15	18.1	17.9	16.3	15.6
	30	17.2	17.4	17.3	17.6
	45	18.7	16.5	17.4	16.0
Hematite	0	8.6	8.6	8.6	8.6
	15	8.8	9.3	9.0	8.4
	30	8.4	9.6	9.3	9.1
	45	9.1	9.9	9.6	9.1
Ferrihydrite	0	205	205	205	205
	15	175	181	182	108
	30	189	257	217	125
	45	158	223	234	79.1
Birnessite	0	50.6	50.6	50.6	50.6
	15	53.0	54.1	60.8	45.4
	30	51.2	54.5	141	45.7
	45	52.9	56.4	104	46.2
Kaolinite	0	11.9	11.9	11.9	11.9
	15	11.7	11.3	9.1	12.3
	30	12.8	11.4	10.4	11.8
	45	14.4	12.2	12.8	14.4
Montmorillonite	0	104	104	104	104
	15	107	86.8	97.5	67.6
	30	106	83.6	104	37.7
	45	108	88.0	84.3	41.4

7.3.2. Effect of Persulfate Formulations on Soil Permeability

Effect of Persulfate Formulations on Commercial Sand Permeability

Commercial silica sand was first used to investigate the effect of persulfate formulations on permeability. Sand permeability variations after treatment with different persulfate concentrations and formulations are shown in Figure 7.3.2.1. The hydraulic conductivity of the sand in control reactors after treatment with deionized water was 1.26 cm/sec. After treatment with unactivated persulfate at concentrations from 0.1 M to 0.5 M, there was no significant difference in the hydraulic conductivity, demonstrating that unactivated persulfate did not have a significant influence on the permeability of silica sand. In contrast, the hydraulic conductivity of sand decreased from 1.28 cm/s to 1.17 cm/s after treatment with sulfate and also decreased with all three persulfate formulations. Treatment with increasing concentrations of iron (III)-EDTA activated persulfate decreased the sand hydraulic conductivity from 1.28 to 1.16 cm/s, which was about the same extent of loss of permeability as the sulfate positive control. Sodium sulfate and iron (III)-EDTA-persulfate solutions are acidic, which may change the surface charge on the sand and decrease its permeability. Furthermore, the addition of sodium may disperse the sand, resulting in decreased sand permeability. Treatment with increasing concentrations of base-activated persulfate decreased the sand hydraulic conductivity even more than the acidic persulfate solution with hydraulic conductivity decreasing from 1.24 to 1.01 cm/s. During the process of persulfate activation by base, gas is produced (Furman et al., 2010). If gasses accumulate in the void spaces of subsurface soil, the result is a substantial decrease in hydraulic conductivity which may be occurring in the base-activated persulfate systems evaluated in this study. In addition, the silicon oxide may react with sodium hydroxide. Silicon oxide particles in the system may have been degraded to smaller size particles by the strong base. These small size particles may have then moved within the porous medium, leading to trapping in the pores and plugging (Amrhein et al., 2004). In summary, unactivated persulfate did not have a significant influence on sand permeability, while iron (III)-EDTA and base activated persulfate decreased sand permeability, similar to the sodium sulfate positive control.

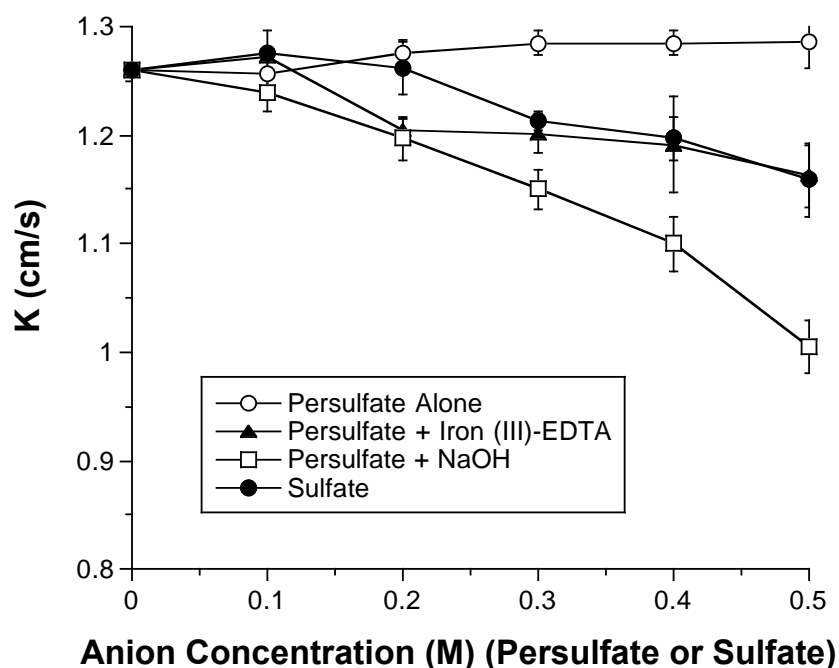


Figure 7.3.2.1. Effect of sodium persulfate and sulfate formulations on sand hydraulic conductivity.

Effect of Persulfate Formulations on Kaolinite Permeability

Permeability tests were also conducted to study the effect of persulfate formulations on kaolinite (Figure 7.3.2.2). There was minimal change in the permeability of kaolinite in the presence of sulfate. After treatment with iron (III)-EDTA-activated persulfate, kaolinite hydraulic conductivity decreased slightly. The iron (III)-EDTA may have precipitated as an iron hydroxide ($\text{Fe}(\text{OH})_3$) or hydrous ferric oxide ($\text{Fe}_2\text{O}_3 \cdot n\text{H}_2\text{O}$) in these systems (Pignatello and Day, 1996; Georgi et al., 2006), possibly decreasing system permeability. Alternatively, the iron hydrolysis complexes in the system may have acted as bonding agents between kaolinite particles (Ma et al., 1997), reducing the kaolinite porosity. Kaolinite permeability increased by 18% when increasing concentrations of unactivated persulfate were applied to the columns. Because persulfate decomposition was less than 6% over 30 d and kaolinite does not promote the activation of persulfate (Ahmad, 2010), minimal change in the permeability of kaolinite would be expected in the presence of unactivated persulfate.

In contrast to the other persulfate systems, base-activated persulfate significantly increased kaolinite permeability with increasing persulfate concentrations (Figure 7.3.2.2). The permeability of the 0.5 M base activated persulfate formulations was 2.8 times that of the 0.1 M base activated persulfate. Under basic conditions, the zeta potential of clay may have become negative, and kaolinite particles may have compacted (Ma et al., 1998) promoting the formation of cracks, resulting in increased hydraulic conductivity (Brown et al., 1987).

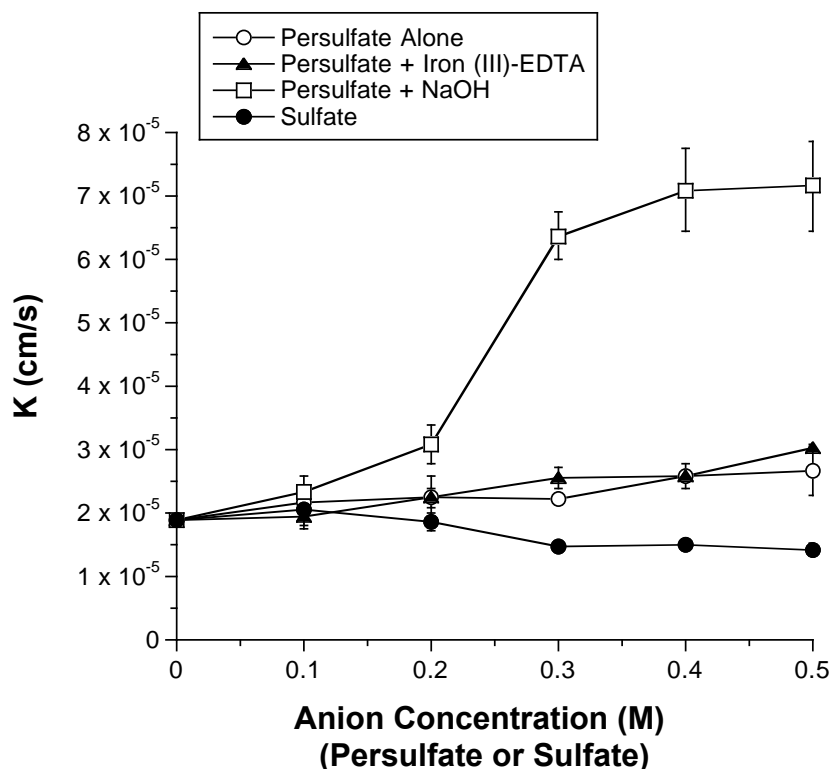


Figure 7.3.2.2. Effect of sodium persulfate and sulfate formulations on kaolinite hydraulic conductivity.

Effect of Persulfate Formulations on the Permeability of Natural Soils

The effect of the three persulfate formulations and the sulfate positive control on the permeability of two horizons of a natural soil, KB1 and KB2, are shown in Figures 7.3.2.3 and 7.3.2.4, respectively. Permeabilities did not change significantly with increasing concentrations of sulfate, unactivated persulfate, or iron (III)-EDTA-activated persulfate. Although the initial (0.1 M) hydraulic conductivities differed significantly in both soils, the trend was the same: there was no change in hydraulic conductivity with increasing treatment concentration when sulfate, unactivated persulfate, and iron (III)-EDTA activated persulfate were applied to the columns.

The trend in changes of hydraulic conductivity was quite different for base-activated persulfate formulations in both soil KB1 and soil KB2. Both soil horizons were characterized by significant increases in hydraulic conductivity with increasing dosages of base-activated persulfate. The hydraulic conductivity of soil KB1 increased by approximately 3.5 times, from 2.2×10^{-5} cm/s to 7.4×10^{-5} cm/s. Although the hydraulic conductivities of the base-activated persulfate systems were lower than the sulfate positive controls, the hydraulic conductivity in base-activated persulfate systems increased two-fold in soil KB2.

Soil minerals may undergo dissolution and precipitation under highly basic conditions (Qafoku et al., 2003), and sodium ion can facilitate the release of silicon from soil structure to promote the dissolution of soil particles (Qafoku et al., 2003), which may compact together thus reducing the permeability. In addition, soil constituents such as aluminum, silicon and iron may precipitate together to form groups of minerals such as sodalite and hematite under basic conditions (Qafoku et al., 2003; Qafoku et al., 2007), which may have reduced the KB1 soil permeability.

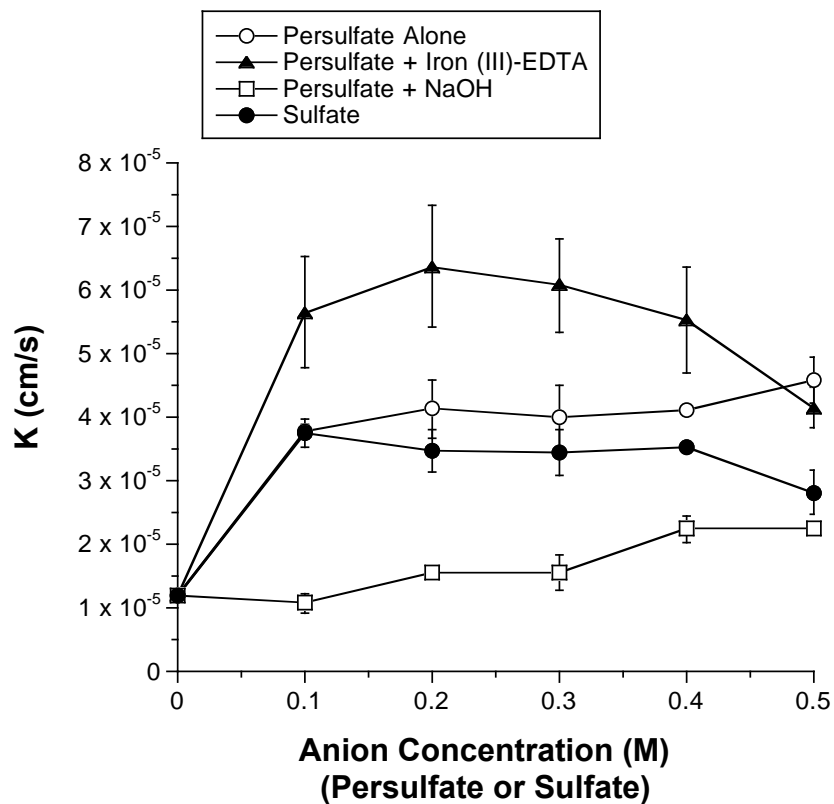


Figure 7.3.2.3. Effect of sodium persulfate and sulfate formulations on soil KB1 hydraulic conductivity.

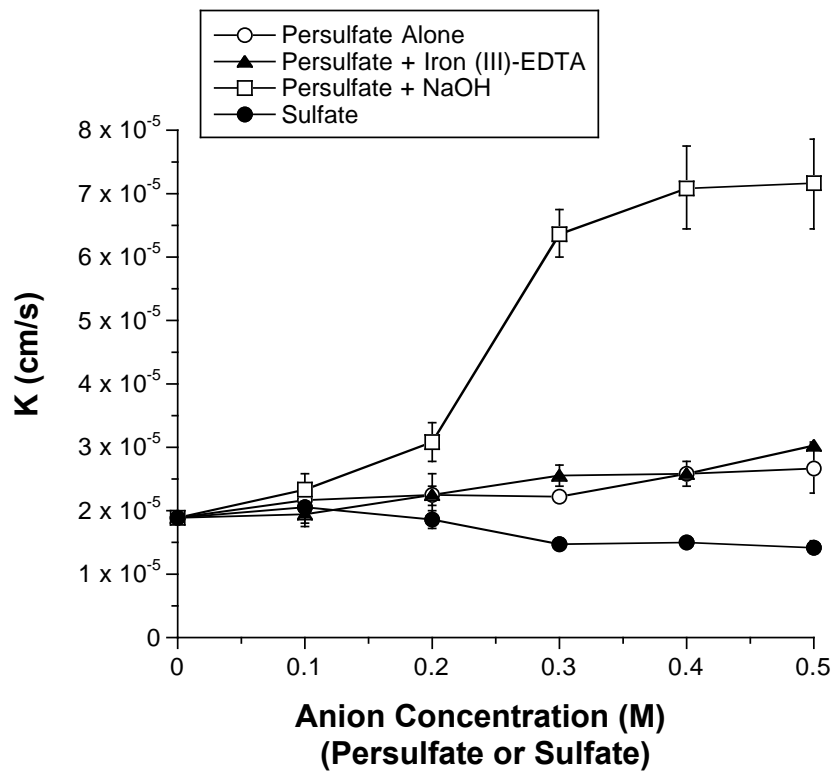


Figure 7.3.2.4. Effect of sodium persulfate and sulfate formulations on soil KB2 hydraulic conductivity.

XRCT Analysis of Soil Porosity

The distribution of porosity of the sand with depth in persulfate-treated soil columns is shown in Figure 7.3.2.5. The porosity of the dry sand (Figure 7.3.2.5a) was distributed relatively uniformly. As shown in Figure 7.3.2.5b, the porosity of the sand sample treated with deionized water distributed uniformly from depth of 1 cm to 5 cm, though it was slightly less uniform above the 1 cm depth. The surface porosity did not distribute uniformly probably due to surface clogging (Manahiloh, et al., 2010). In addition, the sample surface structure was disturbed as the solutions passed through the sample. As shown in Figure 7.3.2.5c and d, the porosity of the sand samples treated by unactivated persulfate and iron (III)-EDTA activated persulfate was even less uniform with depth compared to the dry sand sample and even the deionized water treated sand sample. These results suggest that the persulfate formulation influenced the porosity of the sand samples throughout the entire depth, thus affecting the permeability throughout the entire column. The average porosity of the sand samples treated by unactivated persulfate and iron (III)-EDTA activated persulfate was 0.21 and 0.17, respectively, which is higher than the permeability of the sand in the presence of deionized water. There was little correlation between the mean porosity of samples after treatment and their hydraulic conductivity (Figure 7.3.2.1). However, the minimum hydraulic conductivity in the control, the unactivated persulfate treated

sample, and the iron (III)-EDTA treated sample was approximately 0.1, which may affect hydraulic conductivity more than the mean porosity.

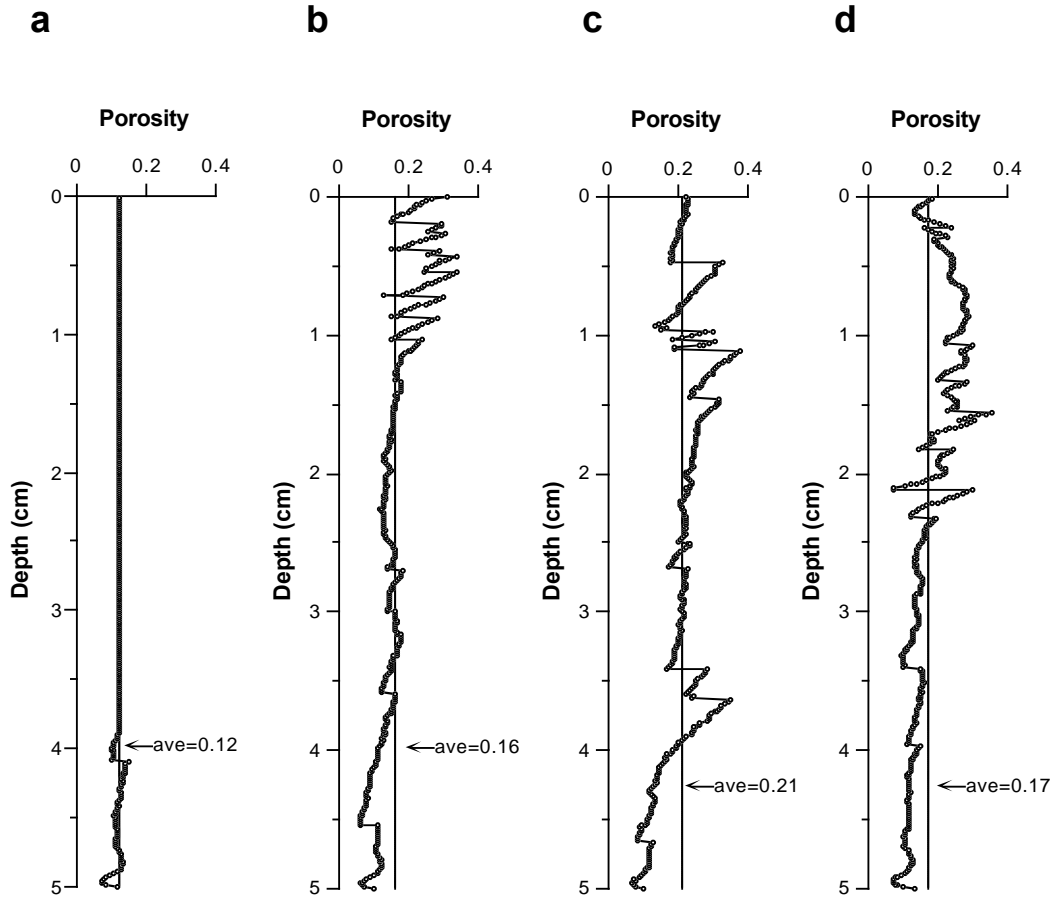


Figure 7.3.2.5. Sand porosity distribution with depth and average porosity; a) untreated; b) deionized water; c) persulfate alone; d) persulfate with iron (III)-EDTA.

The distribution of the porosity of soil KB1 with depth and mean pore radius values are shown in Figure 7.3.2.6. The porosity of the dry KB1 soil and deionized water treated KB1 soil samples were distributed relatively uniformly with depth compared to the distribution of the sample treated with base-activated persulfate. This difference was likely due to changes in soil morphology resulting from the base-activated persulfate. The average porosity of soil KB1 after treatment with base-activated persulfate was 0.26 while the average porosity of soil KB1 treated

with deionized water was 0.16. These results correlate with increased permeability, and are in agreement with the results shown in Figure 7.3.2.3.

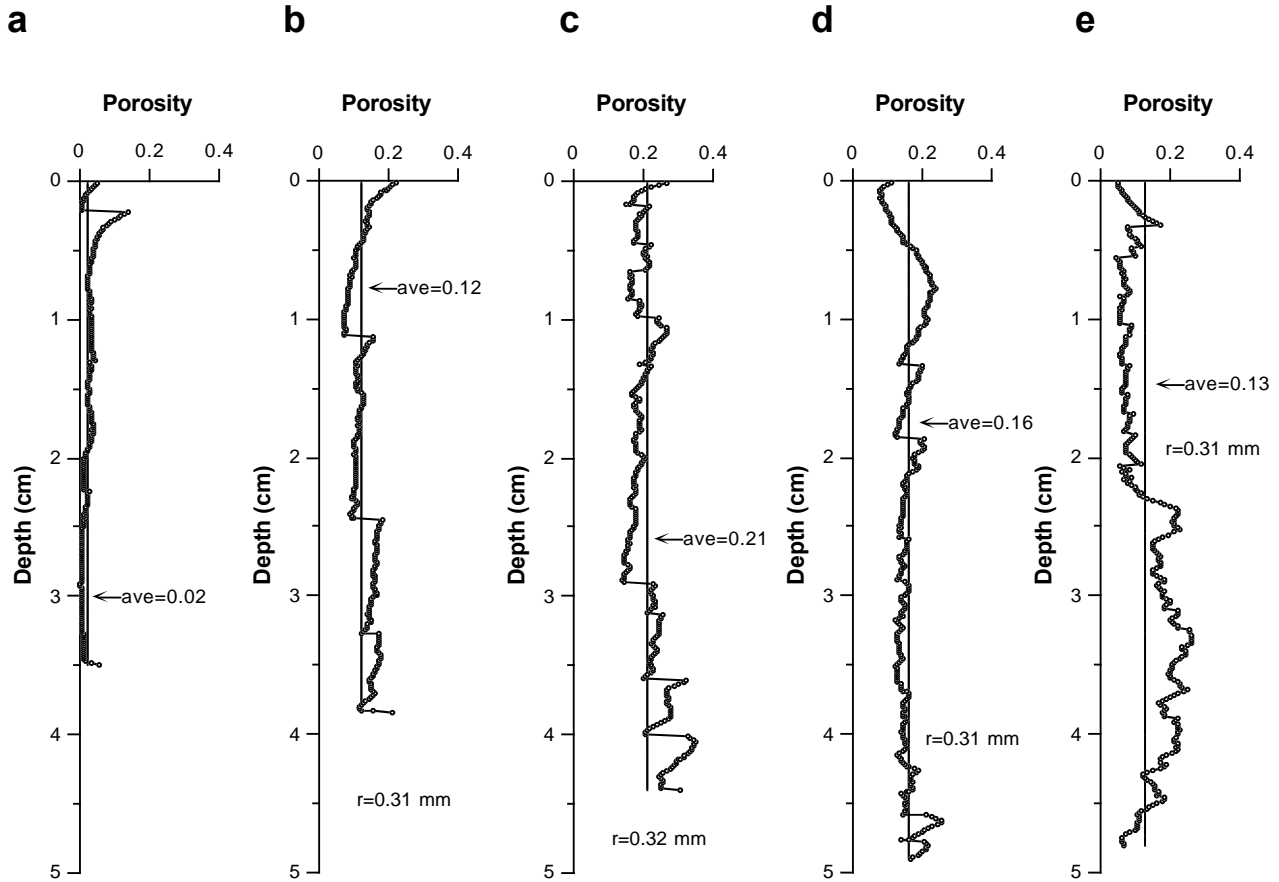


Figure 7.3.2.6. Soil KB1 porosity distribution with depth, average porosity, and mean pore radius; a) dry soil; b) deionized water; c) persulfate alone; d) persulfate with iron (III)-EDTA; e) persulfate with NaOH.

The porosity distribution of soil KB2 with depth and mean pore radius values are shown in Figure 7.3.2.7. Similar to soil KB1, none of the soil KB2 samples treated with persulfate solutions were characterized by uniform pore distribution compared to the dry soil sample. The average porosity of persulfate, iron (III)-EDTA activated persulfate and base activated persulfate samples was 0.21, 0.16 and 0.13 respectively. Neither these mean porosities, nor the minimum porosities shown in Figure 7.3.2.7, correlate with the hydraulic conductivities shown in Figure 7.3.2.4. The porosity data of Figures 7.3.2.5–7 demonstrate that porosity is highly variable and

complex in persulfate-treated samples, and that the changes in porosity do not usually correlate with changes in hydraulic conductivity. Nonetheless, the data shown in Figures 7.3.2.5–7 show that all of the persulfate formulations change the porosity of all of the soils evaluated, and significantly increase the variability in porosity with depth of treatment.

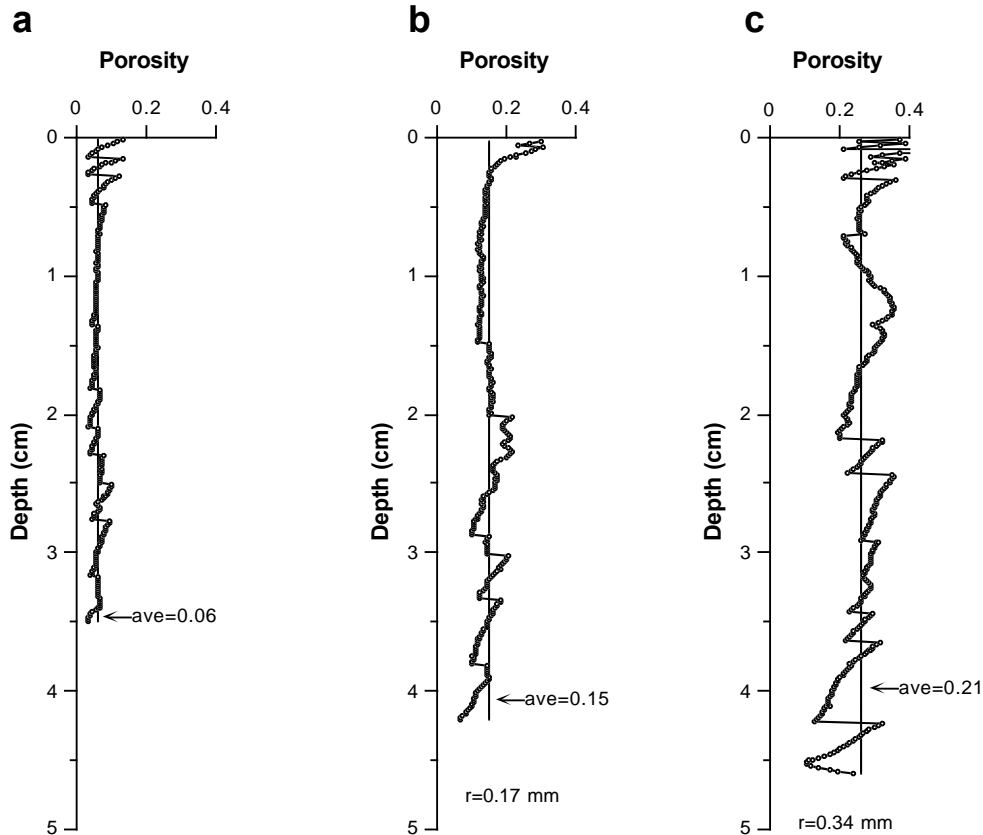


Figure 7.3.2.7. Soil KB2 porosity distribution with depth, average porosity and mean pore radius; a) dry soil; b) deionized water; c) persulfate and NaOH

Conclusion

The results of this research demonstrate that activated persulfate promotes changes in the permeability of different soils, and these changes are dependent on the soil type and the persulfate formulation applied. In the presence of sand, unactivated persulfate and iron (III)-activated persulfate had minimal effect on permeability relative to the sulfate positive control; however, the application of base-activated persulfate resulted in significant decreases in

hydraulic conductivity. These changes in the permeability of sand are likely not important because the hydraulic conductivity of sand is orders of magnitude higher than that of other subsurface solids. Changes in the hydraulic conductivity of kaolinite were only evident for base-activated persulfate, and then only at persulfate concentrations above 0.3 M. Such a dramatic increase (3.5 fold) may significantly increase the potential for treatment of contaminants in low permeability matrices of the subsurface. Similar results of increased hydraulic conductivity with increasing concentrations of base-activated persulfate were found in soils KB1 and KB2. Results of XRCT demonstrated that changes in porosity were minimal in control samples, but all of the soils became highly heterogeneous with respect to porosity. The presence of such wide ranging porosities resulting from the application of persulfate formulations minimizes the potential to correlate soil porosity with hydraulic conductivity.

7.3.3. Summary of the Effect of Persulfate on Subsurface Characteristics

Table 7.3.3.1. Summary of the Effect of Persulfate on Subsurface Characteristics

Subsurface Characteristic	Comments
Soil Mineralogy, pH, and Surface Area	<ul style="list-style-type: none"> • No mineralogy changes were observed for kaolinite, hematite, and goethite in any persulfate system. • Mineralogy changes were found for ferrihydrite, which matured from amorphous into more ordered structures (e.g., goethite, hematite). • Mineral structural changes occurred in one manganese mineral (birnessite) only in iron-EDTA activated persulfate, as a result of Fe (III) substituting for Mn (IV) in the structure. • Montmorillonite may stabilize (e.g., lessen decomposition) persulfate. • No pH changes were observed for kaolinite, hematite, and goethite; however, pH increased slightly for Fe-EDTA-activated persulfate systems containing montmorillonite and ferrihydrite. • The pH of base-activated persulfate containing birnessite decreased substantially. • Hematite, goethite, and kaolinite showed minimal surface area changes. • The surface area of ferrihydrite decreased, which was expected as it transformed from an amorphous, high surface area mineral to a more crystalline species. • The surface area of birnessite decreased slightly. • Montmorillonite showed significant surface area decreases (20-60 m²/g).
Soil Permeability	<ul style="list-style-type: none"> • Activated persulfate promoted changes in the permeability of different soils, dependent on soil type and persulfate formulation. • Iron (III)-activated persulfate resulted in significant decreases in hydraulic conductivity in sand. • Hydraulic conductivity increased in kaolinite and in the two soils whe treated with base-activated persulfate (> 0.3 M persulfate); such a 3.5 fold increase may increase the potential for treatment in low permeability zones • All soils became highly heterogeneous with respect to porosity; the presence of such wide ranging porosities minimizes the potential to correlate soil porosity with hydraulic conductivity.

7.4. Transport of Persulfate into Low Permeability Matrices

7.4.1. Persulfate Transport in Two Low-Permeability Soils

Three treatments were analyzed for persulfate diffusion: persulfate only, iron (III)-activated persulfate (Fe(III) EDTA), and base-activated persulfate (NaOH). The treatments included two initial persulfate concentrations, 1 M and 0.1 M, which were applied to two soil types, Palouse loess and kaolin. The Palouse loess treatment sets included long and short duration tests.

1 M Persulfate Diffusion in Palouse Loess

A concentration versus depth profile for the long-duration (149 days), 1 M persulfate treatment set is shown in Figure 7.4.1.1. Persulfate was detected throughout the column length with a minimum concentration of 0.04 M for the base-activated persulfate treatments and 0.16 M for the iron (III)-activated and persulfate-only treatments. Each treatment had a significantly different persulfate concentration at the end of the testing period ($p < 0.05$): iron (III)-activated persulfate had the lowest persulfate concentration and the persulfate-only treatment had the highest persulfate concentration.

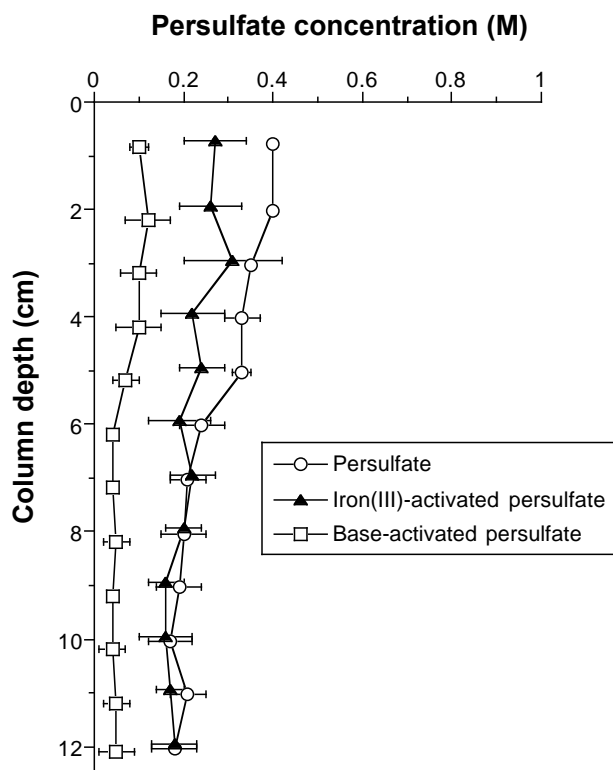


Figure 7.4.1.1. Concentration versus depth profile for diffusion of 1 M persulfate in Palouse loess at 149 days.

The short-duration treatment set (70 d) also showed persulfate diffusion throughout the entire length of each column (Figure 7.4.1.2). However, the concentration of the base-activated treatment approached undetectable levels after approximately 7 cm of transport. There was no significant difference in persulfate diffusion in the persulfate-only and iron (III)-activated treatments ($p > 0.05$), which reached a minimum concentration of approximately 0.15 M. The base-activated treatment was significantly different from the other treatments ($p < 0.05$).

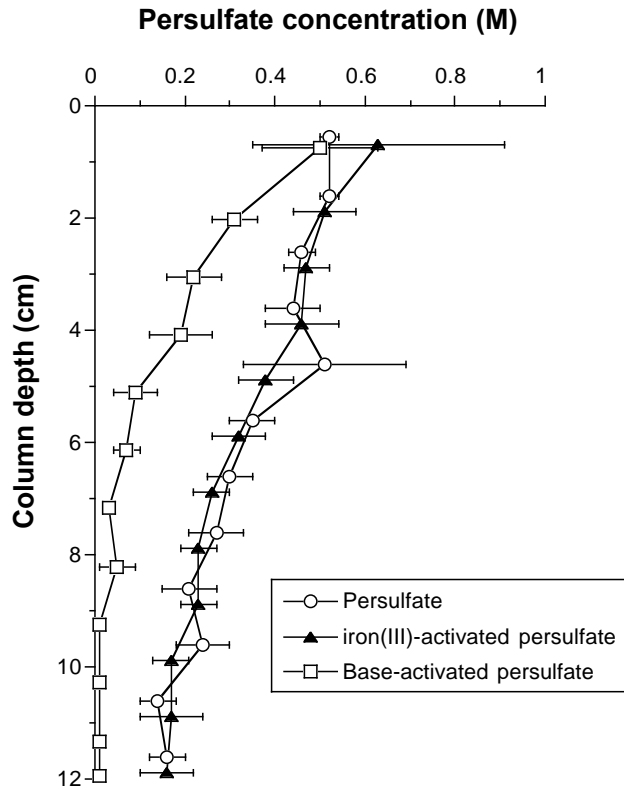


Figure 7.4.1.2. Concentration versus depth profile for diffusion of 1 M persulfate in Palouse loess at 70 days.

Figures 7.4.1.1 and 7.4.1.2 indicate that there are differences between the short and long-duration treatment sets. The results from the long-duration set showed a more uniform persulfate distribution through the columns, especially for the activated treatments. Furthermore, the minimum concentration of the base-activated treatment was higher in the long-duration set. There was no noticeable difference between minimum persulfate concentrations for the iron (III)-activated persulfate and persulfate-only treatments in the short and long duration tests.

0.1 M Persulfate Diffusion in Palouse Loess

No 0.1 M persulfate treatment diffused the full length of the Palouse loess columns over 131 d (Figure 7.4.1.3). The persulfate-only treatment diffused to a depth of approximately 8 cm compared to the iron (III)-activated treatment that diffused to approximately 4 cm. Figure 7.4.1.3 indicates that the base-activated treatment had a lower concentration in the top soil layer than the other treatments and it had a relatively uniform concentration distribution to a depth of approximately 6 cm. The persulfate concentration for each treatment was significantly different ($p < 0.05$).

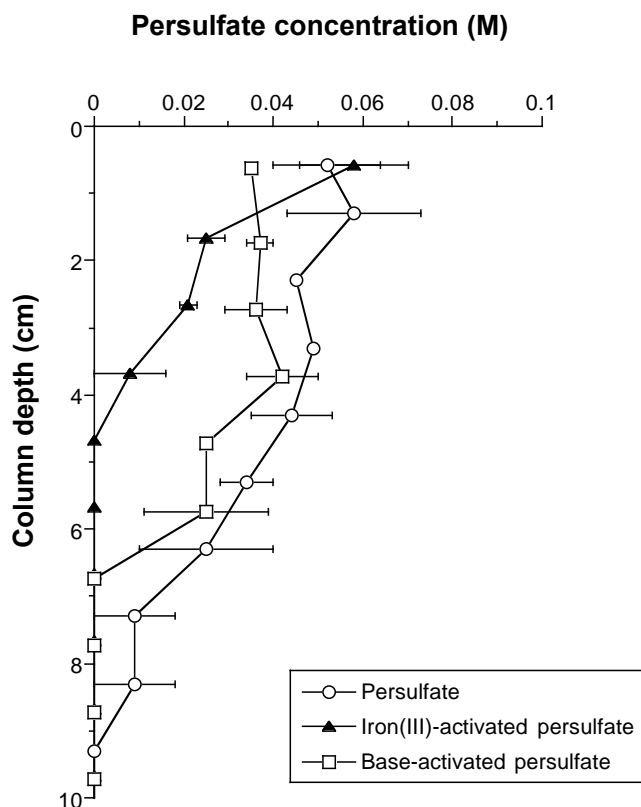


Figure 7.4.1.3. Concentration versus depth profile for diffusion of 0.1 M persulfate in Palouse loess at 131 days.

The short-duration diffusion test (Figure 7.4.1.4) indicated that there were significant differences between the persulfate-only and iron (III)-activated treatments ($p < 0.05$) at 85 d. There were no significant differences between the persulfate-only and base-activated treatments ($p > 0.05$) or the iron (III)-activated and base-activated persulfate treatments ($p > 0.05$). All treatments diffused to an approximate depth of 6 cm (Figure 7.4.1.4).

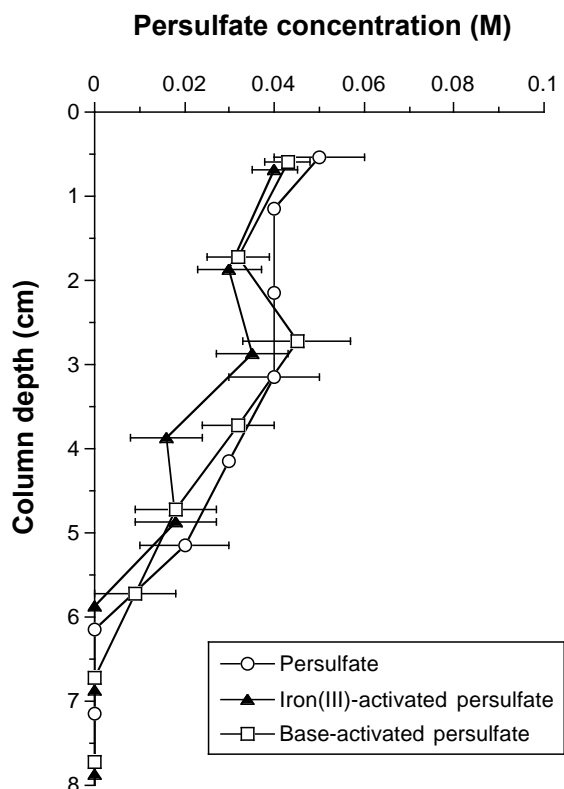


Figure 7.4.1.4. Concentration versus depth profile for diffusion of 0.1 M persulfate in Palouse loess at 85 days.

There was little difference in diffusion depth between the long and short-duration tests (Figures 7.4.1.3 and 7.4.1.4). Also, the depth of diffusion was similar for the activated persulfate treatments; however, the persulfate concentration of the base-activated treatment was higher at a depth of 6 cm in the long-duration test. The persulfate diffused farther into the columns in the persulfate-only treatment when the test duration was longer.

1 M Persulfate Diffusion in Kaolin

Test results indicated that the 1 M persulfate treatments diffused the entire length of the kaolin columns (Figure 7.4.1.5). The persulfate concentration between treatments was significantly different at the 95% confidence level. The base-activated treatment had the lowest concentration, followed by the persulfate-only treatment, and then the iron (III)-activated persulfate treatment.

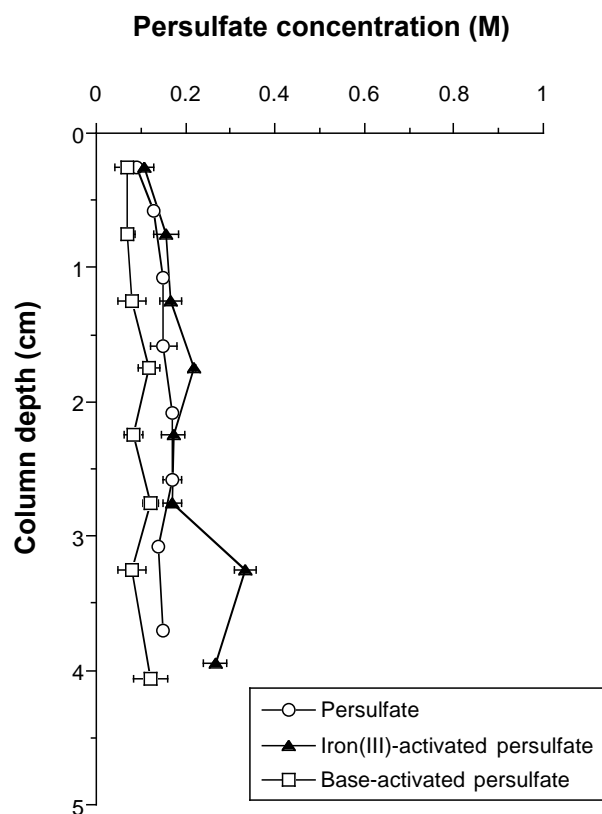


Figure 7.4.1.5. Concentration versus depth profile for diffusion of 1 M persulfate in kaolin at 81 days.

0.1 M Persulfate Diffusion in Kaolin

All of the 0.1M persulfate treatments diffused the full length of the kaolin columns and showed no significant difference in persulfate concentration between treatments at the 95% confidence level (Figure 7.4.1.6).

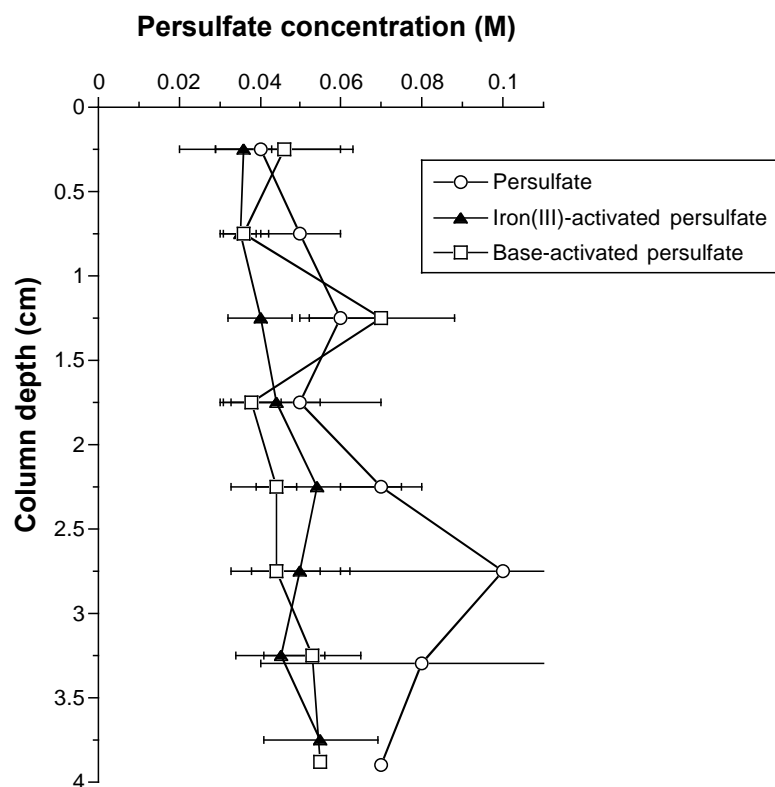


Figure 7.4.1.6. Concentration versus depth profile for diffusion of 0.1 M persulfate in kaolin at 82 days.

Conclusion

The potential for persulfate to diffuse into regions of low permeability was investigated in soil columns studies with two soil types: Palouse loess and kaolin. Initial persulfate concentrations of 1 M and 0.1 M were used to examine the difference in diffusion depths resulting from high and low concentrations. Three persulfate treatments, persulfate, iron (III)-activated persulfate, and base-activated persulfate, were tested.

Persulfate diffused into both soil types under each treatment condition. In addition, higher concentrations increased persulfate diffusion; all 1 M persulfate treatments diffused the full length of the columns, approximately 12 cm for the Palouse loess columns and approximately 4.5 cm for the kaolin columns. The 0.1 M treatment diffused the entire length of the kaolin columns and approximately 6 cm in the loess columns.

Diffusion increased with time and was not substantially hindered by persulfate decomposition. The minimum persulfate concentrations were similar for the iron (III)-activated persulfate and persulfate-only treatments at 70 d and 149 d. Furthermore, the minimum persulfate concentration for the base-activated treatment increased between 70 d and 149 d.

However, the concentration of base-activated persulfate (1 M) was lower throughout the columns compared to the other 1 M persulfate treatments.

The results of this research indicated that persulfate will diffuse into regions of low permeability, where it can potentially destroy contaminants of concern. Furthermore, persulfate diffusion increased with time and concentration, and was not significantly affected by persulfate decomposition.

8. CONCLUSIONS AND IMPLICATIONS FOR FUTURE RESEARCH/IMPLEMENTATION

Iron and manganese oxides can activate persulfate to generate reductants and oxidants; however, iron and manganese oxides in the most subsurface solids are not present in sufficient concentrations to activate persulfate.

Most trace minerals mediate the decomposition of persulfate, but do not promote the generation of reactive oxygen species. Three trace minerals, cobaltite, ilmenite, and pyrite, were found to promote the generation of reactive oxygen species. The majority of the naturally-occurring minerals evaluated do not activate persulfate to generate reactive oxygen species, and other mechanisms of activation are necessary to promote contaminant degradation in the subsurface.

Persulfate activation after base addition as the pH drifts from alkaline to circumneutral showed that hydroxyl radical activity was greatest in persulfate-soil slurries at pH 12 with decreasing hydroxyl radical activity in the systems in which the pH had drifted to pH 10 and pH 8.

Superoxide radical and reductant generation also occurred at all pH systems with lower rates as the pH drifted toward circumneutral, and reductant generation was greatest in soil systems with greater soil organic matter content. Therefore, base-activated persulfate may be more active than previously thought as the pH drifts towards neutral.

Iron (II)-EDTA and iron (III)-EDTA were equally effective for promoting persulfate decomposition and for generating sulfate radical and hydroxyl radical at circumneutral pH, while iron (III)-EDTA was a more effective activator than iron (II)-EDTA for generating reductants. Approximately 75% of the oxidation activity in both iron (II)-EDTA and iron (III)-EDTA activated persulfate systems was due to hydroxyl radical activity.

Minimal persulfate activation occurred in reactions conducted at pH 2 and 7, demonstrating that a low flux of reactants are generated at acidic or neutral pH regimes. In persulfate reactions at pH 12, sulfate and hydroxyl radical were generated but minimal reductants were produced. Scavenging studies showed that the dominant reactive species at basic pH was hydroxyl radical.

The generation of reductants increased at high base:persulfate molar ratios; however, hydroxyl radical generation rates increased only when molar ratios of base:persulfate were $> 3:1$. Hydroxyl radical is the dominant reactive oxygen species in base-activated persulfate formulations, and overall reactivity increases with increasing base:persulfate ratios.

A mechanism for the base activation of persulfate was proposed and confirmed involving the base-catalyzed hydrolysis of persulfate to hydroperoxide anion and sulfate followed by the reduction of another persulfate molecule by hydroperoxide. Reduction by hydroperoxide decomposes persulfate into sulfate radical and sulfate anion, and hydroperoxide is oxidized to superoxide.

Numerous phenoxides, including chlorophenoxides ranging from monochlorophenoxide to pentachlorophenoxide, were found to activate persulfate, with more rapid activation promoted by the more reduced phenoxides. Only the anionic form of phenols (phenoxide) is the activating species in persulfate systems. The proposed mechanism for phenoxide activation is through a reductive pathway, rather than nucleophilic attack on persulfate.

Four classes of organic compounds (ketones, keto acids, dicarboxylic acids, and tertiary alcohols) activate persulfate at high pH. The degree of activation was related to the functional group in the organic compound and its position within the structure. Keto acids were the most effective activator by degrading the hydroxyl radical probe nitrobenzene and the reductant probe hexachloroethane.

Soil organic matter activates persulfate under alkaline conditions to generate both oxidants and reductants. The activation is likely provided by phenoxide moieties associated with the soil organic matter. This pathway of persulfate activation is likely a dominant mechanism for contaminant destruction in soils and the subsurface.

Seven model contaminants (trichloroethylene, perchloroethylene, 1,1-dichloroethane, 1,1,1-trichloroethane, chlorophenol, pentachlorophenol, anisole) were degraded by activated persulfate. The molar ratio of base to persulfate had an effect on the degradation rate of two of the contaminants: 1,1-dichloroethane and trichloroethylene. The two more highly chlorinated aliphatic compounds, 1,1,1-trichloroethane and 1,1,1-trichloroethane, degraded at equal rates regardless of the basicity of the persulfate formulation.

No changes in mineralogy measured by x-ray diffraction were observed for kaolinite, hematite, and goethite in any of the persulfate systems. In contrast, changes in mineralogy were found for ferrihydrite in all persulfate systems with the exception of unactivated persulfate, in which no change in mineralogy occurred. Mineral structural changes also occurred in one of the birnessite-persulfate systems. The manganese oxide birnessite did not transform in the presence of deionized water, unactivated persulfate, or base-activated persulfate, but did transform in the presence of iron-EDTA-activated persulfate.

Hematite, goethite, and kaolinite showed minimal changes in surface area after treatment with persulfate formulations. Ferrihydrite showed a decrease in surface area, which was expected as it transformed from an amorphous high surface mineral to a more crystalline species. Birnessite surface area decreased slightly, which is expected when the mineral is in contact with more oxidizing conditions and becomes more crystalline. Montmorillonite showed significant decreases in surface areas with all persulfate treatments.

Activated persulfate promotes changes in the permeability of different soils, and these changes are dependent on the soil type and the persulfate formulations applied. In the presence of sand, unactivated persulfate and iron (III)-EDTA activated persulfate had minimal effect on permeability relative to the sulfate positive control; however, the application of base-activated persulfate resulted in significant decrease in hydraulic conductivity.

Changes in the hydraulic conductivity of kaolinite were only evident in base activated persulfate above 0.3 M. Such a dramatic increase (3.5 times) may significantly increase the

potential for treatment of contaminants in low permeability matrices of the subsurface. Similar results of increased hydraulic conductivity with increasing concentrations of base-activated persulfate were found in the natural soils evaluated.

Results of x-ray computed tomography demonstrated that changes in porosity were minimal in control samples, but all of the soils became highly heterogeneous with respect to porosity. Such wide ranging porosity can result in minimal potential to correlate soil porosity with hydraulic conductivity.

All persulfate formulations evaluated (unactivated, iron-chelate activated, and base activated) diffused significantly into clay and Palouse loess silty loams. In addition, higher persulfate concentrations increased persulfate diffusion; all 1 M persulfate treatments diffused the full length of the columns, approximately 12 cm for Palouse loess columns and approximately 4.5 cm for kaolin columns. The 0.1 M treatment diffused the entire length of the kaolin columns and approximately 6 cm in the loess columns.

Persulfate diffusion increased with time and was not substantially affected by persulfate decomposition. The minimum persulfate concentrations were similar for the iron (III)-activated persulfate and persulfate-only treatments over 70 d and 149 d.

9. LITERATURE CITED

- Afanas'ev, A.M., Okazaki, K., Freeman, G.R. 1979. Effect of solvation energy on electron reaction rates in hydroxylic solvents. *J. Phys. Chem.* 83, 1244–1249.
- Afanas'ev, I.B. 1989. Superoxide ion: chemistry and biological implications, vol. 1. CRC Press, Boca Raton, FL.
- Ahmad, M. 2008. Persulfate activation by major soil minerals. Thesis, Department of Civil and Environmental Engineering, Washington State University.
- Ahmad, M., Teel, A.L., Watts, R.J. 2010. Persulfate activation by subsurface minerals. *J. Contam. Hydrol.* In Press.
- Amrhein C., Alder, J.R. 2004. Can chemical oxidation improve the permeability of infiltration basins? *Water Environ. Res.* 76, 268.
- Anipsitakis, G.P., Dionysiou, D.D. 2004. Radical generation by the interaction of transition metals with common oxidants. *Environ. Sci. Technol.* 38, 3705-3712.
- Baker, W., Brown, N. 1948. The Elbs persulfate oxidation of phenols, and its adaptation to the preparation of monoalkyl ethers of quinols. *J. Chem. Soc.* 2303-2307.
- Ball, D.L., Edwards, J.O. 1956. The kinetics and mechanism of the decomposition of Caro's acid. *I. J. Am. Chem. Soc.* 78, 1125-1129.
- Barkan, E., Luz, B. 2003. High-precision measurements of $^{17}\text{O}/^{16}\text{O}$ and $^{18}\text{O}/^{16}\text{O}$ of O_2 and O_2/Ar ratio in air. *Rapid Commun. Mass Spectrom.* 17, 2809-2814.
- Behrman, E. 2006. The Elbs and Boyland-Sims peroxydisulfate oxidations. *J. Org. Chem.* 22 (2), 1-10.
- Berlin, A.A. 1986. Kinetics of radical-chain decomposition of persulfate in aqueous solutions of organic compounds. *Kinet. Catalysis.* 27, 34-39.
- Bernthsen, A. 1933. A textbook of organic chemistry. Blackie & Son Limited, London.
- Bissey, L.L., Smith, J.L., Watts, R.J. 2006. Soil organic matter–hydrogen peroxide dynamics in the treatment of contaminated soils and groundwater using catalyzed H_2O_2 propagations (modified Fenton's reagent). *Water Res.* 40(13), 2477-2484.
- Block, P.A. 2004. Comparison of activators for the destruction of organic compounds of concern by sodium persulfate. 3rd International Conference on Oxidative and Reductive Technologies for Environmental Remediation, San Diego, California.
- Block, P.A., Brown, R.A., Robinson, D. 2004. Novel activation technologies for sodium persulfate in situ chemical oxidation, the Fourth International Conference on the Remediation of Chlorinated and Recalcitrant Compounds, Monterey, CA, USA.
- Brown, K.W., Thomas, J.C. 1987. A mechanism by which organic liquids increase the hydraulic conductivity of compacted clay materials. *Soil Sci. Soc. Amer. J.* 51, 1451-1459.
- Brown, R.A. 2009. Director of Technology, Development, Environmental Research Management. Personal Communication .

- Brown, R.A., Robinson, D, Skladany, G. 2003. Response to naturally occurring organic material: permanganate versus persulfate. ConSoil, Ghent, Belgium.
- Brusseau, M.L., Jessup, R.E., Rao, P.S.C. 1990. Sorption kinetics of organic chemicals: evaluation of gas-purge and miscible-displacement techniques. *Environ. Sci. Technol.* 24, 727-735.
- Buxton, G.V., Greenstock, C.L., Helman, W.P., Ross, A.B. 1988. Critical review of rate constants for reactions of hydrated electrons, hydrogen atoms and hydroxyl radicals ($\bullet\text{OH}/\bullet\text{O}^-$) in aqueous solution. *J. Phys. Chem. Ref. Data* 17, 513-531.
- Caregnato, P., David, P. M., Gara, D., Bosio, G., Gonzalez, M., Russo, N., Michelini, M., Martire, D. 2008. Theoretical and Experimental Investigation on the Oxidation of Gallic Acid by Sulfate Radical Anions. *J. Phys. Chem. A* 112, 1188-1194.
- Carter, D.L., Mortland, M.M., Kemper, W.D. 1986. Specific surface. *Methods of soil analysis. part 1: physical and mineralogical methods*, A. Klute ed., American Society of Agronomy and Soil Science Society of America, Madison, WI, 413-423.
- Chao, T.T. 1972. Selective dissolution of manganese oxides from soils and sediments with acidified hydroxylamine hydrochloride. *Soil Sci. Soc. Am. Proc.* 36, 764-768.
- Chen, G., Hoag, G.E., Chedda, P., Nadim, F., Woody, B.A., Dobbs, G.M. 2001. The mechanism and applicability of in situ oxidation of trichloroethylene with Fenton's reagent. *J. Hazard. Mater.* B87 171-186.
- Chlorinated Ethene: DNAPL source zones. 2008. BioDNAPL-3. Washington, D.C.: Interstate Technology & Regulatory Council, Bioremediation of DNAPLs Team.
- Clesceri, L.S. 1989. Standard methods for the examination of water and wastewater, American Public Health Association: Washington, DC.
- Clifton, C.L., Huie, R.E. 1989. Rate constants for hydrogen abstraction reactions of the sulfate radical, $\text{SO}_4^{\cdot-}$ alcohols. *Int. J. Chem. Kinet.* 21, 677-687.
- Cohen, I., Purcell, T. 1967. Spectrophotometric determination of hydrogen peroxide with 8-quinolinol. *Anal. Chem.* 39, 131-132.
- Corbin, J.F., Teel, A.L., Allen-King, M., Watts, R.J, 2007. Reactive oxygen species responsible for the enhanced desorption of dodecane in modified Fenton's systems. *Water Environ. Res.* 79 (1), 37-42.
- Cotton, T.E., Davis, M.M., Shackelford, C.D. 1998. Effects of test duration and specimen length on diffusion testing of unconfined specimens. *Geotech. Test J.* 21, 79-94.
- Couttenye, R.A., Huang, K.C., Hoag, G.E., and Suib, S.L. 2002. Evidence of sulfate free radical ($\text{SO}_4^{\cdot-}$) formation under heat-assisted persulfate oxidation of MtBE. In: *Proceedings of the 19th Petroleum Hydrocarbons and Organic Chemicals in Ground Water: Prevention, Assessment, and Remediation, Conference and Exposition*, Atlanta, GA, November 5-8. pp. 345-350.
- Crimi, M.L., Siegrist, R.L. 2005. Factors affecting effectiveness and efficiency of DNAPL destruction using potassium permanganate and catalyzed hydrogen peroxide. *J. Environ. Eng.* 131, 1724-1732.

- Crooks, V.E., Quigley, R.M. 1984. Saline leachate migration through clay: a comparative laboratory and field investigation. *Can. Geotech. J.* 21, 349-362.
- D'Oliveira, D., Minero, C., Pelizzetti, E., Pichart, P. 1993. Photodegradation of dichlorophenols and trichlorophenols in TiO₂ aqueous suspensions: kinetic effects of the positions of the Cl atoms and identification of the intermediates. *J. Photochem. Photobiol. A: Chem.* 72, 261-267.
- Dahmani, M.A., Huang, K., Hoag, G. E. 2006. Sodium persulfate oxidation for the remediation of chlorinated solvents (USEPA Superfund Innovative Technology Evaluation Program) *Water Air Soil Pollut. Focus* 6(1-2), 127-141.
- Das, K.C., Misra, H.P. 2004. Hydroxyl radical scavenging and singlet oxygen quenching properties of polyamines. *Mol. Cell. Biochem.* 262, 127-133.
- David-Gara, P., Bosio, G., Gonzalez, M., Martire, D. 2008. Kinetics of the sulfate radical-mediated photo-oxidation of humic substances. *Int. J. Chem. Kinet.* 40 (1), 19-24.
- Davies, M. J., Gilbert, B.C., Stell, J.K., Whitwood, A.C. 1992. Nucleophilic substitution reactions of spin adducts. Implications for the correct identification of reaction intermediates by EPR/spin trapping. *J. Chem. Soc., Perkin Trans. 2*, 333-335.
- Davies, M., Gilbert, B., Thomas, B., Young, J. 1985. Electron spin resonance studies. Part 69. oxidation of some aliphatic carboxylic acids, carboxylate anions, and related compounds by the sulfate radical anion (SO₄^{•-}). *J. Chem. Soc., Perkin Trans. 2*, 1199 - 1204.
- Dogliotti, L., Hayon, E. 1967. Flash photolysis of persulfate ions in aqueous solutions. Study of the sulfate and ozonide radical anions. *J. Phys. Chem.* 71 (8), 2511-2516.
- Droste, E., Marley, M., Parikh, J., Lee, A., Dinardo, P., Bernard, W., Hoag, G., Chheda, P. 2002. Proceedings of the Third International Conference on Remediation of Chlorinated and Recalcitrant Compounds, May 20-23, Monterey, CA, 1107-1114.
- Ebersson, L. 1987. Electron transfer reactions in organic chemistry. Springer-Verlag, Berlin.
- Eisenberg, G.M. 1943. Colorimetric determination of hydrogen peroxide. *Ind. Eng. Chem. Anal. Ed.* 15, 327-328.
- Elbenberger, H., Steenken, S., O'Neill, P., Schulte-Frohlinde, D. 1978. Pulse radiolysis and electron spin resonance studies concerning the reaction of SO₄^{•-} with alcohols and ethers in aqueous solution. *J. Phys. Chem.* 82,749-750.
- England, W.A., Mackenzie, A.A. 1987. The movement and entrapment of petroleum fluids in the subsurface. *J. Geol. Soc., London* 144, 327-347.
- EPA. 2006. Research on Chemical Oxidation/In-situ Chemical Oxidation. <http://www.epa.gov/ada/topics/oxidation.html>.
- Finkelstein, E., Rosen, G.M., Rauckman, E.J. 1980. Spin trapping. Kinetics of the reaction of the superoxide and hydroxyl radicals with nitrones. *J. Am. Chem. Soc.* 102, 4994-4999.
- Freeze, R.A., Cherry, J.A. 1979. Groundwater. Prentice-Hall, Englewood Cliffs, N.J.
- Furman, O. 2009. Reactivity of oxygen species in homogenous and heterogeneous aqueous environments. PhD Dissertation, Department of Civil and Environmental Engineering, Washington State University.

- Furman, O.S., Teel, A.L., Watts, R.J. 2010. Mechanism of base activation of persulfate. Environ. Sci. Technol. Under review.
- Furman, O., Laine, D.F., Blumenfeld, A., Teel, A. L., Shimizu, K., Cheng, I.F., Watts, R.J. 2009a. Enhanced reactivity of superoxide in water-solid matrices. Environ. Sci. Technol. 43(5), 1528-1533.
- Furman, O., Teel, A.L., Watts, R.J. 2010. Effect of basicity on persulfate reactivity. J. Environ. Eng. In press.
- Gee, B.W., Bauder, J.W. 1986. Particle size analysis in: A. Klute (Ed), Methods of soil analysis, part 1. physical and mineralogical methods, American Society of Agronomy, Madison, WI, p. 399.
- George, C., El Rassy, H., Chovelon, J. 2001. Reactivity of selected volatile organic compounds (VOCs) toward the sulfate radical ($\text{SO}_4^{\cdot-}$). Int. J. Chem. Kinet. 33, 539-547.
- Georgi, A., Schierz, A., Kopinke, F.D. 2006. Activation of hydrogen peroxide by complexes of iron(III) with humic acid for chemical degradation of organic compounds in water. Proceeding of the EAAOP Conference (Environmental Applications of Advanced Oxidation Processes), Chania, Greece, September 7–9.
- Haag, W.R., Yao, C.C.D. 1992. Rate constants for reaction of hydroxyl radicals with several drinking water contaminants. Environ. Sci. Technol. 26, 1005-1013.
- Hakoila, E. 1963. Ann. Univ. Turku., Ser A, 66.
- Hamdi, N., Della, M. 2005. Experimental study of the permeability of clays from the potential sites for acid effluent storage. Desalination 185, 523-534.
- Hammar, A.D. 2004. Measurement and characterization of clay microstructure under one-dimensional compression. Master's thesis. Washington State University.
- Hasan, M.A., Zaki, M.I., Pasupulety, L., Kurmari, K. 1999. Promotion of the hydrogen peroxide decomposition activity of manganese oxide catalysts. Appl. Catal. A. 181, 171-179.
- Hayon, E., McGarvey, J.J. 1967. Flash photolysis in the vacuum ultraviolet region of sulfate, carbonate, and hydroxyl ions in aqueous solutions. J. Phys. Chem. 71(5), 1472-1477.
- Hayon, E., Treinin, A., Wilf, J. 1972. Electronic spectra, photochemistry, and autoxidation mechanism of the sulfite-bisulfite-pyrosulfite systems. The $\text{SO}_2^{\cdot-}$, $\text{SO}_3^{\cdot-}$, $\text{SO}_4^{\cdot-}$, and $\text{SO}_5^{\cdot-}$ radicals. J. Am. Chem. Soc. 1972, 94, 47-57.
- Hong, C.S., Davis, M.M., Shackelford, C.D. 2009. Non-reactive solute diffusion in unconfined and confined specimens of a compacted soil. Waste Manage., 29, 404-417.
- House, D.A. 1962. Kinetics and mechanism of oxidations by peroxydisulfate. Chem. Rev. 62, 185-203.
- Houston, P.L. 2006. Chemical kinetics and reaction dynamics, Dover Publications: Mineola, NY.
- Huang, H.H., Lu, M.C., Chen, J.N. 2001. Catalytic decomposition of hydrogen peroxide and 2-chlorophenol with iron oxides. Water Res. 35 (9), 2291-2299.
- Huang, K.C., Couttenye, R.A., Hoag, G. H. 2002. Kinetics of heat-assisted persulfate oxidation of methyl tert-butyl ether (MTBE). Chemosphere 49, 413-420.

- Huang, K.C., Zhao, Z., Hoag, G.E., Dahmani, A., Block, P.A. 2005. Degradation of volatile organic compounds with thermally activated persulfate oxidation. *Chemosphere* 61, 551-560.
- Huling, S.G., Pivetz, B.E. 2006. In-situ chemical oxidation. United States Environmental Protection Agency.
- Interstate Technology Regulatory Council., (ITRC) 2005. Overview of groundwater remediation technologies for MTBE and TBA.
- Jackson, M.L., Lim, C.H., Zelazny, L.W. 1986. In: A. Klute et al. (Eds.), *Methods of soil analysis, Part 1: Physical and mineralogical methods*. American Society of Agronomy and Soil Science Society of America, Madison, WI, p. 124
- Kao, C.M., Chien, H.Y., Surampalli, R.Y., Chien, C.C., Chen, C.Y. 2010. Assessing of natural attenuation and intrinsic bioremediation rates at a petroleum-hydrocarbon spill site: laboratory and field sites. *J. Environ. Eng.*, 136, 54-67.
- Keszler, A., Kalyanaraman, B., Hogg, N. 2003. Comparative investigation of superoxide trapping by cyclic nitron spin traps: the use of singular value decomposition and multiple linear regression analysis. *Free Radical Biol. Med.* 35, 1149-1157.
- Khan, M.A.J., Watts, R.J. 1996. Mineral-catalyzed peroxidation of perchloroethylene. *Water Air Soil Pollut.* 88, 247-260.
- Killian, P.F., Bruell, C.J., Liang, C.J., Marley, M.C. 2007. Iron (II) Activated persulfate oxidation of MGP contaminated soil. *Soil Sed. Contam.* 16, 523-537.
- Kirino, Y., Ohkuma, T., Kwan, T. 1981. Spin trapping with 5,5-dimethylpyrroline-N-oxide in aqueous solution. *Chem. Pharm. Bull.* 29, 29-34.
- Kolthoff, I.M., Belcher, R. 1957. *Volumetric analysis, volume III, Titration methods: oxidation-reduction reactions*, John Wiley & Sons, Inc., New York.
- Kolthoff, I.M., Medalia, A.I., Raaen, H.P. 1951. The reaction between ferrous iron and peroxides. IV. Reaction with potassium persulfate. *J. Amer. Chem. Soc.* 73(4), 1733-1739.
- Kolthoff, I.M., Miller, J.K. 1951. The chemistry of persulfate: I. The kinetics and mechanism of the decomposition of the persulfate ion in aqueous medium. *J. Am. Chem. Soc.* 73, 3055-3059.
- Kolthoff, I.M., Stenger, V.A. 1947. *Volumetric analysis, second ed. Vol. I: Theoretical fundamentals. Vol. II: Titration methods: acid-base, precipitation and complex reactions*. Interscience Publishers Inc., New York.
- Koubek, E., Levey, G., Edwards, J.O. 1964. An isotope study of the decomposition of Caro's acid. *Inorg. Chem.* 3, 1331-1332.
- Kwan, C.Y., Chu, W. 2007. The role of organic ligands in ferrous-induced photochemical degradation of 2,4-dichlorophenoxyacetic acid. *Chemosphere* 67, 1601-1611.
- Kwan, W.P., Voelker, B.M. 2003. Rates of hydroxyl radical generation and organic compound oxidation in mineral-catalyzed Fenton-like systems. *Environ. Sci. Technol.* 37(60), 1150-1158.

- Larson, R.A. Weber, E.J. 1994. Reaction mechanisms in environmental organic chemistry, Lewis Publishers, Inc, Chelsea, Michigan.
- Latimer, W.M. 1952. Oxidation Potentials. Prentice-Hall, Inc., Englewood Cliffs, NJ.
- Ledwith, A., Russell, P. J., Sutcliffe, L.H. 1971. Cation Radicals: formation of methoxy-radicals by photochemical and thermal oxidation of methanol. Chem. Commun. 964-965.
- Li X.D., Schwartz, F.W. 2004. DNAPL mass transfer and permeability reduction during in-situ chemical oxidation with permanganate. Geophys. Res. Lett. 31, L06504.
- Liang, C.J. Lee, I.-L. 2008. In situ iron activated persulfate oxidative fluid sparging treatment of TCE contamination — A proof of concept study. J. Contam. Hydrol. 100, 91–100.
- Liang, C.J., Bruell, C J. 2008. Thermally activated persulfate oxidation of trichloroethylene: experimental investigation of reaction orders. Ind. Eng. Chem. Res. 47, 2912–2918.
- Liang, C.J., Bruell, C.J., Marley, M.C., Sperry, K.L. 2003. Thermally activated persulfate oxidation of trichloroethylene (TCE) and 1,1,1-trichloroethane (TCA) in aqueous systems and soil slurries. Soil Sediment Contam. 12 (2), 207–228.
- Liang, C.J., Bruell, C.J., Marley, M.C., Sperry, K.L. 2004a. Persulfate oxidation for in situ remediation of TCE. I. Activated by ferrous ion with and without a persulfate-thiosulfate redox couple. Chemosphere 55, 1213–1223.
- Liang, C.J., Bruell, C.J., Marley, M.C., Sperry, K.L. 2004b. Persulfate oxidation for in situ remediation of TCE. II. Activated by chelated ferrous ion. Chemosphere 55, 1225–1233.
- Liang, C.J., Liang, C.-P., Chen, C.-C. 2009. pH dependence of persulfate activation by EDTA/Fe(III) for degradation of trichloroethylene. J. Contam. Hydrol., 106, 173–182
- Liang, C.J., Su, H.-W. 2009. Identification of sulfate and hydroxyl radicals in thermally activated persulfate. Ind. Eng. Chem. Res. 48, 5558–5562.
- Liang, C.J., Wang, Z.-S., Bruell, C.J. 2007. Influence of pH on persulfate oxidation of TCE at ambient temperatures. Chemosphere 66, 106–113.
- Liang, C.J., Huang, C.F., Yan-Jyun Chen, Y.J. 2008a. Potential for activated persulfate degradation of BTEX contamination. Water Res. 42, 4091–4100.
- Liang, C.J., Lee, I.-L., Hsu, I.-Y., Liang, C.-P., Lin, Y.-L. 2008b. Persulfate oxidation of trichloroethylene with and without iron activation in porous media. Chemosphere 70, 426–435.
- Lighty, J.S., Silcox, G.D., Pershing, D.W. 1990. Fundamentals for the thermal remediation of contaminated soils. particle and bed desorption models. Environ. Sci. Technol. 24, 750-757.
- Linde D.R., editor, 2009. CRC Handbook of chemistry and physics [Internet]. London: Taylor & Francis, c2009 [cited 2009 Jun 16], [about 10 screens]. Available from: <http://www.hbcpnetbase.com/>
- Lipczynska-Kochany, E. 1992. Degradation of nitrobenzene and nitrophenol in homogeneous aqueous solution. direct photolysis versus photolysis in the presence of hydrogen peroxide and the Fenton reagent. Water Pollut. Res. J. Can. 27, 97–122.

- Lunenok-Burmakina, V.A., Aleeva, G.P. 1972. Mechanism of the decomposition of peroxomonosulphates and peroxomonophosphates in alkaline aqueous solution. *Russ. J. Phys. Chem.* 46, 1591-1592.
- Ma, K.S., Pierre, A.C. 1997. Effect of interaction between clay particles and Fe^{3+} ions on colloidal properties of kaolinite suspensions. *Clays Clay Min.* 45(5), 733-744.
- Ma, K.S., Pierre, A.C. 1999. Clay sediment-structure formation in aqueous kaolinite suspensions. *Clays Clay Min.* 47(4), 522-526.
- Mabey, W., Mill, T. 1978. Critical review of hydrolysis of organic compounds in water under environmental conditions. *J. Phys. Chem. Ref. Data* 7, 383-415.
- Madigan, M.T., Martinko, J.M., Parker, J. 1997. *Brock biology of microorganisms*. Prentice Hall, NJ.
- Manahiloh, K.N. 2010. Evaluation of clogging through scanning of field samples. In Preparation.
- Marlier, J.F., Dopke, N.C., Johnstone, K.R., Wirdzig, T.J. 1999. A heavy-atom isotope effect study of the hydrolysis of formamide. *J. Am. Chem. Soc.* 121, 4356-4363.
- Maruthamuthu, P., Neta, P. 1977. Reactions of phosphate radicals with organic compounds. *J. Phys. Chem.*, 81, 1622-1625.
- Masel, R.I. 2001. *Chemical kinetics and catalysis*, Wiley, Inc., New York.
- McBride, M.B., 1994. *Environmental chemistry of soils*. Oxford university press, New York. 240-242.
- McKeague, J.A., Day, J.H. 1966. Dithionite- and oxalate-extractable Fe and Al as aids in differentiating various classes of soils. *Can. J. Soil Sci.* 46, 13-22.
- McKenzie, R.M. 1971. The synthesis of birnessite, cryptomelane, and some other oxides and hydroxides of manganese. *Mineralogical Mag.* 38, 493-502.
- Mees F., Swennen, R. 2003. Applications of X-ray computed tomography in the geosciences. *Geol. Soc.* 215, 1-6.
- Merz, J.H., Waters, W.A. 1949. The oxidation of aromatic compounds by means of the free hydroxyl radicals. *J. Chem. Soc.* 2427-2433.
- Metelitsa, D.I. 1971. Mechanisms of the hydroxylation of aromatic compounds. *Russ. Chem. Rev.* 40, 563 – 579.
- Miller, C.M., Valentine, R.L. 1995. Hydrogen peroxide decomposition and quinoline degradation in the presence of aquifer material. *Water Res.* 29, 2353-2359.
- Miller, C.M., Valentine, R.L. 1999. Mechanistic studies of surface catalyzed H_2O_2 decomposition and contaminant degradation in the presence of sand. *Water Res.* 33, 2805-2816.
- Minisci, F., Citterio, A., Giordano, C. 1983. Electron-transfer processes: peroxydisulfate, a useful and versatile reagent in organic chemistry. *Acc. Chem. Res.* 16, 27-32.
- Monig, J., Bahnemann, D., Asmus, K.-D. 1983. One electron reduction of CCl_4 in oxygenated aqueous solutions: a CCl_3O_2 -free radical mediated formation of Cl^- and CO_2 . *Chem. Biol. Interact.* 47, 15-27.

- Murphy, A.P., Boegli, W.J., Price, M.K., Moody, C.D. 1989. A Fenton-like reaction to neutralize formaldehyde waste solutions. *Environ. Sci. Technol.* 25, 166-169.
- Myrand, D., Gillham, R.W., Sudicky, E.A., O'Hannesin, S.F., Johnson, R.L. 1992. Diffusion of volatile organic compounds in natural clay deposits. *J. Contam. Hydrol.* 10, 159-177.
- Nadim, F., Huang, K., Dahmani, A. 2006. Remediation of soil and ground water contaminated with PAH using heat and Fe(II)-EDTA catalyzed persulfate oxidation. *Water Air Soil Pollut. Focus* 6, 227-232.
- Nebe, J., Baldwin, B.R., Kassab, R.L., Nies, L., Nakatsu, C.H. 2009. Quantification of aromatic oxygenase genes to evaluate enhanced *bioremediation* by oxygen releasing materials at a gasoline-contaminated site. *Environ. Sci. Technol.* 43, 2029–2034.
- Neta, P., Hule, R.E., Ross, A.B. 1988. Rate constants for reactions of inorganic radicals in aqueous solution. *J. Am. Chem. Soc.* 110 (3), 1027-1284.
- Neta, P., Madhavan V., Zemel H., Fessenden R. 1977. Rate constants and mechanism of reaction of sulfate radical anion with aromatic compounds. *J. Am. Chem. Soc.* 99, 163-164.
- Norman, R., Storey, P.M., West, P.R. 1970. Electron spin resonance studies. Part XXV. Reactions of the sulphate radical anion with organic compounds. *J. Chem. Soc. (B)* 1970, 1087-1095.
- O'Neill, P., Steenken, S., Schulte-Frohlinde, D. 1975. Formation of radical cations of methoxylated benzenes by reaction with OH radicals, Ti^{2+} , Ag^{2+} , and $SO_4^{\cdot-}$ in aqueous solution. An optical and conductometric pulse radiolysis and in situ radiolysis electron spin resonance study. *J. Phys. Chem.* 79(25), 2773–2779.
- Ocampo, A.M. 2009. Persulfate activation by organic compounds. Ph.D. Dissertation, Washington State University.
- Ocampo, A., Teel, A., Vaughn, R., Watts, R., Brown, R., Block, P. 2007. Persulfate activation by phenoxide derivatives. oxidation and reduction technologies for in-situ treatment of soil and groundwater (ORTs-6) conference. Niagara Falls, New York.
- Ogram, A.N., Jessup, R.E., Ou, L.T., Rao, P.D.C. 1985. Effects of sorption on biological degradation of 2,4-dechlorophenoxy acetic acid in soils. *Appl. Environ. Microbiol.* 49(3), 582-587.
- Ossadnik, S., Schwedt, G. 2001. Comparative study of the determination of peroxomonosulfate, in the presence of other oxidants, by capillary zone electrophoresis, ion chromatography, and photometry. *Fresenius J. Anal. Chem.* 371, 420-424.
- Padmaja, S., Alfassi, Z. B., Neta, P., Huie, R.E. 1993. Rate constants for reactions of $SO_4^{\cdot-}$ radicals in acetonitrile. *Int. J. Chem. Kinet.* 25, 193–198.
- Pankow, J.F., Cherry, J.A. 1996. Dense chlorinated solvents and other DNAPLs in groundwater, Waterloo Press, Portland, Oregon.
- Perret, J., Prasher, S.O. 1999. Three-dimensional quantification of macropore networks in undisturbed soil cores. *Soil Sci. Soc. Amer. J.* 63, 1530-1543.
- Perrin, D.D., Dempsey, B., Serjeant, E.P. 1981. pKa predictions for organic acids and bases. Chapman and Hall, New York.

- Peyton, G.P. 1993. The free-radical chemistry of persulfate-based total organic carbon analyzers. *Marine Chem.* 41, 91-103.
- Piechowski, M., Nauser, T., Hoigne, J., Buhler, R. 1993. O₂- decay catalyzed by Cu²⁺ and Cu⁺ ions in aqueous solutions: a pulse radiolysis study for atmospheric chemistry. *Ber. Bunsenges. Phys. Chem.* 6, 762-771.
- Pignatello, J.J., Day, M. 1996. Mineralization of methyl parathion insecticide in soil by hydrogen peroxide activated with iron(III)-NTA or HEIDA complexes. *Hazard. Waste Hazard. Mater.* 13, 237-244.
- Qafoku, N.P., Qafoku, O. 2007. Fe-solid phase transformations under highly basic conditions. *Appl. Geochem.* 22, 2054-2064.
- Quan, H. N., Teel, A. L., Watts, R. J. 2003. Effect of contaminant hydrophobicity on H₂O₂ dosage requirements in the Fenton-like treatment of soils. *J. Hazard. Mater.* 102(2-3), 277-289.
- Robinson, W.O. 1927. The determination of organic matter in soils by means of hydrogen peroxide. *J. Agric. Res.* 34, 339-356.
- Root, D.K., Lay, E.M., Block, P.A., Cutler, W.G. 2005. Investigation of chlorinated methanes treatability using activated sodium persulfate, the First International Conference on Environmental Science and Technology, New Orleans, Louisiana, USA.
- Roso, J.A., Allegretti, P.E., Martire, D., Gonzalez, M. 1999. Reaction of sulfate and phosphate radicals with α - α - α -trifluorotoluene. *J. Chem. Soc., Perkin Trans 2*, 205-210.
- Rowe, R.K., Caers, C.J., Barone, F. 1988. Laboratory determination of diffusion and distribution coefficients of contaminants using undisturbed clayey soil. *Can. Geotech. J.*, 25, 108-118.
- SAS 2003. The SAS system for Windows, Release 9.1. SAS Institute, Cary, NC.
- Schumb, W.C., Satterfield, C.N., Wentworth, R.L. 1955. Hydrogen Peroxide, ACS Monograph 128, American Chemical Society: Washington, DC.
- Scott, D., McKnight, D., Blunt-Harris, E.L., Kolesar, S.E., Lovley, D.R. 1998. Quinones moieties act as electron acceptors in the reduction of humic substances by humic-reducing microorganisms. *Environ. Sci. Technol.* 32, 2984-2989.
- Sedlak, D.L., Andren, A.W. 1994. The effect of sorption on the oxidation of polychlorinated biphenyls (PCBs) by hydroxyl radical. *Water Res.* 28(5), 1207-1215.
- Selvararani, S., Medona, B., Ramachandran, M.S. 2005. Studies on the ketone-catalyzed decomposition of caroate in aqueous alkaline medium. *Int. J. Chem. Kinet.* 37, 483-488.
- Sethna, S.M. 1951. The Elbs persulfate oxidation. *Chem. Rev.* 49 (1), 91-101
- Shackelford, C.D., Daniel, D.E., Liljestrand, H.M. 1989. Diffusion of inorganic chemical species in compacted clay soil. *J. Contam. Hydrol.* 4, 241-273.
- Shackelford, C.D. 1991. Laboratory diffusion testing for waste disposal – a review. *J. Contam. Hydrol.* 7, 177-217.
- Sheeran, D.E., Krizek, R.J. 1971. Preparation of homogeneous soil samples by slurry consolidation. *J. Hazard. Mater.* 6, 356-373.

- Sheldon, R.A., Kochi, J.K. 1981. Metal-catalyzed reactions of organic compounds: mechanistic principles and synthetic methodology including biochemical processes, Academic Press: New York, NY.
- Siegrist, R.L., Urynowicz, M.A., West, O.R., Crimi, M.L., Lowe, K.S. 2001. Principles and practices of in situ chemical oxidation using permanganate, Battelle Press, Columbus, OH.
- Siegrist, R.L., Urynowicz, M.A., Crimi, M.L., Lowe, K.S. 2002. Genesis and effects of particles produced during in situ chemical oxidation using permanganate. *J. Environ. Eng.* 128 (11), 1068-1079.
- Singh, U. C., Venkatarao, K. 1976. Decomposition of peroxodisulphate in aqueous alkaline solution. *J. Inorg. Nucl. Chem.* 38, 541-543.
- Slebocka-Tilk, H., Neverov A.A., Brown, R.S. 2003. Proton inventory study of the base-catalyzed hydrolysis of formamide. Consideration of the nucleophilic and general base mechanisms. *J. Am. Chem. Soc.* 125, 1851-1858.
- Smith, B., Teel, A.L., Watts, R.J. 2004. Identification of the species responsible for the degradation of carbon tetrachloride by modified Fenton's reagent. *Environ. Sci. Technol.* 38, 5465-5469.
- Smith, B.A., Teel, A.L., Watts, R.J. 2006. Mechanism for the destruction of carbon tetrachloride and chloroform DNAPLs by modified Fenton's reagent. *J. Contam. Hydrol.* 85(3-4), 229-246.
- Sommeling, P., Mulder, P., Louw, R., Avila, D., Luszyk, J., Ingold, K. 1993. Rate of reaction of phenyl radicals with oxygen in solution and in the gas phase. *J. Phys. Chem.* 97 (32), 8361-8363.
- Staehelin, J., Hoigné, J. 1982. Decomposition of ozone in water—rate of initiation by hydroxide ions and hydrogen peroxide. *Environ. Sci. Technol.* 16, 676-681.
- Steliga, T., Kapusta, P., Jakubowicz, P. 2009. Effectiveness of bioremediation processes of hydrocarbon pollutants in weathered drill wastes. *Water Air Soil Pollut.* 202, 211-228.
- Stenuit, B., Eyers, L., Schuler, L., Agathos, S.N., George, I. 2008. Emerging high-throughput approaches to analyze bioremediation of sites contaminated with hazardous and/or recalcitrant wastes. *Biotechnol. Adv.* 26, 561-575.
- Stumm, W., Morgan, J.J. 1996. Aquatic chemistry. Wiley-Interscience, New York.
- Sun, Y., Pignatello, J.J. 1992. Chemical treatment of pesticide wastes. Evaluation of Fe(III) chelates for catalytic hydrogen peroxide oxidation of 2,4-D at circumneutral pH. *J. Agric. Food Chem.* 40(2), 322-327.
- Suthersan, S.S. 1997. Remediation engineering: design concepts, Lewis Publishers: Boca Raton, FL.
- Teel, A.L., Watts, R.J. 2002. Degradation of carbon tetrachloride by Fenton's reagent. *J. Hazard. Mater.* 94, 179-189.
- The SAS system for Windows, 2003. Release 9.1., SAS Institute: Cary, NC,

- Todres, Z.V. 2003. Organic ion radicals. chemistry and applications. Marcel Dekker, Inc. New York.
- Trantnyek, P.G., Waldemer, R.H. 2006. Kinetics of contaminant degradation by permanganate. *Environ. Sci. Technol.* 40(3), 1055-1061.
- Tsai, T.T., Kao, C.M., Yeh, T.Y., Lee, M.S. 2008. Chemical oxidation of chlorinated solvents in contaminated groundwater: review. *Pract. Period. Hazard., Toxic, Radioact. Waste Manage.*, 12, 116-126.
- U.S. DOE 1999. Innovative technology summary report: Fenton's reagent (DOE/EM-0484), Office of Science and Technology: Washington, D.C.
- U.S. Soil Conservation Service. 1972. Soil survey investigation: Report 1. U.S. Government Printing Office, Washington, DC.
- Valentine, R.L., Wang, H.C.A. 1998. Iron oxide surface catalyzed oxidation of quinoline by hydrogen peroxide. *J. Environ. Eng.* 127(1), 31-38.
- Wahba, N., El Asmar, M.F., El Sadr, M.M. 1959. Iodometric method for determination of persulfates. *Anal. Chem.* 31 1870-1871.
- Waldemer, R.H., Trantnyek, P.G., Johnson, R.L., Nurmi, J. 2007. Oxidation of chlorinated ethenes by heat-activated persulfate: kinetics and products. *Environ. Sci. Technol.* 41, 1010-1015.
- Walkley A., Black I. A. 1934. An examination of the Degtjareff method for determining soil organic matter and a proposed modification of the chromic acid titration method. *Soil Sci.* 37, 29-38.
- Watts, R.J., 1998. Hazardous wastes: sources, pathways, receptors. John Willey and Sons, New York.
- Watts, R.J., Bottenberg, B.C., Hess, T.F., Jensen, M.D., Teel, A.L. 1999. Role of reductants in the enhanced desorption and transformation of chloroaliphatic compounds by modified Fenton's reactions. *Environ. Sci. Technol.* 33, 3432-3437.
- Watts, R.J., Dilly, S.E. 1996. Evaluation of iron catalysts for the Fenton-like remediation of diesel-contaminated soils. *J. Hazard. Mater.* 51(1-3), 209-224.
- Watts, R.J., Finn, D.D., Cutler, L.M., Schmidt, J.T., Teel, A.L. 2007. Enhanced stability of hydrogen peroxide in the presence of subsurface solids. *J. Contam. Hydrol.* 91, 312-326.
- Watts, R.J., Furman, O.S., Teel, A.L., Brown, R.A., Block, P.A. 2008. Mechanism of base activation of persulfate for in situ chemical oxidation (ISCO). Partners in Environmental Technology Technical Symposium & Workshop, Washington, D.C., December 2-4.
- Watts, R.J., Howsawkung, J., Teel, A.L. 2005. Destruction of a carbon tetrachloride dense nonaqueous phase liquid by modified Fenton's reagent. *J. Environ. Eng.* 131(7), 1114-1119.
- Watts, R.J., Kong, S., Dippre, M., Barnes, W.T. 1994. Oxidation of sorbed hexachlorobenzene in soils using catalyzed hydrogen peroxide. *J. Hazard. Mater.* 39(1), 33-47.
- Watts, R.J., Stanton, P.C. 1999. Mineralization of sorbed and NAPL-phase hexadecane by catalyzed hydrogen peroxide. *Water Res.* 33(6), 1405-1414.

- Watts, R.J., Stanton, P.C., Howsawheng, J., Teel, A.L. 2002. Mineralization of a sorbed polycyclic aromatic hydrocarbon in two soils using catalyzed hydrogen peroxide. *Water Res.* 36(17), 4283-4292.
- Watts, R.J., Teel, A.L. 2006. Treatment of contaminated soils and groundwater using in situ chemical oxidation. *Pract. Period. Haz. Waste Manag.* 10(1), 2-9.
- Watts, R.J., Teel, A.L. 2005. Chemistry of modified Fenton's reagent (catalyzed H_2O_2 Propagations-CHP) for in situ soil and groundwater remediation. *J. Environ. Eng.* 131(4), 612-622.
- Watts, R.J., Teel, A.L., Finn, D.D., Schmidt, J.T., Cutler, L.M. 2007. Rates of trace mineral-catalyzed decomposition of hydrogen peroxide. *J. Environ. Eng.* 133(8), 853-858.
- Yeh, C.K.-J., Wu, H.-M., Chen, T.-C. 2003. Chemical oxidation of chlorinated non-aqueous phase liquid by hydrogen peroxide in natural sand systems. *J. Hazard. Mater.* 96(1), 29-51.
- Zafiriou, O.C., Voelker, B.M., Sedlak, D.L. 1998. Chemistry of the superoxide radical (O_2^-) in sea water: reactions with inorganic copper complexes. *J. Phys. Chem. A.* 102, 5693-5700.

10. APPENDICES

List of Technical Publications

Articles or papers published in peer-review journals

- Ahmad, M., Teel, A. L., Ocampo, A.M., and Watts, R. J., 2011. Mechanism of Phenoxide Activation of Persulfate. *Environ. Sci. Technol.* In preparation.
- Teel, A. L., and Watts, R. J. 2011. Activation of Persulfate by Ketones. *J. Hazard. Mater.* In preparation.
- Ahmad, M., Teel, A. L., Furman, O., and Watts, R. J., 2011. Oxidative and Reductive Pathways in Iron-Ethylenediaminetetraacetic acid (EDTA) Activated Persulfate Systems. *J. Environ. Engr.* Under review.
- Corbin, J. C., Teel, A.L., and Watts, R.J. 2011. Activation of Persulfate by Trace Minerals . *Chemosphere.* Under review.
- Furman, O., Teel, A. L., and Watts, R. J. 2011. Effect of Basicity on Persulfate Reactivity. *J. Environ. Engr.* In press; scheduled for April 2011 publication.
- Furman, O., Teel, A. L., and Watts, R. J. 2010. Mechanism of Base Activation of Persulfate. *Environ. Sci. Technol.* 44(16), 6423-6428.
- Ahmad, M., A.L. Teel, and R.J. Watts. 2010. Persulfate Activation By Major Soil Minerals. *J. Contam. Hydrol.* 115(1-4), 34-45.
- Teel, A.M, L. M. Cutler, and R.J. Watts. 2009. Effect of Sorption on Contaminant Oxidation in Activated Persulfate Systems. *J. Environ. Health Sci. A. Toxic/Hazard. Substance. Environ. Engr.* 44(11), 1098-1103.

Conference/symposium proceedings

- Watts, R.J and A.L. Teel. 2010. Retrospective on 20 Years of Peroxygen Research. 2010. Second Southeastern In Situ Soil & Groundwater Remediation Conference, Raleigh, NC, February 23-24, 2010.
- Watts, R.J and A.L. Teel. Recent Advances in Peroxygen Mechanisms and Contaminant Degradation Pathways for In Situ Chemical Oxidation. 2009. RemTec09 Conference. Atlanta, GA March 3-5, 2009.
- Watts, R.J., A.M. Ocampo, A.L. Teel, R.A. Brown, P.A. Block. 2009. Mechanism of Phenoxide Activation of Persulfate for In Situ Chemical Oxidation (ISCO). 2009. Partners in Environmental Technology Technical Symposium & Workshop, Washington, D.C. December 1-3, 2009.
- Watts, R.J. J.F. Corbin, O.S. Furman, A.M. Ocampo, J.I. Reed, R.E. Vaughan, A.L. Teel, R.A. Brown, and P.A. Block. 2008. Recent Advances in Persulfate Activation for In Situ

Chemical Oxidation. Sixth International Conference on Remediation of Chlorinated and Recalcitrant Compounds, Monterey, CA , May 19-22, 2008.

- Watts, R.J., O.S. Furman, A.L. Teel, R.A. Brown, P.A. Block. 2008. Mechanism of Base Activation of Persulfate for In Situ Chemical Oxidation (ISCO). Partners in Environmental Technology Technical Symposium & Workshop, Washington, D.C. December 2-4, 2008.
- Watts, R.J and A.L. Teel. 2008. Current Research on Enhancing In Situ Chemical Oxidation (ISCO) Reactant-Contaminant Contact. Partners in Environmental Technology Technical Symposium & Workshop, Washington, D.C. December 2-4, 2008.
- Watts, R.J and A.L. Teel. 2008. Catalyzed Peroxygens: Chemistry and Applications. First Southeastern In Situ Soil & Groundwater Remediation Conference, Raleigh, NC, February 26-27, 2008
- R.A. Brown, P.A. Block, R.J. Watts, and A.L. Teel. 2006. Perspectives on mechanisms of persulfate activation and process chemistry. The Fifth International Conference on Remediation of Chlorinated and Recalcitrant Compounds. Monterey, CA. May 22-26, 2006.
- J. Corbin and R.J. Watts. 2006. Kinetics of mineral-catalyzed decomposition of persulfate. 4th International Conference on Oxidation –Reduction Technologies for the Remediation of Contaminated Soils and Groundwater. Chicago, IL October 22-25, 2006.
- Watts, R.J and A.L. Teel. 2006. Fundamentals and Recent Advances in In Situ Chemical Oxidation. Combined Technologies Symposium, Tufts University. July 22-24, 2006.
- Watts, R.J. 2006. Recent Advances in Peroxygen ISCO. Monterey Conference on Chlorinated and Recalcitrant Compounds. May 21-25, 2006